Dissertation

submitted to the
Combined Faculty of Natural Sciences and Mathematics
of the Ruperto-Carola University of Heidelberg, Germany
for the degree of
Doctor of Natural Sciences

Presented by
M.Sc. Hendrik Welsch
Born in Hameln, Germany
Oral examination: 21.09.2021

Investigating the Effects of Chronic Stimulation of Innate Antiviral Immune Responses

Referees:

Prof. Dr. Ralf Bartenschlager

Dr. Marco Binder

Declaration

The applicant, Hendrik Welsch, declares that he is the sole author of the submitted dissertation and no other sources or help apart from those specifically referred to have been used. Additionally, the applicant declares that he has not applied for permission to enter an examination procedure at any other institution and that this dissertation has not been presented to any other faculty and has not been used in its current or in any other form in another examination.

.....	.....
Date	Signature

Acknowledgements

I would like to express my gratitude to the many friends and colleagues without whom this work would not have been possible.

First of all, I would like to thank Dr. Marco Binder for accepting me as a PhD student in his lab, for supervising this work, for always being available for discussion and advice, and for providing a pleasant working environment.

I would also like to thank Prof. Dr. Ralf Bartenschlager for being my first referee and chairing my defense. Furthermore, I thank Prof. Dr. Martin Müller and PD Dr. Dr. Angelika Riemer for accepting to be part of my defense committee.

I would like to thank the members of my thesis advisory committee – Prof. Dr. Ralf Bartenschlager, Dr. Steeve Boulant, Prof. Dr. Andreas Pichlmair, and Prof. Dr. Volker Lohmann – for helpful discussions and valuable input from which this work has greatly benefitted.

Special thanks to Katharina Heine and our partners within TRR179 (TP11), Christian Urban and Andreas Pichlmair, for the productive collaboration.

The members of F170, past and present, I want to thank for the great working environment, the many interesting discussions (science-related as well as off-topic), the get-togethers and events. Shout-outs to the F170 running group!

Big thanks to my fellow DKFZ PhD students, my Pen & Paper group, and all the other friends in and around Heidelberg that made my stay here so much more enjoyable.

I want to express my gratitude to all the former and present members of the Binder Lab. The friendly atmosphere, the level of teamwork and support, and the friendships that were formed here made my time in the lab very special. I will miss our coffee breaks together! I want to specifically mention Sandra, Vladimir, and Catherine, for accompanying and supporting me during a substantial period of my PhD. In addition, I want to thank Vladimir, Sandy, David, and Christopher for proofreading and helpful comments.

Finally, my time in Heidelberg wouldn't have been nearly that great if it weren't for my fellow Binder Lab doctoral students Sandy Burkart, Christopher Dächert, and David Zander. Thank you for your support and the many hours spent together in and out of the lab. Our cooking events were truly highlights that I will not forget! I consider myself lucky that we were able to tackle the big milestone "doctoral thesis" together.

Vielen Dank meinen Freunden in der Heimat. Trotz der Distanz ist unsere Freundschaft sogar noch zusammengewachsen, und ich bin sehr dankbar für all die wundervollen gemeinsamen Aktionen.

Abschließend möchte ich meiner Familie, allen voran meinen Eltern Anette und Michael, für die Unterstützung auf meinem bisherigen Lebensweg und in allen Lebenslagen von ganzem Herzen danken! Euch widme ich diese Arbeit.

Summary

Hepatotropic viruses constitute a global health concern, as the WHO estimates over 300 million people worldwide suffering from chronic viral hepatitis. One of the causative agents is the Hepatitis C virus (HCV). In many infected, HCV is able to evade clearance by the immune system and establish a persistent infection. Here, the characteristics of a constantly activated immune response turn from antiviral to pro-inflammatory, thereby establishing a chronic inflammation of the liver, which promotes increasingly severe levels of liver damage, liver failure, and the development of liver cancer. In this study, we investigated the consequences of prolonged activation of antiviral signaling pathways in a virus-free cell culture system, using the lung adenocarcinoma cell line A549 and the immortalized hepatocyte cell line PH5CH. Ectopic expression of NS5B, the RNA-dependent RNA polymerase of HCV, produced double-stranded RNA (dsRNA) that was sensed by the pattern recognition receptor retinoic acid-inducible gene I (RIG-I). This induced the expression and secretion of interferons (IFNs) β and λ1, pro-inflammatory cytokines tumor necrosis factor and interleukin 6, and chemokines CCL3, -4, -17, and CXCL10. Cells expressed interferon-stimulated genes (ISGs) and exhibited reduced proliferation, which we could attribute to a concerted effect of IFN-β and IFN-λ1. We showed that IFN-λ1 expression correlated with NS5B expression on a single cell level, while ISG induction and impairment of proliferation was exerted through paracrine IFN signaling. NS5B expression was sufficiently high to trigger the RIG-I pathway for over 14 days, before unspecific downregulation of the transgene, likely in combination with counterselection of NS5B high-expressing cells, led to ceasing production of IFNs. We compared the supernatant from NS5B-expressing cells to a defined mix of IFN-β and IFN-λ1 in elicited changes in global gene transcription of exposed cells. In A549 and in PH5CH, both treatments triggered a very similar response in the upregulation of, for the most part, well-defined ISGs. Long-term exposure of naïve A549 cells to NS5B-derived supernatant for one month showed only subtle differences in ISG gene expression, suggesting that cells do not become refractory to IFN-β or IFN-λ1. Of three genes that were significantly upregulated only after treatment for one month, the tetraspanin TM4SF4 warrants further investigation due to its implication in hepatocellular carcinoma and a possible link to SARS-CoV2 infection. In summary, this study describes a cell culture system that enables to study the effects of continuous antiviral signaling for over two weeks, thereby mimicking a persistent viral infection while excluding virus-mediated interference. Furthermore, the system allows to produce a mix of secreted factors that resembles the epithelial-derived secretome present in an infected organ. Further elucidating the composition of this mix as well as long-term co-culture experiments of NS5B-expressing cells and non-parenchymal liver-resident or -infiltrating cells may help elucidate the complex intercellular dynamics that form the basis of HCV-associated chronic infection, inflammation, and liver deterioration.

Zusammenfassung

Hepatotrope Viren stellen ein globales Gesundheitsproblem dar, denn nach Schätzungen der WHO leiden weltweit über 300 Millionen Menschen an chronischer Virus-Hepatitis. Einer der Erreger ist das Hepatitis-C-Virus (HCV). Bei vielen Infizierten ist HCV in der Lage, sich der Beseitigung durch das Immunsystem zu entziehen und eine persistente Infektion zu etablieren. Dabei wechseln die Eigenschaften einer ständig aktivierten Immunantwort von antiviral zu pro-inflammatorisch und etablieren so eine chronische Entzündung der Leber, die immer schwerere Leberschäden, Leberversagen und die Entwicklung von Leberkrebs fördert. In dieser Studie untersuchten wir die Folgen einer verlängerten Aktivierung der antiviralen Signalwege in einem virusfreien Zellkultursystem unter Verwendung der Lungenadenokarzinom-Zelllinie A549 und der immortalisierten Hepatozyten-Zelllinie PH5CH. Die ektopische Expression von NS5B, der RNA-abhängigen RNA-Polymerase von HCV, produzierte doppelsträngige RNA (dsRNA), die von dem Mustererkennungsrezeptor (engl. *pattern recognition receptor*) *retinoic acid-inducible gene I* (RIG-I) erkannt wurde. Dies induzierte die Expression und Sekretion der Interferone (IFN) β und λ1, der pro-inflammatorischen Zytokine Tumornekrosefaktor und Interleukin 6, sowie der Chemokine CCL3, -4, -17, und CXCL10. Die Zellen exprimierten Interferon-stimulierte Gene (ISGs) und wiesen eine reduzierte Proliferation auf, was wir auf einen konzertierten Effekt von IFN-β und IFN-λ1 zurückführen konnten. Wir zeigten, dass die IFN-λ1-Expression mit der NS5B-Expression auf Einzelzellebene korrelierte, während die ISG-Induktion und die Beeinträchtigung der Proliferation durch parakrine IFN-Signalübertragung erfolgte. Die NS5B-Expression war ausreichend hoch, um den RIG-I-Signalweg für mehr als 14 Tage auszulösen, bevor eine unspezifische Herunterregulierung des Transgens, wahrscheinlich in Kombination mit einer Gegenselektion der stark NS5B-exprimierenden Zellen, zu einem Ende der Produktion von IFNs führte. Wir verglichen Veränderungen der globalen Gentranskription in Zellen, die durch Exposition mit dem Überstand von NS5B-exprimierenden Zellen oder mit einer definierten Mischung aus IFN-β und IFN-λ1 hervorgerufenen worden waren. In A549 und in PH5CH lösten beide Behandlungen eine sehr ähnliche Reaktion in der Hochregulierung von größtenteils wohldefinierten ISGs aus. Eine Langzeitexposition von naiven A549-Zellen mit Überstand von NS5B-exprimierenden Zellen für einen Monat zeigte nur subtile Unterschiede in der ISG-Genexpression, was darauf hindeutet, dass die Zellen nicht refraktär gegenüber IFN-β oder IFN-λ1 werden. Von den drei Genen, die nur nach einmonatiger Behandlung signifikant hochreguliert waren, verdient das Tetraspanin TM4SF4 weitere Untersuchungen aufgrund seiner Bedeutung für das hepatozelluläre Karzinom und einer möglichen Verbindung zu SARS-CoV2-Infektionen. Zusammenfassend wird in dieser Arbeit ein Zellkultursystem beschrieben, das es ermöglicht, die Auswirkungen einer kontinuierlichen antiviralen Signalübertragung über zwei Wochen zu untersuchen und damit eine persistente

virale Infektion zu imitieren, während eine virusvermittelte Interferenz ausgeschlossen wird. Darüber hinaus erlaubt das System, eine Mischung von sekretierten Faktoren zu produzieren, die dem epithelialen Sekretom in einem infizierten Organ ähnelt. Die weitere Aufklärung der Zusammensetzung dieser Mischung sowie Langzeit-Kokulturexperimente mit NS5B-exprimierenden Zellen und nicht-parenchymalen, leber-residenten oder -infiltrierenden Zellen können dazu beitragen, die komplexe interzelluläre Dynamik zu entschlüsseln, die die Grundlage für HCV-assoziierte chronische Infektion, Entzündung und Leberschädigung bildet.

Abbreviations

25-HC	25-hydroxycholesterol
aCKRs	Atypical chemokine receptors
ACTB	Beta-actin
ADAR1	Adenosine deaminase acting on RNA 1
AIM2	Absent in melanoma 2
APO	Apolipoprotein
APOBEC	Apolipoprotein B mRNA-editing enzyme catalytic polypeptide-like
APS	Ammonium persulfate
ATAC	assay for transposase-accessible chromatin using sequencing
ATP	Adenosin triphospate
BSA	Bovine serum albumin
BTN3A3	Butyrophilin subfamily 3 member A3
CANX	Calnexin
CARD	Caspase activation and recruitment domain
cCKRs	Conventional chemokine receptors
CD	Cluster of differentiation
cDNA	Complementary DNA
cGAMP	Cyclic GMP-AMP
cGAS	Cyclic GMP-AMP synthase
CH25H	Cholesterol-25-hydroxylase
CHC	Chronic hepatitis C
CLDN1	Claudin 1
CLR	C-type lectin receptor
CMPK2	Cytidine/uridine monophosphate kinase 2
CoV	Coronavirus
CRISPR	Clustered regularly interspaced short palindromic repeats
CTD	C-terminal domain
d.p.t.	Days post transduction
Da	Dalton
DAMP	Danger-associated molecular pattern
DAPI	4',6-Diamidin-2-phenylindol
DBD	DNA binding domain
DC	Dentritic cell
DD	Death domain
ddH_2O	Double distilled H_2O
DDX60(L)	DExD/H-Box helicase 60 (like)
DED	Death effector domain
DENV	Dengue virus
DMEM	Dulbecco's modified eagle medium
DMSO	Dimethyl sulfoxid
DMV	Double membrane vesicle
DNase	Desoxyribonuclease
dNTP	Desoxyribonucleotide triphosphate
DR	Death receptor
dsDNA	Double-stranded DNA
dsRNA	Double-stranded RNA
DTT	Dithiothreitol
DUB	Deubiquitinating enzymes
E. coli	*Escherichia coli*
e.v.	Empty vector
ECM	Extracellular matrix
EDTA	Ethylenediaminetetraacetic acid
EF1α	Elongation factor 1 α
eIF-2α	Eukaryotic translation initiation factor 2 subunit alpha
EPSTI1	Epithelial stromal interaction 1
ER	Endoplasmic reticulum
FACS	Fluorescence-activated cell sorting
FADD	Fas-associated via death domain
FCS	Fetal calf serum
fwd	forward
GAF	IFN gamma activated factor
GAPDH	Glyceraldehyde-3-phosphate dehydrogenase
GAS	IFN gamma activation sequence
GDD	Glycine aspartate aspartate
GFP	Green fluorescent protein
HA	Human influenza hemagglutinin
HCC	Hepatocellular carcinoma
HCMV	Human cytomegalovirus
HCV	Hepatitis C virus
HGD	Homogentisate 1,2-dioxygenase
HIV	Human immunodeficiency virus
HLA	Human leukocyte antigen
HRP	Horseradish peroxidase
HSC	Hepatic stellate cells
IκB	Inhibitor of κB
IAP	Inhibitor of apoptosis
IAV	Influenza A virus
IDO	Indoleamine 2,3-deoxygenase
IFI	Interferon-induced protein
IFIT	Interferon-induced with tetratrico-peptide repeats
IFITM	Interferon-induced transmembrane
IFN	Interferon
IKK	IκB kinase
IL	Interleukin
IP-10	IFN-γ induced protein 10
IRES	Internal ribosomal entry site

IRF	Interferon regulatory factor
ISG	Interferon stimulated gene
ISGF3	Interferon stimulated gene factor 3
ISRE	Interferon stimulated response element
IU	international units
JAK	Janus kinase
LAP3	Leucine aminopeptidase 3
LB	Lysogeny broth
LCMV	Lymphocytic choriomeningitis virus
LFQ	Label-free quantification
LGALS3BP	Lectin galactoside-binding soluble 3-binding protein
LGP2	Laboratory of genetics and physiology 2
lncRNA	Long non-coding RNA
LPS	Lipopolysaccharides
LSEC	Liver sinusoidal endothelial cells
LY6E	Lymphocyte antigen 6 family member E
MAVS	Mitochondrial antiviral signalling protein
MCP	Monocyte chemoattractant protein
MDA5	Melanoma differentiation-associated 5
MHC	Major histocompatibility complex
MIP	Macrophage inflammatory protein
MLKL	Mixed lineage kinase domain like pseudokinase
MNase	Micrococcal nuclease
MOI	Multiplicity of infection
MyD88	Myeloid differentiation primary response 88
NADH	Nicotinamide adenine dinucleotide
NEMO	NF-κB essential modulator
NF-κB	Nuclear factor κ light chain enhancer of activated B cells
NK	Natural killer cell
NLR	Nucleotide-binding oligomerization domain-like receptor
NLS	Nuclear localization signal
NMI	N-myc and STAT interactor
NS	non-structural
OAS	Oligoadenylate synthetase
OCLN	Occludin
ORF	Open reading frame
PAMP	Pathogen-associated molecular pattern
PARP	Poly(ADP-Ribose) polymerase
PBS	Phosphate buffered saline
PCR	Polymerase chain reaction
PD-1	Programmed cell death 1
PD-L1	Programmed cell death 1 ligand
PFA	Paraform aldehyde
PIAS	Protein inhibitors of activated STAT
PKR	Protein kinase R
poly(C)	Polycytidylic acid potassium salt
poly(I:C)	Polyinosinic:polycytidylic acid
PP	Protein phosphatase
PRR	Pattern recognition receptor
PSMB9	Proteasome 20S subunit beta 9
PTM	Posttranslational modification
qRT-PCR	Quantitative real time PCR
RdRp	RNA-dependent RNA polymerase
RE	Restriction endonuclease
rev	reverse
RIG-I	Retinoic acid inducible gene I
RIPA	RIG-I-like receptor-induced IRF3-mediated pathway of apoptosis
RIPK	Receptor-interacting serine/threonine protein kinase
RLR	RIG-I-like receptor
RNase	Ribonuclease
RNF	Ring finger protein
RT	Reverse transcription
SAMHD1	SAM and HD domain containing deoxy-nucleoside triphosphate triphospho-hydrolase 1
SARS	Severe acute respiratory syndrome
SDS	Sodium dodecyl sulfate
SeV	Sendai virus
SOCS	Suppressor of cytokine signaling
SRB1	Scavenger receptor class B type I
ssRNA	Single-stranded RNA
STAT	Signal transducer and activator of transcription
STING	Stimulator of interferon genes
TAE	Tris acetate EDTA
TANK	TRAF family member-associated NF-κB activator
TARC	Thymus and activation-regulated chemokine
TBK1	TANK binding kinase 1
TBS	Tris-buffered saline
TEMED	N, N, N', N'-tetramethylethylenediamine
TGF-β	Transforming growth factor β
TGS	Tris glycine sulfate
TIR	Toll/IL-1 receptor
TLR	Toll-like receptor
TM4SF4	Transmembrane 4 L six family member 4
TMEM63B	Transmembrane protein 63B
TNF	Tumor necrosis factor
TNFR	TNF receptor
TRADD	TNF receptor type 1-associated death domain
TRAF	TNF receptor-associated factor
TRAIL	TNF-related apoptosis-inducing ligand

TRANK1	Tetratricopeptide repeat and ankyrin repeat containing 1
TREX1	Three prime repair exonuclease 1
TRIF	TIR-domain-containing adapter-inducing IFN-β
TRIM	Tripartite motif containing
TYK	Tyrosine kinase
U	units
UBE2L6	Ubiquitin/ISG15-conjugating enzyme E2 L6
UGT1A1	UDP glucuronosyltransferase family 1 member A1
USP	Ubiquitin-specific protease
UTR	Untranslated region
WT	wild type
XAF1	XIAP-associated factor 1
XIAP	X-linked IAP

List of Figures

List of Tables

Contents

1 Introduction

The human body is subject to constant attack by a variety of pathogens, ranging from intracellular microbes to multicellular parasites. Survival under these conditions is only possible due to a complex immune system that is able to sense the pathogen, mount a fast and – if necessary – organism-wide counterattack, and "remember" the pathogen to be prepared in case of future attacks[1]. Evolutionary pressure resulted in an ongoing co-evolution of improvement and adaptation of the host immune system on one side and pathogen countermeasures and evasion strategies on the other side[2].

Viruses are intracellular pathogens that require the host cell for production of progeny virions[3]. A viral infection is usually terminated by a powerful but time-restricted response of the immune system; however, certain viruses can establish a persistent infection and/or induce chronic disease manifestations[4]. A prominent example is Hepatitis C virus (HCV) that may persist in infected livers for decades despite the presence of a constantly active immune response[5]. Strikingly, it is the permanent inflammation of the liver – targeted at the virus but ultimately futile – that causes detrimental effects on the organ. Patients with chronic hepatitis C (CHC) often develop liver cirrhosis, which can later lead to liver failure or hepatocellular carcinoma[6].

This work exploited components of HCV to investigate how cells cope with the stress of a constantly active immune response. The following introduction will therefore cover properties of viral infection, with a focus on HCV and chronic hepatitis, as well as the signaling networks of the immune system that are involved in combating viral infections.

1.1 Hepatitis C Virus

According to a 2017 study of the World Health Organization, around 71 million people world-wide are estimated to suffer from CHC[7]. The virus causing the disease, HCV, belongs to the *Flaviviridae* family of enveloped viruses with a single strand RNA (ssRNA) genome[8]. HCV is of the genus *Hepacivirus* and closely related to viruses from the genus *Flavivirus*, with prominent members such as Dengue virus (DENV) and Zika virus (ZIKV)[8–10].

HCV measures 56–65 nm in diameter and contains a 9.6 kilobases (kb) long ssRNA genome of positive orientation ((+)ssRNA), coding for ten viral proteins[11,12] (Fig Ia). The genome is surrounded by a capsid made up from multiple units of viral core protein, and a host cell membrane-derived envelope that contains viral glycoproteins E1 and E2[12]. The virus particle is furthermore coated with host-derived lipoproteins such as apolipoprotein E[13] (APOE).

HCV was first isolated more than three decades ago from blood of infected patients[15].

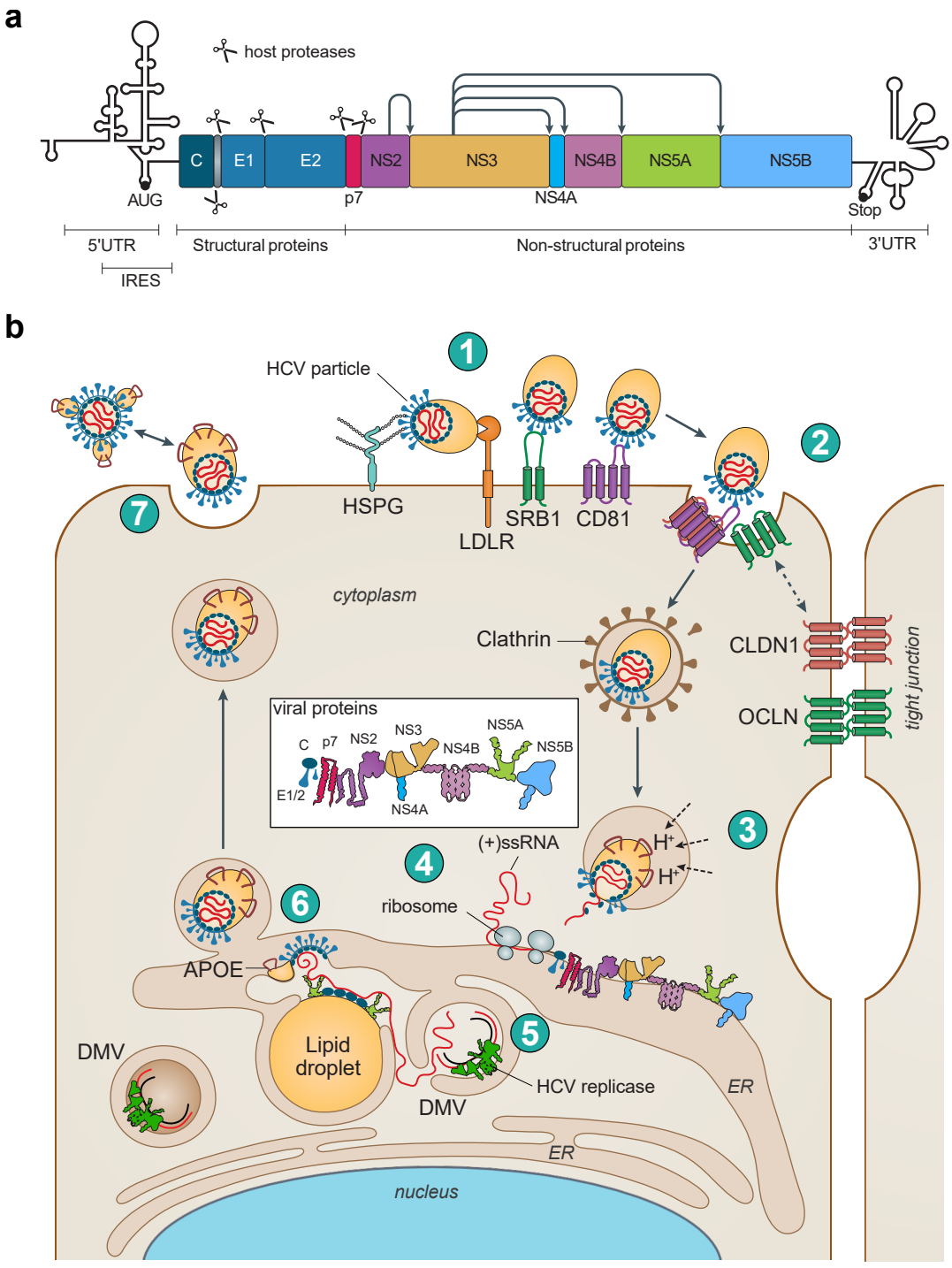

Figure I: Hepatitis C virus genome structure and life cycle.

(**a**) Positive single strand RNA genome of Hepatitis C virus (HCV). Open reading frame encodes structural proteins core (C), glycoproteins E1 and E2, and non-structural proteins p7, NS2, -3, -4A,- 4B, -5A, and -5B. The polyprotein is processed through proteolytic cleavage by host proteases (scissor symbol) and viral proteases NS2 and NS3 (arrows). UTR: untranslated region; IRES: internal ribosomal entry site; AUG: methionine start codon. (**b**) HCV life cycle steps in infected hepatocytes: (1) Attachment, (2) internalization, (3) fusion with endosome membrane, (4) translation of viral proteins, (5) genome replication, (6) virion assembly, and (7) secretion. HSPG: heparan sulfate proteoglycan; LDLR: low-density lipoprotein receptor; CD81: cluster of differentiation 81; SRB1: scavenger receptor class B member 1; CLDN1: claudin 1; OCLN: occluding; DMV: double membrane vesicle; APOE: apolipoprotein E. Figure adapted and modified from [14].

It is primarily transmitted through exposure to virus-containing blood, for example via shared needles during drug abuse or contaminated medical equipment[16]. In the blood stream, the virus is carried into the liver, where it attaches to hepatocytes via rather unspecific interactions between virus-associated lipoproteins and their receptors on the hepatocyte cell surface[17] (Fig Ib). Exposure of viral glycoproteins then allows for more specific binding with several cell surface proteins such as scavenger receptor class B type I (SRB1) and cluster of differentiation 81 (CD81)[17–20]. These interactions, combined with co-localization of SRB1 and CD81 with other membrane associated factors like the tight-junction proteins claudin 1 (CLDN1) and occludin (OCLN), lead to the formation of the HCV co-receptor complex[17,21–23]. Binding of E2 to CD81 activates signaling pathways that initiate and regulate viral entry[17,24–26]. The HCV particle is internalized through endocytosis mediated by clathrin and dynamin[17,27–29]. Within the endosome, pH changes and interactions with CD81 are believed to induce conformational changes of E1 and E2 that result in exposure of a fusion peptide[17]. Membrane fusion of the viral particle membrane and the endosome releases the viral genome into the cytoplasm[17].

The host ribosomal machinery immediately commences with translation, initiated via an internal ribosomal entry site (IRES) in the 5' untranslated region (UTR)[30] (Fig Ia). Downstream of the IRES, the HCV genome contains a single open reading frame (ORF) coding for a polyprotein that will later yield three structural proteins (Core, E1, E2) and seven non-structural (NS) proteins (viroporin p7, NS2, -3, -4A, -4B, -5A, and -5B)[12]. The polyprotein is first processed by two cellular proteases, ER signal peptidase and signal peptid peptidase, yielding mature proteins Core to p7[12,31]. Viral protease NS2 then cleaves the connection to NS3, and NS3/4A protease activity in turn liberates the remaining non-structural proteins[12,31].

Viral genome replication of (+)ssRNA viruses takes place in specialized replication organelles[3]. Flaviviruses like DENV induce invaginations of the ER membrane, while HCV replication happens in ER membrane protrusions of about 200 nm in diameter, termed double-membrane vesicles (DMV)[3,32]. Spatial confinement to replication organelles entails several advantages for viral genome replication (summarized in [3] and [33]): First, within a replication organelle, viral proteins of the replicase complex (NS3 to NS5B for HCV), the RNA genome, and necessary co-factors and nucleotides are concentrated to facilitate replication. Moreover, the viral genome and replication intermediates are protected from detection and degradation by host antiviral factors. Finally, since many viral proteins as well as the RNA genome are involved in multiple steps of the viral life cycle, spatial separation of genome replication prevents attenuation through interference with other steps.

The HCV replicase complex is comprised of viral non-structural proteins NS3 to NS5B, which are associated to the inner membrane of DMVs via transmembrane domains[33–35]. Responsible for complement strand synthesis and replication of the positive strand genome is the RNA-dependent RNA polymerase (RdRp) NS5B, a 68 kDa protein of 591

amino acids[36]. It is anchored to the membrane via a C-terminal α-helix of 21 amino acids and a 40 amino acid long linker[36–38]. The catalytic domain (530 amino acids) displays the right-hand shape typical for single subunit polymerases, consisting of the subdomains palm, fingers, and thumb[36,39–41] (Fig. II). The palm domain contains the catalytic center of the enzyme with the hallmark sequence of one glycine and two aspartate residues (GDD)[12,40]. Here, the two catalytic aspartate residues chelate two divalent metal ions (Mg^{2+} or Mn^{2+}), which are the only co-factors needed for RNA polymerization[12]. NS5B can *de novo* synthesize the complementary strand of its template without the need for primers[36,43,44]. Membrane bound NS5B exists in a closed conformation, where the active site is obstructed by fingers and thumb domains on one side and linker domain and the beta-flap motif of the thumb domain on the other side[36,39–41] (Fig. II). In this closed state, only ssRNA can enter the active site, and the 3' end of the template strand does so through a groove between fingers and thumb domains[36,41]. During the initiation step, multiple dinucleotide primers are synthesized, until the synthesis of a third nucleotide stabilizes the complex and initiates transition to the elongation step[36,45]. This is accompanied by a conformational change of the enzyme into a more open shape that allows the binding of double-stranded RNA (dsRNA) in the active site, which is necessary for stable oligonucleotide synthesis progression[36,41,46–48]. NS5B proceeds to synthesize 100–400 nucleotides per minute with a relatively high error rate of 10^{-3} per nucleotide[36,48,49].

Assembly of progeny virions takes place in the proximity of DMVs at lipid droplets[14]. Here, the viral genome is encapsulated and cellular lipoproteins such as APOE associate with the particle, before matured virions leave the cell, supposedly via secretion

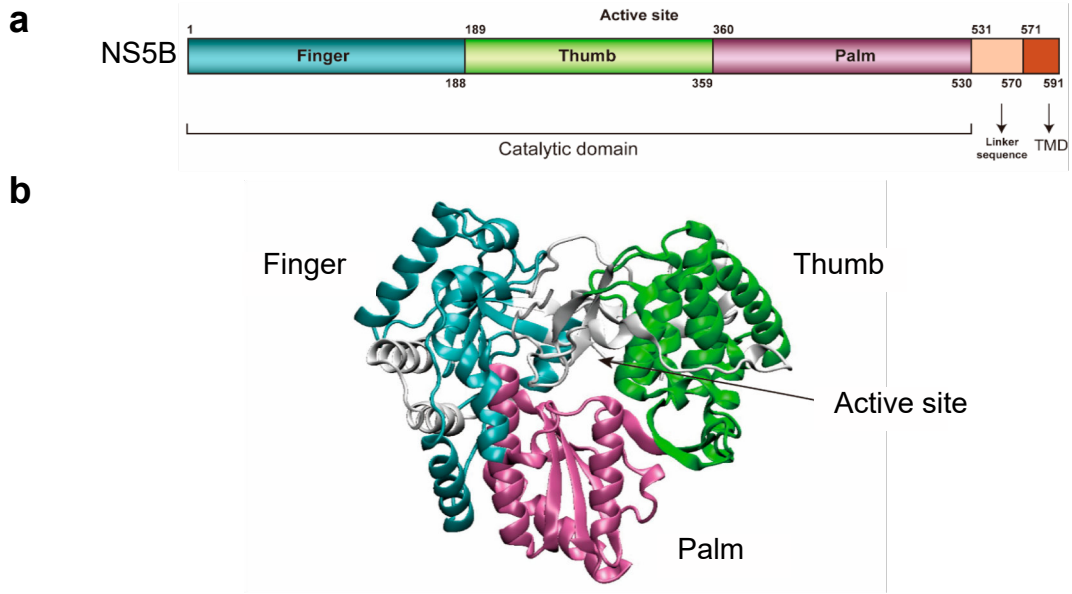

Figure II: Hepatitis C virus RNA-dependent RNA polymerase NS5B.
(**a**) Schematic organization of Hepatitis C virus (HCV) RNA-dependent RNA polymerase (RdRp) NS5B. N-terminal catalytic domain, consisting of subdomains finger, thumb, and palm, is followed by linker and C-terminal transmembrane domain (TMD). Numbers indicate amino acid position. (**b**) 3-Dimensional structure of HCV NS5B catalytic domain. Figure adapted and modified from [42].

pathways[50]. HCV replication is highly efficient and is estimated to produce new virions in the range of 10^{12} per day in an infected person[51,52]. Before going into detail on the progression of acute HCV infection and the development of chronic hepatitis C, the following chapters will describe how cells are able to sense viral infections, mount intracellular defenses and alarm surrounding tissues and immune cells.

1.2 Innate Immunity of the Cell

Intracellular pathogens exploit their host cells for resources and, in the case of viruses, even hijack cellular machineries. Cells are consequently equipped with a multitude of security systems to constrain an infection. The first step, the detection of the pathogen, is executed by pattern recognition receptors (PRRs), which survey specific cellular compartments for pathogen-associated molecular patterns (PAMPs)[53,54]. PAMPs are molecular structures conserved among microbial species[53], and in a broader sense can be defined as non-self, i.e. they are not present in a given compartment under homeostatic conditions[54]. Usually, these PAMPs are components of the pathogen itself, but also endogenous molecules may be sensed when homeostasis is disturbed during an infection, causing them to be modified or translocate to another compartment[53,54].

Different classes of PRRs are specialized to sense defined molecular structures. On the cell surface, C-type lectin receptors (CLR) like dectin 1 can detect fungal pathogens[55,56]. Bacterial components such as cell wall fragments may be recognized by nucleotide-binding and oligomerization domain (NOD)-like receptors (NLRs)[56,57]. Viral genomes and nucleic acid intermediates that are transiently exposed during replication represent a prime target of PRRs, since these oligonucleotides are either structurally different from cellular DNA or RNA and/or are encountered in the incorrect compartment[54]. DNA sensors, for example absent in melanoma 2 (AIM2) or cyclic GMP–AMP synthase (cGAS), can bind to double-stranded DNA (dsDNA) of DNA viruses such as herpesviruses[56,58,59]. Conversely, RNA viruses are detected by RNA-sensing PRRs, among them representatives of the Toll-like receptor (TLR) and RIG-I-like receptor (RLR) classes[60].

Upon binding of their ligands, all PRRs induce signaling pathways that activate antiviral responses ranging from expression of signaling molecules, such as interferons and cytokines, to the induction of cell death[54,61]. The following paragraphs will explore these responses in more detail for the TLR- and RLR-class dsRNA sensors that play an important role in sensing an HCV infection[62].

1.2.1 dsRNA-Sensing PRRs – TLR and RLR Signaling

Toll-like receptors are transmembrane proteins present on the cell surface or in endosomes, where they sense a variety of PAMPs, such as bacterial components like

lipopolysaccharides (LPS)[54,63]. The endosomal subset of TLRs specializes in nucleic acid binding via an N-terminal leucine rich repeat[54,63,64]. For most TLRs, ligand binding induces homodimerization and cytoplasmic signal transduction from the C-terminal Toll/IL-1 receptor (TIR) domain to myeloid differentiation primary response 88 (MyD88) and associated proteins, including TNF receptor associated factor (TRAF) 6[54,63,65]. Endosomal TLR3, which specifically binds short dsRNA in a sequence-independent manner, is able to detect double-stranded HCV genome replication intermediates[54,66]. Instead of MyD88, TLR3 recruits TIR-domain-containing adapter-inducing IFN-β (TRIF), which can relay the signal to TRAF6 and TRAF3, thus converging with downstream signaling of other TLRs and with RLR signaling[54,63,67,68] (described below).

The RIG-I-like receptor class of cytosolic RNA sensors is specialized to detect dsRNA and is comprised of three members: the namesake retinoic acid-inducible gene I (RIG-I), melanoma differentiation-associated 5 (MDA5), and laboratory of genetics and physiology 2 (LGP2)[60]. They belong to the SF2 helicase superfamily of NTP-dependent helicases, and are very similar in structure[54]. In RIG-I and MDA5, two N-terminal caspase recruitment and activation domains (CARD) are followed by a DExD/H-box helicase domain and a C-terminal domain[54]. The helicase contains two RecA-like helicase domains (Hel1 and -2) that flank an insert domain (Hel2i)[56]. LGP2 is composed of a helicase domain and a CTD, but lacks the CARD domains that are essential for downstream signaling. It is nonetheless able to bind to dsRNA and acts as a regulator of the other two sensors[54,69]. LGP2 inhibits RIG-I signaling by competitive binding of its dsRNA ligand[54,56,70]. Conversely, LGP2 is suggested to enhance MDA5 signaling by facilitating binding to dsRNA[54,56,71,72].

Although similar in domain structure, RIG-I and MDA5 differ in ligand affinity and how ligand binding proceeds[60]. Three canonical characteristics of RIG-I RNA ligands have been determined (summarized in [54] and [60]): First, a short (10-19 bp) terminal dsRNA region, preferentially forming a blunt end[54,73,74]. RIG-I binds this section in a sequence-independent manner and can tolerate mismatches and secondary structures, but certain sequence motifs, such as a poly(U/UC) stretch in the 3'-UTR of HCV, may positively influence binding[54,75]. Second, a 5' di- or triphosphate group (5'-(p)pp), which is usually absent in cellular RNA species but common in viral replication intermediates[54,76,77]. Similar to host RNAs, genomes of many RNA virus families are modified at the 5' end after transcription, thus removing the 5'-(p)pp, but this is not the case for pestiviruses and hepaciviruses, which retain the triphosphate group[78]. Interestingly, the HCV (+)ssRNA genome is a weak RIG-I ligand, and immune response is markedly increased if 5'-(p)pp and a dsRNA stretch are present[52,73,79]. It has been suggested that this could give HCV a head start in protein translation and replication organelle establishment, before the cell is able to sense dsRNA replication intermediates[52]. And third, a 5'-terminal nucleotide that lacks 2'-O-methylation, which aids in discrimination between foreign RNA and self RNA[60,80]. Although these properties greatly improve detection by RIG-I, they are not always required. For example, it has been shown that increased length of dsRNA

molecules can compensate for missing 5'-(p)pp[81].

RIG-I is present in the cytoplasm in an autoinhibitory conformation, where the CARD domains are sequestered due to interactions with the helicase insert domain Hel2i[54,82] (Fig IIIa). RNA sensing is initiated when a pocket in the CTD binds the 5'-(p)pp. Subsequently, the helicase wraps around the dsRNA, which in turn releases the sequestered CARD domains[56,82–84]. RIG-I adopts a more open conformation that allows for post-translational modifications (PTMs), such as CARD dephosphorylation by phosphatases PP1α or PP1γ (Fig IIIb) (reviewed in detail in [60]). Multiple RIG-I molecules can bind to a single RNA molecule, where the CARDs oligomerize into a helical assembly termed "lock washer"[54,56]. This process is facilitated and stabilized by the binding of lysine-63 (K63) linked poly-ubiquitin chains, which are subsequently covalently attached to RIG-I CTD and CARDs by ubiquitin ligases ring finger protein 135 (RNF135/Riplet) and tripartite motif-containing protein 25 (TRIM25), respectively[54,85–87]. In addition, our group recently demonstrated in a collaborative effort that RIPLET facilitates RIG-I signaling by bridging RIG-I filaments on dsRNA, and that the signaling augmentation correlated with dsRNA molecule length[88].

MDA5 exists in a more open and flexible conformation when no ligand is bound[54,56,91]. It preferentially senses longer dsRNA molecules (> 300 bp) that may exist in complex, higher-order conformations[54,92,93]. Unlike RIG-I, which binds RNA ligands in a terminal approach, MDA5 wraps around dsRNA with its CTD and Hel1 domains, beginning from internal sites of the dsRNA molecule[56,94,95]. From here on, MDA5 also forms oligomeric filaments that are stabilized by PTMs, for instance dephosphorylation via PP1α/γ and K63-linked poly-ubiquitination via TRIM65[54,96,97].

RIG-I or MDA5 filaments, now fully signaling competent, are recruited to mitochondria via 14-3-3 proteins ε and η, respectively, where they interact with mitochondrial antiviral signaling protein (MAVS)[54,98]. MAVS is anchored to the outer mitochondrial membrane through a C-terminal transmembrane domain and contains an N-terminal CARD domain[54,99]. Via CARD-CARD interaction with MAVS, filaments of RIG-I or MDA5 act as nuclei for the induction of prion-like MAVS aggregation[56,100,101]. These MAVS aggregates in turn serve as a signaling hub, recruiting several proteins – among others, ubiquitin ligases TRAF2, -5, -6, and TNF receptor type 1-associated death domain (TRADD) – that activate downstream signaling pathways[54,102]. Of note, HVC is able to inhibit RLR signaling through NS3/4A-mediated proteolytic cleavage of MAVS[103,104], and possibly TLR3 signaling through TRIF cleavage[105]. TRAF family member associated NF-κB activator (TANK) aids MAVS in recruitment of the kinases TANK binding kinase 1 (TBK1) and I-kappa-B kinase ε (IKKε), which then phosphorylate interferon regulatory factor 3 (IRF3)[54,102,106]. IRF3 is a transcription factor that is constitutively expressed, but remains in an inactive form in the cytoplasm when dephosphorylated[107,108]. Upon phosphorylation, IRF3 forms homodimers via C-terminal IRF-association domains and translocates into the nucleus[106,107]. Here, IRF3 induces the expression of major signaling

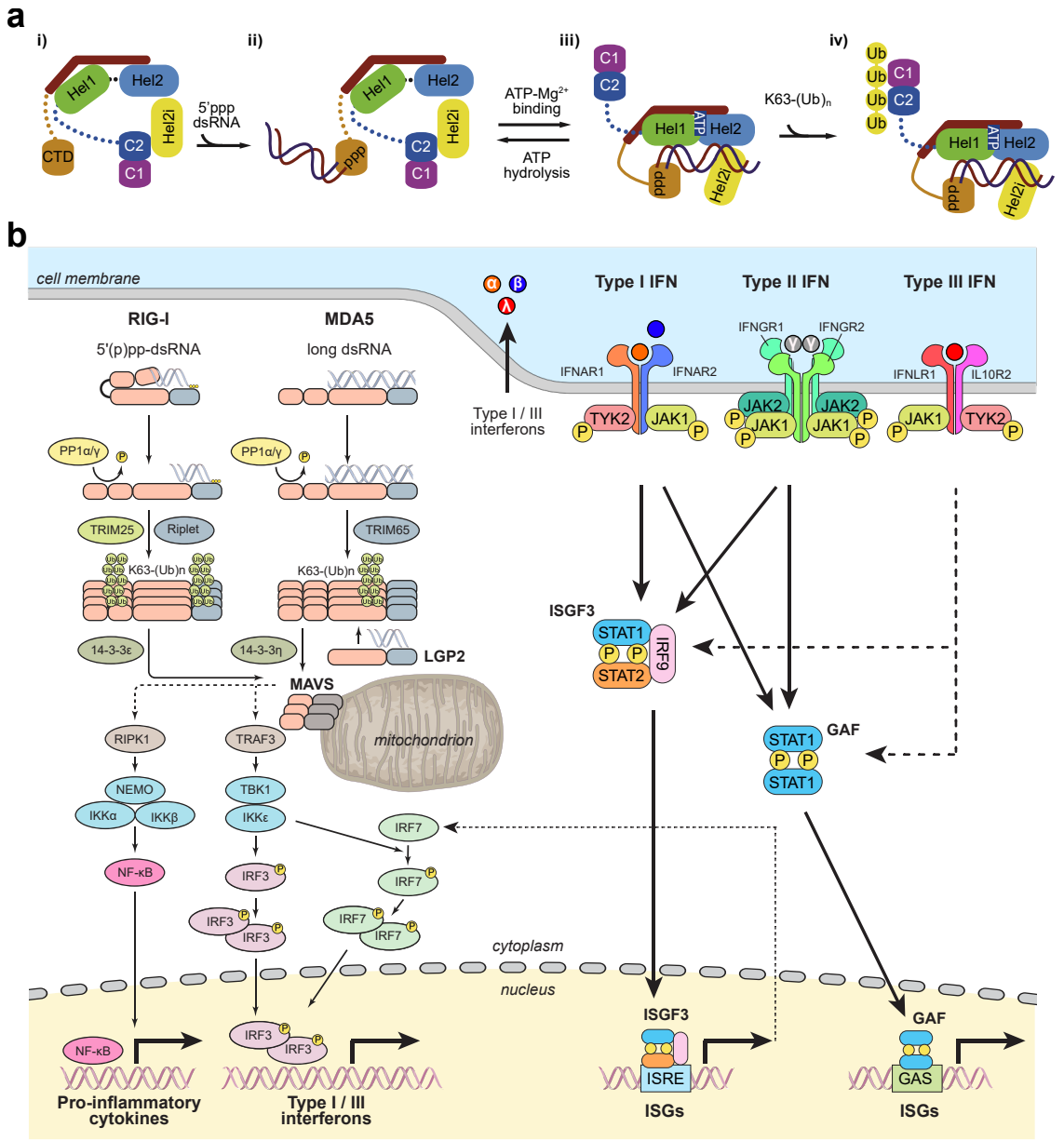

Figure III: Antiviral signaling via RIG-I-like receptors and interferons.

(**a**) Schematic process of retinoic acid-inducible gene I (RIG-I) binding to 5'-di- or triphosphorylated (5'-(p)pp) dsRNA. CTD: C-terminal domain; Hel: Helicase subdomain; C: CARD domain; K63-$(Ub)_n$: lysine-63-linked polyubiquitin. (**b**) Simplified signaling pathways of pattern recognition receptors RIG-I and melanoma differentiation-associated 5 (MDA5), which bind 5'-di- or triphosphorylated (5'-(p)pp) dsRNA or long dsRNA and initiate downstream signaling via mitochondrial antiviral signaling protein (MAVS). Transcription factors nuclear factor kappa-light-chain-enhancer of activated B cells (NF-κB) and interferon regulatory factors (IRF) 3 and 7 induce the expression of pro-inflammatory cytokines and interferons (IFNs) of type I (α, β) and III (λ). Secreted IFNs bind to IFN receptors and induce signaling via Janus kinases (JAK) and signal transducers and activators of transcription (STAT) transcription factors. Interferon-stimulated gene factor 3 (ISGF3) and IFN gamma activated factor (GAF[89]) transcriptional complexes induce the expression of interferon-stimulated genes (ISGs). PP1: protein phosphatase 1; (P): phosphate group; TRIM: tripartite motif-containing protein; LGP2: laboratory of genetics and physiology 2; RIPK1: Receptor-interacting serine/threonine protein kinase 1; NEMO: NF-κB essential modulator; IKK: inhibitor of NF-κB kinase; TRAF3: TNF receptor-associated factor 3; TBK1: TANK binding kinase 1; IFN*R: interferon * receptor subunit (*: A for α, G for γ, and L for λ); IL10R2: interleukin 10 receptor subunit 2; TYK2: tyrosine kinase 2; ISRE: interferon stimulated response element; GAS: IFN gamma activation sequence. Figure adapted and modified from [82], [54] and [90].

molecules of the antiviral immune response, type I and type III interferons[54,107].

1.2.2 Interferon Signaling

Interferons (IFNs) belong to the class of cytokines, small signaling proteins involved in cell-cell communication in many biological processes, including immune response and inflammation[109]. IFNs are grouped into three types based on their target receptors[89,110]: IFNs of type I include several IFN-α subtypes, IFN-β, and several lesser known interferons such as ε, κ, and ω. Type II consists of only one interferon, IFN-γ, and type III includes IFN-λ1–4. While type I and III IFNs can be expressed by many cell types, IFN-γ expression is more restricted to immune cells, such as natural killer (NK) cells, T lymphocytes, and professional antigen presenting cells (e.g. macrophages)[111].

Type I and III interferon expression is induced by many PRRs, including RLRs[107]. Upon secretion, IFNs stimulate cells in an autocrine or paracrine fashion via transmembrane cell surface receptors[90] (Fig III). Type I interferons bind to IFN alpha receptor (IFNAR) subunit 2, which induces recruitment of IFNAR subunit 1 and the formation of a ternary receptor complex[89,90]. Although all type I interferons interact with the same receptor, differences in signaling intensities and gene expression patterns have been observed[90,112,113]. As a reason for these seemingly unintuitive differences, ternary complex stability has been suggested[90]. One of the parameters affecting ternary complex formation and stability is the receptors' binding affinity for different type I IFNs[90]. For example, IFNAR displays a stronger affinity to IFN-β than to IFN-α subtypes[112,113]. Type II and III IFNs each have only one receptor as well: IFN-γ is bound as a homodimer by IFN gamma receptor (IFNGR) subunits 1 and 2, while type III interferons form a ternary complex with IFN lambda receptor (IFNLR) subunits IFNLR1 and a subunit of the interleukin 10 (IL-10) family receptor, IL-10 receptor 2 (IL10R2)[90,114–116]. While type I and II receptors as well as the type III receptor subunit IL10R2 are expressed ubiquitously, IFNLR1 expression seems to be restricted to epithelial cells and a subset of innate immune cells[116]. The affinity of the IFNLR complex to type III IFNs is lower than that of IFNAR to type I IFNs, and interleukins of the IL-10 family were reported to synergize with or antagonize IFNLR signaling[116].

In the cytoplasm, the formation of the ternary receptor complex results in the recruitment and phosphorylation of signal transducers and activators of transcription (STAT) proteins by receptor-associated tyrosine kinases of the Janus kinase (JAK) family[107,116] (Fig IIIb). JAK1 and tyrosine kinase 2 (TYK2) downstream of IFNAR and IFNLR phosphorylate STAT1 and STAT2[90,107]. Both proteins form a heterotrimer with IRF9, called interferon-stimulated gene factor 3 (ISGF3)[107,117]. This transcriptional complex translocates to the nucleus and binds to interferon-stimulated response elements (ISRE) in the promoters of interferon-stimulated genes (ISGs), inducing the expression of a broad set of genes that are involved in counteracting the viral infection[90,118,119] (described in section 1.2.4). Similarly, type II IFN signaling results in the JAK1/2-mediated phosphorylation of

STAT1 and the formation of phospho-STAT1 homodimers termed IFN gamma activated factor (GAF)[90,107]. It translocates to the nucleus and induces the expression of ISGs with an IFN gamma activation sequence (GAS) in their promoter[90,120]. It is important to note the entanglement of JAK/STAT signaling, resulting in crosstalk between different IFN types[90,107]. For example, phosphorylation of STAT1 by IFNAR-associated kinases can also lead to the formation of GAF and subsequent expression of type II stimulated ISGs[90]. Furthermore, different combinations of phosphorylated STAT1-6 proteins , as homo- or heterodimers, all show affinity to the GAS element, and ISG promoter regions may contain different combinations of GAS and ISRE elements[116].

Signaling through RLRs and INF receptors is able to potentiate the signal intensity and translate the detection of PAMPs in a single cell to the expression of large gene sets in whole tissue areas[90]. An important aspect of the signal amplification is the fact that some molecules involved in the signaling pathways are themselves ISGs[121]. RIG-I and MDA5 are both upregulated by IFN sensing, and intracellular protein levels of those PRRs correlate with pathway activity[121]. JAK/STAT signaling members STAT1, STAT2, and IRF9 are upregulated in response to IFN-β signaling[90,122]. IRF7 is another member of the IRF transcription factor family and is expressed by early IFN signaling[107,123]. Upon TBK1- and TRAF6-mediated phosphorylation and polyubiquitination, IRF7 forms homodimers or heterodimers with IRF3 and translocates to the nucleus[107,124]. Here it induces the expression of a broader IFN type I and III response than IRF3 homodimers and thus aids in further increase of signaling strength[107,125–127]. For example, one report suggested that IFN-λ1 is expressed already early after RLR activation in an IRF3-dependent manner, while IFN-λ3 expression sets on later and is IRF7-dependent, thus resembling the different expression dynamics of IFN-β and IFN-α[126,128].

1.2.3 Negative Regulators of RLR and IFN Signaling

Deregulated RLR and IFN signaling can have detrimental effects on the host. This is exemplified by several autoimmune diseases collectively called interferonopathies that are characterized by a constant overproduction of IFNs[129]. To avoid positive feedback loops from accelerating the antiviral system out of control, many negative regulators tightly control PRRs and the connected signaling pathways.

RLR signaling is controlled on many levels and is reviewed in detail in [130]. One of the inhibitory concepts is modulation of PTMs. For example, RIG-I can be targeted for proteasomal degradation by RNF125-mediated K48-linked polyubiquitination[130,131]. Conversely, removal of K63-linked polyubiquitin by USP21 inhibits RIG-I[130,132]. In addition, our group recently demonstrated that RIG-I activity is inhibited in a negative feedback loop through phosphorylation by death associated protein kinase 1 (DAPK1)[133]. Other concepts include, but are not limited to, autophagy of PRRs, competition of MAVS binding and activation, inhibition of activating regulators like TRIM25, and interference through other classes of PRRs such as NLRs[130].

IFN signaling is immediately regulated by internalization of the ternary receptor complex through endocytosis and subsequent degradation or recycling of receptor subunits[121,134]. Furthermore, IFN receptor signaling leads to the expression of several ISGs that act as negative regulators. Suppressor of cytokine signaling (SOCS) proteins are expressed by and negatively regulate JAK/STAT signaling[90]. SOCS1 and -3 for instance inhibit cross-phosphorylation of JAK1 and TYK2, thereby destabilizing the IFN receptor complexes and attenuating signal transduction[90,135,136]. SOCS1, but not SOCS3, was also shown to inhibit type III IFN signaling[90,137]. The ubiquitin-specific protease 18 (USP18) interacts with the cytosolic fraction of IFNAR, thereby inhibiting type I signaling in response to weaker ligands such as IFN-α subtypes, and reducing signal intensity in response to IFN-β[90,138,139]. USP18 is stabilized by ISG15, a 15 kDa protein that resembles in its tertiary structure ubiquitin and is attached to several proteins of the antiviral immune response by specific ligases such as ubiquitin/ISG15-conjugating enzyme E2 L6 (UBE2L6)[90,140,141]. This modification is termed “ISGylation” and, in the case of USP18, has a negative effect on antiviral signaling; however, depending on the target of the modification, ISG15 also exerts beneficial effects on the antiviral response[121,141]. STAT protein function can be inhibited, for instance, through dephosphorylation by tyrosine phosphatase family members, and their transcription factor ability can be blocked by binding to protein inhibitors of activated STAT (PIAS) proteins[116].

1.2.4 Interferon-Stimulated Genes

IFN signaling in general induces the expression of a broad set of ISGs. One study estimated that up to 10 % of all genes could be regulated by IFNs, although only a small set of around 60 ISGs seems to be conserved across species[118,142]. ISG gene products can have direct antiviral properties, be involved in antiviral sensing and signaling (e.g. RIG-I, IRF7) or regulate the antiviral response (e.g. USP18, ISG15)[118]. Furthermore, ISG transcription may also yield micro RNAs (miRNA) and long non-coding RNAs (lncRNA) with various regulatory functions[118,143,144]. Of note, IFN signaling also suppresses the expression of certain genes[118,145]. Due to the sheer number of ISGs discovered to date, a collection of well-studied ISGs will be described below.

Many classical ISGs possess direct antiviral properties and collectively impair the viral life cycle at every possible step[118]. Proteins of the interferon-induced transmembrane (IFITM) family are enriched in late endosomes and lysosomes, and inhibit entry of enveloped viruses[62,118,121,146]. IFITM3 for example inhibits the fusion of viral particles with the endosomal membrane and directs the trafficking of endocytosed viral particles for lysosomal degradation[118,147,148]. Cholesterol-25-hydroxylase (CH25H) is thought to inhibit viral entry by perturbing cell membrane composition through conversion of cholesterol to 25-hydroxycholesterol[121,149]. Some viruses such as Influenza A virus (IAV) and Human immunodeficiency virus (HIV) require post-entry nuclear import, which can be inhibited by MX dynamin like GTPases (MX) 1 and 2[118,150]. Importantly, many ISGs

act on multiple steps of the viral life cycle. MX1 for example also inhibits HCV genome replication[118,151].

Viral genome translation and replication are overrepresented as targets of ISGs[118]. Protein kinase R (PKR) is a dsRNA-dependent kinase that attenuates RNA translation through phosphorylation of eukaryotic translation initiation factor 2 subunit alpha (eIF-2α)[118,152]. Interestingly, HCV translation, which is initiated via the IRES in the HCV genome, is not affected by this[5,153]. Oligoadenylate synthetases (OAS), upon binding to viral dsRNA, synthesize 2'-5'-linked oligoadenylates that activate ribonuclease latent (RNaseL), which subsequently degrades host and viral RNA molecules[118,154]. Several proteins of the interferon-induced with tetratricopeptide repeats (IFIT) family inhibit viral translation and replication through interaction with viral RNA or the translational machinery[118,155]. IFIT1 for instance recognizes and sequesters RNA molecules with a 5'-ppp group, thus also affecting HCV replication[62,156,157]. Apolipoprotein B mRNA-editing enzyme catalytic polypeptide-like (APOBEC) deaminases convert cytosine to uracil, thereby hypermutating viral genomes and thus perturbing correct translation and replication[118,158]. Flavivirus replication organelle formation is suppressed by IFI6, but formation of HCV DMVs is not affected[118,159].

Viral assembly and egress are less affected by ISG activity[118]. One mode of action is the inhibition of viral particle release from the cell membrane. For example, enveloped viruses such as HCV and HIV are immobilized to the cell surface by the transmembrane protein tetherin/BST2[62,118,160,161]. Another ISG, viperin/RSAD2, was shown to inhibit budding of several enveloped viruses[121,162]. Possessing multifunctionality typical for many ISGs, viperin can also impair genome replication of HCV and potentially DENV through interaction with proteins of the viral replication complex[121,163,164].

1.2.5 RLR-Induced NF-κB Signaling

RLR signaling in infected cells does not only induce the activation of IRF transcription factors and the expression of IFNs, but also activates the canonical nuclear factor κ light chain enhancer of activated B cells (NF-κB) signaling pathway[54] (Fig. IIIb). The NF-κB family of transcription factor proteins encompasses 5 members that can form homo- or heterodimers via their N-terminal DNA binding domains[165,166]. NF-κB1/p50 and NF-κB2/p52 are processed from larger precursor proteins p105 and p100, respectively[166,167]. They do not possess C-terminal transactivation domains and may repress transcription as homodimers[166]. RelA, RelB, and c-Rel on the other hand contain transactivation domains, and heterodimers containing one of those proteins are able to induce gene expression[165,168]. Like IRF3, NF-κB proteins are retained in the cytoplasm, as inhibitors of κB (IκB) proteins sequester the nuclear localization signal (NLS) and facilitate nuclear export[168,169].

During RLR signaling, MAVS aggregates activate receptor-interacting serine/threonine

protein kinase 1 (RIPK1), which in turn activates the heterotrimeric IκB kinase (IKK) consisting of the regulatory subunit NF-κB essential modulator (NEMO/IKKγ) and the catalytic subunits IKKα and -β[102,165] (Fig. IIIb). IKK proceeds to phosphorylate IκB proteins, inducing their ubiquitination and subsequent proteasomal degradation[165,170]. NF-κB subunits then form dimers, translocate to the nucleus and induce gene expression[165,168]. Among the targets of NF-κB are pro-inflammatory cytokines and chemokines, which will be discussed in the next section. Furthermore, NF-κB induces expression of IκB proteins, which shut down the NF-κB pathway in a negative feedback regulation[165]. NF-κB can furthermore act as part of transcriptional complexes with IRF proteins, for instance as member of the IFN-β promoter enhanceosome, thereby supporting IFN production[107,171,172].

1.3 A Call for Help: Chemokines and Pro-Inflammatory Cytokines

The previous sections have covered how cells sense the intrusion of pathogens and respond with the secretion of warning signals. IFNs are efficient in inducing and amplifying the expression of antiviral effector molecules, but they are not the only immune signaling molecules produced by cells upon sensing an infection. A subset of cytokines termed chemokines is crucial in guiding immune cells to the infected area. Furthermore, cells produce pro-inflammatory cytokines that activate the recruited immune cells, thereby boosting the immune response.

1.3.1 Chemokines

Chemokines are a subset of cytokines with chemoattractant properties. They navigate immune cells to enter or leave certain tissues and organs during development, immune surveillance, and in response to tissue damage and infection[173,174]. Based on the configuration of two cysteine residues near the N-terminus, chemokines are categorized into four subfamilies[174]. In CC chemokines, the residues are adjacent, while they are separated by one or three amino acids in CXC and CX_3C chemokines, respectively. Finally, XC family chemokines lack one of the cysteine residues.

Upon secretion, chemokines are quickly immobilized on cell surfaces and in the extracellular matrix (ECM), for example through binding to glycosaminoglycans (GAG)[174,175]. This generates a concentration gradient from infected tissue to surrounding blood vessels, where chemokines are bound to and presented on endothelial cell surfaces[174,176,177]. Immune cells travelling through the blood stream now can detect the chemokines and extravasate into the affected tissue region[174,178]. Binding to chemokines occurs via two heptahelical receptor classes[174,179,180]. Conventional chemokine receptors (cCKRs) are G-protein coupled receptors that activate various

downstream signaling pathways, including JAK/STAT signaling, that modulate the cellular response[174, 181]. Atypical chemokine receptors (aCKRs), on the other hand, do not signal upon chemokine binding. They rather act as binding antagonists to cCKRs and indirectly control chemokine-cCKR binding by affecting localization and abundance of chemokines[174, 182].

The signaling network of chemokines and chemokine receptors is highly complex. Interactions involved in essential processes of development and homeostasis show clear dependencies of ligands and receptors, and low redundancy between ligands[174]. For example, the interaction of CXC ligand 12 (CXCL12) and receptors CXC receptor 4 (CXCR4) and ACKR3 are essential in the development of several organs and in the guidance of maturing T cells into the thymus[174, 183]. The chemokine-receptor-network in response to homeostasis disturbances, e.g. infection, on the other hand shows increased promiscuity between chemokines and receptors, which has been suggested to protect functional chemokine signaling from pathogen interference through redundancy as well as to enable signaling fine-tuning[174, 184]. For instance, CCL5, one of the chemokines secreted by hepatocytes in response to HCV infection[177, 185], can form signaling-competent heterodimers or oligomers with 20 different chemokines[174, 186].

The types of chemokines present, their tissue half-life and concentration, and the composition of receptors present on immune cells are among the factors tightly regulating which immune cell types respond to what kind of insult at what step of the immune response[174, 184]. Moreover, the expression profile of chemokine receptors changes and diversifies when immune cells are activated[174]. Although the functions of chemokines have been mostly studied in the context of immune cell attraction, most cell types express chemokine receptors and can respond to their binding (reviewed in [174]). For example, airway epithelial cells exhibited increased wound healing capacities and produced profibrogenic growth factors and several chemokines upon CC receptor 3 (CCR3)-mediated stimulation with eotaxin chemokines (CCL11, -24, and -26)[174, 187].

1.3.2 Pro-Inflammatory Cytokines

Pro-inflammatory cytokines are potent immune signaling molecules that are involved in the recruitment and activation of innate and adaptive immune cells, and are key factors in the cross-talk between cells of the immune system[188]. Most pro-inflammatory cytokines are produced exclusively by immune cells; however, other cell types including epithelial cells are able to express subsets of pro-inflammatory cytokines[188], of which a selection will be described below.

NF-κB activation leads to the production of pro-inflammatory cytokines such as tumor necrosis factor (TNF) and interleukin 6 (IL-6)[189, 190]. TNF signaling via TNF receptors (TNFRs) takes part in mediating a cells fate during inflammation. Depending on target cell type and other signals that are integrated with TNF signaling, TNF can either protect

cell survival or push a cell towards cell death (reviewed in [191]). Survival signals are transduced through several mitogen-activated protein kinase (MAPK) pathways as well as through activation of NF-κB[191]. The ubiquitination status of RIPK1 is a central parameter in the regulation of TNF signaling via TNF receptor 1 (TNFR1), as ubiquitinated RIPK1 allows activation of canonical NF-κB signaling and subsequent production of cell death inhibitors[192]. Pro-apoptotic signaling of TNF will be described in section 1.4.

IL-6 possesses both anti- and pro-inflammatory properties (reviewed in [193] and [194]). The classical signaling pathway involves the detection of IL-6 by a receptor complex consisting of IL-6 receptor (IL6R) and glycoprotein 130 (gp130)[194]. The signal is then transduced via JAK-mediated phosphorylation of STAT3 and activates an anti-inflammatory response. Interestingly, IL6R is also produced as a soluble version (sIL6R), and an IL-6:sIL6R complex may activate any cell that is expressing gp130 on their cell surface[194–196]. In contrast to the classical signaling pathway, this so-called trans-signaling also leads to STAT3 phosphorylation, and downstream signaling activates pro-inflammatory pathways that favor chronic inflammation and processes such as proliferation, angiogenesis, and in the context of cancer, metastasis[193,194]. One of the transcriptional targets of phospho-STAT3 dimers is SOCS3, which negatively regulates the pathway by inhibiting JAKs[197]. Of note, STAT3 can also influence IFN signaling, for example by sequestering phospho-STAT1[90,198]. IL-6 stimulates B and T cells and is involved in the activation of cluster of differentiation 4 positive ($CD4^+$) T cells and their differentiation into T-helper cell subtypes[188]. Furthermore, IL-6 regulates the temporal recruitment of different types of leukocytes during infection by modifying chemokine expression patterns[188]. Because of these properties, IL-6 plays a central role in the transition from acute to chronic inflammation[193].

Epithelial cells can also produce interleukins of the IL-1 family (reviewed in [199]). Many members of this cytokine family are produced constitutively, but are retained in the cell as inactive pro-peptides. For instance, IL-1β and IL-18 are processed via proteolytic cleavage and subsequently released as signaling-competent molecules during inflammatory forms of programmed cell death[200] (described in section 1.4.2). Conversely, IL-1α and IL-33 are cleaved and thereby inactivated during programmed cell death, but are released as signaling-competent full-length proteins during uncontrolled cell death, thus functioning as alarm signals[199].

As the immune crosstalk during infection is quite complex, relevant cytokines and chemokines will be described later in the context of acute and chronic HCV infection (Section 1.5).

1.4 Ultima Ratio: Programmed Cell Death

The last resort in combating infection is the removal of infected cells. This is achieved through programmed cell death, where intrinsic or extrinsic signals set in motion mostly

irreversible processes that result in the controlled decay of a cell[201].

1.4.1 Apoptosis

The most studied form of programmed cell death is termed apoptosis and is the standard mode of cell removal in tissue development and homeostasis as well as in response to infection, cell damage, and malignant degeneration (reviewed in [201]). In a controlled fashion, the cell is fragmented into small, vesicle-like organelles that retain plasma membrane integrity and present surface markers that induce phagocytosis by macrophages and surrounding cells, thus preventing the release of cellular components with potential toxic effects into the surrounding tissue[201,202]. Importantly, apoptosis is an energy-dependent process, and upon energy shortage (e.g. insufficient ATP levels), cells switch into the passive and energy-independent process of necrosis. Here, cells they disintegrate in an uncontrolled fashion, and plasma membrane disruption leads to the release of intracellular contents into the tissue[201]. Necrosis therefore commonly affects whole tissue areas and is the result of insufficient energy supply or excessive tissue damage, especially if this damage regards cell membrane integrity[201].

Apoptosis may be activated by intrinsic signals in response to stress or damage (e.g. during hypoxia or after radiation), viral infection, or in response to the absence of survival signals such as growth factors[201]. Various intrinsic signals are integrated at the mitochondria. Here, the composition of members of the B cell lymphoma 2 (BCL2) protein family controls further signal transduction[203,204]. Pro-apoptotic Bcl2 proteins like BCL2 associated X (BAX) and BCL2 antagonist/killer (BAK) are involved in opening a pore in the inner mitochondrial membrane, which leads to the collapse of the mitochondrial transmembrane potential[201,204]. Subsequently, proteins such as cytochrome C and second mitochondria-derived activator of caspase (SMAC/DIABLO) are released from the intermembrane space into the cytoplasm[201]. Cytochrome C forms a multiprotein complex with apoptotic peptidase activating factor 1 (APAF1) and procaspase 9 termed “apoptosome”[201,205,206]. Within this complex, procaspase 9 units cleave and activate each other, and proceed to activate downstream caspases[201]. Caspases are cellular proteases that are constitutively expressed as catalytically inactive procaspases and are activated through proteolytic cleavage[207]. The catalytic signal is amplified through a series of caspase activation steps, termed caspase cascade[201,207]. Ultimately, so-called executioner caspases activate several key enzymes that – together with the caspases themselves – perform processes that entail the irreversible morphological changes taking place during apoptosis, such as degradation of the cytoskeleton and nuclear DNA[201,207]. Executioner caspases also inactivate pro-inflammatory cytokines such as IL-33 that are typically released during necrotic cell death[200]. Anti-apoptotic members of the Bcl2 family, such as its namesake BCL2, are involved in counteracting pro-apoptitic Bcl2 proteins[201,208]. Furthermore, inhibitor of apoptosis proteins (IAPs) such as x-linked inhibitor of apoptosis (XIAP) play a central role in controlling intrinsic and extrinsic pathway signal transduc-

tion (reviewed in [209]). IAPs in turn are inhibited by SMAC/DIABLO and other factors released from mitochondria during apoptosis inhibition[209].

Apoptosis can also be induced externally through binding of death ligands (DL) to their specific death receptors (DR) of the TNF receptor superfamily[201]. Those include, among others, TNF and its receptor TNFR1, Fas ligand (FASL) and Fas receptor (FASR), and TNF-related apoptosis-inducing ligand (TRAIL) and DR4 and -5[201,210]. Ligands are bound as trimers by clustered DRs, which then recruit adaptor proteins, such as TRADD and Fas-associated via death domain (FADD), via cytoplasmatic death domains (DD)[201,211–213]. With its death effector domain (DED), FADD dimerizes with procaspase 8 and forms the death inducing signaling complex (DISC)[201,214]. Analogous to the "apoptosome", the DISC promotes autocatalytic activation of caspase 8 and subsequent induction of the caspase cascade.[201,214]. Another extrinsic pathway of apoptosis induction is mediated by CD8-expressing cytotoxic T lymphocytes ($CD8^+$)[215]. They survey cell surfaces for major histocompatibility complex (MHC) molecules that present antigen epitopes, e.g. from viral proteins or mutated proteins produced in the presenting cell[201]. Essentially, this presentation serves as a danger signal, and $CD8^+$ cells react by sending pro-apoptotic signals through two modes of action[201,215]: First, they can activate extrinsic DR-mediated signaling via FASL. Second, they can secrete perforin, which forms transmembrane pores in the cell membrane of the target cells. Subsequently, $CD8^+$ cells shuttle granules containing proteases granzyme A and B through these pores[201,216,217]. While granzyme B activates the caspase cascade, granzyme A induces apoptosis via an alternative pathway that involves the induction of DNA damage through single strand breaks[201,218]. In a similar fashion, NK cells survey cell surfaces for the presence of "self" signals and induce cell death, if those signals are missing (e.g. on cancerous cells)[219].

1.4.2 Necroptosis and Pyroptosis

Apoptosis can be described as a "silent" form of programmed cell death, as the cell is broken down without the release of intracellular components[200]. There are, however, alternative cell death programs that involve the release of danger-associated molecular patterns (DAMPs) from inside the cell. These signals can induce an inflammatory response, and the alternative cell death modes necroptosis and pyroptosis are therefore classified as inflammatory cell death pathways (reviewed in [200] and [220]).

Necroptosis may for example be induced via DR signaling, which activates RIPK1 to form the "necrosome" complex with RIPK3, which in turn phosphorylates mixed lineage kinase domain like pseudokinase (MLKL)[200,221,222]. Activated MLKL forms pores in the cell membrane and allows for release of DAMPs such as IL-1 family cytokines (IL-1α, IL-33), mitochondrial DNA, or ATP[200,223,224]. Under normal conditions, apoptosis is favored over necroptosis. This is controlled through ubiquitination and proteolytic cleavage of RIPK1 and RIPK3 by IAPs and caspase 8, respectively[200,225]. In the case of infection, however, apoptotic pathways might be inhibited by the pathogen and necroptosis may

serve as a backup cell death pathway[200, 226, 227].

The main biological function of pyroptosis is thought to be the release of inflammasome-activated cytokines and DAMPs in response to the detection of events that could potentially damage cell integrity and may necessitate an immune response[200]. Ligand sensing by a variety of intracellular PRRs, including AIM2 and several NLRs, is integrated at "inflammasome"-termed multiprotein complexes[228]. Analogous to necroptosis, autocatalytically activated caspase 1 proceeds to cleave proteins of the gasdermin family, such as gasdermin D[228]. Activated gasdermins form oligomeric death-inducing pores in the cell membrane that allow the release of IL-1β and IL-18 previously activated by caspase 1-mediated proteolytic cleavage[200].

1.4.3 Cell Death Induction via RLR Signaling

MAVS plays a key role in the induction of apoptosis upon RLR signaling, and several modes of action have been reported. For one, MAVS aggregates can act as a FADD-independent DISC, recruit and activate procaspase 8, and thus start the caspase cascade indepentently of BAX/BAK-mediated cytochrome C release[229]. The second mode of action involves the disruption of mitochondrial outer membranes, resulting in the release of pro-apoptotic factors like cytochrome C[230]. Finally, RLR signaling can lead to the ubiquitination of IRF3, which subsequently together with BAX induces cytochrome C release from mitochondria in a process termed RIG-I-like receptor-induced IRF3-mediated pathway of apoptosis (RIPA)[231]. Of note, other RNA sensors such as TLR3, some members of the NLR and DEAH-box protein families, and Z-DNA-binding protein 1 (ZBP1), which can bind dsRNA in the Z-conformation, were shown to be involved in the activation of cell death programs (reviewed in [54] and [61]).

1.5 Hepatitis C – from Acute to Chronic Infection

1.5.1 Acute Hepatitis C

The course of an HCV infection is influenced by the features of the liver. Blood flow through the liver is directed through liver sinusoids, where exchange of nutrients and metabolites between blood and parenchymal cells (hepatocytes) is facilitated[232] (Fig. IVa). Next to its many metabolic functions, the liver also exhibits a unique immunological function and state. The organ is enriched in cells of both, the innate and the adaptive immune system, and filters the blood for microbe-associated molecular patterns, DAMPs, and blood-borne pathogens[232]. Constant activation of the immune response and chronic inflammation due to the permanent exposure to harmless molecules is avoided through the establishment of an immunosuppressive state. Here, anti-inflammatory cytokines such as IL-10 and transforming growth factor β (TGF-β) bal-

ance out pro-inflammatory cytokines, leading to immune tolerance[232,233]. Nevertheless, the liver is able to respond to an actual hazard (e.g. an infection with HCV), where additional pro-inflammatory signals override the tolerance state and start an immune response[232,233].

The acute phase of an HCV infection describes a period of several weeks after initial infection (reviewed in [5], [52] and [234]). Within days, patients exhibit high viral titers, accompanied by an IFN response in the infected liver[5,234] (Fig. IVb). Both type I and type III IFNs have been reported to be elevated; however, the impact of individual IFNs on the immune response is still subject to research[5]. The liver is enriched with NK cells that respond to IFN signals from infected hepatocytes and act in an antiviral manner by expressing type II IFN and inducing apoptosis of infected cells via death receptor signaling and perforin[5,234].

As mentioned before, expression of chemokines and pro-inflammatory cytokines mediates the recruitment of cells of the adaptive immune system. Pro-inflammatory cytokines typical for HCV infection are, among others, TNF, IL-6, IL-1β, IL-18, and IL-33[199,236]. Hepatocytes infected with HCV also secrete chemokines, including (but not limited to) CCR5 ligands CCL3, -4, and -5, and CXCR3 ligands CXCL9, -10, and -11[177,185,236]. In addition to hepatocytes, the liver is composed of a variety of different cell types[235] (Fig. IVa), such as liver sinusoidal endothelial cells (LSEC), liver-resident macrophages called Kupffer cells, hepatic stellate cells (HSC), and NK cells, which all add to the mix of cytokines and chemokines produced during infection[5,185,234,236]. In general, many

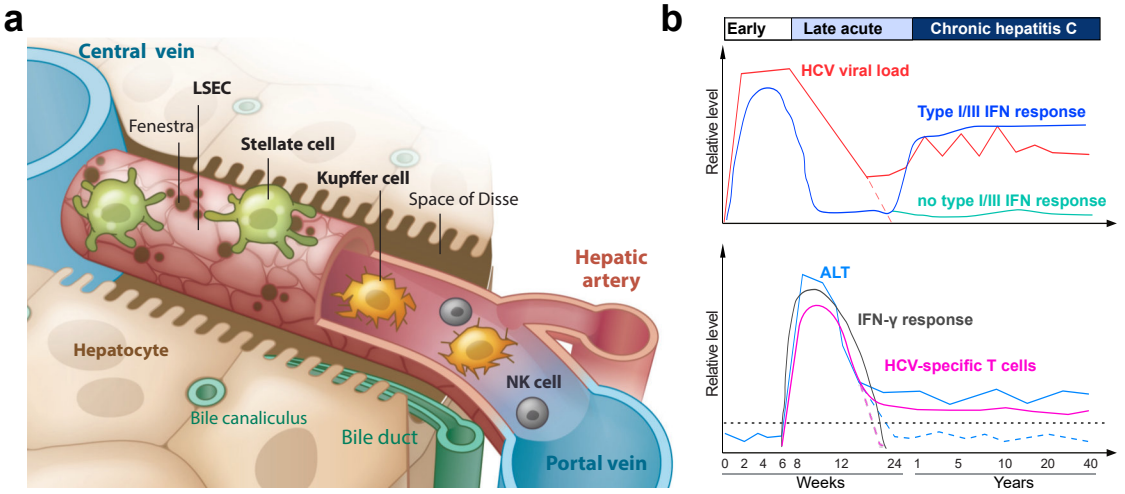

Figure IV: Schematics of liver sinusoid organization and HCV infection time course.
(**b**) Schematic organization of the liver sinusoid. LSEC: liver sinusoidal endothelial cell; NK: natural killer cell. (**a**) Time course of Hepatitis C virus (HCV) infection from acute phase to chronic phase, displaying relative levels of selected disease parameters. Patients either clear the infection (dashed lines) or develop a chronic infection (continued solid lines). About half of the patients in the chronic infection phase exhibit elevated ISG expression related to type I and III IFNs (top, dark blue line), while the other half does not (top, light blue line). Likewise, patients who clear the infection display no elevated liver damage marker levels (bottom; alanine transaminase, ALT), while levels of ALT and infiltrating T cells remain elevated in the chronic infection (dotted grey line indicates upper limit of normal ALT levels). Due to the inability of lymphocytes to efficiently produce type II IFN in the chronic phase, IFN-γ-related ISG expression is diminished (bottom). Figure adapted and modified from [235] and [5].

of these immunostimulatory factors correlate with viral load as well as with the progression and severity of chronic inflammation and liver damage[185,199,236]. The adaptive immune response includes the activation and proliferation of antigen-specific T- and B-lymphocytes[237]. The CD8-bearing cytotoxic T cells act, similar to NK cells, in a cytolytic fashion against infected cells, while B cells proliferate into plasma cells and produce antigen-specific antibodies[237]. The immune response is amplified, regulated, and ultimately terminated by CD4-expressing T-helper cells (T_h) and regulatory T cells (T_{reg})[238]. T_{h1} cells, a T_h subset with an important role in the immune response to viral infections, express both CCR5 and CXCR3 and are therefore typical targets of the hepatocyte-derived chemokines[238]. Due to the activation and differentiation processes these immune cells have to undergo, the adaptive immune response requires a few days to become effective[239]. Strikingly, though, this development is delayed several weeks in the context of an HCV infection[5,52,240]. Onset and sustainment of the adaptive response as well as antigen specificity seem to be fate-deciding factors for disease progression and outcome[5]. Patients usually exhibit an antibody response against various HCV epitopes during the acute phase, but most antibodies have no effect on the infection status[5]. An early onset in the production of neutralizing antibodies was shown to correlate with clearance of the infection[5,241]. Research suggests that the T cell response is of greater importance in eliminating the infection: Patients with an early, strong, and sustained response, which includes both $CD4^+$ and $CD8^+$ T cells and targets multiple viral epitopes, are generally more likely to eliminate the virus[5]. Conversely, patients with a delayed, low-level T cell response or patients that exhibit T cell depletion are more prone to develop a chronic form of hepatitis C[5].

1.5.2 Chronic Hepatitis C

Patients in the acute phase are often unaware of their infection due to the frequently asymptomatic disease progression, or due to presence of symptoms not readily connected to liver disease[5,242]. In about 70-80 % of patients, HCV establishes a persistent infection that is characterized by continued viral replication[5,52]. The host response, however, seems to vary greatly between patients. Conflicting results regarding IFN levels, types of IFNs, presence of ISG expression, and incoherencies between detected IFNs and ISG expression patterns paint an overall inconclusive picture[5]. In a study with CHC patients of Caucasian ethnicity, about half of the patients showed high type I and III ISG expression levels, whereas no ISG induction was detectable in the other half[5,243]. Furthermore, the detected ISG expression did not correlate with viral load. Importantly, though, studies indicate that the continuous expression of ISGs is not able to clear the viral infection[5,52,234].

NK cells and HCV-specific $CD8^+$ T cells are thought to exert their antiviral effects primarily through non-cytolytic ways, importantly via secretion of IFN-γ[5,234]. In CHC patients, both cell types are enriched in the liver, but are unable to effectively combat the infection[5,234].

Prolonged type I IFN signaling stimulates NK cells to change from an IFN-γ-producing phenotype to a cytotoxic TRAIL-producing phenotype that is thought to promote liver damage[234]. T cell function is also impaired, in part due to the expression of several receptors with inhibitory potency that prevent efficient proliferation and cytokine production[234]. T cell control is reported to be deregulated in CHC patients: Support by T_h cells is weak or dysfunctional, while the number of suppressive regulatory T cells, which repress $CD8^+$ T cell function via IL-10, is increased[5]. Consequently, T cell response to HCV resembles a state of exhausted immune cells, and the expression of IFN-γ-specific ISGs is underrepresented[5,233] (Fig. IVb). T cell exhaustion moreover seems to prevent the establishment of a potent T cell memory, thus allowing re-infection after viral clearance through antiviral therapy[233]. Escape mutations in HCV structural proteins and HCVs property to hide surface antigens under lipoproteins may add to the delayed and weak adaptive immune response[5,52].

Despite the inability of the immune system to clear the infection, the liver remains in an inflamed state. The continued presence of pro-inflammatory signals and chemokines activates non-parenchymal liver cells, especially Kupffer cells, and attracts neutrophils[177]. These cells proceed to secrete, among other factors, pro-apoptotic TNF and necrosis-inducing reactive oxygen species (ROS), inducing inflammatory forms of cell death in hepatocytes[177]. This further accelerates the inflammation of the liver through the release of pro-inflammatory signal molecules, a process termed “necroinflammation”[244]. The liver possesses regenerative capacities, as differentiated hepatocytes can regain the ability to proliferate; however, repetitive compensatory proliferation can lead to the accumulation of pre-oncogenic alterations in hepatocytes[232]. The damaged parenchymal tissue is also replaced by connective tissue. Here, HSCs differentiate into myofibroblasts and, together with other cell types, produce components of the ECM, such as collagen, thus forming scar tissue[177,245]. This process of wound healing is termed fibrosis, constitutes a balance between fibrogenesis and fibrolysis, and is usually reversible; however, prolonged and excessive fibrosis has adverse effects, such as permanent scar formation, and subsequently leads to the development of liver cirrhosis[177,245]. Necroinflammation, compensatory hepatocyte regeneration and cirrhosis may ultimately lead to patients experiencing liver failure or developing hepatocellular carcinoma (HCC)[177,232,245].

1.6 Aim of the Work

The advent of direct acting antivirals (DAA) against HCV has revolutionized therapy in recent years, with ~95 % of patients being able to eliminate the virus[246]. Nevertheless, due to the lack of a vaccine against HCV, often undetected infections, and the poor state of medical care in many parts of the developing world, hepatitis C remains a substantial worldwide health concern[7]. Moreover, many infected suffer from the damages caused by CHC-related liver inflammation[6].

To be able to tailor effective treatments and design specific-acting drugs against these challenges, it is important to understand the consequences of aberrant immune responses on healthy cells. In this work, we aimed to simulate a persistent infection *in vitro* to study how cells react to a constantly activated antiviral response, and to study how cells are affected by the immunostimulatory factors secreted from infected cells.

2 Materials

2.1 Consumables

Table 1: Consumables.

Product	Supplier
1.5 ml reaction tube	Sarstedt AG & Co.
10 cm bacteria culture plate Falcon	Corning GmbH
12 well cell culture plate	Corning GmbH
15 ml Falcon	Corning GmbH
2 ml reaction tube	Sarstedt AG & Co.
24 well cell culture plate	Corning GmbH
50 ml Falcon	Corning GmbH
6 well cell culture plate	Greiner Bio-One GmbH
96 well cell culture plate	Corning GmbH
96 well flat bottom plate	Corning GmbH
Blotting paper	Bio-Rad Laboratories GmbH
Cell scraper	Sarstedt AG & Co.
CELLSTAR Cell Culture Dishes 10 cm	Greiner Bio-One GmbH
CELLSTAR Cell Culture Dishes 15 cm	Greiner Bio-One GmbH
CELLSTAR Cell Culture Dishes 6 cm	Greiner Bio-One GmbH
Cover slips	Glaswarenfabrik Karl Hecht GmbH
Cryo vials	Greiner Bio-One GmbH
Filter 0.2 µm	GE Healthcare
Filter 0.45 µm	GE Healthcare
Glas slides SuperfrostTM	Thermo Fisher Scientific
Hard-Shell 96-Well PCR Plates	Bio-Rad Laboratories GmbH
Neubauer counting chamber	Neolab
PVDF Western blot membrane	Bio-Rad Laboratories GmbH
Round-bottom tube with cell-strainer cap	Corning GmbH
Scalpel	B. Braun Melsungen AG
Sealing sheets PCR plates	Bio-Rad Laboratories GmbH
Stericup 0.2 µm	Thermo Fisher Scientific
Stericup 0.45 µm	Merck Millipore
Stripetten 2, 5, 10, 25 and 50 ml	Corning GmbH
Syringe 5, 10, 20 ml	Becton Dickinson
Tips 10, 100 and 1000 µl, filtered	STARLAB GmbH
Tips 10, 200 and 1000 µl, refill pack	Greiner Bio-One GmbH
Tips 10, 200 and 1000 µl, Stecksystem	STARLAB GmbH
Transwell 12-well insert (0.4 µm, high density)	Corning GmbH
Whatman filter paper	GE Healthcare Life Sciences, UK
XCEED Nitrile Gloves	Barrier Safe Solutions International, Inc.

2.2 Chemicals, Reagents, and Kits

Table 2: Chemicals, Reagents, and Kits.
Table continues on the next page.

Product	Supplier	Identifier
Acrylamide:Bisacrylamide (BAA; 29:1)	Roth	A515.1
Adenosine 5'-triphosphate (ATP)	Sigma Aldrich	A2383
Agarose	Roth	3810.3
Alkaline Phosphatase, Calf Intestinal (CIP)	NEB	M0290
Ammonium persulfate (APS)	Roth	9592.1
Benzonase	Merck Millipore	70746-4
Blasticidin S hydrochloride	MP Biomedicals	15047750
CalPhos Mammalian Transfection Kit	Takara Bio Europe	631312
Carbenicillin disodium salt	Sigma Aldrich	C1389
Clarity Western ECL Substrate	Bio-Rad Laboratories GmbH	170-5061
Cytofix/Cytoperm	Becton Dickinson	554722
Cytotox Green Dye	Sartorius	4633
DAPI (4',6-diamidino-2-phenylindole)	Sigma Aldrich	10236276001
D-Luciferin	PJK GmbH	N/A
DMEM, high glucose	Thermo Fisher Scientific	41965062
Dimethyl sulfoxide (DMSO)	VWR	23.500.297
deoxyribose nucleoside triphosphates (dNTPs)	VWR	733-1270
double-strand RNA (dsRNA; 200 bp)	produced in-house by Sandy Burkart	N/A
Ethylenediaminetetraacetic acid (EDTA)	AppliChem GmbH	A3553
Fetal calf serum (FCS)	Thermo Fisher Scientific	10270106
Fluoromount-G	Southern Biotech	0100-01
Gateway BP Clonase II Enzyme mix	Thermo Fisher Scientific	11789-100
Gateway LR Clonase II Enzyme mix	Thermo Fisher Scientific	1946833
Gel electrophoresis DNA loading dye	Thermo Fisher Scientific	R0611
Gel electrophoresis RNA loading dye	Thermo Fisher Scientific	R0641
Gene Ruler 1 kb	Thermo Fisher Scientific	SM0311
Geneticin (G418) Sulfate	Santa Cruz Biotechnology	SC-29065B
Gentamicin (50 mg/mL)	Thermo Fisher Scientific	15750037
Glycerol	Sigma Aldrich	15523-1L-M
Glycyl Glycin	Sigma Aldrich	G3915-500G
High-Capacity cDNA Reverse Transcription Kit	Thermo Fisher Scientific	43-688-14
IFN-α	BIOZOL GmbH	11100-1
IFN-β	R & D Systems	8499-IF-010/CF
IFN-λ1	PeproTech	300-02L
iTaq Universal SYBR Green Supermix	Bio-Rad Laboratories GmbH	17251525
Kanamycin sulphate	Thermo Fisher Scientific	15470594
L-Glutathion	Sigma Aldrich	G-4251-25G
Lipofectamine 2000 Transfection Reagent	Thermo Fisher Scientific	11668030
LumiKine Xpress hIFN-beta 2.0 ELISA	InvivoGen	luex-hifnbv2
MEM Non-Essential Amino Acids Solution (NEAA; 100X)	Thermo Fisher Scientific	11140050

Product	Supplier	Identifier
Midori Green Advance	Biozym	617004
Monarch DNA Gel Extraction Kit	NEB	T1020
Monarch Plasmid Miniprep Kit	NEB	T1010
Monarch Total RNA Miniprep Kit	NEB	T2010
Necrostatin 7 (Nec-7) Necroptose inhibitor	Sigma Aldrich	N3040
NucleoBond PC 500	Macherey-Nagel	740574.50
NucleoSpin RNA Plus	Macherey-Nagel	740984250
OptiMEM	Thermo Fisher Scientific	31985047
Pan Caspase Inhibitor Z-VAD-FMK	R & D Systems	FMK001
PBS (10X Dulbecco's) powder	AppliChem GmbH	A0965,9050
PEI (Polyethylemine) 25kDa linear	Polysciences, Inc.	23966-2
Penicillin-Streptomycin (10.000 U/mL)	Thermo Fisher Scientific	15140122
Peptone from casein, tryptic digest	Thermo Fisher Scientific	70172
Perm/Wash	Becton Dickinson	554723
Poly(I:C)	Sigma Aldrich	P9582
poly(C)	Sigma Aldrich	P4903
Polybrene Transfection Reagent	Merck Millipore	TR-1003-G
Polyethylenglycol 8000 (PEG)	Roth	0263.2
Protease-free milk powder	Roth	T145.1
Puromycin dihydrochloride	Sigma Aldrich	P7255
Q5 High-Fidelity PCR Kit	NEB	E0555
qScript XLT One-Step RT-qPCR ToughMix	VWR	733-2230
Restriction Enzymes and Buffers	NEB	N/A
ssRNA ladder	NEB	N0362S
T4 DNA Ligase	NEB	M0202S
T4 DNA Ligase Reaction Buffer	NEB	B0202S
T4 Polynucleotide Kinase	NEB	M0201S
Tetramethylenediamine (TEMED)	Roth	8142.1
Triton X-100	AppliChem GmbH	A497
TriTrack 6x DNA Loading Dye	Thermo Fisher Scientific	R1161
Trypsin-EDTA (0.05 %), phenol red-20	Thermo Fisher Scientific	25300-096
U-PLEX Interferon Combo Human Kit	Meso Scale Diagnostics	K15094K
V-PLEX Chemokine Panel 1 Human Kit	Meso Scale Diagnostics	K15047D
V-PLEX Proinflammatory Panel 1 Human Kit	Meso Scale Diagnostics	K15049D
Western Lightning Plus ECL	PerkinElmer	NEL104001EA
Yeast Extract BioChemica	AppliChem GmbH	A1552

2.3 Media, Buffers, and Solutions

If not listed in Table 2, chemicals mentioned here were purchased from Sigma Aldrich (Munich, Germany) or Roth (Karlsruhe, Germany). Percentages given refer to % (v/v) for liquids and % (w/v) for solids.

Table 3: Media, Buffers, and Solutions.
If not noted otherwise, solutions were prepared in ddH_2O.

Solution	Composition
DMEM complete	DMEM with 10 % fetal calf serum, 1x MEM NEAA, 1x Penicillin-Streptomycin
FACS buffer	PBS with 1 % FCS
KPO4 buffer	90.8 mM K_2HPO_4, 9.2 mM KH_2PO_4
LB Agar	LB medium with 0.5 % Agar
Luciferase Assay Buffer	25 mM Glycyl Glycin, 15 mM KPO_4 buffer, 15 mM $MgSO_4$, 4 mM EGTA, 2 mM ATP, 1 mM DTT, 80 µM D-Luciferin
Luciferase Lysis Buffer	10 % Glycerol, 1 % Triton X-100, 25 mM Glycyl Glycin, 15 mM $MgSO_4$, 4 mM EGTA, 1 mM DTT
Lysogeny broth (LB) medium	1 % Bacto-Trypton, 0.5 % Yeast extract, 0.5 % NaCl
PBS-Tween (PBS-T)	PBS with 0.1 % Tween-20
Phosphate-buffered saline (PBS)	0.01 % PBS powder
Protein sample buffer	5 % glycerol, 16.25 mM TRIS (pH 6.8), 0.5 % SDS, 1.25 % β-mercaptoethanol, bromophenol blue
Reverse Transcription Mix	20 % RT Buffer (10x), 20 % RT Random Primers (10x), 8 % dNTP Mix (25x), 10 % RNase Inhibitor, 10 % MultiScribe Reverse Transcriptase
SDS-PAGE resolving gel	25 % resolving gel buffer, 8-12 % BAA, 0.1 % TEMED, 0.1 % saturated ammonium persulfate solution
SDS-PAGE resolving gel buffer	1.5 M Tris Base, 0.4 % SDS pH 8.8
SDS-PAGE stacking gel	13 % stacking gel buffer, 10 % BAA, 0.1 % TEMED, 0.15 % saturated ammonium persulfate solution
SDS-PAGE stacking gel buffer	1 M Tris Base, 0.8 % SDS, pH 6.8
Semi-dry blotting buffer	2.5 mM Tris Base (pH 8.3), 15 mM Glycine, 10 % Methanol
T4 dimerization mix	10 % T4 10x ligation buffer, 10 % T4 PNK, 10 µM forward oligo, 10 µM reverse oligo
T4 DNA ligation mix (10 µl)	1 µl ligation buffer (10 x), 1 µl T4 DNA ligase, 1 µl DNA oligo dimers (pre-diluted 1:200), 100 ng linearized vector backbone
TE buffer	10 mM Tris, 1 mM EDTA, pH 8.0
Tris-acetate-EDTA (TAE) buffer	40 mM Tris, 20 mM acetic acid, 1 mM EDTA
Tris-glycine-sulfate (TGS) buffer	192 mM Glycine, 25 mM Tris Base, 0.1 % SDS, pH 8.3
Western Blot blocking buffer	PBS with 0.5 % Tween-20, 5 % protease free milk powder

2.4 Bacteria and Viruses

For all cloning experiments and re-transformations, the following bacteria strain was used: *E. coli* DH5α: F'/endA1 hsdR17A (rk-mk+) supE44 thi-1 recA1 gyrA (Nalr) relA1Δ(lacZYA-argF)U169 deoR (ϕ80dlacΔ(lacZ)M15).

Sendai virus (SeV) was provided by Prof. Dr. Rainer Zawatzky (DKFZ, Heidelberg).

2.5 Cell Lines

Table 4: Cell Lines.

Cell line	Source
A549	Heidelberg University Hospital
A549 IFNAR1$^{-/-}$ IFNLR1$^{-/-}$	Sandra Wüst, Binder Lab, DKFZ, Heidelberg
A549 IFNAR1$^{-/-}$ IFNLR1$^{-/-}$ IFNGR1$^{-/-}$	Sandy Burkart, Binder Lab, DKFZ, Heidelberg
A549 IFNLR1$^{-/-}$	Sandra Wüst, Binder Lab, DKFZ, Heidelberg
A549 IRF3$^{-/-}$	[247]
A549 MAVS$^{-/-}$	[248]
A549 RIG-I$^{-/-}$	[133]
HEK293T	DKFZ, Heidelberg
PH5CH	Volker Lohmann, Heidelberg University Hospital
A549 IFNB1$^{-/-}$	This study
A549 IFNLR1$^{-/-}$ IFNB1$^{-/-}$	This study

2.6 DNA Oligonucleotides

Table 5: DNA Oligonucleotides.
Orientation of oligos relative to coding strand (5' to 3': forward (fwd); 3' to 5': reverse (rev)). Table continues on the next page.

Oligo	Purpose	Sequence
attB1-NS5B-fwd	PCR primer for cloning	GGGGACAAGTTTGTACAAAAAAGC-AGGCTTCATGTCATACTCCTGGAC-CGG
attB2-GFP-rev	PCR primer for cloning	GGGGACCACTTTGTACAAGAAAGC-TGGGTTTTACTTGTACAGCTCGTCC
cppt-fwd	sequencing	TAATAGCAACAGACATAC
IFNB1-gRNA-2-fwd	CRISPR/Cas9 guide RNA	CACCGATGAACTTTGACATCCCTG
IFNB1-gRNA-2-rev	CRISPR/Cas9 guide RNA	AAACCAGGGATGTCAAAGTTCATC
IFNB1-gRNA-3-fwd	CRISPR/Cas9 guide RNA	CACCGCTGCAGCAGTTCCAGAAGG
IFNB1-gRNA-3-rev	CRISPR/Cas9 guide RNA	AAACCCTTCTGGAACTGCTGCAGC
GAPDH-fwd	qPCR primer	TCGGAGTCAACGGATTTGGT
GAPDH-rev	qPCR primer	TTCCCGTTCTCAGCCTTGAC

Oligo	Purpose	Sequence
hU6-promoter	sequencing	ACGATACAAGGCTGTTAGAGAGA
IFIT1-fwd	qPCR primer	GAATAGCCAGATCTCAGAGGAGC
IFIT1-rev	qPCR primer	CCATTTGTACTCATGGTTGCTGT
IFN-β-fwd	qPCR primer	CATTCGGAAATGTCAGGAGC
IFN-β-rev	qPCR primer	TGGAGCATCTCTTGGATGG
IFN-λ1-fwd	qPCR primer	GGTGACTTTGGTGCTAGGCT
IFN-λ1-rev	qPCR primer	TGAGTGACTCTTCCAAGGCG
MX1-fwd	qPCR primer	ACCATTCCAAGGAGGTGCAG
MX1-rev	qPCR primer	TGCGATGTCCACTTCGGAAA
NS5B-GFP-fwd	PCR primer for cloning	CGCGCGCCCGACCCCGCGTGAGCA-AGGGCGAGG
NS5B-GFP-rev	PCR primer for cloning	CCTCGCCCTTGCTCACGCGGGGTCG-GGCGCG
SOCS1-fwd	qPCR primer	GACGCCTGCGGATTCTACTG
SOCS1-rev	qPCR primer	AGGCCATCTTCACGCTAAGG
USP18-fwd	qPCR primer	ATCCTAACTACCACTGGCAGGA
USP18-rev	qPCR primer	AGCGTGTCAATCTCTGAAGGT

2.7 Plasmids

Table 6: Plasmids.
Antibiotic resistance for selection in eukaryotic cells: Blr, blasticidin; Neo, neomycin/G418; Puro, puromycin.

Plasmid	Source
pDONR207	Invitrogen/Thermo Fisher Scientific
pCMV-dr8.91	Didier Trono, EPFL, Lausanne, Switzerland
pMD2.G	Didier Trono, EPFL, Lausanne, Switzerland
pWPI EF1a Blr Con1 NS3/4A^{WT}	Volker Lohmann, Heidelberg University Hospital
pWPI EF1a Blr Con1 NS3/4A^{mut} (S139A)	Volker Lohmann, Heidelberg University Hospital
pWPI EF1a Neo H2B-mCherry	Sandy Burkart, Binder Lab, DKFZ, Heidelberg
pWPI BLR rfB	[79]
pWPI Puro rfB	[79]
pWPI EF1a Blr NS5B^{WT} Δc21	Volker Lohmann, Heidelberg University Hospital
pWPI EF1a Blr NS5B^{Δ} Δc21	Volker Lohmann, Heidelberg University Hospital
pWPI EF1a Puro n-HA NS5B^{WT} (B22) Δc21	Volker Lohmann, Heidelberg University Hospital
pWPI EF1a Puro n-HA NS5B^{GND} (B22) Δc21	Volker Lohmann, Heidelberg University Hospital
pWPI EF1a Blr NS5B^{WT}Δc21-eGFP	This study
pWPI EF1a Blr NS5B^{Δ}Δc21-eGFP	This study
pWPI EF1a Puro n-HA NS5B^{WT}Δc21-eGFP	This study
pWPI EF1a Puro n-HA NS5B^{GND}Δc21-eGFP	This study
lentiCRISPRv2 Puro	Feng Zhang, Addgene # 52961
lentiCRISPRv2 Puro IFNB1 guideRNA 2	This study
lentiCRISPRv2 Puro IFNB1 guideRNA 3	This study

2.8 Antibodies

Table 7: Antibodies.

Antibody	Host	Clonality	Source
anti-beta-actin	mouse	mono	Santa Cruz Biotechnology (SC-47778)
anti-calnexin	rabbit	poly	Enzo Life Sciences (ADI-SPA-865-F)
anti-IFIT1	rabbit	poly	Abnova, Taiwan (H00003434-DO1)
anti-mouse-HRP	goat	poly	Sigma Aldrich (A4416)
anti-NS5B	rabbit	poly	Volker Lohmann, Heidelberg University Hospital
anti-rabbit-AlexaFluor647	donkey	poly	Invitrogen (A-31573)
anti-rabbit-HRP	goat	poly	Sigma Aldrich (A6154)

2.9 Equipment

Table 8: Equipment.

Device	Supplier
BioRad SDS-PAGE gel casting system	Bio-Rad Laboratories GmbH
Centrifuges, tabletop (5424, 5424R)	Eppendorf
Centrifuge, Rotina 380 R	Hettich GmbH & Co. KG
Centrifuge, Sorvall RC 5C	Thermo Fisher Scientific
CFX96 Real-Time PCR Detection System	Bio-Rad Laboratories GmbH
ECL Chemocam	Intas Science Imaging Instruments GmbH
FACSAria cell sorter	Becton Dickinson
IncuCyte S3 Live-Cell Analysis System	Sartorius AG
LSRFortessa flow cytometer	Becton Dickinson
MESO QuickPlex SQ 120	Meso Scale Diagnostics
MilliQ Barnstead GenPure Pro	Thermo Fisher Scientific
Mini-PROTEAN Tetra Vertical Electrophoresis Cell	Bio-Rad Laboratories GmbH
Mithras LB 943	Berthold Technologies GmbH & Co. KG
NanoDrop	Thermo Fisher Scientific
Nikon Eclipse Ti	Nikon Corporation, Japan
Trans-Blot Turbo Transfer System	Bio-Rad Laboratories GmbH

2.10 Software

Table 9: Software.

Software	Source
Affinity Designer	Serif Ltd.
BD FACSDiva (V8.0.1)	Becton Dickinson
BioRender	biorender.com
CFX Manager (V3.1)	Bio-Rad Laboratories GmbH
DeepL (EN to DE translator)	deepl.com
e-crisp.org	Boutros Lab, DKFZ
FlowJo (V10)	Becton Dickinson
ImageLab	Bio-Rad Laboratories GmbH
IncuCyte Software (2019B Rev2)	Sartorius AG
MaxQuant (V1.6.10.43)	Cox Lab, MPI of Biochemistry, Munich
MSD Discovery Workbench	Meso Scale Diagnostics
PANTHER GO Enrichment Analysis	pantherdb.org[249, 250]
Perseus (V1.6.10.43)	Cox Lab, MPI of Biochemistry, Munich
Prism (V8)	GraphPad Software
Python Jupyter Notebook	jupyter.org

3 Methods

If not noted otherwise, purchased kits and assays were used following the protocol provided by the manufacturer (see Table 2 for product details). Media, buffers, solutions, and reaction mixtures referred to herein are listed in Table 2 and Table 3.

3.1 Basic Molecular Biology Techniques

3.1.1 Agarose Gel Electrophoresis

Agarose gel electrophoresis was used to separate nucleic acid fragments based on molecular weight. For a 1 % gel, 0.5 g agarose were dissolved in 50 ml 1x TAE buffer by heating in a microwave until the solution was free of visible agarose. Once the solution had cooled down to 60 °C, 2 µl Midori Green were added and the solution was poured into a gel chamber. A comb was inserted to introduce pockets while the solution solidified, yielding the agarose gel. The chamber was filled with 1x TAE buffer up until covering the gel. Nucleic acids in H_2O were supplemented with TriTrack 6x DNA Loading Dye to a final concentration of 1x. 6 µl of molecular weight standard Gene Ruler 1 kb or 0.5-1.0 µg of nucleic acids were loaded into a pocket, and gel electrophoresis was performed at 100 V until bands were distinguishable under UV light.

3.1.2 Restriction Digest

For restriction digestion of DNA, restriction endonucleases (RE) from New England Biolabs (NEB) were used. 1-3 µg DNA were digested with 1 U RE in a 20 µl ddH_2O reaction volume containing 1x of the enzyme-specific NEBuffer. Digestion was performed for 1.5 h at 25 °C or 37 °C, depending on the RE.

3.1.3 Q5 Polymerase Chain Reaction

Polymerase chain reaction (PCR) with the NEB Q5 High Fidelity Polymerase was used to amplify DNA fragments. A 50 µl reaction mix contained 22.5 µl ddH_2O, 10 µl 5x Q5 Reaction Buffer, 10 µl Q5 High GC Enhancer, 2.5 µl each of forward primer and reverse primer (10 µM), 1 µl dNTPs (10 mM), 1 µl template DNA, and 0.5 µl Q5 High-Fidelity DNA Polymerase. The PCR reaction was performed on a thermal cycler with the following program: initial denaturation for 30 s at 98 °C; then 35 cycles of 10 s at 98 °C, 20 s at 50-72 °C*, 30 s/kb at 72 °C; then final extension for 2 min at 72 °C. The annealing temperature (*) was dependent on primer sequence and was calculated with SnapGene for each primer pair.

3.2 Cloning

3.2.1 Handling of Bacteria and Plasmid Production

Plasmids generated or used in this study were transformed into chemo-competent *E. coli* DH5α. 100 µl bacteria solution were incubated with 50 ng plasmid on ice for 5 min, then heat-treated at 42 °C for 45 s and then incubated again on ice for 20 min. Bacteria were then incubated in LB medium for 30 min, plated on LB agar plates containing the required selection antibiotic and incubated 16 h at 37 °C. Single colonies were transferred into 2 ml LB medium containing the appropriate selection antibiotic and cultured at 37 °C for 16 h. Plasmid DNA was isolated using Monarch Plasmid Miniprep Kit and integrity was confirmed via sequencing (GATC/Eurofins). For large-scale plasmid preparation, plasmid DNA was isolated from 300 ml cultures with the NucleoBond PC 500 kit.

3.2.2 Generation of Lentiviral pWPI NS5B-eGFP Expression Vectors

NS5B-eGFP recombinant DNA fragments required for generation of pWPI NS5B-eGFP expression vectors were generated via Q5 High-Fidelity PCR. First, DNA fragments of NS5BΔc21 WT or ΔGDD were amplified from template plasmids

i) pWPI EF1a BLR NS5B^{WT} Δc21,

ii) pWPI EF1a BLR NS5B$^{\Delta}$ Δc21,

iii) pWPI EF1a Puro n-HA NS5B^{WT} (B22) Δc21, and

iv) pWPI EF1a Puro n-HA NS5B^{GND} (B22) Δc21

(see Table 6) using primers attB1-NS5B-fwd and NS5B-GFP-rev (Table 5). Then, a DNA fragment coding for eGFP was generated with primers NS5B-GFP-fwd and attB2-GFP-rev based on a template plasmid coding for eGFP-IRF3[133]. Primers NS5B-GFP-rev and NS5B-GFP-fwd introduced an area of sequence homology to the 3' and 5' ends of the NS5B and eGFP DNA fragments, respectively. This subsequently allowed for fusion of both fragments via overlap-extension PCR. Here, both DNA fragments were added to the Q5 reaction mix and primers were omitted during initial denaturation and the first amplification cycle (annealing temperature 60 °C). Then, primers attB1-NS5B-fwd and attB2-GFP-rev were added and subsequent amplification cycles were performed with annealing temperature 64 °C. These primers added *attB* sites to both ends of the fusion product.

Quality of DNA fragments after each PCR reaction was assessed with agarose gel electrophoresis (1 % agarose), and DNA fragments were purified from gel with the Monarch DNA Gel Extraction Kit.

The recombinant NS5B-eGFP DNA fragment was then first cloned into entry vector pDONR207 in a Gateway BP reaction. Here, 150 ng each of pDONR207 and recombi-

nant DNA were mixed with 1 µl BP clonase in TE buffer (final volume: 8 µl) and incubated for 1 h at 25 °C. The reaction mix was transformed into *E. coli*; selection with gentamicin (7 µg/ml) and further steps of plasmid preparation were performed as described in 3.2.1. From the pDONR207 vector, the recombinant NS5B-eGFP DNA was then shuttled into a pWPI destination vector (pWPI Blr rfB or pWPI Puro rfB) in a Gateway LR reaction. Here, 150 ng each of pDONR207 NS5B-eGFP and the destination vector were mixed with 1 µl LR clonase in TE-buffer (final volume: 8 µl) and incubated for 1 h at 25 °C. The reaction mix was transformed into *E. coli* and selection with carbenicillin (100 µg/ml) and further steps of plasmid preparation were performed as described in 3.2.1. Correct insertion of the recombinant DNA fragment was confirmed by sequencing with the primer cppt-fwd.

3.3 Cell Culture

Cells were cultured in complete DMEM at 37 °C, 85 % humidity and 5 % CO_2. Cells were passaged twice per week at a ratio of 1:5 to 1:20, depending on the level of confluence, using 0.05 % Trypsin-EDTA for detachment. For long-term storage of cell lines, cells were centrifuged (5 min, 450 rcf), resuspended in FCS with 10 % DMSO (2x10^6 cells/ml), frozen at -80 °C, and stored in liquid nitrogen.

3.4 Cell Line Generation

Both overexpression cell lines and knockout cell lines were generated by transduction with lentiviral vectors.

3.4.1 Lentiviral Vector Particle Production

Human embryonic kidney (HEK293T) cells were seeded a day before transfection (1x10^6/6 cm dish) and received fresh medium (4 ml/1x10^6 cells) 30 min prior to transfection. In this study, two different chemical-based transfection methods for lentiviral particle production were employed. In both, 1x10^6 cells were transfected with a total of 15 µg DNA, consisting of plasmids pCMV-dr8.91, pMD2.G, and retroviral vector (Table 6) at a ratio of 3:1:3.

For calcium phosphate transfection with the Takara CalPhos Mammalian Transfection Kit, DNA was mixed with 62 µl 2 M CaCl2 and ddH_2O to a final volume of 500 µl. An equal volume of 2x HBS was then slowly added, while air was constantly introduced to the solution to facilitate mixing. The transfection mixture was added drop-wise to the dish. Formation of calcium phosphate precipitates were confirmed after 4 h.

For PEI transfection, DNA in OptiMEM was mixed with an equal volume of OptiMEM containing 1 mg/ml PEI solution, incubated for 30 min at room temperature and then added

drop-wise onto the cells.

In both methods, medium was refreshed 6 h after transfection. Supernatant was harvested 48 h, 56 h and 72 h after transfection, sterile-filtered through a 0.2 µM filter, pooled and stored at -80 °C.

3.4.2 Generation of Overexpression Cell Lines

Cells seeded the day prior at $8x10^3/cm^2$ were transduced twice for 24 h each by adding 1 ml/$4x10^4$ cells of lentiviral particle containing medium. Overexpression cell lines were continuously cultured under the presence of the required selection antibiotic to ensure stable transgene expression (blasticidin: 5 µg/ml; neomycin resistance: 1 mg/ml of geneticin (G418); puromycin: 1 µg/ml).

3.4.3 Generation of Knockout Cell Lines

The IFNB1 gene coding for IFN-β was deleted in A549 through CRISPR/Cas9-mediated gene knockout. Guide RNA sequences against human IFNB1 were designed with e-crisp and ordered as DNA oligos from Sigma (Table 5). Oligos were dimerized in a T4 dimerization reaction mix (Table 3) at 37 °C for 30 min, followed by 5 min at 95 °C and subsequent temperature reduction to 25 °C at 5 °C/min. DNA dimers were diluted 1:200 in ddH_2O. 3 µg of the vector plasmid lentiCRISPRv2 with a puromycin resistance were digested with *Bsm*BI and incubated with calf intestinal phosphatase (CIP; 0.2 U/ml) for 1.5 h at 37 °C. Digested fragments were separated on an agarose gel, and vector backbone (larger band) was cut out and DNA was purified from the gel fragment with the Monarch DNA Gel Extraction Kit. Vector backbone and DNA dimers were annealed in a 1:1 ratio in a T4 DNA ligation mix (Table 3) at 16 °C overnight. Afterwards, the complete reaction mix was transformed into competent bacteria and plated onto LB agar containing carbenicillin (100 µg/ml). Subsequent steps included picking colonies, culturing in LB medium, plasmid extraction, and sequencing, and were performed as described in section 3.2. Guide RNA sequence integrity and orientation was confirmed by sequencing with the hU6 promotor primer (Table 5).

With the generated lentiCRISPRv2 IFNB1 plasmids, lentiviral particles were generated and A549 cells were transduced as described above. From the transduced cell pools, cells were seeded on 96-well plates at a limiting dilution of 0.5 cells/well. Wells were checked regularly for the presence of a cell population descending from a single cell, and single cell clones were step-wise expanded up to 6-well plates.

To confirm successful knockout of IFNB1, $1x10^6$ cells were infected with Sendai virus at MOI = 0.1 for 16 h before supernatant harvest. Then, IFN-β contents in the supernatants were determined with the LumiKine Xpress IFN-β 2.0 ELISA following the manufacturer's protocol (Fig. S4).

3.4.4 Generation and Handling of NS5B-Overexpressing Cells

Cells overexpressing NS5B were freshly generated for each experiment as described above for overexpressing cell lines. If not noted otherwise, experiments were performed 5 days post transduction.

3.5 RNA Quantification by RT-qPCR

Relative RNA levels were determined by reverse transcription (RT) of RNA into cDNA and subsequent quantitative PCR (qPCR). Cells were lysed in Monarch RNA lysis buffer, and RNA was purified using the Monarch Total RNA Miniprep Kit and eluted in 50 µl RNase-free ddH_2O. 3 µl RNA was mixed with an equal volume of Reverse Transcription Mix, and cDNA synthesis was performed on a thermal cycler (25 °C for 10 min, 37° C for 2 h, then 85 °C for 5 min). cDNA was diluted 1:20 in ddH_2O, and 6 µl cDNA were mixed with 9 µl iTaq Universal SYBR Green Supermix containing both forward and reverse primers for target gene (Table 5) at a final concentration of 0.25 µM, resulting in 15 µl final reaction volume per well. qPCR was performed in Hard-Shell 96-Well PCR Plates in a CFX96 Real-Time PCR Detection System (program: 3 min at 95 °C, then 44 cycles of 10 s at 95 °C, 30 s at 60 °C, fluorescence emission measurement). Ct values were exported with CFX Manager 3.1 and fold change over reference gene GAPDH was calculated with the $2^{-\Delta\Delta Ct}$ method[251]. If not noted otherwise, mRNA levels were plotted as mean ± standard deviation (s.d.) of three technical replicates.

3.6 Protein Quantification by Immunoblotting

Protein quantification of whole cell populations was performed by SDS-polyacrylamide gel electrophoresis (PAGE) and immunoblotting (Western Blot). 5x10^5 cells were washed in 500 µl PBS, then lysed in 150 µl 1x Sample buffer at 95 °C for 5 min. Genomic DNA was digested with Benzonase (1 U) for 1 h at room temperature and residual cell debris was removed by centrifugation.

An 8 % SDS-polyacrylamide gel was cast in a BioRad gel casting system. First, the resolving gel containing polyacrylamide (BAA) at a final concentration of 8 % was prepared as described in Table 3 and poured between the glas slides of the casting system. To avoid air bubbles on top of the gel, 200 µl isopropanol was added on top. Once the resolving gel had solidified, the isopropanol was removed and the stacking gel (Table 3) was poured on top. A comb was inserted and the gel was stored at 4 °C over night to completely solidify.

For electrophoresis, the gel was inserted into a Mini-PROTEAN Tetra Vertical Electrophoresis Cell and covered with 1x TGS buffer. 5x10^4 lysed cells were loaded onto the gel and proteins were separated for 90 min at 120 V. Proteins were transferred onto a

methanol-activated PVDF membrane (pore size: 0.2 µM) with the Trans-Blot Turbo Transfer System in 1x Semi Dry Transfer buffer at 25 V and 1 A for 30 min. Membranes were dried, rehydrated in ethanol, washed in PBS-T and blocked by incubation in Western Blot blocking buffer for 30 min. After incubation with primary antibodies (Table 7) for 16 h at 4 °C, membranes were washed 4x with PBS-T for 15 min each, incubated with secondary antibodies (Table 7) for 1 h at room temperature and washed again 4x with PBS-T. Protein bands were visualized in an ECL Chemocam using Clarity Western ECL Substrate and quantified with ImageLab.

3.7 Chemical-based Transfection of RLR Agonists

Cells were seeded the day prior to transfection at $5x10^4$ cells/well on a 24-well plate. The next day, cells received 400 µl complete DMEM without penicillin and streptomycin at least 30 min before transfection. For one well, 1 µl Lipofectamine 2000 was diluted in 50 µl OptiMEM, mixed and incubated at room temperature for 5 min. Furthermore, dsRNA or poly(I:C) were diluted in 50 µl OptiMEM, and nucleic acid content was increased to 1 µg per transfection reaction with poly(C). Both reactions were added together, mixed, incubated for 20 min at room temperature and added dropwise to the cells. After 4 h, medium was replaced with 500 µl fresh complete DMEM, and RNA was harvested 6 h after start of transfection.

3.8 Sendai Virus Infection

$1x10^5$ cells/well in a 24-well plate were infected 10 h after seeding with Sendai virus at MOI = 0.004. RNA was harvested 16 h after infection.

3.9 LucUbiNeo Luciferase Reporter Assay

The potential of supernatants harvested from NS5B-expressing cells to inhibit viral replication was assessed in Huh7 LucUbiNeo-ET cells by measuring luciferase levels that correlate with LucUbiNeo reporter construct replication[252].

Huh7 cells harboring the LucUbiNeo reporter construct were seeded at $5x10^4$ cells/well on a 24-well plate in complete DMEM. Next day, medium on cells was exchanged with medium harvested from NS5B-expressing A549. After 48 h, cells were washed with 500 µl PBS and lysed in 100 µl luciferase lysis buffer at -80 °C. Lysates were thawed and directly measured in a Mithras plate reader by adding 400 µl luciferase assay buffer and then measuring firefly luciferase signal for 10 s.

3.10 Cell Imaging

3.10.1 Determination of NS5B Subcellular Localization by Fluorescence Microscopy

Images of subcellular NS5B-eGFP localization were taken with a Nikon Eclipse Ti microscope equipped with an X-Cite 120 LED, a SD-Qi2 camera and the NIS-Elements AR 4.40.00 software. $5x10^4$ cells expressing NS5B$^{\Delta}$-eGFP or the corresponding wild-type variant were grown on cover slips in a 24-well plate for 24 h, washed with 500 µl PBS and fixed in 100 µl 4 % paraformaldehyde for 10 min at room temperature. Then, cells were washed thrice with PBS and permeabilized for 10 min in 0.5 % Triton X-100 in PBS. After three washing steps, cells were blocked with 3 % BSA in PBS for 30 min at 4 °C. Then, cells were stained with DAPI (1:5000 in ddH_2O) for 5 min protected from light. After three final washing steps with PBS and an additional washing step with ddH_2O, residual liquid was carefully removed from the cover slip, and the cover slip was mounted onto 4 µl Fluoromount-G on a microscope glass slide. After drying overnight, DAPI and NS5B-eGFP were imaged with a 20x lens at 20 % or 100 % LED intensity for 50 ms or 1 s, respectively.

Cells expressing NS5B^{GND}-eGFP or the corresponding wild-type variant were imaged alive and in PBS to avoid fluorescence interference from phenol red-containing DMEM. Images were taken at 100 % LED intensity for 1 s using a 10x lens.

3.10.2 Temporal Resolution of Cell Proliferation and Cell Death via Live Cell Imaging

Cell proliferation and cell death was monitored over time by live cell imaging in an IncuCyte S3 Live-Cell Analysis System. On a 96-well plate, $2x10^3$ cells were seeded per well and supplemented with Cytotox Green dye at 100 nM and with the appropriate selection antibiotics. Four images per well were taken with a 10x objective and 400 ms acquisition time in channels phase, red and green every 6 h and analyzed with IncuCyte S3 2019B Rev2 software; analysis parameters were adapted from David Zander (DKFZ, Heidelberg) and are listed below:

Confluence mask parameters – Segmentation Adjustment: 1.1; Hole Fill: 500; Filters: Area minimum: 200.

Red mask parameters – Segmentation: Top-Hat; Radius: 100; Threshold: 0.4; Edge Split: On; Edge Sensitivity: -35; Area minimum: 60; Area maximum: 1000; Integrated Intensity minimum: 60.

Green mask parameters – Segmentation: Top-Hat; Radius: 100; Threshold: 10; Edge Split: On; Edge Sensitivity: -40; Area minimum: 10; Area maximum: 700; Eccentricity maximum: 0.9; Mean intensity minimum: 7; Mean intensity maximum: 1000.

Overlap mask – Area minimum: 20.

Number of cells were determined by counting red events per image equaling number of

H2B-mCherry containing nuclei. Then, cell numbers were normalized to t = 0 h to compensate for variations in starting cell number:

$$n_t^{norm} = n_t * \frac{n_0^{ref}}{n_0}$$

(n_t^{norm}: normalized cell number at time point t, n_t: cell number at time point t, n_0^{ref}: reference cell number at time point 0 h, n_0: cell number at time point 0 h)

Fraction of dead cells was calculated by dividing number of green events (Cytotox Green stained dead cells) through the sum of red events and green events minus overlap events:

$$dead\,cells\,(\%) = \frac{n_{green}}{n_{green} + n_{red} - n_{overlap}}$$

3.11 Flow Cytometry and Fluorescence-Activated Cell Sorting

Single cell protein levels were determined by flow cytometry. Cells were detached from the culture dish by trypsinization with 0.05 % Trypsin-EDTA. If only proteins tagged with a fluorescent dye such as NS5B-eGFP were analyzed, 5x10^4 cells were washed once with 500 µl PBS, resuspended in 300 µl FACS buffer and separated with a cell strainer before measurement. For intracellular staining of IFIT1, 5x10^4 cells were washed in 500 µl FACS buffer, fixated in 100 µl Cytofix/Cytoperm buffer for 20 min at 4 °C protected from light and then washed twice with 100 µl 1x Perm/Wash buffer. Afterwards, cells were incubated with anti-IFIT1 (1:500) in 50 µl 1x Perm/Wash buffer for 30 min on ice and then washed thrice with 100 µl 1x Perm/Wash buffer. Incubation with fluorophore-coupled secondary anti-rabbit Alexa-647 (1:1000) in 50 µl 1x Perm/Wash was performed on ice for 30 min in the dark. Then cells were washed thrice with 100 µl 1x Perm/Wash buffer, resuspended in 300 µl FACS buffer and separated with a cell strainer. Flow cytometry was performed with a LSRFortessa flow cytometer and the FACSDiva software. Laser voltage values were set as follows: Forward Scatter (FSC): 50; Side Scatter (SSC): 225; FITC: 350; Alexa-647: 450. NS5B-eGFP signal (FITC channel) and IFIT1-Alexa-647 signals of at least 2x10^4 single events were measured, and gating was performed to remove cell debris and cell aggregates from the analysis.

Fluorescence-activated cell sorting (FACS) of NS5B-eGFP-expressing cells was performed with assistance from the DKFZ Flow Cytometry Core Facility. 1x10^7 cells were washed with 5 ml PBS and resuspended in 1 ml FACS buffer. Cells were sorted with a FACSAria cell sorter based on signal intensity of the NS5B-associated eGFP-tag; sorting gates were slightly tilted to compensate for GFP signal differences due to cell size. Cells were seeded in DMEM; depending on cell number per fraction after sorting and calculating with 70 % survival, cells were seeded on appropriate dish formats to avoid stress due to low cell layer density.

3.12 Mass Spectrometry

Unbiased whole proteome analysis was performed by mass spectrometry. A confluent cell layer in a 10 cm dish was washed with PBS, then 5 ml ice-cold PBS was added to the dish and cells were detached with a cell scraper. Cells were precipitated by centrifugation (3 min, 700 rcf, 4 °C), PBS was aspirated and cells were shock-frozen in liquid nitrogen. Samples were stored at -80 °C. Further sample handling, mass spectrometry and data analysis were performed by Christian Urban and Andreas Pichlmair as described in detail in [247].

3.13 Multiplex Electrochemiluminescence Assay

Concentrations of interferons, pro-inflammatory cytokines and chemokines in supernatants of NS5B-transduced cells were measured with Meso Scale Diagnostics' (MSD) electrochemiluminescence technology in a multiplex approach. NS5B-transduced cells received fresh complete DMEM three days post transduction. Supernatant was harvested 48 h later, sterile-filtered and stored at -80 °C. Concentrations of IFN-α2a, IFN-β, IFN-λ1, and IFN-γ were determined with the MSD U-PLEX Interferon Combo Human Kit. Pro-inflammatory cytokines IL-1β, IL-2, IL-4, IL-6, IL-8, IL-10, IL-12p70, IL-13, and TNF were analyzed with the MSD V-PLEX Proinflammatory Panel 1 Human Kit. Chemokines CCL11/eotaxin, CCL4/MIP-1β, CCL26/eotaxin-3, CCL17/TARC, CCL3/MIP-1α, CCL2/MCP-1, CCL22/MDC, CCL13/MCP-4, CXCL10/IP-10, and CXCL8/IL-8 were analyzed with the MSD V-PLEX Chemokine Panel 1 Human Kit. All three assays were performed with undiluted supernatant following the manufacturer's protocols. In brief, the MSD U-PLEX Interferon Combo Human Kit was first incubated overnight at 4 °C with linker-coupled biotinylated capture antibodies against the four interferons, thereby coating four defined spots in the well with only one of the four detection antibodies each. V-PLEX plates were purchased pre-coated with capture antibodies. The assay protocols for all three panels followed the same steps: First, plates were washed three times with PBS-T. Then, the same volume of undiluted sample, or standards at different dilutions, were added to the wells and incubated on a shaker at room temperature for 1-2 h. Plates were washed again three times with PBS-T, followed by incubation with a mix of all required detection antibodies for 1-2 h on a shaker at room temperature. After three wash steps with PBS-T, Read Buffer was added to the plates. Plate measurement was performed in a MESO QuickPlex SQ 120. Analyte concentrations were calculated based on standard dilution series with the MSD Discovery Workbench software. MSD electrochemiluminescence assays were performed with assistance from Sandy Burkart and Sandra Wüst (DKFZ, Heidelberg).

3.14 RNA Expression Profiling

RNA was harvested and purified as described in section 3.5, and RNA integrity was confirmed by agarose gel electrophoresis (10 µl RNA, 1.5 % agarose). The DKFZ Genomics and Proteomics Core Facility measured RNA levels of n > 19000 genes on a Clariom S (human) micro array (Applied Biosystems), and supplied analysis data (normalized mean expression values and mean fold changes between two conditions) and statistics (two-sample t-test p-values corrected for multiple testing with Benjamini-Hochberg (BH)). Data cleanup, hit calling and visualization was performed with Python (v3.8.5) in Jupyter Notebook. Genes were determined to be significantly regulated (= hits) if i) at least 2-fold up- or downregulated, and ii) BH-corrected p-value < 0.05.

PANTHER[249, 250] (v16.0) was used for Gene Ontology (GO) enrichment analysis. Sets of significantly regulated genes were compared to all genes included in the microarray, and pathways were classified as enriched with a false discovery rate (FDR) of < 0.05.

The Interferome database[253] (interferome.org; accessed on 24.04.2021) was used to separate significantly regulated genes into ISGs and non-ISGs. Database was filtered for genes in human-derived samples with a log2 fold difference >= 1 after type I or type III interferon treatment, and returned genes were classified as ISGs.

3.15 Graphics

If not noted otherwise before, data was plotted with GraphPad Prism. Schematic depictions of NS5B variants and experimental procedures were generated with BioRender. Figures were generated with Affinity Designer. Figures adapted from publications were done so with permission (refs. [14], [54], [82], [90], [235]) or covered by a Creative Commons license (refs. [5], [42], [247]).

4 Results

PRRs such as RIG-I sense a viral infection in infected cells and trigger the production of signaling molecules including interferons, which are secreted into the surrounding tissue[54]. Here, they induce an antiviral response both in infected as well as in uninfected cells, priming them for an upcoming infection[118,254].

In this work, we aimed to investigate the consequences of a chronic antiviral response both on infected cells and on cells in their proximity that are themselves not infected. The most straightforward approach to study the effects of prolonged immune stimulation on cells *in vitro* would be to infect cells with a virus that is able to establish a persistent infection. However, viruses bring along potent countermeasures against a cells' antiviral system, and thus would obscure what changes to a cell over time could be attributed to constantly activated antiviral signaling. Conversely, the use of genetically modified viruses lacking those countermeasures would likely prevent the virus from establishing a persistent infection. In this work, we, therefore, pursued technical approaches to establish a virus-free cell culture system that would allow for constant activation of a cell's antiviral signaling through the permanent presence of RLR ligands.

4.1 Exploiting HCV NS5B as a Molecular Tool to Activate RLR Signaling

Various methods are available to study a cell's immediate response to non-self molecular patterns such as viral RNA. Virus-derived RNA-replication intermediates can be mimicked by *in vitro* transcribed dsRNA or its synthetic analog poly(I:C). These substances are typically introduced through chemical- or electroporation-based transfection[255]. While these approaches activate the cell's innate immune response within a short time frame, they also represent cytotoxic stress factors and thus have to be well-adjusted to avoid severe side effects that might compromise the experimental outcome. Hence, repeated transfection of stimulating factors was deemed not feasible for constant stimulation over a long period.

In the case of HCV, one of the patterns detected by PRRs is the viral dsRNA produced during viral genome replication by HCVs RdRp NS5B. It has been shown before that the expression of NS5B alone is sufficient to produce small RNA species that can induce the interferon response in human embryonic kidney cells and hepatocytes[256–258]. We tested whether we could circumvent transfection of stimulating factors by exploiting NS5B as a molecular tool to produce dsRNA within the cell. Recombinant versions of HCV NS5B were cloned into pWPI lentiviral expression vectors and introduced into cells through transduction and expressed under the control of an EF1α promoter (Fig. 1a, Fig. S1). Of note, all NS5B variants used in this study lacked the C-terminal 21 amino acids that

comprise the transmembrane domain. As a negative control to catalytically active NS5B ($NS5B^{WT}$), a NS5B variant with a 10 amino acid deletion in the palm domain, including the catalytic glycine-aspartate-aspartate (GDD) sequence, was used ($NS5B^{\Delta}$). The IFN-competent lung adenocarcinoma cell line A549 expressed mRNA of both NS5B variants at similar levels 6 days post transduction (d.p.t.), but only $NS5B^{WT}$-transduced cells showed an increase in mRNA and protein levels of the interferon stimulated gene IFIT1 (Fig. 1b,d). We then generated C-terminally eGFP-tagged versions of both $NS5B^{WT}$ and

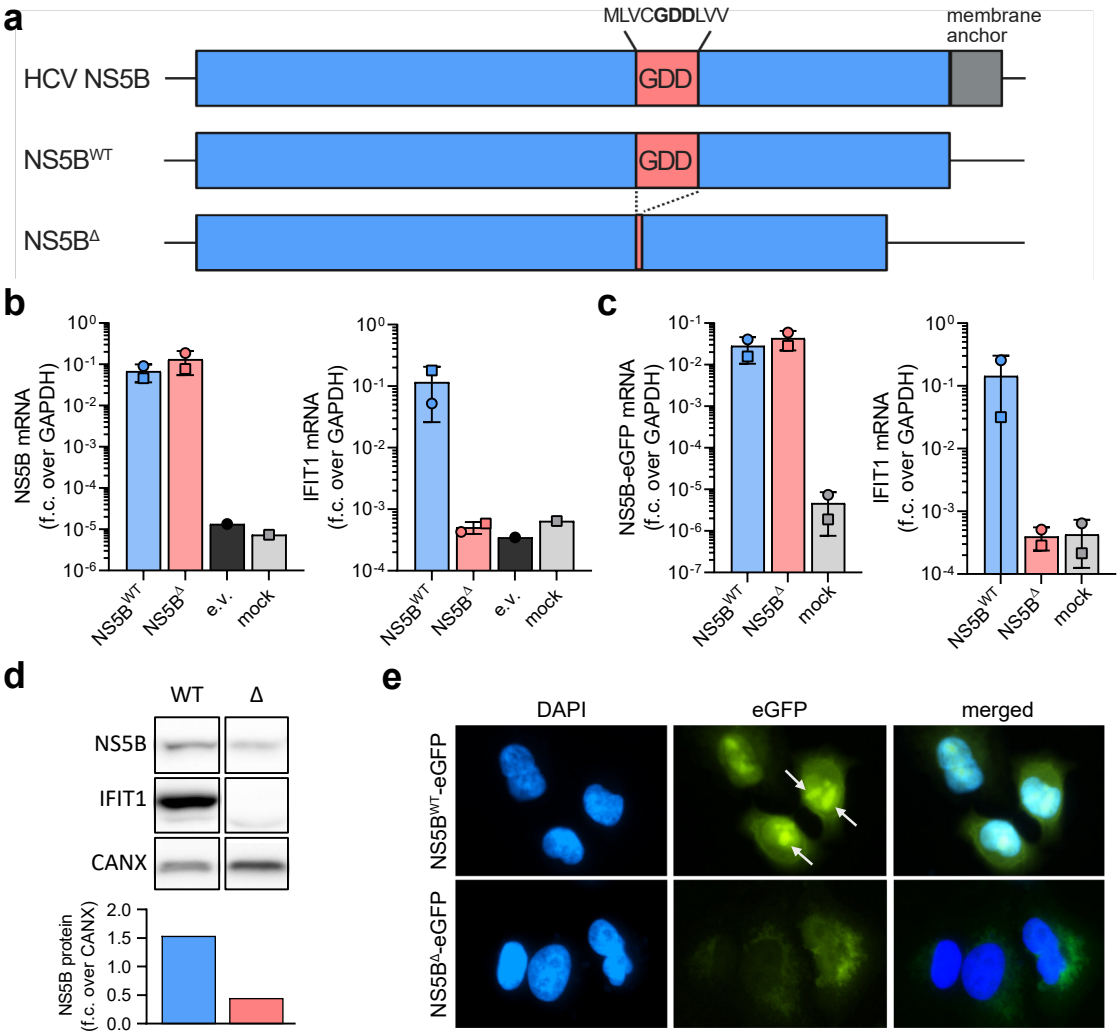

Figure 1: Expression of recombinant HCV RNA-dependent RNA polymerase NS5B activates the innate antiviral response in A549 cells.

(**a**) Simplified display of full-length HCV NS5B and recombinant NS5B variants used in this study. A 10 amino acid segment (red), including the catalytic triad GDD, is deleted in $NS5B^{\Delta}$. (**b**) NS5B (left) and IFIT1 (right) mRNA levels in $NS5B^{WT}$-, $NS5B^{\Delta}$-, empty vector- (e.v.), or mock-transduced A549 cells 6 days post transduction. mRNA level fold change (f.c.) was calculated over GAPDH (mean $\pm$ s.d. of $n = 2$ biological replicates; values below detection limit are not shown). (**c**) NS5B-eGFP (left) and IFIT1 (right) mRNA levels in $NS5B^{WT}$-eGFP-, $NS5B^{\Delta}$-eGFP-, or mock-transduced A549 cells 6 days post transduction ($n = 2$ biological replicates). (**d**) Western blot of NS5B and IFIT1 protein expression in A549 wild-type cells 6 days post transduction with $NS5B^{WT}$ or $NS5B^{\Delta}$. Fold change (f.c.) in NS5B protein level was calculated over loading control calnexin (CANX). Representative of $n = 2$ independent experiments is shown. (**e**) Subcellular localization of NS5B-eGFP (green) in A549 cells 5 days post transduction with $NS5B^{WT}$-eGFP or $NS5B^{\Delta}$-eGFP. Cells were fixed on cover slips and DNA was stained with DAPI (blue). Arrows indicate $NS5B^{WT}$-eGFP cluster. Data in this figure was generated together with Katharina Heine (DKFZ, Heidelberg) as part of collaborative work within TRR179.

NS5B$^{\Delta}$, which induced a similar response (Fig. 1c). Unlike as observed for NS5B mRNA, however, NS5B protein levels of NS5B$^{\Delta}$ were significantly lower than NS5B^{WT} (Fig. 1d). Fluorescence microscopy analysis of the subcellular localization of both NS5B variants in cells expressing the eGFP-tagged NS5B variants revealed that NS5B^{WT} clustered in several small loci within the nucleus (Fig. 1e, arrows), while NS5B$^{\Delta}$ exhibited a more diffuse distribution throughout the whole cell. In the absence of viral RNA, NS5B has to rely on host RNA as a template for generation of dsRNA. We argued that NS5B protein lacking membrane anchorage might accumulate in areas with high RNA concentrations. The detected cluster in the nuclei of NS5B^{WT}-transduced cells could therefore be nucleoli, which exhibit high density of ribosomal RNA[259], although it is unclear how NS5B would translocate into the nucleus. Conversely, due to deletion of a highly conserved part of the palm domain, NS5B$^{\Delta}$ might not be able to bind to RNA as well as the wild type and thus would not accumulate at RNA-dense regions. Different localization alone could in principle affect protein half-life; furthermore, the deletion of a part of NS5B$^{\Delta}$ might also cause a decrease in protein stability.

To eliminate differences in protein level and localization between active and inactive NS5B, we employed pWPI vectors coding for NS5B^{GND}, which harbored a point mutation in the catalytic triad exchanging aspartate (D) with asparagin (N), and its corresponding wild-type variant (Fig. 2a, Fig. S1). These new variants of NS5B, both with or without a C-terminal eGFP tag, showed similar potency in activating the innate antiviral response (Fig. 2b-c). The point mutation did not affect protein levels between the active and inactive version, and subcellular localization in nucleolar clusters was indistinguishable (Fig. 2d-e). Of note, NS5B^{GND} and its corresponding wild-type variant had been previously HA-tagged at the N-terminus and had been furthermore mutated to match the epitope sequence recognized by a HCV-specific CD8^{+} T cell clone[252]. The epitope optimization had been reported to have no effect on NS5B's catalytic activity[252], and our data indicated that both modifications did not influence NS5B's primary function in this study (Fig. 2c). Thus, we concluded that both modifications were of no further relevance. Although we switched to the more stable mutant NS5B^{GND} after discovering the caveats of NS5B$^{\Delta}$, some early experiments shown in this work were performed with NS5B$^{\Delta}$.

To quantify the magnitude of NS5B-induced immune responses, we compared IFIT1 induction 5-6 days post transduction to the response to lipofectamine-based transfection of dsRNA or poly(I:C) in A549 cells (Fig. 3). NS5B^{WT}-transduced cells reached IFIT1 mRNA levels comparable to the response to 0.1-1.0 ng dsRNA, or 10 ng poly(I:C). Even though A549 cells could be stimulated to reach ~10-fold higher IFIT1 mRNA levels than after expression of NS5B^{WT}, we estimated a 100-fold induction over non-treated cells to be sufficiently strong and possibly closer to a real chronic virus infection.

Furthermore, data from our group indicated that transfection of A549 with dsRNA already at low amounts (2.5 ng/ml) leads to cell death of about 80 % of cells within 48 hours[260]. Thus, lower level induction of innate immune pathways that avoid excessive induction of

cell death were considered advantageous for monitoring long-term stimulation effects.

dsRNA species are mainly sensed by two cytosolic PRRs, RIG-I and MDA5, in a structure and length dependent fashion[54]. While RIG-I exhibits a high affinity for shorter dsRNA molecules that possess a 5'-triphosphate and lack 2'-O-methylation, MDA5 targets longer dsRNA molecules. As we did not know the precise nature of NS5B-derived dsRNA species in our cell culture system, both receptors could potentially be involved. Furthermore, it had been reported previously that NS5B-derived dsRNA is sensed by transmembrane TLR3 in immortalized hepatocytes[257]. To determine through which path-

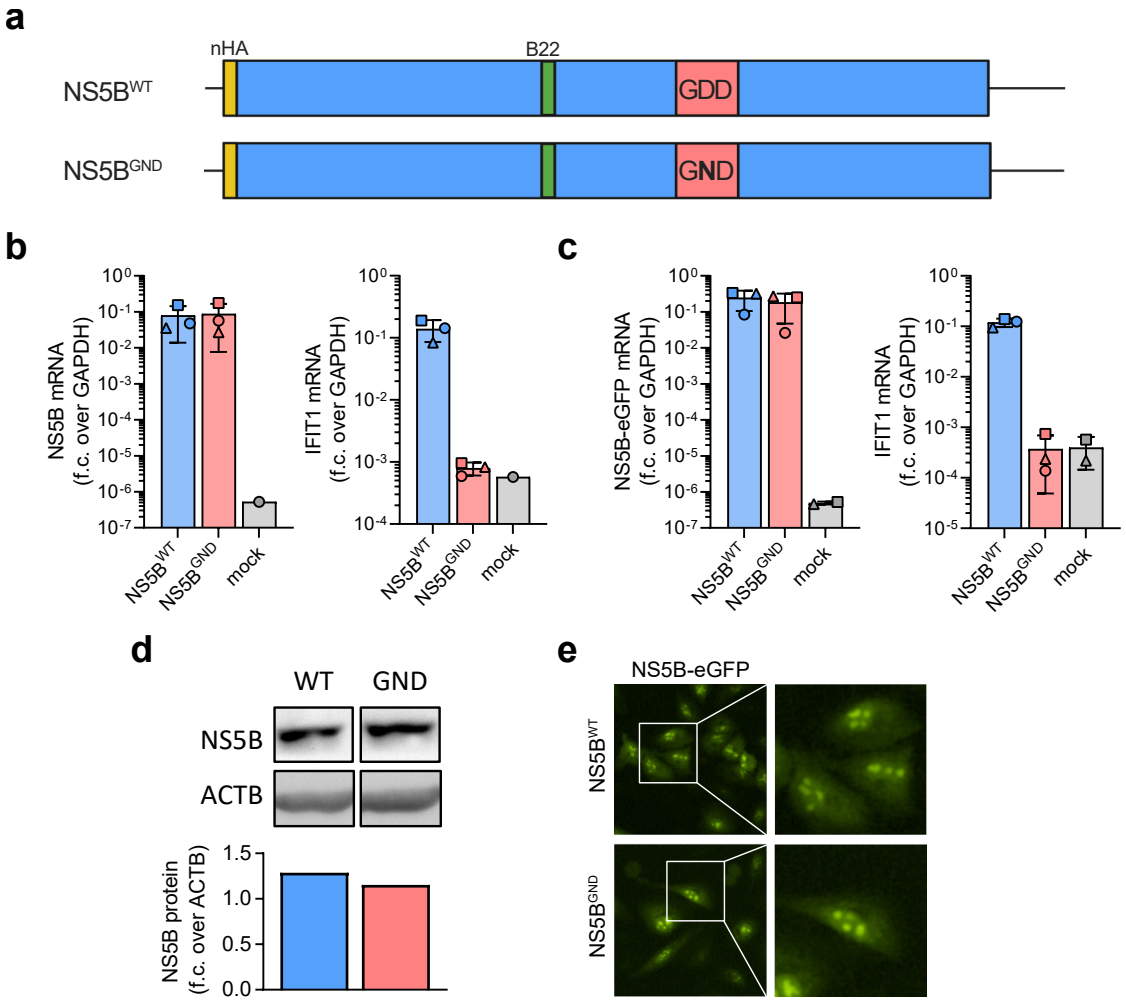

Figure 2: A point mutation in the catalytic triad renders NS5B inactive without affecting protein abundance and subcellular localization.

(**a**) Schematic display of additional recombinant NS5B variants used in this study. In NS5B^{GND}, a point mutation introduced an amino acid switch from aspartate (D) to asparagine (N). NS5B^{GND} and its corresponding wild-type variant harbor an N-terminal HA tag (nHA) and are optimized for epitope recognition by HCV-specific CD8$^+$ T cells (B22 epitope; amino acid sequence change ITQ to VVT[252]). (**b**) NS5B (left) and IFIT1 (right) mRNA levels in NS5B^{WT}-, NS5B^{GND}-, or mock-transduced A549 cells at 5 days post transduction (n = 3 biological replicates). (**c**) NS5B (left) and IFIT1 (right) mRNA levels in NS5B^{WT}-eGFP-, NS5B^{GND}-eGFP-, or mock-transduced A549 cells 5 days post transduction (n = 3 biological replicates). (**d**) Western blot of NS5B protein expression in A549 wild-type cells 6 days post transduction with NS5B^{WT} or NS5B^{GND}. Fold change (f.c.) in NS5B protein level was calculated over loading control beta-actin (ACTB). (**e**) Subcellular localization of NS5B-eGFP (green) in NS5B^{WT}-eGFP- or NS5B^{GND}-eGFP- transduced A549 cells 4 days post transduction (magnification of marked area shown on the right).

way NS5B activates the innate antiviral response in our system, we analyzed IFIT1 expression in NS5B-transduced A549 cell lines where RIG-I or MAVS, a signaling adaptor downstream of both RIG-I and MDA5, had been knocked out through CRISPR/Cas9-mediated deletion. RIG-I knockout completely abrogated IFIT1 expression, suggesting that NS5B activates the innate antiviral response in A549 cells solely through this PRR (Fig. 4a-b). Because functional MAVS is required for RIG-I signaling, its deletion also prevented NS5B-induced IFIT1 expression (Fig. 4b). Furthermore, NS5B was able to activate IFIT1 expression in the immortalized hepatocyte cell line PH5CH[261] (Fig. 4b).

Our data proves that transgene expression of catalytically active NS5B is sufficient to induce antiviral signaling via RIG-I and MAVS.

4.2 NS5B Expression Does Not Maintain a Constant ISG Response

We successfully established NS5B as a molecular tool that is able to activate the antiviral response shortly after transduction. In order to simulate a persistent infection, the system would need to be able to stimulate the RIG-I pathway for an extended period. We therefore examined NS5B and ISG expression over several weeks in NS5B-transduced A549 cells. NS5B mRNA level remained relatively constant over the course of four weeks for both $NS5B^{WT}$ and $NS5B^{\Delta}$, and abrogation of RLR signaling through knockout of MAVS did not affect $NS5B^{WT}$ transcript levels either (Fig. 5a). IFIT1 expression was upregulated ~100-fold in $NS5B^{WT}$-transduced A549 cells in the first week after transduction (Fig. 5b). Surprisingly, however, transcript levels gradually returned to near background over the course of three weeks. Flow cytometry analysis revealed that NS5B protein levels peaked around 4 d.p.t. and then decreased over time until they stabilized at a lower

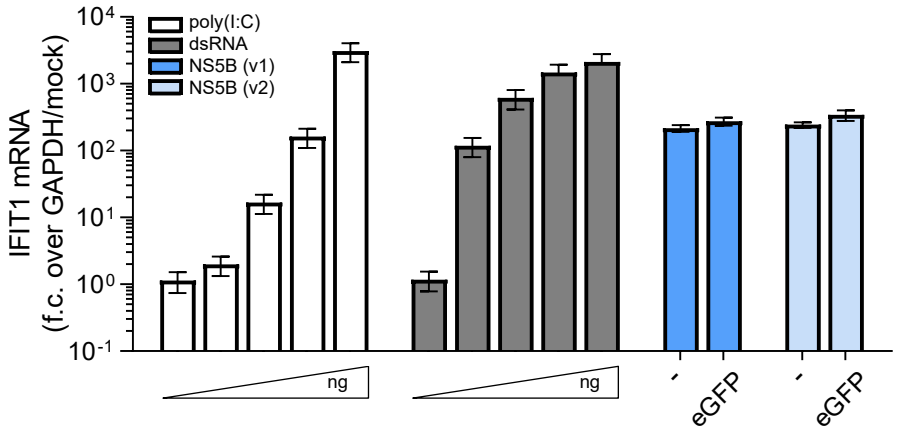

Figure 3: Comparison of NS5B-derived immune response with transfection of RLR agonists.

IFIT1 mRNA level in A549, either 6 hours after transfection with 0, 0.1, 1.0, 10, or 100 ng poly(I:C) or dsRNA, or transduced with untagged $NS5B^{WT}$ (-) or $NS5B^{WT}$-eGFP. Variant 1 (v1), corresponding to $NS5B^{\Delta}$, 5 days post transduction; variant 2 (v2), corresponding to $NS5B^{GND}$, 6 days post transduction. mRNA level fold change (f.c.) was calculated over GAPDH and untreated, non-transduced A549 wild-type cells.

level (Fig. 5c). It is important to note that within the transduced cell pool, NS5B-eGFP signals of individual cells scattered over a range of two magnitudes, indicating huge intercellular differences in NS5B protein levels. IFIT1 protein levels lagged behind with a peak at 8 d.p.t. and intercellular differences were less pronounced. In accordance with mRNA data, IFIT1 protein returned to basal levels three weeks after transduction (Fig. 5d).

The unexpected loss of ISG induction led us to investigate possible causes. For one, the decline in average NS5B protein content per cell could have caused dsRNA concentrations to drop below a threshold level necessary to induce detectable IFIT1 levels. Another potential cause could have been active downregulation of ISG expression through negative feedback regulation. The intensity of the interferon response is amplified at different steps throughout the antiviral signaling cascade and results in the expression of a broad range of proteins. Thus, a tight regulation through negative factors such as inhibitors of the pathway is necessary to keep the system from overshooting.

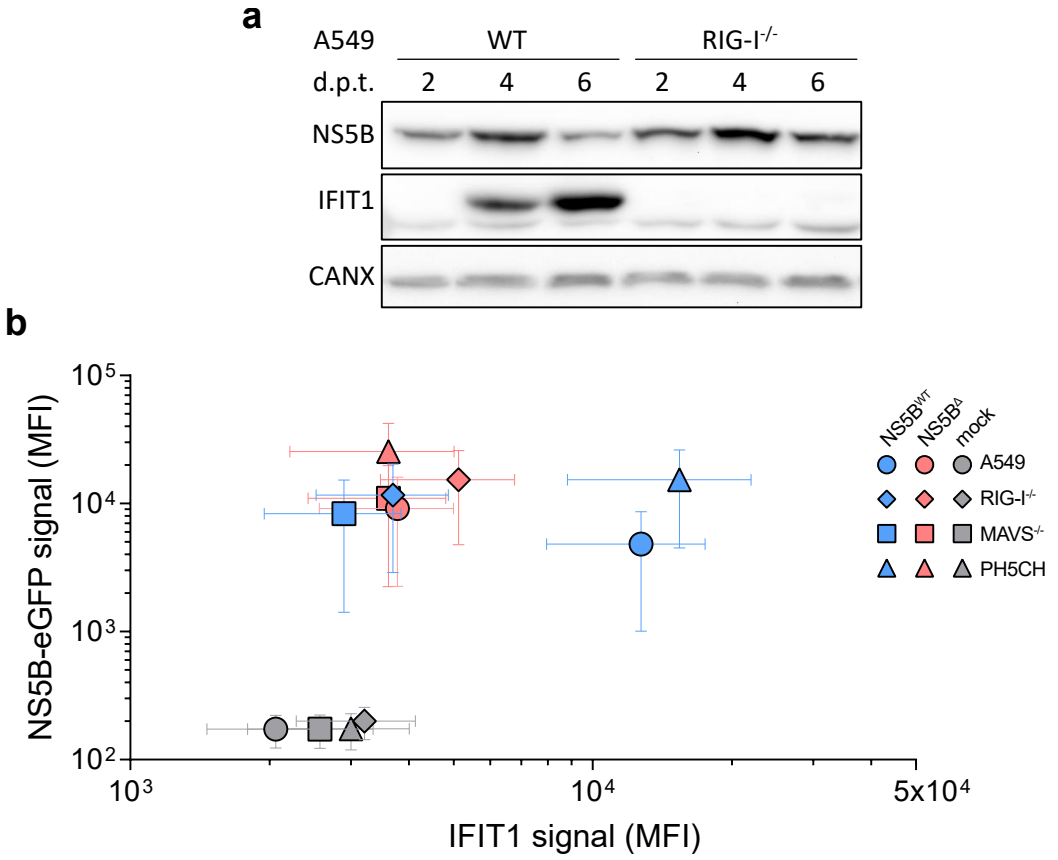

Figure 4: Stimulation of innate antiviral activity by recombinant NS5B depends on functional RIG-I and MAVS.

(**a**) Western blot of NS5B and IFIT1 protein expression in $NS5B^{WT}$-transduced A549 wild-type or RIG-I knockout cells at 2, 4 and 6 days post transduction (d.p.t). Calnexin (CANX) served as loading control. (**b**) NS5B and IFIT1 signal determined by flow cytometry in A549 wild-type, RIG-I knockout or MAVS knockout cells, or PH5CH wild-type cells, 6 days post transduction with $NS5B^{WT}$, $NS5B^{GND}$ or mock. Per cell line, $n > 1.5x10^4$ cells after gating were measured (mean fluorescent intensity (MFI) $\pm$ robust s.d.). NS5B-eGFP levels were directly measured via the eGFP tag, while IFIT1 levels were indirectly measured via staining with anti-IFIT1 (rabbit) primary antibody and anti-rabbit-AlexaFluor647 fluorophore-tagged secondary antibody. Subfigure (a) originally published in [247].

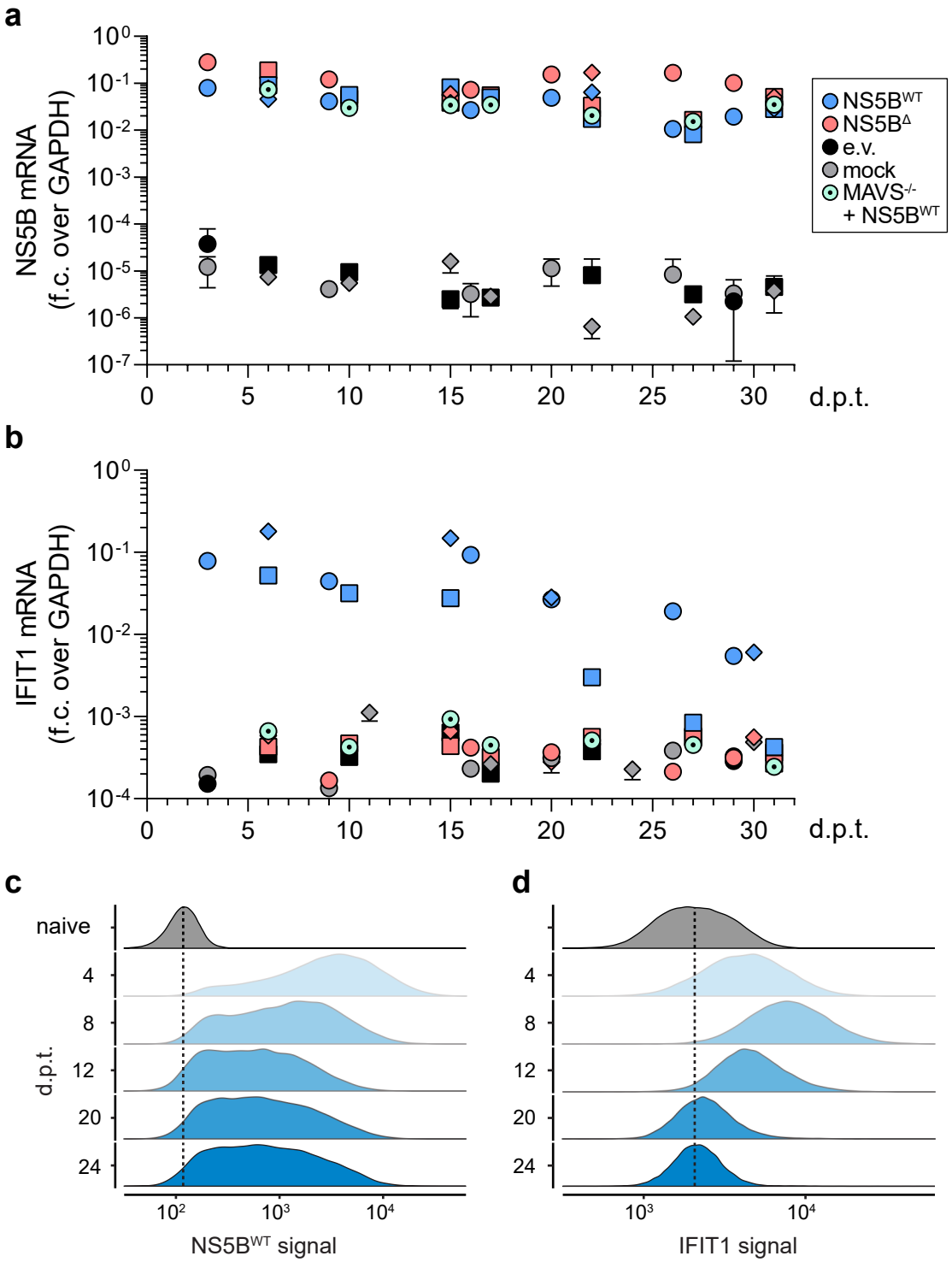

Figure 5: Long-term NS5B expression does not maintain stable ISG expression.

(**a-b**) NS5B (a) and IFIT1 (b) mRNA levels in NS5B^{WT}-, NS5B$^{\Delta}$-, empty vector- (e.v.), or mock-transduced wild-type A549 cells, and NS5B^{WT}-transduced A549 MAVS knockout cells. mRNA level fold changes (f.c.) at the indicated days post transduction (d.p.t.) were calculated over GAPDH. Different data point shapes indicate biological replicates. (**c-d**) NS5B^{WT} (c) and IFIT1 (d) protein levels in A549 transduced with NS5B^{WT} were determined by flow cytometry at the indicated days. Scaled density plots show fluorescent intensity of $n > 1.5x10^4$ transduced cells after gating for each time point, or all time points combined for naïve A549 (dashed line indicates median of naïve A549). Data in this figure was generated together with Katharina Heine (DKFZ, Heidelberg) as part of collaborative work within TRR179. Parts of data in subfigures (a) and (b), and subfigures (c) and (d) were originally published in [247].

We first examined whether continuous NS5B^{WT} expression had led cells to become refractory to the stimulus exerted by NS5B. To determine whether cells were still able to sense a viral infection after prolonged activation of RLR signaling, NS5B-transduced cells were infected with Sendai virus (SeV) at different time points after transduction. SeV is a negative single-strand RNA virus of the *Paramyxoviridae* family[262]. It is not pathogenic for humans, but can infect cancer cell lines and induce a RIG-I-dependent immune response[262–264]. An increase in IFIT1 mRNA levels at all time points suggested that cells were still able to sense viral infections via RIG-I after weeks of NS5B^{WT} expression (Fig. 6a). Moreover, infecting cells with SeV at a low MOI of 0.004 allowed us to detect additive effects of NS5B- and SeV-derived ISG induction. On day 7 after NS5B^{WT} transduction, SeV infection was followed by a ~10-fold increase in IFIT1 transcript levels over baseline levels of SeV infection at later timepoints or in NS5B$^{\Delta}$-transduced A549 (dashed line in Fig. 6a). This supported our earlier observation that NS5B levels reached

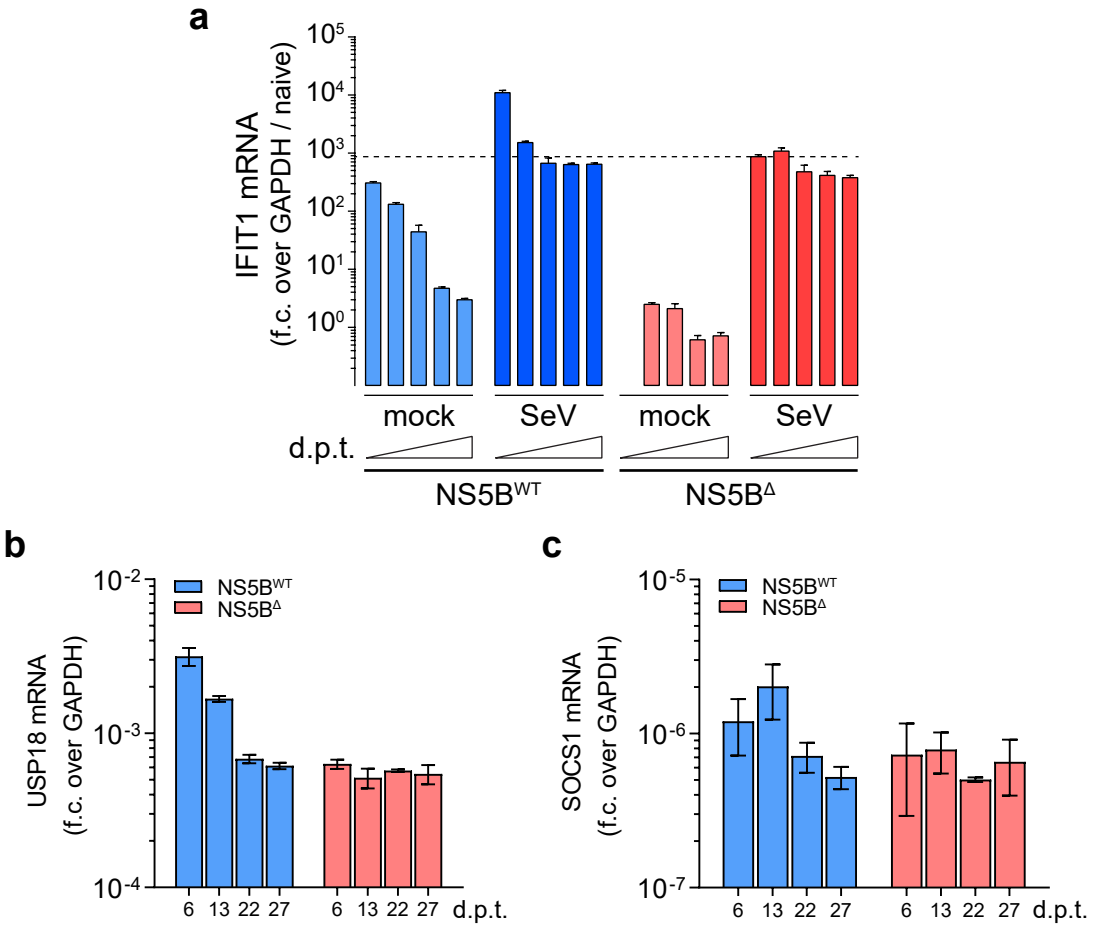

Figure 6: NS5B-expressing cells do not become refractory to stimulation of antiviral signaling.

(**a**) IFIT1 mRNA levels in NS5B^{WT}- or NS5B$^{\Delta}$-transduced A549 cells infected with Sendai Virus (SeV) at 7, 11, 15, 19, and 23 days post transduction (d.p.t.) (mRNA fold change over GAPDH and naïve, uninfected cells). Dashed line indicates IFIT1 mRNA fold change induced by SeV infection alone. (**b-c**) USP18 (b) and SOCS1 (c) mRNA levels in NS5B^{WT}- or NS5B$^{\Delta}$-transduced A549 cells, 6 to 27 days post transduction. mRNA fold change (f.c.) was calculated over GAPDH. Data in subfigure (a) was generated by Katharina Heine (DKFZ, Heidelberg) and originally published in [247]. Data in subfigures (b) and (c) were generated together with K. Heine as part of collaborative work within TRR179.

early after transduction do not produce RIG-I-saturating amounts of dsRNA (Fig. 3).

We next assessed whether inhibitors of interferon sensing were affected by NS5B activity. USP18 negatively regulates IFN signaling by rendering the IFN type I receptor IFNAR unresponsive to IFN-α[90, 138]. mRNA levels of USP18 were elevated 6 days after transduction with NS5B^{WT}, but returned to basal levels after three weeks, following the same trend as IFIT1 (Fig. 6b). Likewise, SOCS1, which inhibits IFN signaling by preventing JAK1-mediated tyrosine phosphorylation downstream of IFN type I and III receptors[90], was slightly upregulated early after transduction, but also here mRNA levels returned to basal levels (Fig. 6c).

Finally, we performed a mass spectrometry-based unbiased whole-proteome analysis of NS5B-transduced A549 cells at different days post transduction. Compared to NS5B$^{\Delta}$-transduced cells, 67 proteins were significantly upregulated 6 days post transduction with NS5B^{WT}, however, the number diminished over the course of three weeks (Fig. 7a, Fig. S2). We compared NS5B^{WT}-transduced cells to A549 cells treated for two weeks with 8.25 ng/mL IFN-α (Fig. 7b-c). Interestingly, IFN-α-treated cells did not exhibit a gradual decline in the number of significantly upregulated proteins. Hierarchical clustering of proteins upregulated in NS5B^{WT}-expressing cells 6 d.p.t. revealed four distinct clusters that could be separated based on temporal changes in protein levels (Fig. 7b,d; Fig. S3). IFN-α treatment resulted in the upregulation of a majority of proteins that were also upregulated in NS5B^{WT} (Fig. 7d). Conversely, there were no proteins detected that were specifically upregulated by IFN-α but not by NS5B^{WT}.

NS5B^{WT} was significantly upregulated on days 6, 12, and 24 post transduction compared to NS5B$^{\Delta}$ protein levels (Fig. 7b; Fig. S2), underlining the differences described earlier (Fig. 1). Apart from NS5B^{WT} itself, six proteins were specifically upregulated in NS5B^{WT}-transduced cells, but not in IFN-α treated cells. Those included two MHC class I proteins of HLA groups B and C, respectively, while other class I HLAs of groups A, B and C were upregulated also by IFN-α. Temporal regulation of cluster of differentiation (CD38) and three prime repair exonuclease 1 (TREX1) was very similar to NS5B^{WT} (cluster 2). CD38 is a receptor and a multifunctional ecto-enzyme involved in, among others, extracellular nucleotide homeostasis, Ca^{2+} signaling, and in the establishment of an effective immune response[265, 266]. TREX1 is a 3' -> 5' DNA exonuclease implicated in DNA proofreading and DNA degradation during granzyme A-mediated cell death[267]. Impaired exonuclease activity of TREX1 resulted in the cytosolic accumulation of immunostimulatory DNA molecules[268]. Another protein selectively upregulated in NS5B^{WT}-expressing A549 cells was the chaperone PET100 that acts in the formation of complex IV, also known as cytochrome C oxidase, of the mitochondrial electron transportation chain[269]. Transmembrane protein 63B (TMEM63B), an osmosensitive Ca^{2+} channel[270, 271], was upregulated in NS5B^{WT} cells in a similar fashion to PET100.

Genes upregulated by both NS5B^{WT} and IFN-α are dominated by known ISGs. Cluster 1 and 2 behaved rather similar and protein levels returned to baseline at day 18. Cluster

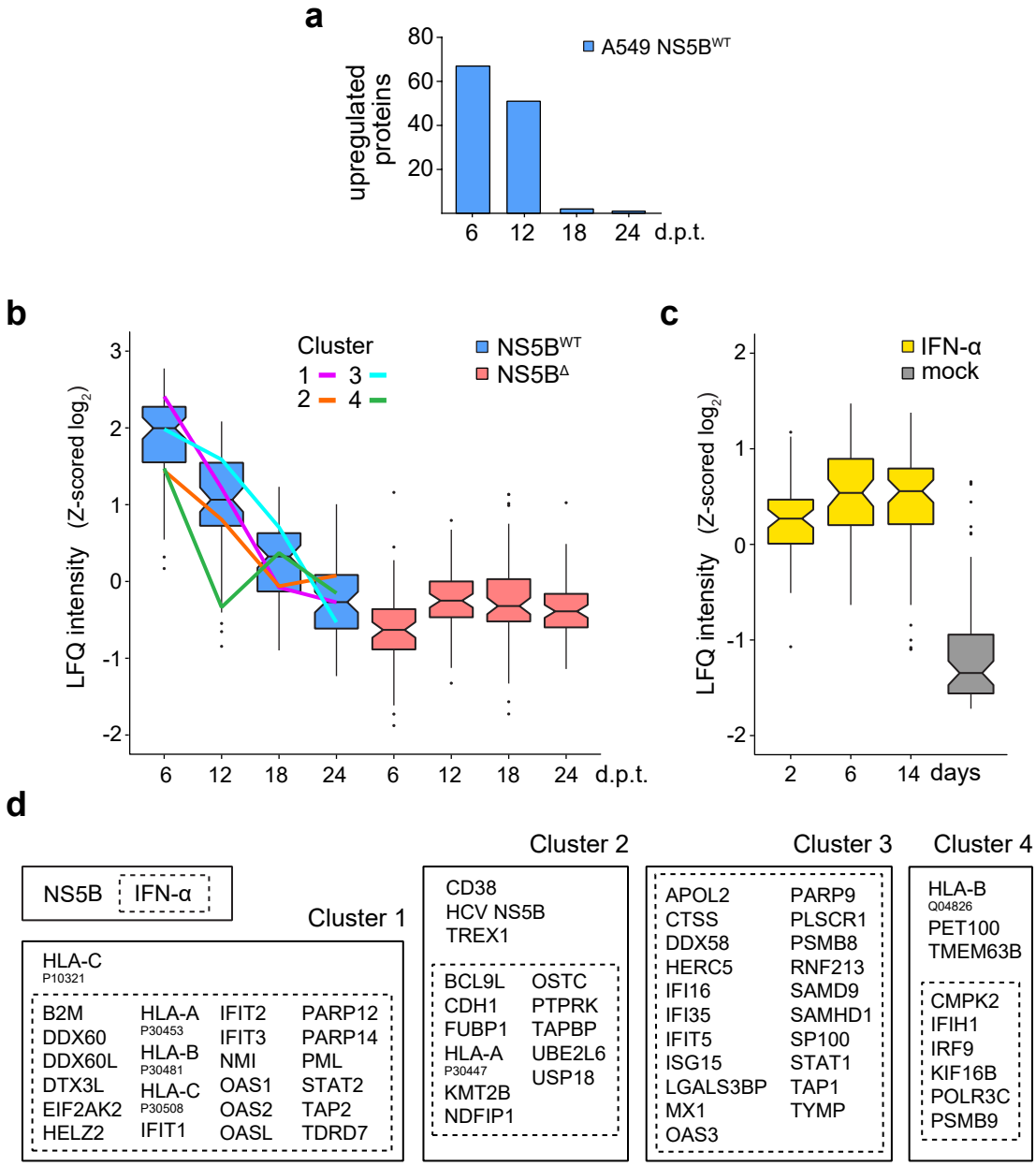

Figure 7: Time-resolved proteome analysis of NS5B-transduced or IFN-α-treated A549 cells.

(**a**) Number of significantly upregulated proteins at the indicated days post NS5B^{WT} transduction as compared to NS5B$^{\Delta}$ (two-tailed Student's t-test, S0 = 1, permutation-based FDR < 0.01, n = 4 technical replicates). Volcano plots containing all significantly regulated proteins at each time point are shown in Fig. S2. (**b-c**) Box and whisker plots (median; hinges: 1st and 3rd quartiles; whiskers: ± 1.5 x inter-quartile-range) of Z-scored median $\log_2$ label-free quantification (LFQ) intensities of proteins, significantly upregulated at 6 days post NS5B^{WT} transduction, tracked over time in NS5B^{WT}- and NS5B$^{\Delta}$-transduced (b) cells, or in IFN-α- (8.25 ng/mL every three days) and mock-treated (c) cells. Hierarchical clustering (Euclidean distances, Ward agglomeration method) of Z-scored $\log_2$ LFQ intensities of these proteins in NS5B^{WT}-transduced cells across time points identified four main clusters of differentially upregulated proteins (cluster 1, pink; cluster 2, orange; cluster 3, light blue; cluster 4, green). A detailed heat-map of all clusters is shown in Fig. S3. (**d**) Intersection of upregulated proteins at day 6 post NS5B^{WT} transduction (solid box) with data of IFN-treated cells (dashed box). NS5B transduction experiment and sample generation performed together with Katharina Heine (DKFZ, Heidelberg) as part of collaborative work within TRR179. IFN-α treatment experiment and mass spectrometry analysis of all samples performed by Christian Urban and Andreas Pichlmair (Technical University Munich). Figure adapted from joint publication [247].

1 contained many proteins involved in antigen presentation (HLA-A, -B, -C) and proteins involved in binding and degradation of nucleic acids (DDX60, DDX60L, EIF2AK2, IFIT1, IFIT2, IFIT3, OAS1, OAS2, OASL)[247]. Cluster 3 exhibited the slowest downregulation over time, reaching baseline levels after 24 days. Negative regulators of IFN signaling such as N-Myc and STAT interactor (NMI; cluster 1), UBE2L6 and USP18 (cluster 2), IFI35, ISG15, and lectin galactoside-binding soluble 3-binding protein (LGALS3BP; cluster 3), were spread over the three clusters[142,247,272]. Cluster 4 experienced the fastest reduction in protein levels with baseline levels reached already 12 days after transduction. It contained ISGs MDA5 (encoded by IFIH1) and IRF9, which is involved in IFN receptor downstream signaling[89], but no negative regulators of either RLR or IFN signaling.

Proteome profiling of NS5B-expressing cells revealed a response very similar to the response to IFN-α. The overall reduction in significantly regulated genes, including negative immune signaling regulators, suggested that negative regulation of RLR or IFN signaling was not involved in the loss of ISG response in NS5B^{WT}-expressing A549 cells.

4.3 IFN-λ1 Expression Positively Correlates with NS5B^{WT} Protein Levels

After we had ruled out downregulation of ISG expression through endogenous inhibitors, we switched focus to examine in more detail NS5B expression levels in our cell culture system. We previously had observed that NS5B levels varied greatly between cells (Fig. 5c). Flow cytometry-based measurement of both NS5B-eGFP as well as IFIT1 protein levels on a single cell level confirmed this variety for cells transduced with NS5B^{WT} as well as NS5B$^{\Delta}$ (Fig. 8a). Significant numbers of cells with elevated IFIT1 protein levels could only be detected for NS5B^{WT}-transduced cells and made up about 35 % of the population. Interestingly, instead of clearly defined IFIT1-positive and IFIT1-negative subpopulations, the cell pool showed a high variability in IFIT1 protein levels. We observed that cells expressing NS5B^{WT} at very high levels and cells without detectable NS5B^{WT} experienced a very similar distribution of IFIT1 signals. We therefore argued that on a single cell level, IFIT1 expression is independent of NS5B protein levels. Since IFIT1 is a classical ISG, it was reasonable to assume that its expression was induced by paracrine signaling, most likely through secreted interferons.

We wondered how different NS5B protein levels would affect production of interferons. To test this, we separated via fluorescence-activated cell sorting (FACS) NS5B^{WT}-expressing cells based on NS5B-eGFP signal into several subpopulations (Fig. 8b-c). Indeed, mRNA levels of IFN-λ1 positively correlated with NS5B protein levels in the subpopulations (Fig. 8d). Population 6, containing the cells with the highest NS5B content and making up 2 % of the whole cell population, showed a ~15-fold increase in IFN-λ1 transcript levels over the NS5B^{WT} cell pool. We then tested the antiviral potency of supernatant from NS5B-expressing cells in a more general approach. Here, Huh7 cells stably replicating a

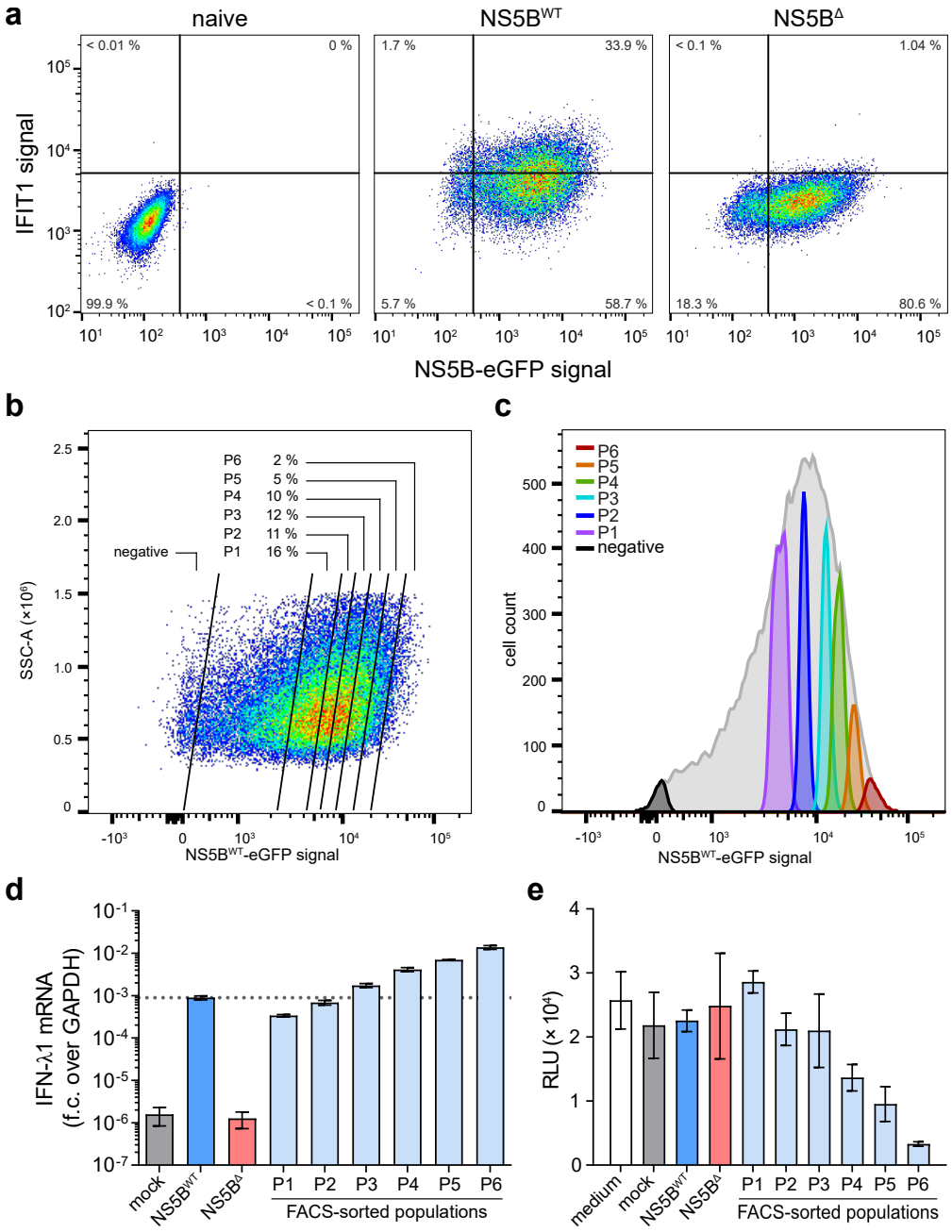

Figure 8: Expression levels of NS5B and IFN-λ1 correlate on a single cell level.

(**a**) Fluorescent signal intensity of NS5B-eGFP and IFIT1 in naïve A549 cells or 5 days after transduction with NS5B^{WT}-eGFP or NS5B$^{\Delta}$-eGFP. Data of n > 1.5x10^4 cells after gating was acquired by flow cytometry and plotted as a heat-map scatter plot (event density: blue, low; red, high). Quadrant gates separate double negative cells (bottom left), NS5B-positive (bottom right), IFIT1-positive (top left) and double positive (top right) cells. (**b**) Fluorescence-activated cell sorting (FACS) of A549 cells 6 days post transduction with NS5B^{WT}-eGFP. Acquired GFP fluorescence intensity was plotted against side scatter area (SSC-A), and sorting gates (black lines) were set to separate cells into six populations of different NS5B expression levels (P1-P6; total percentage is indicated) as well as cells negative for NS5B signal. (**c**) Histograms of GFP levels in each sorted population. (**d**) IFN-λ1 mRNA levels in NS5B^{WT}-, NS5B$^{\Delta}$-, or mock-transduced A549 cells 8 days post transduction as well as in the FACS-sorted populations 2 days after sorting. mRNA fold change (f.c.) was calculated over GAPDH. Dashed line indicates IFN-λ1 mRNA level in NS5B^{WT}-transduced A549 cell pool. (**e**) Luciferase activity in LucUbiNeo cells treated with medium or supernatant from NS5B^{WT}-, NS5B$^{\Delta}$-, or mock-transduced A549 cells, or supernatant from FACS-sorted populations of NS5B^{WT}-transduced A549 cells harvested 2 days post sorting (relative light units (RLU) mean ± s.d. of n = 2 technical replicates). Data in subfigure (a) generated together with Katharina Heine (DKFZ, Heidelberg) as part of collaborative work within TRR179. Subfigures (b)–(d) originally published in [247].

luciferase-expressing HCV reporter replicon (Huh7 LucUbiNeo[252]) were cultured in supernatant harvested from the sorted subpopulations. A decrease in luciferase signal represented a decrease in replicon replication and indicated the presence of antiviral agents. In fact, reduction of replication by NS5B-derived supernatant positively correlated with NS5B protein levels in the donor subpopulations (Fig. 8e). Taken together, we concluded that ISG induction in the majority of cells was predominantly triggered through paracrine signaling factors, such as interferons, that are in large part produced by a minority of NS5B high-expressing cells.

4.4 FACS-Based Enrichment Does Not Stabilize NS5B High-Expressing Subpopulation

We previously had established that cells expressing high levels of NS5B also produced high levels of IFN-λ1. Long-term single cell NS5B expression data, however, suggested that those cells disappeared over the course of three weeks (Fig. 5c). It was not clear at this point whether these cells disappeared, e.g. because of cell death or other disadvantages that led to counterselection, or if transgene expression was downregulated over time. Regardless, we hypothesized that loss of NS5B high-expressing cells resulted in an overall decrease in interferon concentration that would subsequently lead to a reduction of ISG levels.

To test this, we aimed to stabilize the NS5B high-expressing subpopulation by repeated FACS-based enrichment. A549 cells were sorted 4 days post transduction with $NS5B^{WT}$ (Fig. 9a), and only NS5B high-expressing cells were kept in culture. Surprisingly, six days after sorting (10 d.p.t.) the cell population again showed a huge spread in NS5B protein level, indicating that NS5B transgene expression on a single cell level was subject to varying degrees of downregulation (Fig. 9b). Although cells were sorted again at 10, 17, and 24 d.p.t., the overall distribution of NS5B protein exhibited a shift to a lower average level (Fig. 9c). Total NS5B protein levels decreased despite sorting, and IFIT1 protein was not detected by immunoblotting at 17 d.p.t. (Fig. 9d). Quantification of mRNA levels confirmed the decrease in expression of NS5B, IFIT1, and the ISG MX1 (Fig. 9e-g).

The downregulation of NS5B expression could not be fully attributed to NS5B activity, since $NS5B^{\Delta}$ and $NS5B^{GND}$ cells exhibited similar behavior over time (data not shown). We suspected that the loss of NS5B high-expressing cells could at least in part have been caused by downregulation of transgene expression. We concluded that repeated enrichment is unable to stabilize the subpopulation of NS5B high-expressing cells that seemed to be required for successful ISG induction.

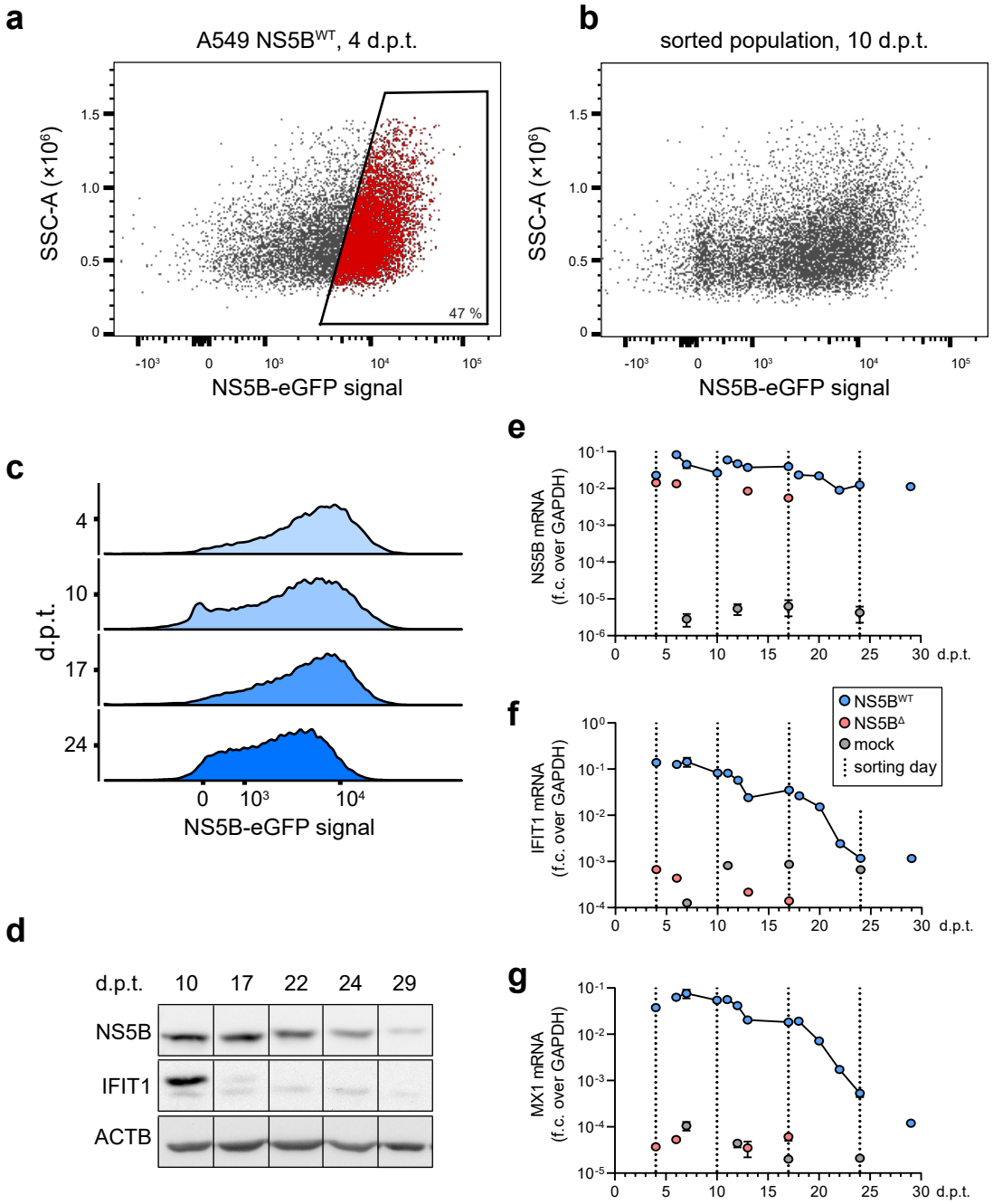

Figure 9: Repeated FACS sorting does not stabilize the NS5B high-expressing A549 subpopulation.

(**a**) Scatter plot of NS5B-eGFP signal and side scatter area (SSC-A) signal in NS5B^{WT}-transduced cells 4 days post transduction (d.p.t.). Gate (black box) indicates cells that were sorted (red) and kept in culture. (**b**) Scatter plot of cells sorted in (a) and kept in culture until 10 d.p.t. (**c**) Scaled density plots show distribution of NS5B^{WT}-eGFP protein levels at the indicated time points before FACS-sorting (sorting gate was set as indicated in (a)). NS5B^{WT}-eGFP signal was determined by flow cytometry. Y-axis shows normalized cell numbers. (**d**) Western blot of NS5B and IFIT1 protein expression in NS5B^{WT}-transduced A549 cells at the indicated time points before sorting. Actin (ACTB) served as a loading control. Samples from indicated time points were detected on the same membrane. (**e-g**) NS5B (e), IFIT1 (f) and MX1 (g) mRNA levels in A549 cells at the indicated time points after NS5B^{WT}-, NS5B$^{\Delta}$-, or mock-transduction. NS5B^{WT}-transduced cells were sorted at 4, 10, 17, and 24 d.p.t. (dashed lines), and RNA was collected before sorting. Data generated together with Katharina Heine (DKFZ, Heidelberg) as part of collaborative work within TRR179.

4.5 NS5B^{WT} Expression Elicits Cytotoxic and Cytostatic Effects

To elucidate whether NS5B^{WT}-expressing cells were counterselected, we further investigated their behavior over time. Interestingly, monitoring cell growth by continuous live cell imaging revealed that both A549 and PH5CH cells exhibited a strong cell growth defect 5 days post transduction with NS5B^{WT} (Fig. 10a-b). Since this phenotype coincided with elevated ISG levels and was not observed at later time points after transduction (from 14 d.p.t. onwards; data not shown), we wondered whether RLR signaling was involved. Depletion of MAVS through CRISPR/Cas9-mediated gene knockout completely restored cell growth in NS5B^{WT}-transduced A549 cells (Fig. 10c). Likewise, overexpression of the HCV protease NS3/4A, which targets MAVS for cleavage[103, 104], resulted in restoration of normal cell growth in cells co-transduced with NS5B^{WT} (Fig. 10d). Conversely, overexpression of the catalytically inactive NS3/4A mutant S139A (NS3/4A^{mut}) did not affect the NS5B^{WT}-related cell growth phenotype. Similar to MAVS knockout, CRISPR/Cas9-mediated deletion of IRF3, a transcription factor downstream of MAVS, was able to prevent the NS5B-derived growth defect. This data suggested that functional RLR signaling via MAVS and IRF3 is required for NS5B-related cell growth impairment.

We wondered whether the impaired cell growth was a result of cytostatic effects, cytotoxic effects, or a combination of both. To monitor cell death events during live cell imaging, cells were cultured in the presence of the nucleic acid dye Cytotox Green (CG). As cell membrane integrity decreases during cell death progression, CG can pass the cell membrane and bind to cellular DNA. NS5B^{WT}-transduced A549 cells exhibited slightly increased cell death rates, typically peaking between 5 % to 15 % in the period of 24-48 hours after seeding (Fig. 11a-b). Later, cells recovered as the fraction of dead cells slowly decreased.

MAVS had been previously reported to be involved in the induction of cell death[229, 230], and the fact that its deletion fully rescued cell growth would support a MAVS-related induction of cell death in NS5B-transduced A549. The fact, however, that an IRF3 knockout in cells with functional MAVS restored cell growth suggested that the observed cell death had to be independent of cell death-related functions of MAVS. IRF3 as well has been implicated in the induction of cell death through a pathway termed RIG-I-like receptor-induced IRF3-mediated pathway of apoptosis (RIPA)[231]. Here, IRF3 receives linear polyubiquitination through the LUBAC complex involving, among others, MAVS TRAF2, and TRAF6[231, 247]. This modification facilitates the recruitment of IRF3 and BAX to the mitochondrial membrane, which triggers the release of pro-apoptotic factors such as cytochrome C and the subsequent activation of caspase 9[231, 247]. Both MAVS- and IRF3-mediated cell death involves caspase activity[61, 229, 231]. Treatment of NS5B-expressing A549 cells with the pan-caspase inhibitor ZVAD-FMK did not affect cell growth (Fig. 11c). It is known that cells with an impaired apoptosis may activate alternative modes of cell

death such as necroptosis[221]. We therefore treated NS5B-transduced A549 cells with a combination of ZVAD-FMK and the necroptosis inhibitor Nec7. The combined treatment exerted a further decrease in cell growth that might be due to cytotoxic properties of Nec7; a positive effect on cell growth in NS5B^{WT}-transduced cells, however, could not be observed (Fig. 11d).

As noted before, cell growth defects in NS5B-transduced cells were only observed early

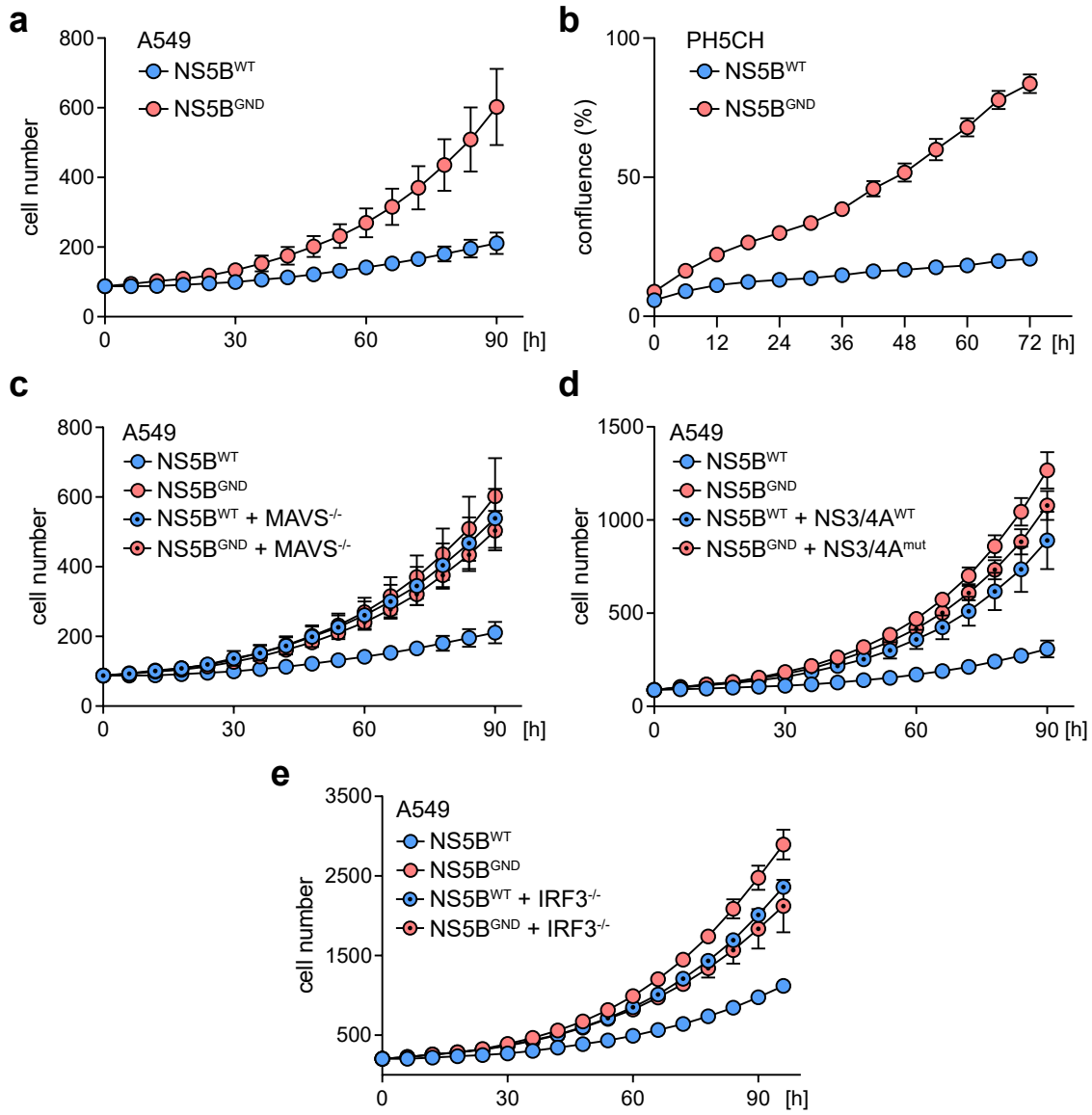

Figure 10: NS5B activity reduces cell growth in cells with functional MAVS and IRF3.

(**a-b**) Cell growth of NS5B^{WT}- or NS5B^{GND}-transduced A549 (a) and PH5CH (b) cells as determined by live cell imaging (mean ± s.d. of n = 5 technical replicates). One representative of n = 4 independent experiments is shown. (**c**) Cell growth of NS5B^{WT}- or NS5B^{GND}-transduced A549 wild-type or MAVS knockout cells (mean ± s.d. of n = 5 technical replicates). One representative of n = 3 independent experiments is shown. (**d**) Cell growth of NS5B^{WT}- or NS5B^{GND}-transduced and NS3/4A^{WT}- or NS3/4A^{mut}-transduced A549 cells (mean ± s.d. of n = 3 technical replicates). One representative of n = 3 independent experiments is shown. (**e**) Cell growth of NS5B^{WT}- or NS5B^{GND}-transduced A549 wild-type or IRF3 knockout cells (mean ± s.d. of n = 5 technical replicates). One representative of n = 3 independent experiments is shown. Data originally published in [247].

after transduction, when NS5B expression in the cell pool was high enough to trigger RLR signaling and subsequent ISG induction. We therefore investigated the effect of

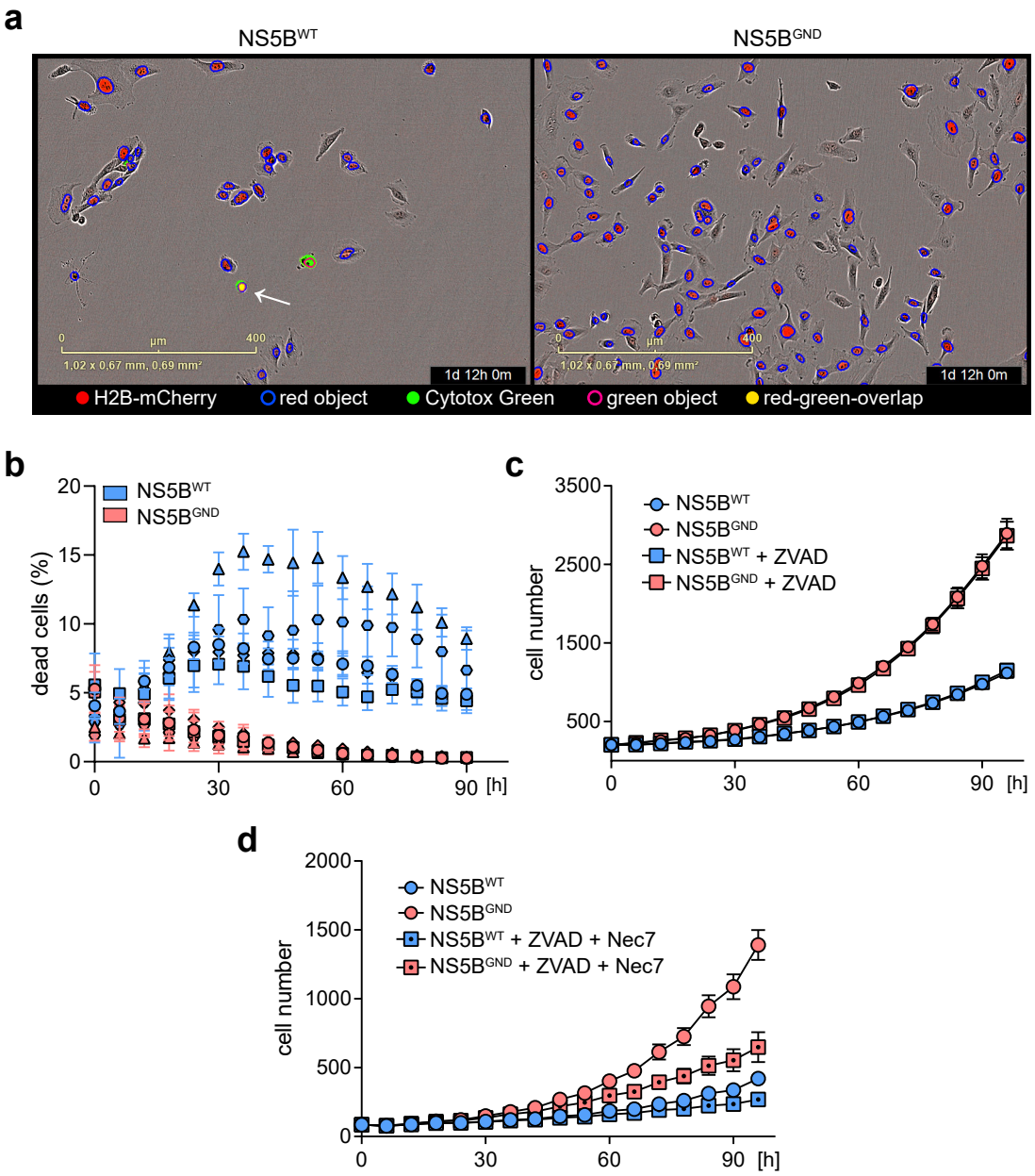

Figure 11: Caspase-mediated cell death does not have a major impact on NS5B-related cell growth reduction.

(**a**) Live cell images of NS5B^{WT}- or NS5B^{GND}-transduced A549 cells 36 hours after seeding (6.5 days post transduction). Image analysis detected individual cells as red objects (marked with blue circles) based on nuclear localization of transgenically expressed, mCherry-tagged histone 2B (H2B-mCherry; red). Dead or dying cells were detected as green objects (pink circles) by Cytotox Green staining (green). Cells positive for both H2B-mCherry and Cytotox Green (arrow) were accounted for by detection as overlap events (yellow). (**b**) Fraction of dead A549 cells transduced with NS5B^{WT} or NS5B^{GND} (mean ± s.d. of n = 4 technical replicates). Data point shapes indicate n = 5 individual experiments. (**c**) Cell growth of NS5B^{WT}- or NS5B^{GND}-transduced A549 cells treated with Z-VAD-FMK (ZVAD, 40 µM, in DMSO) or DMSO control (0.2 % (v/v)) (mean ± s.d. of n = 4 technical replicates). One representative of n = 2 independent experiments is shown. (**d**) Cell growth of NS5B^{WT}- or NS5B^{GND}-transduced A549 cells treated with Z-VAD-FMK (ZVAD, 40 µM) and Necrostatin-7 (Nec7, 10 µM; in DMSO) or DMSO control (0.2 % (v/v)) (mean ± s.d. of n = 4 technical replicates). One representative of n = 2 independent experiments is shown. Data in subfigures (c) and (d) originally published in [247].

NS5B expression levels on cell growth by live cell imaging of A549 cells transduced with different dilutions of NS5B coding lentivirus particles. As expected, increasing lentivirus dilution during transduction led to a reduction in NS5B mRNA levels (Fig. 12a). The decrease in overall NS5B expression correlated with a decrease of the observed growth defect (Fig. 12b). Cell growth recovered at a dilution factor of 1:4. Of note, transduction with undiluted lentiviral particles alone had a negative effect on cell growth independently of NS5B activity, as cells transduced with $NS5B^{GND}$ also exhibited slightly reduced cell growth. The severity of cell growth impairment positively correlated with the expression levels of IFN-λ1 (Fig. 12c). Interestingly, cells transduced with $NS5B^{WT}$ at a dilution factor of 1:4 exhibited undisturbed growth while IFN-λ1 transcript levels were about two magnitudes higher compared to mock-transduced cells. IFIT1 mRNA levels on the other hand did not display a correlation with NS5B expression (Fig. 12d).

In summary, expression of $NS5B^{WT}$ results in reduced cell growth rate that correlates with NS5B and IFN-λ1 mRNA expression. $NS5B^{WT}$-expressing cells furthermore exhibit cell death that seemed to be independent of caspase activity. Due to its low frequency, we estimated cell death not to be the sole cause for the observed growth defect.

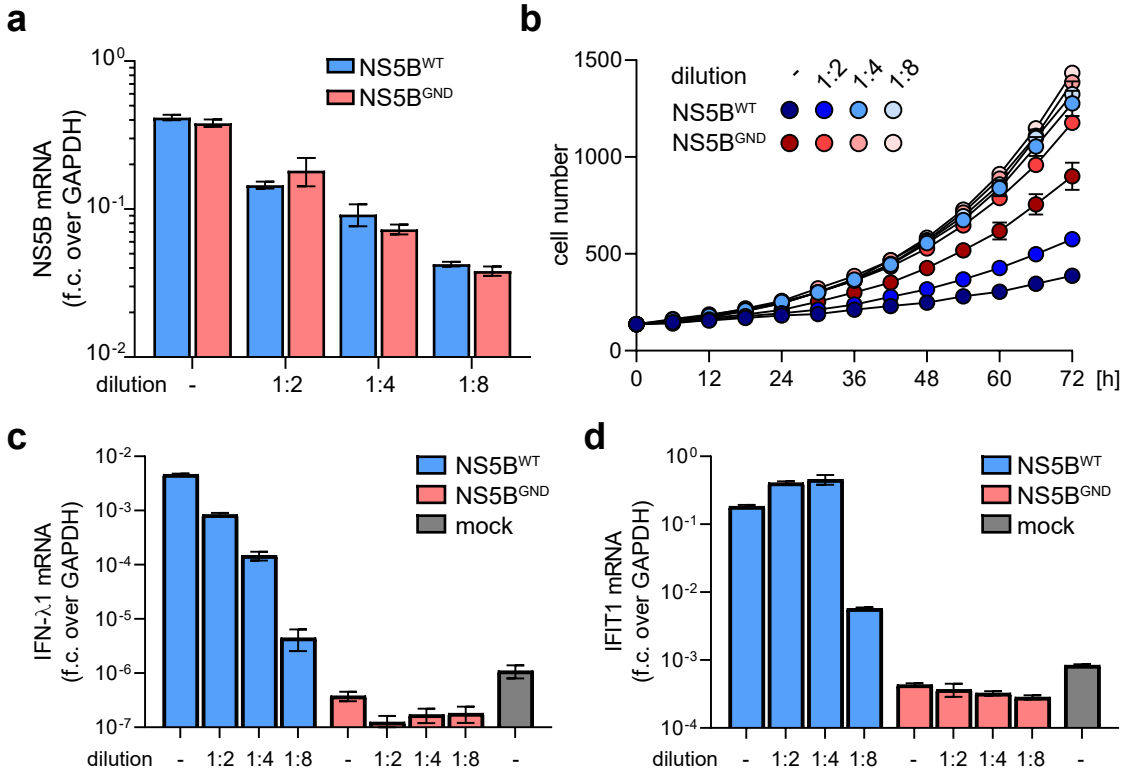

Figure 12: Severity of NS5B-induced growth defect correlates with NS5B and IFN-λ1 expression levels.

(**a**) NS5B mRNA levels in A549 cells 5 days post transduction with $NS5B^{WT}$ or $NS5B^{GND}$ at increasing lentivirus dilutions (fold change (f.c.) over GAPDH, mean ± s.d. of n = 3 technical replicates). (**b**) Cell growth of A549 cells transduced with $NS5B^{WT}$- or $NS5B^{GND}$-expressing lentivirus at increasing dilution (mean ± s.d. of n = 4 technical replicates). (**c-d**) IFN-λ1 (c) and IFIT1 (d) mRNA levels in A549 cells 5 days after transduction with $NS5B^{WT}$ or $NS5B^{GND}$ at increasing lentivirus dilutions (fold change (f.c.) over GAPDH, mean ± s.d. of n = 3 technical replicates). Subfigures (a) and (c) originally published in [247].

4.6 NS5B^{WT} Expression Induces Cytostasis via Paracrine Signaling

At the start of this work, we aimed to simulate a persistent viral infection in cell culture. Single cell analysis of NS5B-transduced cells revealed that cells were expressing NS5B to varying degrees and were producing different amounts of IFN-λ. Intriguingly, this distribution may reflect the situation in an infected organ: only a subset of cells is infected, and infected cells differ in stage of viral life cycle and magnitude of antiviral response. Evidence collected so far suggested that cells expressing NS5B at high levels also produce the highest amounts of immunostimulatory factors, and that the observed cytostatic response correlated with the magnitude of expression of these factors.

Although NS5B was successfully employed as a molecular tool to activate a cells antiviral response, we were not able to stabilize this activation over a longer period. We therefore shifted our focus to study the effects of a persistent infection on uninfected cells, termed "bystander" cells. In the infected organ, those cells would receive continuous stimulation through cytokines and other factors secreted by infected cells in their proximity. To translate this situation to our cell culture system, we tested different approaches to continuously provide naïve cells serving as bystanders with the factors secreted from cells with activated RLR signaling.

The first approach aimed at replenishing the subpopulation of NS5B high-expressing cells in a co-culture system with naïve bystander cells. Using FACS, we recovered from A549 cells freshly transduced with NS5B^{WT}-eGFP the top 2 % fraction with the highest NS5B protein levels. These cells were then co-cultured with naïve A549 at different ratios, and two days later NS5B-eGFP and IFIT1 protein levels on single cell level were determined with flow cytometry (Fig. 13a). Increasing the fraction of NS5B^{WT}-expressing cells resulted in an increase in cells with elevated IFIT1 levels. Although the approach was – in principle – able to achieve the aim of presenting bystander cells with immunomodulating agents, we recognized several technical downsides. For one, even at an NS5B cell fraction of 10 %, the majority of bystander cells was negative for IFIT1 (Fig. 13a, right panel). Increasing the fraction of NS5B cells further would render the approach obsolete once NS5B cells would make up the majority of the cell pool. Furthermore, naïve and NS5B-expressing cells would have to be separated again before further analysis, making the approach technically challenging. Finally, repeated sorting for a very small fraction of cells requires large scale production of lentiviral particles to ensure the required yield of NS5B high-expressing cells. This point is exacerbated by the fact that FACS sorting poses a major stress factor to cells, reducing cell survival and yield even further.

To avoid the need for regularly sorting of NS5B cells, we tested a transwell co-culture system. Here, naïve A549 cells were continuously passaged in cell culture dishes while being in close proximity to recently NS5B-transduced cells in the transwell insert (Fig. 13b). The transwell membrane separated both cell populations while allowing secreted factors

to transfer from NS5B-transduced cells to the bystander cells in the bottom well. We regularly exchanged NS5B-expressing cells with newly transduced cells to ensure continuous production of stimulatory factors. RNA analysis revealed that this co-culture system achieved stable induction of IFIT1 in naïve bystander cells over the course of three weeks (Fig. 13c). With ~100-fold upregulation, IFIT1 levels were in the same range as observed before in NS5B^{WT}-transduced cells (Fig. 3). Compared to the FACS-based replenishment approach, the transwell co-culture system greatly reduced workload and material cost while allowing for continuous paracrine stimulation of bystander cells.

A weakness of the transwell system, however, was the incompatibility with long-term live cell imaging, as the transwell membranes disrupted automatic focusing. To study the effect of messenger molecules secreted by NS5B^{WT}-transduced cells on cell growth, we

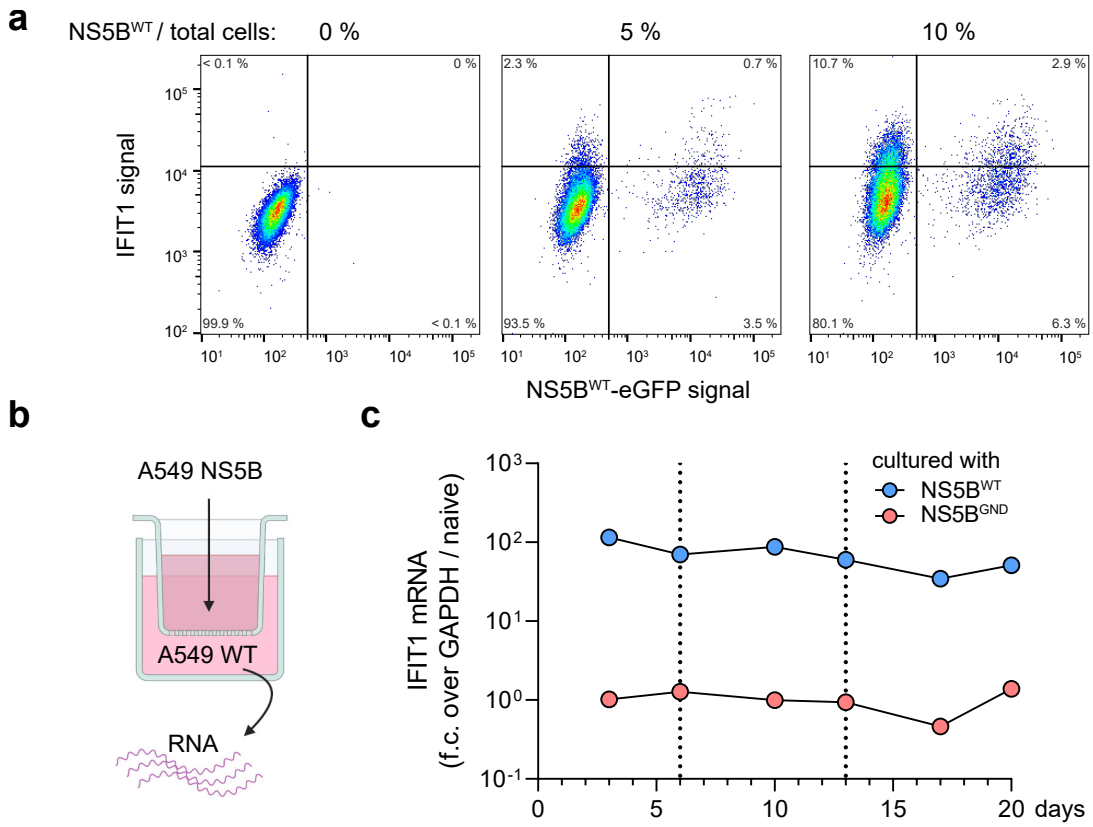

Figure 13: Approaches to maintain constant stimulation of naïve bystander cells by NS5B-derived immune stimulatory factors.

(**a**) Scatter plots of NS5B-eGFP and IFIT1 fluorescence signal in A549 wild-type cells co-cultured with NS5B^{WT}-transduced A549 cells. NS5B-transduced cells had been sorted for high NS5B expression (top 2 % of whole population; data not shown) 5 days post transduction and were co-cultured with wild-type A549 at the indicated ratios for two days before flow cytometry analysis. Data of $n > 1.5x10^4$ cells after gating was acquired by flow cytometry and plotted as a heat-map scatter plot (event density: blue, low; red, high). Quadrant gates indicate double negative cells (bottom left), NS5B-positive (bottom right), IFIT1-positive (top left) and double positive (top right) cells. (**b**) Wild-type A549 cells were continuously passaged in a cell culture dish, while NS5B^{WT} or NS5B^{GND} cells in the transwell insert above were routinely exchanged with freshly transduced cells. RNA was harvested from wild-type cells in the bottom well. (**c**) IFIT1 mRNA levels in A549 wild-type cells cultured in a transwell system together with A549 cells 2 days after transduction with NS5B^{WT} or NS5B^{GND}. NS5B-transduced cells were exchanged at days 6 and 13 of the experiment (dashed lines). mRNA levels were calculated over GAPDH and A549 wild-type cells co-cultured with mock-transduced A549 (mean $\pm$ s.d. of $n = 3$ technical replicates).

chose the simpler alternative of supernatant transfer. Here, supernatant from recently NS5B-transduced cells was harvested, sterile-filtered and then used as culture medium for naïve cells. We cultured NS5B-transduced A549 cells for 48 h in complete DMEM before harvesting the supernatant on day 5 post transduction. Subsequently, naïve cells were cultured in the supernatant for four days while cell growth and cell death were monitored via live cell imaging. Both A549 and PH5CH wild-type cells exhibited reduced growth rates in supernatant from $NS5B^{WT}$-transduced cells (Fig. 14a,c). As opposed to cells expressing $NS5B^{WT}$, cell lines only receiving NS5B-derived supernatant did not exhibit elevated cell death rates (Fig. 14b,d). We previously showed that deletion of MAVS or IRF3 was able to restore cell growth in $NS5B^{WT}$-transduced cells. When cultured in $NS5B^{WT}$-derived supernatant, however, both knockout cell lines experienced reduced cell growth (Fig. 14e,g). Again, cell death was not affected in IRF3 knockout cells (Fig. 14h), while MAVS knockout cells experienced a mildly increased cell death rate (< 5 %; Fig. 14f). We concluded that cytostasis had to be induced by a paracrine signal and was independent on functional RLR signaling.

Main transcriptional targets of RLR signaling are type I and type III interferons, which are secreted and then induce the ISG response through auto- and paracrine signaling via interferon receptors and JAK/STAT signaling. In addition to their antiviral role, studies have assigned these interferons antiproliferative capacities (reviewed in [113] and [128] for type I and type III IFNs, respectively). We therefore considered interferons to be the prime suspects for the observed impaired cell growth. Indeed, when A549 cells deleted for interferon receptors IFNAR, IFNLR, and IFNGR (IFNR triple knockout) were cultured in $NS5B^{WT}$ supernatant, both cell growth and cell death were not affected (Fig. 15a-b). Conversely, $NS5B^{WT}$ transduction of IFNR triple knockout cells did not affect cell growth either (Fig. 15c). Single cell analysis of IFNR triple knockout cells revealed that IFIT1 levels were not elevated throughout the cell pool after transduction with $NS5B^{WT}$(Fig. 15d). Interestingly, though, the exception was a very small fraction (~1.3 %) of cells with high NS5B protein levels. Here, cells exhibited in part strongly elevated IFIT1 levels (Fig. 15d, box gate). Recent studies have shed light on different modes of interferon-independent ISG production (reviewed in [273]). For example, IFIT1 expression was induced in IFN signaling-incompetent cells upon infection with human cytomegalovirus (HCMV)[274] or after transfection of A549 cells with dsRNA (unpublished data from our group). We argued that in the small subset of cells experiencing elevated IFIT1 protein levels, NS5B protein levels and consequently dsRNA levels might have been high enough to trigger RLR signaling to an extent that direct IFIT1 expression was induced.

Taken together, our data suggested that NS5B-derived cytostasis could be conferred via paracrine signaling and was not limited to NS5B-expressing cells. As depletion of IFN receptors abrogated the cytostatic phenotype completely, we concluded that IFN sensing plays an important role in inducing, and possibly amplifying, cytostasis.

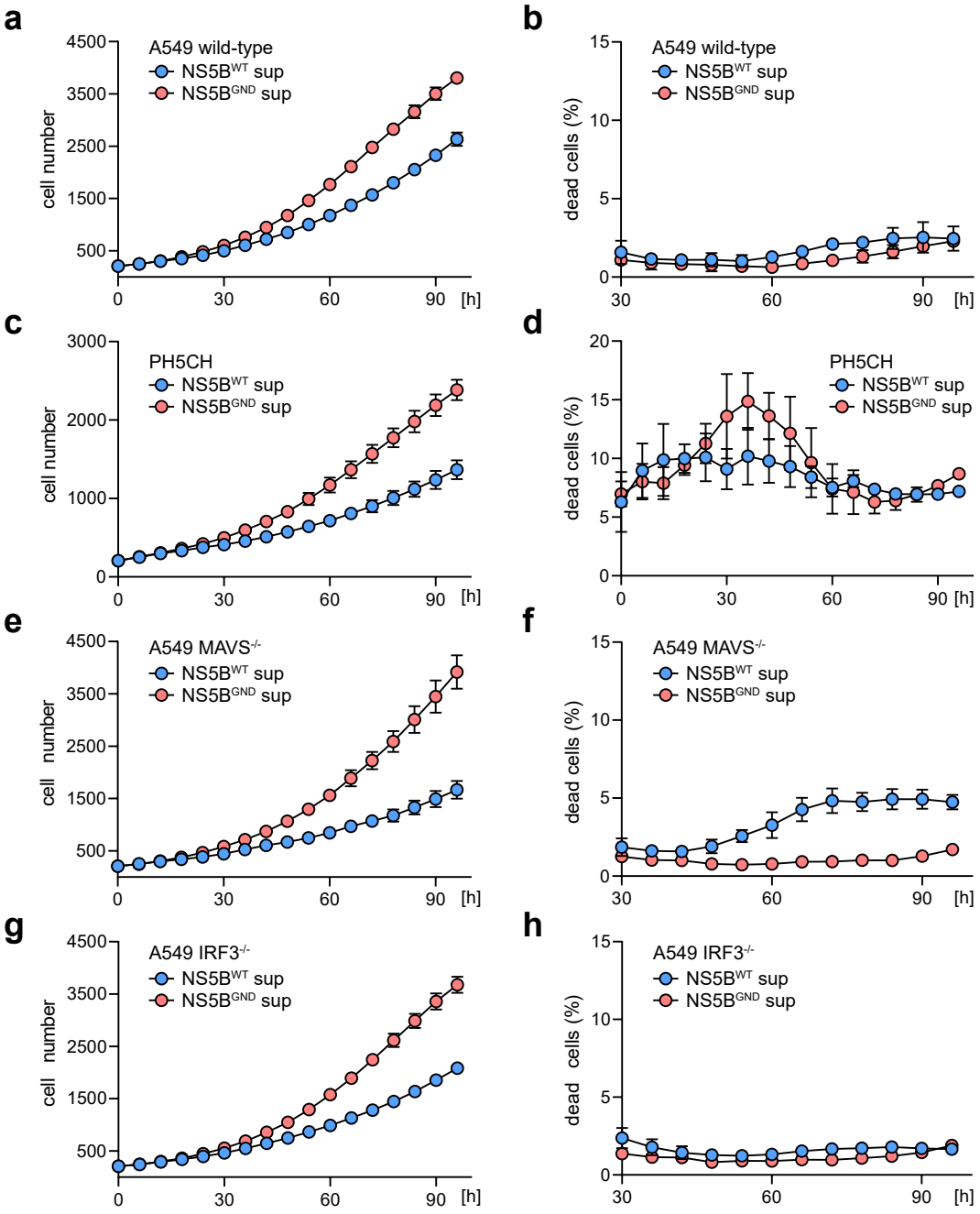

Figure 14: NS5B-derived growth defect is induced by paracrine signaling independent of functional MAVS or IRF3.

Cell growth and fraction of dead cells of cells cultured in supernatant (sup) from NS5B^{WT}- or NS5B^{GND}-transduced A549 harvested 5 days post transduction, as determined by live cell imaging (mean $\pm$ s.d. of n = 5 technical replicates). (**a-b**) Cell growth (a) and fraction of dead cells (b) of A549 wild-type cells. One representative of n = 3 independent experiments is shown. Due to Cytotox Green artifacts, calculation of percentage of dead cells was not possible before t = 30 h. (**c-d**) Cell growth (c) and fraction of dead cells (d) of PH5CH wild-type cells. One representative of n = 3 independent experiments is shown. (**e-f**) Cell growth (e) and fraction of dead cells (f) of A549 MAVS knockout cells. One representative of n = 2 independent experiments is shown. Due to Cytotox Green artifacts, calculation of percentage of dead cells was not possible before t = 30 h. (**g-h**) Cell growth (g) and fraction of dead cells (h) of A549 IRF3 knockout cells. One representative of n = 3 independent experiments is shown. Due to Cytotox Green artifacts, calculation of percentage of dead cells was not possible before t = 30 h.

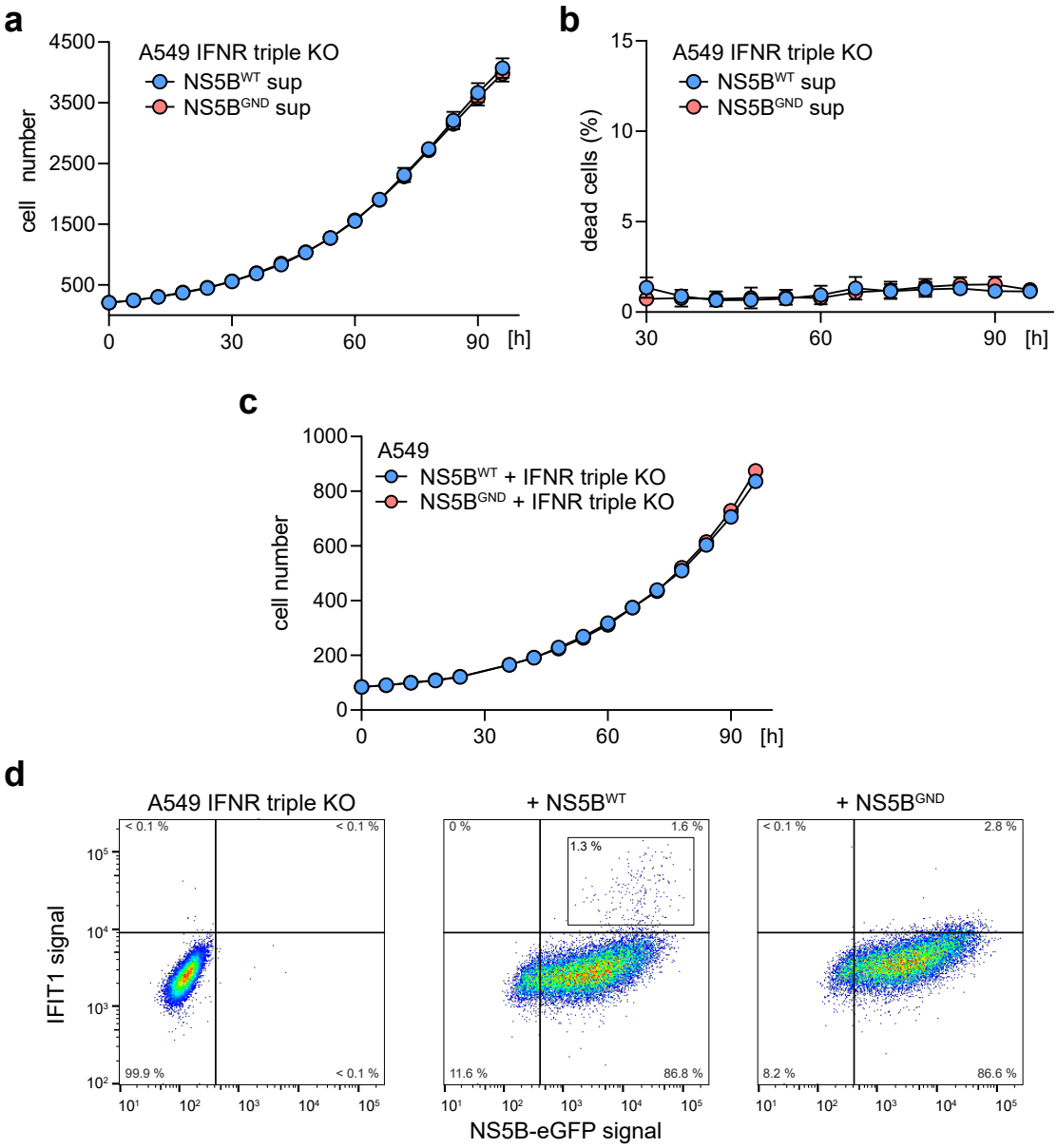

Figure 15: Depletion of IFN receptors prevents NS5B-derived growth defect.

(**a-b**) Cell growth (a) and fraction of dead cells (b) of A549 IFNR triple knockout cells cultured in supernatant (sup) from NS5B^{WT}- or NS5B^{GND}-transduced A549 cells harvested 5 days post transduction, as determined by live cell imaging (mean ± s.d. of n = 5 technical replicates). One representative of n = 3 independent experiments is shown. Due to Cytotox Green artifacts, calculation of percentage of dead cells was not possible before t = 30 h. (**c**) Cell growth of NS5B^{WT}- or NS5B^{GND}-transduced A549 IFNR triple knockout cells. One representative of n = 3 independent experiments is shown. Due to a measurement error, no images were acquired at t = 30 h. (**d**) Scatter plots of NS5B-eGFP and IFIT1 fluorescence signal in NS5B^{WT}-, NS5B^{GND}-, or mock-transduced A549 IFNR triple knockout cells. Data of n > 1.5x10^4 cells after gating was acquired by flow cytometry and plotted as a heat-map scatter plot (event density: blue, low; red, high). Quadrant gates indicate double negative cells (bottom left), NS5B-positive (bottom right), IFIT1-positive (top left) and double positive (top right) cells. Box gate indicates IFNR triple knockout cells transduced with NS5B^{WT} that exhibit elevated IFIT1 levels.

4.7 NS5B-Derived Cytostasis is Conferred by IFN-β and IFN-λ

We previously had concluded that the NS5B-derived growth defect depended on functional interferon sensing and downstream signaling. Next, we aimed to narrow down which interferons were responsible for growth inhibition in NS5B-transduced cells. A549 wild-type cells were treated with recombinant human interferons of type I (IFN-α, IFN-β) and type III (IFN-λ1), and both cell growth and cell death were monitored via live cell imaging. While treatment with 1000 IU/ml of IFN-α or 100 ng/ml of IFN-λ1 resulted only in marginal reduction of cell growth, treatment with 1000 IU/ml IFN-β negatively affected cell growth more strongly (Fig. 16a). None of the IFNs impacted the cell death frequency (Fig. 16b). We investigated the effects of IFN concentration as well as the combination of different IFNs. Impairment of cell growth correlated with IFN-β concentration and was slightly amplified by combining IFN-β with IFN-λ1 (Fig. 16c). Again, no relevant cell death effects were observed (Fig. 16d).

We wondered which interferons were expressed by NS5B-transduced cells, and at what concentrations they were present in the supernatant. We used electrochemiluminescence-based detection to measure the concentration of several analytes per sample at the same time. Here, the analyte binds to immobilized capture anti-

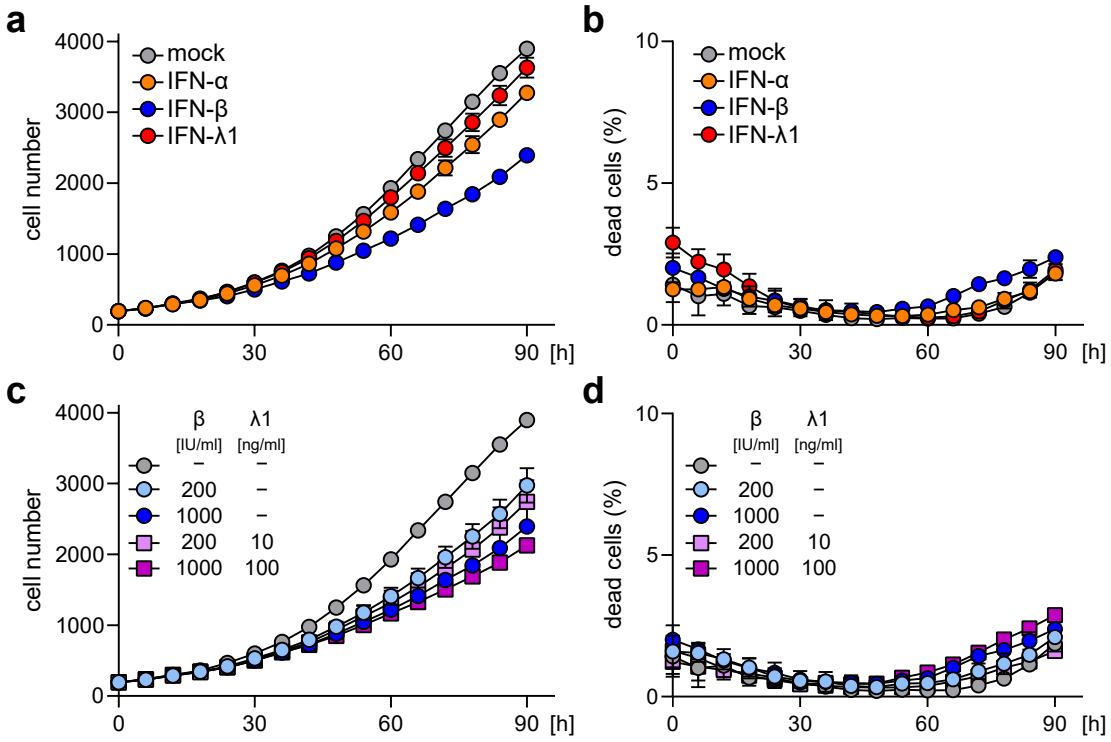

Figure 16: IFN-β impairs cell growth in A549.
(**a-b**) Cell growth (a) and fraction of dead cells (b) of A549 wild-type cells treated with IFN-α (1000 IU/ml), IFN-β (1000 IU/ml), or IFN-λ1 (100 ng/ml), as determined by live cell imaging (mean ± s.d. of n = 3 technical replicates). One representative of n = 2 independent experiments is shown. (**c-d**) Cell growth (c) and fraction of dead cells (d) of A549 wild-type cells treated with IFN-β and IFN-λ1 at the indicated concentrations (mean ± s.d. of n = 3 technical replicates). One representative of n = 3 independent experiments is shown.

bodies in a specific region of the well. Then, SULFO-TAG-conjugated detection antibodies bind to their target analytes. A voltage is applied, inducing a chemical reaction that results in emission of light from the SULFO-TAG. Like other chemiluminescence techniques, the light signal intensity is proportional to the analyte concetration. We quantified the concentration of several interferons in supernatant from NS5B^{WT}-transduced A549 and PH5CH cells (Fig. 17a). In both cell lines, IFN-α2a and IFN-γ were at or below detection limits of 4.0 pg/ml and 1.7 pg/ml, respectively. The concentration of IFN-β on the other hand was at 230 pg/ml in A549 and 190 pg/ml in PH5CH. IFN-λ1 levels were in the lower nanogram range and showed a greater difference between A549 (13 ng/ml) and PH5CH (3 ng/ml). We wondered whether a combination of IFN-β and IFN-λ1 alone would suffice to mimic the NS5B-derived cytostasis. Before treatment, IFN-β concentrations were converted from pg/ml to UI/ml of recombinant IFN-β, and IFN-λ1 concentrations were adjusted to compensate for assay-derived differences between input amount and measurement result (data not shown). Then, A549 cells were treated either with NS5B^{WT} supernatant, NS5B^{GND} supernatant or with NS5B^{GND} supernatant supplemented with a combination of recombinant IFN-β (130 IU/ml) and recombinant IFN-λ1 (12 ng/ml). Live cell imaging revealed that the addition of both interferons was sufficient to reduce cell growth to the same extent as NS5B^{WT} supernatant (Fig. 17b). The same was true for PH5CH cultured in NS5B^{GND} supernatant supplemented with IFN-β (110 IU/ml) and IFN-λ1 (2.5 ng) (Fig. 17d). Cell death was slightly elevated in PH5CH cells treated with NS5B^{WT} supernatant, while adding interferons to NS5B^{GND} supernatant had no effect on cell death in both cell lines (Fig. 17c,e).

We finally investigated whether IFN-β and IFN-λ1 were also responsible for the growth defect observed in NS5B^{WT}-transduced cells. We used CRISPR/Cas9-mediated gene knockout to delete the IFN-β gene IFNB1 in A549 wild-type cells and A549 cells already harboring an IFNLR knockout. This allowed us to study specifically the effects of preventing either IFN-β signaling or IFN-λ signaling. Deletion of IFNLR alone had no effect on cell growth or cell death after NS5B^{WT} transduction (Fig. 18a-b). We next evaluated four IFNB1 knockout single cell clones generated with two different guide RNAs. Three clones were able to partly rescue cell growth to varying degrees, while one clone (cl. 3.2) completely rescued cell growth in NS5B^{WT}-transduced cells (Fig. 18c). The percentage of cell death correlated with the extent of cell growth impairment, with clone 3.2 showing no elevated cell death compared to NS5B^{GND}-transduced cells (Fig. 18d). The picture was clearer for the IFNB1 IFNLR double knockout: all four clones completely rescued cell growth in NS5B^{WT}-transduced cells, and no elevated rates of cell death were observed (Fig. 18e,f).

All four IFNB1 knockout cell lines were of single cell origin and their inability to secrete IFN-β after Sendai virus infection had been validated by IFN-β enzyme-linked immunosorbent assay (ELISA; Fig. S4). The cause of the observed clonal variations are unknown, however, they may be direct consequences of NS5B-induced IFN-λ signaling.

Taken together, the secretion of IFN-β and IFN-λ1 from RLR-stimulated cells and the subsequent auto- and paracrine stimulation via the IFN type I and III receptors are likely to be responsible for NS5B-derived cytostasis.

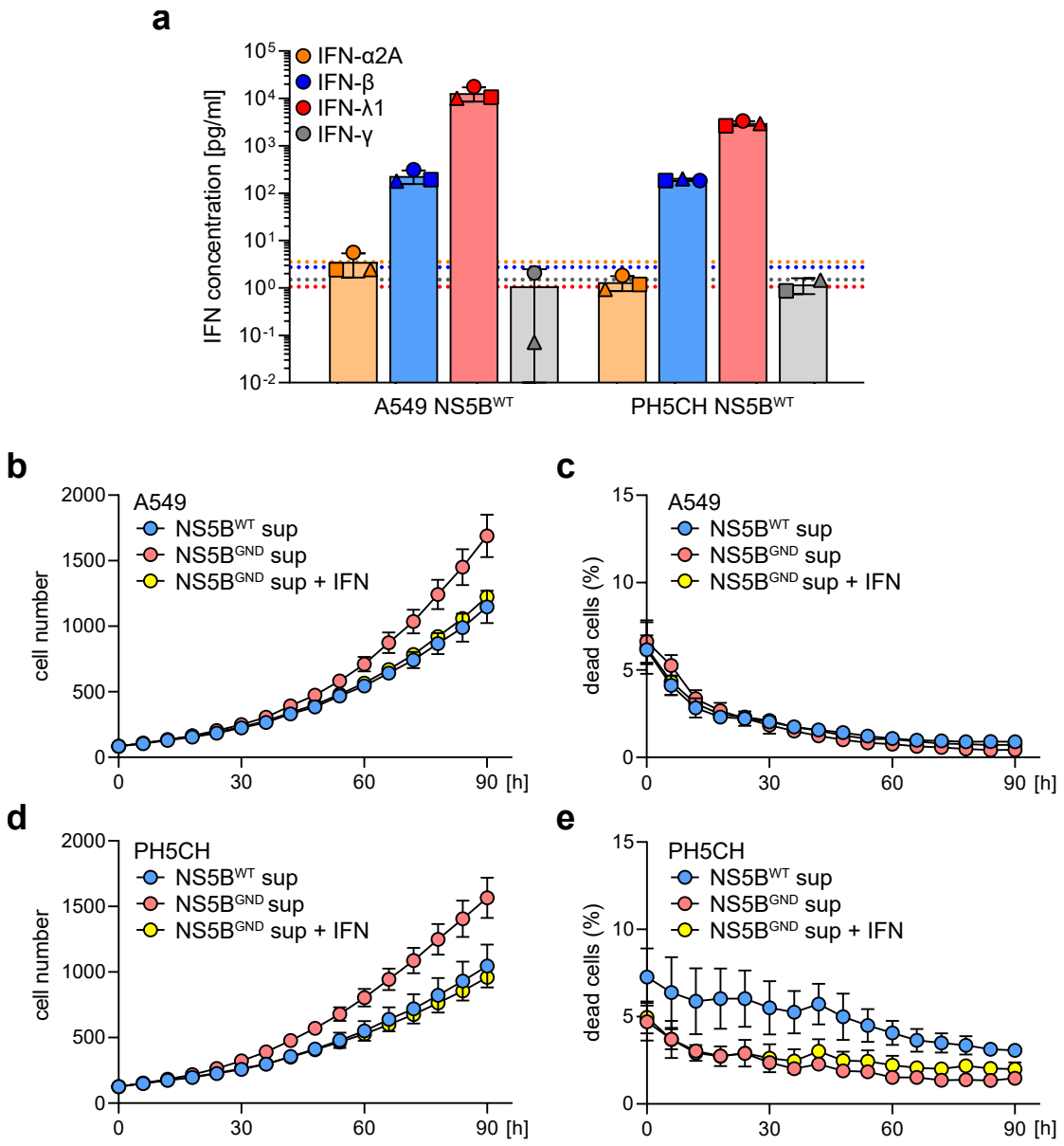

Figure 17: Defined combination of IFN-β and IFN-λ1 mimics growth impairment through NS5B^{WT}-derived supernatant.

(**a**) IFN content in supernatant from NS5B^{WT}-transduced A549 or PH5CH cells, as determined by MSD multiplex electrochemiluminescence assay (mean ± s.d. of n = 3 independent experiments). Supernatant was harvested after 48 h at 5 days post transduction. Dashed lines indicate lower assay detection limits (IFN-α2a: 4.0 pg/ml, IFN-β: 3.1 pg/ml, IFN-γ: 1.7 pg/ml, IFN-λ1: 1.2 pg/ml). (**b-c**) Cell growth (b) and fraction of dead cells (c) of A549 wild-type cells cultured in supernatant from NS5B^{WT}- or NS5B^{GND}-transduced A549 cells, or cultured in NS5B^{GND} supernatant supplemented with a combination of IFN-β (130 IU/ml) and IFN-λ1 (12 ng/ml) (mean ± s.d. of n = 3 biological replicates). (**d-e**) Cell growth (d) and fraction of dead cells (e) of PH5CH wild-type cells cultured in supernatant from NS5B^{WT}- or NS5B^{GND}-transduced PH5CH cells, or cultured in NS5B^{GND} supernatant supplemented with a combination of IFN-β (110 IU/ml) and IFN-λ1 (2.5 ng/ml) (mean ± s.d. of n = 3 biological replicates).

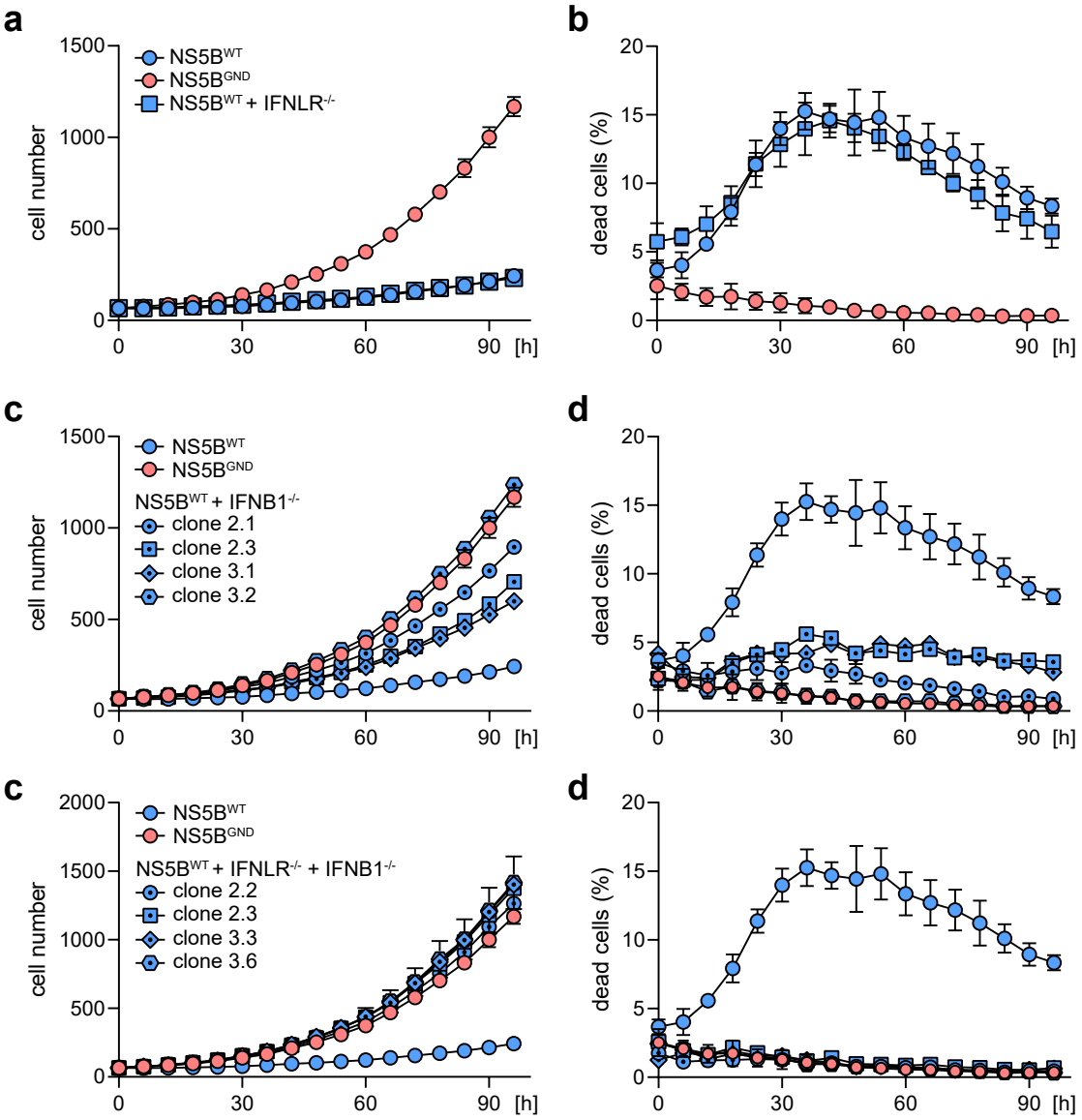

Figure 18: Depletion of both IFN-β and IFNLR completely reverses NS5B-induced growth defect in A549 cells.

Cell growth and fraction of dead cells of $NS5B^{WT}$- or $NS5B^{GND}$-transduced cells, as determined by live cell imaging (mean ± s.d. of n = 4 technical replicates). To account for differences in basal cell growth between cell lines, growth data of $NS5B^{WT}$-transduced knockout cell lines were normalized to their $NS5B^{GND}$-transduced variants and then normalized to A549 wild type transduced with $NS5B^{GND}$. (**a-b**) Cell growth (a) and fraction of dead cells (b) of A549 wild-type or IFNLR knockout cells. (**c-d**) Cell growth (c) and fraction of dead cells (d) of A549 wild-type cells or four different IFNB1 knockout single cell clones (clone IDs refer to guide RNAs 2 and 3, respectively). (**e-f**) Cell growth (e) and fraction of dead cells (f) of A549 wild-type cells or four different IFNLR IFNB1 double knockout single cell clones.

4.8 $NS5B^{WT}$ Expression Induces the Secretion of Several Pro-Inflammatory Cytokines and Chemokines

We were able to attribute the NS5B-derived growth defect phenotype observed in the cell lines A549 and PH5CH to the concerted effects of IFN-β and IFN-λ1. While our NS5B cell culture model contained only cells of epithelial origin, an infected organ constitutes a far more complex interaction system of different cell types. Infected epithelial cells secrete

various chemokines and cytokines to attract and activate immune cells. We wondered what cytokines apart from IFN-β and IFN-λ1 are secreted by cells with NS5B-activated RLR signaling.

To elucidate the composition of the secretome of NS5B-transduced cells – termed the NS5B secretome – we employed multiplex electrochemiluminescence detection of a selection of pro-inflammatory cytokines as well as chemokines. Secreted levels of pro-inflammatory cytokine TNF were slightly, but significantly, elevated in supernatants from both A549 cells and PH5CH cells transduced with $NS5B^{WT}$, with concentrations in the single-digit picogram region (Fig. 19a). Interleukin 6 (IL-6) levels were increased in A549 $NS5B^{WT}$ supernatant as well (90 pg/ml; Fig. 19b). In PH5CH cells, IL-6 levels were higher than in A549, and the detected concentration in PH5CH $NS5B^{WT}$ supernatant was above the assay detection range of 488 pg/ml. Secretion of other tested cytokines – interleukins IL-1b, -2, -4, -8, -10, -12p70 and -13 – was not affected by NS5B activity (data not shown).

We also measured the concentrations of several chemotactic cytokines, or chemokines, from the CC-motif and CXC-motif subtypes. In $NS5B^{WT}$ supernatant from both A549 and PH5CH, three CC chemokines (CCL3, -4, -17) and one CXC chemokine (CXCL10) exhibited elevated levels (Fig. 19c-f). CCL17 was increased ~37-fold (9.5 pg/ml) in A549 supernatant and ~7-fold (1 pg/ml) in PH5CH supernatant, respectively (Fig. 19c). Also known as thymus and activation-regulated chemokine (TARC), it binds to the chemokine receptor CCR4 and is involved in the activation and maturation of T cells and in attraction of T_h cells and T_{reg} cells[275–277]. CCL3 and CCL4, or macrophage inflammatory proteins (MIP) 1α and 1β, respectively, were also strongly elevated in both cell line supernatants after $NS5B^{WT}$ transduction (Fig. 19e-f). While the concentration of CCL4 exhibited a stronger increase than CCL3 in A549 $NS5B^{WT}$ derived supernatant (230-fold vs. 50-fold; 317 pg/ml vs. 224 pg/ml), in PH5CH the increase in CCL3 levels was more pronounced than that of CCL4 (105-fold vs. 65-fold; 326 pg/ml vs. 58 pg/ml). CXCL10, or interferon gamma-induced protein 10 (IP-10), secretion was increased several hundred fold upon $NS5B^{WT}$ expression in both cell lines (A549: 337 pg/ml; PH5CH: 396 pg/ml) (Fig. 19d). CXCL10 binds to the CXCR3 receptor and attracts monocytes, NK cells, and T cells, but was also shown to target hepatic stellate cells[177]. Moreover, increased CXCL10 levels were associated with liver fibrosis and apoptosis[177,278–280].

Other chemokines of the assay panel were not affected by $NS5B^{WT}$ activity (data not shown). These included CCL2 and CCL13, also known as monocyte chemoattractant proteins 1 (MCP-1) and 4 (MCP-4), CCL11 (eotaxin) and CCL26 (eotaxin-3), and CCL22 (macrophage-derived chemokine, MDC).

In summary, we detected two pro-inflammatory cytokines (TNF, IL-6) and four chemokines (CCL3, -4, -17, CXCL10) that were secreted upon expression of $NS5B^{WT}$. It is important to note that, despite the differences between the two cell lines (a cancer cell line from the lung and an immortalized cell line from the liver), the secretion profiles were remarkably similar.

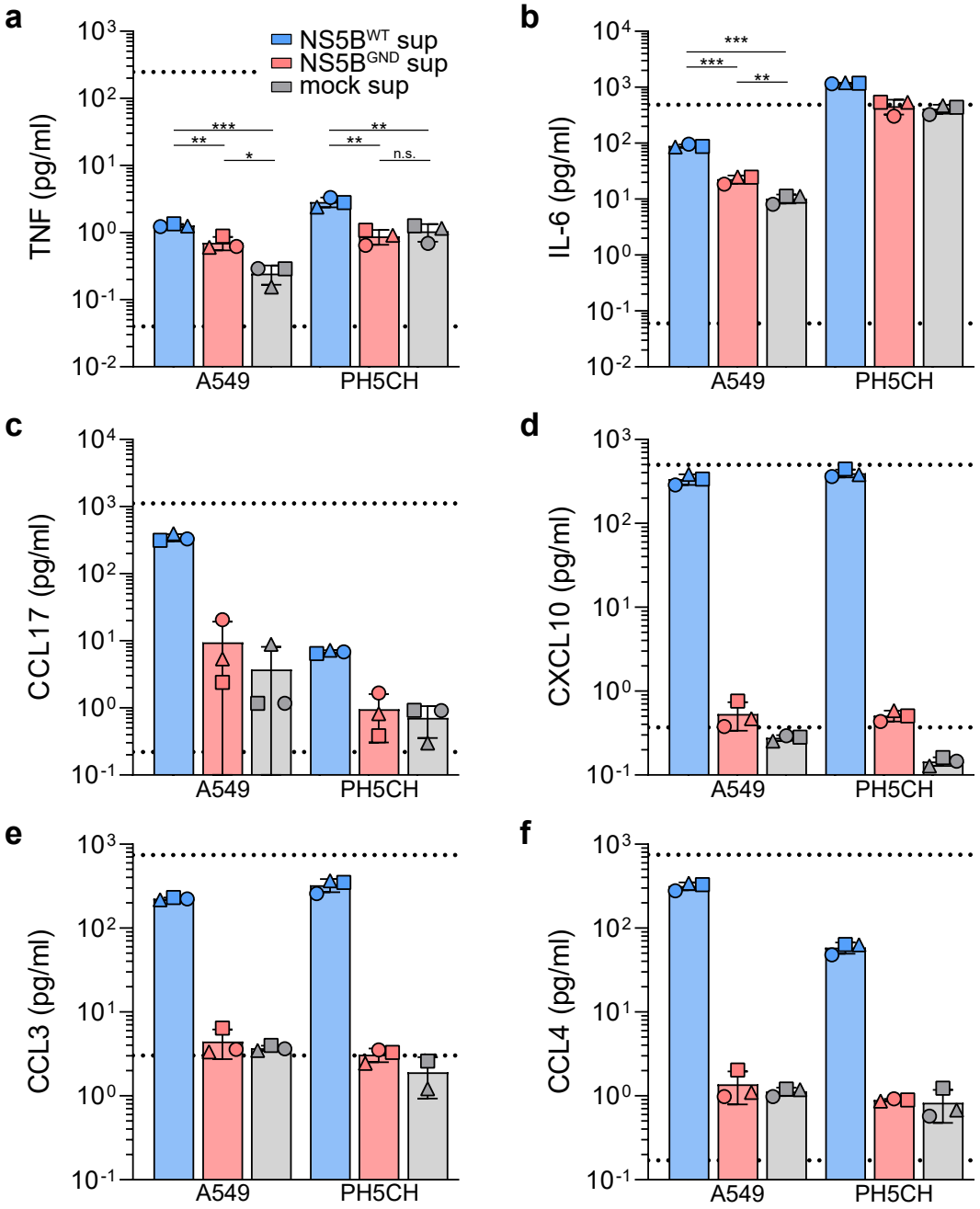

Figure 19: NS5B activity induces secretion of pro-inflammatory cytokines and chemokines.

Concentrations of cytokines TNF (a) and IL-6 (b) as well as concentrations of chemokines CCL17 (c), CXCL10 (d), CCL3 (e), and CCL4 (f) in supernatant (sup) from $NS5B^{WT}$-, $NS5B^{GND}$-, or mock-transduced A549 or PH5CH cells, as determined by MSD multiplex electrochemiluminescence assay (mean $\pm$ s.d. of $n = 3$ independent experiments). Supernatant was harvested after 48 h incubation on day 5 post transduction. Dashed lines indicate lower and upper assay detection limits (TNF: 0.04-248 pg/ml; IL-6: 0.06-488 pg/ml; CCL17: 0.22-1120 pg/ml; CXCL10: 0.37-500 pg/ml; CCL3: 3.02-743 pg/ml; CCL4: 0.17-750 pg/ml). Statistical significance was determined with Student's t-test corrected for multiple testing (***: $p < 0.001$, **: $p < 0.01$, *: $p < 0.05$, n.s.: not significant).

4.9 The Transcriptional Response to the NS5B Secretome is Dominated by ISGs and is Maintained Over an Extended Treatment Period

Previous experiments had revealed that RLR stimulation through NS5B transgene expression led to the secretion of interferons β and λ1, pro-inflammatory cytokines TNF and IL-6, and chemokines CCL3, -4, -17, and CXCL10. We now wondered how exposure to this mix of secreted factors, together with potential additional factors not covered by the assay panels, would affect the transcriptional landscape of uninfected bystander cells.

4.9.1 RNA Expression Profiles of A549 Cells Stimulated with IFNs or A549 NS5B^{WT} Supernatant

We cultured naïve A549 cells for 24 h in the NS5B^{WT} supernatant that was described in the previous sections (Fig. 20a). Changes in transcriptional levels were analyzed in a microarray-based expression profiling approach. Of special interest were potential effects caused by secreted factors other than IFN-β or IFN-λ1. To distinguish those, we also treated naïve A549 cells for 24 h only with a combination of IFN-β and IFN-λ1 matching the concentrations detected in the NS5B^{WT} supernatant (see Fig. 17), and then compared transcriptome data from both conditions (Fig. 20). We classified genes as significantly up- or downregulated if they exhibited at least a two-fold change in mRNA levels compared to naïve cells at the start of the treatment (t = 0 h), and if the p-value after correction for multiple testing was below 0.05. This reduced the list of over 19,000 analyzed genes dramatically: only two genes, MX1 and IFIT3, were significantly upregulated after IFN treatment, while treatment with NS5B^{WT} supernatant resulted in 18 significantly upregulated genes (Fig. 20b, Fig. S5a-b). Most strongly upregulated genes were classical ISGs MX1 (55-fold) and IFIT1 (90-fold), respectively. Although all genes except IFIT3 were only classified as significant in one of the treatment conditions but not in the other, we chose to compare fold changes from both conditions in a scatter plot, indicating the p-value of the non-significant condition by color (Fig. 20b). In fact, most of the genes showed very similar responses to the different treatments, and some of them, such as MX1 or IFIT1, were only excluded based on their p-values being marginally shy of the significance threshold. Overall, most of the genes exhibited slightly higher fold changes after NS5B^{WT} supernatant treatment compared to IFN treatment; however, differences between the two treatments are mostly smaller than two-fold. IFIT3 was upregulated 37-fold and 18-fold after NS5B^{WT} supernatant or IFN treatment, respectively, representing a 2.1-fold difference. IFIT2 shows the highest fold-change difference between conditions (3.7-fold higher after NS5B^{WT} supernatant treatment), however, since the significance threshold was not met in the IFN treatment condition, such a value has to be considered with caution.

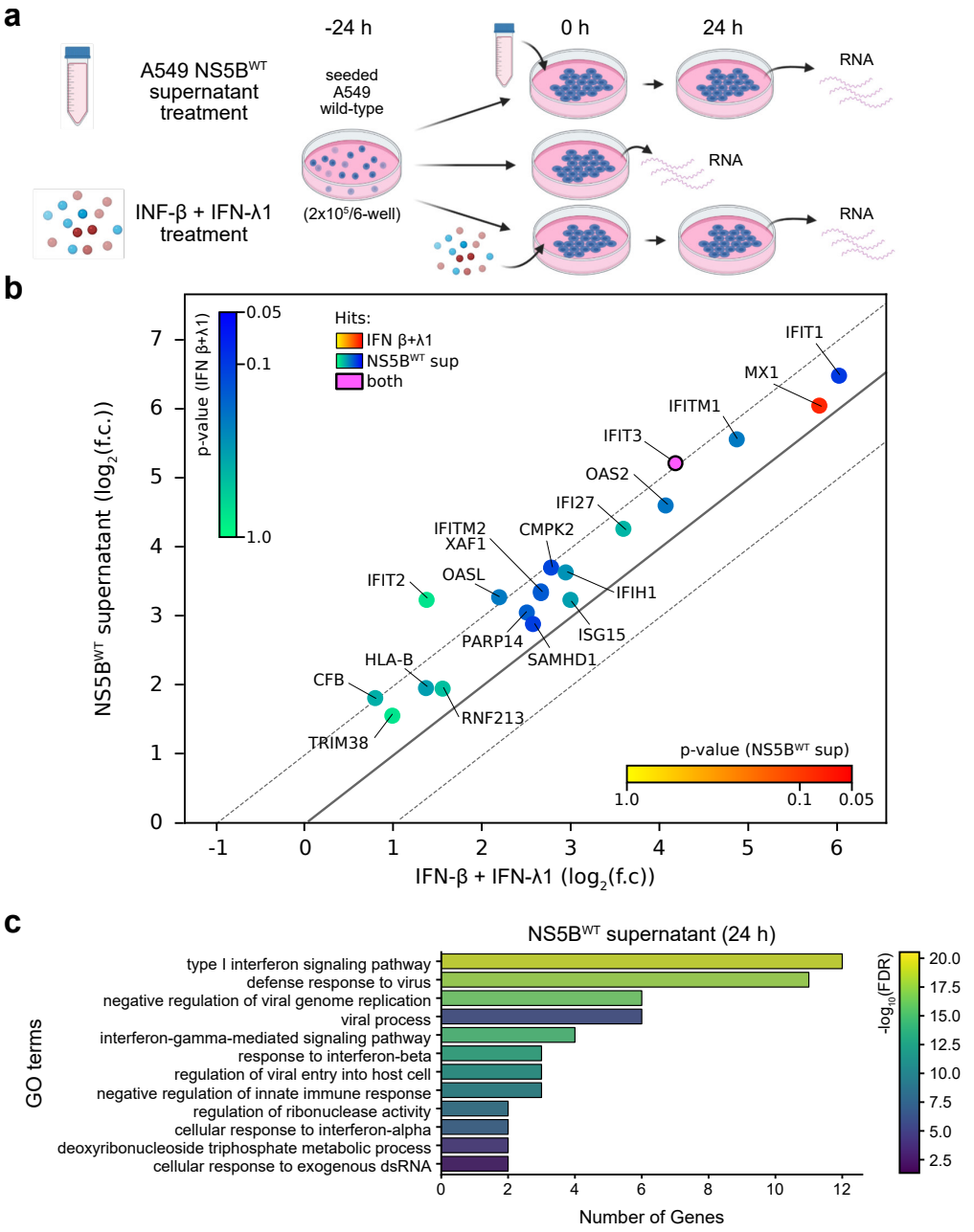

Figure 20: RNA expression profiles of stimulated A549 cells.

(**a**) Schematic of experimental process. A549 wild-type cells were seeded at 2x10^5 cells/6-well. 24 h later, RNA was harvested, or cells were treated with either 2 ml supernatant derived from NS5B^{WT}-expressing A549 cells, or 2 ml DMEM containing a combination of IFN-β (130 IU/ml) and IFN-λ1 (12 ng/ml). RNA was harvested 24 h later. (**b**) Scatter plot displaying mRNA level fold changes (f.c.) of significantly regulated genes in A549 wild-type cells treated for 24 h with a combination of IFN-β and IFN-λ1 or with A549 NS5B^{WT} supernatant (sup) ($\log_2$ of mean f.c. over t = 0 h from n = 3 independent experiments). Genes were classified as significantly regulated if they fulfilled the requirements of i) at least 2-fold up- or downregulation, and ii) p-value < 0.05 (after Benjamini-Hochberg correction for multiple testing). Gene color indicates whether a gene was significantly regulated in both conditions (pink with black border) or only in one (IFN treatment: yellow to red; NS5B^{WT} supernatant: green to blue). The color of a gene significantly regulated only in one condition also indicates the p-value in the respective other condition (see color bars in the top left and bottom right). Diagonal lines indicate fold change differences between both conditions (continuous line: no difference; dashed lines: 2-fold difference). Detailed volcano plots for each condition are shown in Fig. S5a-b. (**c**) Gene ontology (GO) terms for biological processes (BP) enriched in A549 cells cultured in supernatant derived from NS5B^{WT}-transduced A549 cells (false discovery rate (FDR) < 0.05). Analysis for enriched GOBP terms was performed with PANTHER, and most specific terms from the hierarchically sorted results are shown (list of annotated genes: Table S1).

The set of 18 significantly regulated genes after NS5B^{WT} supernatant treatment allowed us to search for enriched Gene Ontology terms of biological processes (GOBP). We focused only on the most specific terms from a hierarchically sorted set of results to exclude terms that were too generic to provide meaningful insights. Unsurprisingly, terms “type I interferon signaling pathway” (13 genes) and “defense response to virus” (12 genes) were the most prominent hits (Fig. 20c). Both terms showed a high overlap in annotated genes with IFIT1, -2, -3, IFITM1, -2, IFI27, OAS2, OASL, ISG15, and SAM and HD domain-containing deoxynucleoside triphosphate triphosphohydrolase 1 (SAMHD1) (for a complete list of genes per term, see Table S1).

Out of the 18 significantly regulated genes, complement factor B (CFB) and ring finger protein 213 (RNF213) were not annotated to any of the listed terms, however, they could be annotated to the more generalized terms “immune effector process” (CFB) and “biological process involved in symbiotic interaction” (RNF213). CFB protein circulates in the blood stream and is involved in the early steps of the alternative activation of the complement system[281]. RNF213, an E3 ubiquitin ligase, was reported to be an ISG conserved over different species[142]. Recently, a preliminary report indicated that IFN signaling induces ISGylation of RNF213 and its subsequent oligomerization on lipid droplets, where it senses ISGylated proteins and possesses broad antimicrobial properties[282]; however, a peer-reviewed publication was not available as of yet.

4.9.2 RNA Expression Profiles of PH5CH Cells Stimulated with IFNs or PH5CH NS5B^{WT} Supernatant

We performed the same experiment also with PH5CH cells. Here, treatment with NS5B^{WT} supernatant or interferons resulted in the upregulation of 14 and 13 genes, respectively (Fig. 21a, Fig. S5c-d). Both sets showed an overlap of six upregulated genes, namely MX1, IFIT3, XAF1, EPSTI1, UBE2L6, and BTN3A3. As observed in the experiment with A549 cells, upregulated proteins in PH5CH cells behaved very similar in both treatment conditions, with a very slight trend towards higher fold-changes after NS5B^{WT} treatment for the majority of the hits. MX1 shows the greatest fold increase over naïve cells in both conditions (~50-fold each). GOBP enrichment analysis of IFN and NS5B^{WT} supernatant treatment revealed a picture very similar to data from A549 cells, with terms “type I interferon signaling pathway” and “defense response to virus” again containing the most genes (Fig. 21b-c; for a complete list of genes per term, see Tables S2 and S3). Four biological processes returned as enriched after NS5B^{WT} supernatant treatment covering mitochondrial fission, synaptic budding and synaptic receptor internalization are all based on the same two genes, MX1 and MX2. Three genes upregulated in both treatment conditions – ubiquitin/ISG15-conjugating enzyme E2 L6 (UBE2L6), epithelial stromal interaction 1 (EPSTI1), and butyrophilin subfamily 3 member A3 (BTN3A3) – were not annotated to any of the specific terms. UBE2L6 is involved in the process of ISGylation and thus in regulation of innate immune signaling[141]. BTN3A3 is associated with the broader

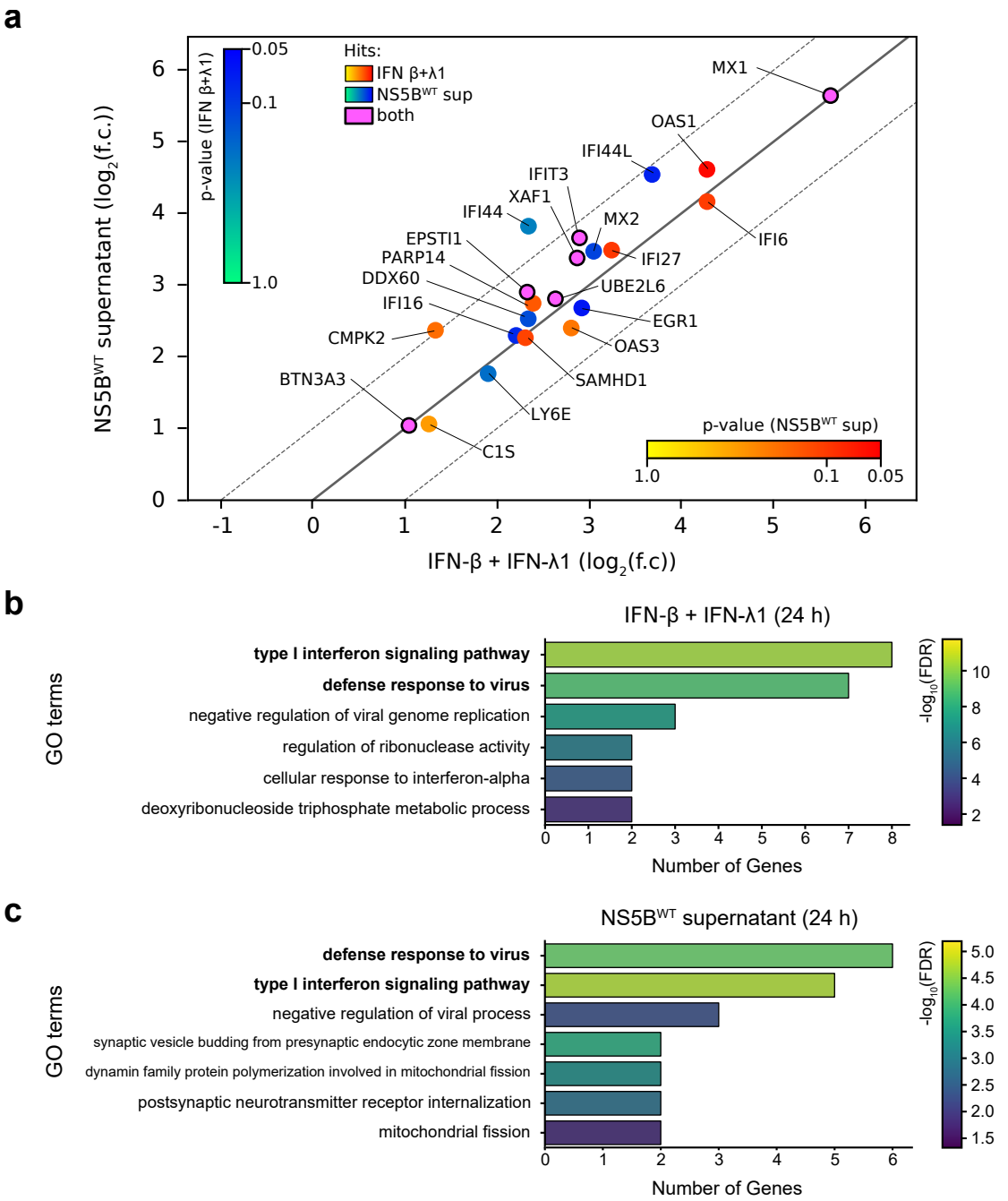

Figure 21: RNA expression profiles of stimulated PH5CH cells.

(**a**) Scatter plot displaying mRNA level fold changes (f.c.) of significantly regulated genes in PH5CH wild-type cells treated for 24 h with a combination of IFN-β (110 IU/ml) and IFN-λ1 (2.5 ng/ml) or with supernatant (sup) derived from NS5B^{WT}-expressing A549 cells (log_2 of mean f.c. over t = 0 h from n = 3 independent experiments). Genes were classified as significantly regulated if they fulfilled the requirements of i) at least 2-fold up- or downregulation, and ii) p-value < 0.05 (after Benjamini-Hochberg correction for multiple testing). Gene color indicates whether a gene was significantly regulated in both conditions (pink with black border) or only in one (IFN treatment: yellow to red; NS5B^{WT} supernatant: green to blue). The color of a gene significantly regulated only in one condition also indicates the p-value in the respective other condition (see color bars in the top left and bottom right). Diagonal lines indicate fold change differences between both conditions (continuous line: no difference; dashed lines: 2-fold difference). Detailed volcano plots for each condition are shown in Fig. S5c-d. (**b-c**) Gene ontology (GO) terms for biological processes (BP) enriched in PH5CH cells treated with IFN-β and IFN-λ1 (b) or with PH5CH NS5B^{WT} supernatant (c) (false discovery rate (FDR) < 0.05). Analysis for enriched BP terms was performed with PANTHER, and most specific terms from the hierarchically sorted results are shown (lists of annotated genes: Tables S2 and S3). Terms enriched in both conditions are highlighted in bold print.

term “immune response”, encodes a MHC type I-associated transmembrane protein, and exhibits antiviral properties against Ebola virus and alphaviruses[283,284]. Expression of BTN3A3 in the hepatoma cell line Huh-7 was induced by both IFN type I and II signaling, with a stronger induction through IFN-γ[285,286]. EPSTI1 did not come up in any of the significantly enriched GOBP terms. It is involved in activation and differentiation of macrophages as well as tumor invasion and metastasis in some cancers[287,288]. One study showed that EPSTI1 expression is induced by IFN-λ2 in HCV-infected Huh7.5 cells and induces expression of IFN-β and early ISGs through activation of PKR[289]. Complement component 1s (C1S), a hit in the interferon treatment experiment that was also not annotated, is another component of the complement system[281].

Expression profiles from both cell lines, A549 and PH5CH, display a strong correlation of upregulated genes between treatment with $NS5B^{WT}$ supernatant and treatment with a defined mix of IFNs mimicking IFN content of the supernatant. This suggests that the early transcriptional response to stimulation with factors secreted from cells with activated RLR signaling is predominantly mediated by IFNs.

4.9.3 Long-Term Exposure to NS5B Secretome Does Not Alter Transcriptional Response

We finally used the NS5B supernatant transfer approach to tackle one of the questions from the start of this work: how do cells react and adapt to long-term immune stimulation? Within the scope of this work, we treated naïve A549 cells for a month with supernatant from $NS5B^{WT}$ or $NS5B^{GND}$-transduced A549 cells (Fig. 22a). Cells were passaged twice per week, where they were seeded at defined cell numbers per well to compensate for treatment related differences in cell growth. As observed before, $NS5B^{WT}$ supernatant reduced the proliferation rate of A549 cells (data now shown). We then identified genes significantly regulated by $NS5B^{WT}$ supernatant treatment compared to $NS5B^{GND}$ supernatant treatment after 1 day or after 29 days of culture, and mRNA level fold changes of both time points were then compared (Fig. 22b; Fig. S5e-f). Three genes – IFIT1, IFITM1, and CMPK2 – were classified as significantly upregulated at both time points, while 8 and 26 genes were significantly upregulated only on day 1 or day 29, respectively. In general, fold changes over the $NS5B^{GND}$ control did not change dramatically over time, as they clustered around the diagonal line that represents no difference in mRNA transcript level between the two time points (Fig. 22b). For example, interferon alpha inducible protein 27 (IFI27) shows a 2.6-fold increase in mRNA levels at day 29 compared to day 1. As seen before, GOBP term enrichment analysis revealed “type I interferon pathway”, “defense against virus” and “negative regulation of viral genome replication” as the most prominent enriched processes (Fig. 23; for a complete list of genes per term, see Tables S4 and S5).

All six terms enriched on day 1 are closely related to processes active during viral infection (Fig. 23a). Many enriched terms on day 29 contained only 2–3 genes. Among them are

"negative regulation of type I interferon production" (IFIH1, ISG15, UBE2L6) as well as several terms related to regulation of immune cell cytotoxicity and antigen presentation, which is mainly due to the upregulation of HLA-B and HLA-E.

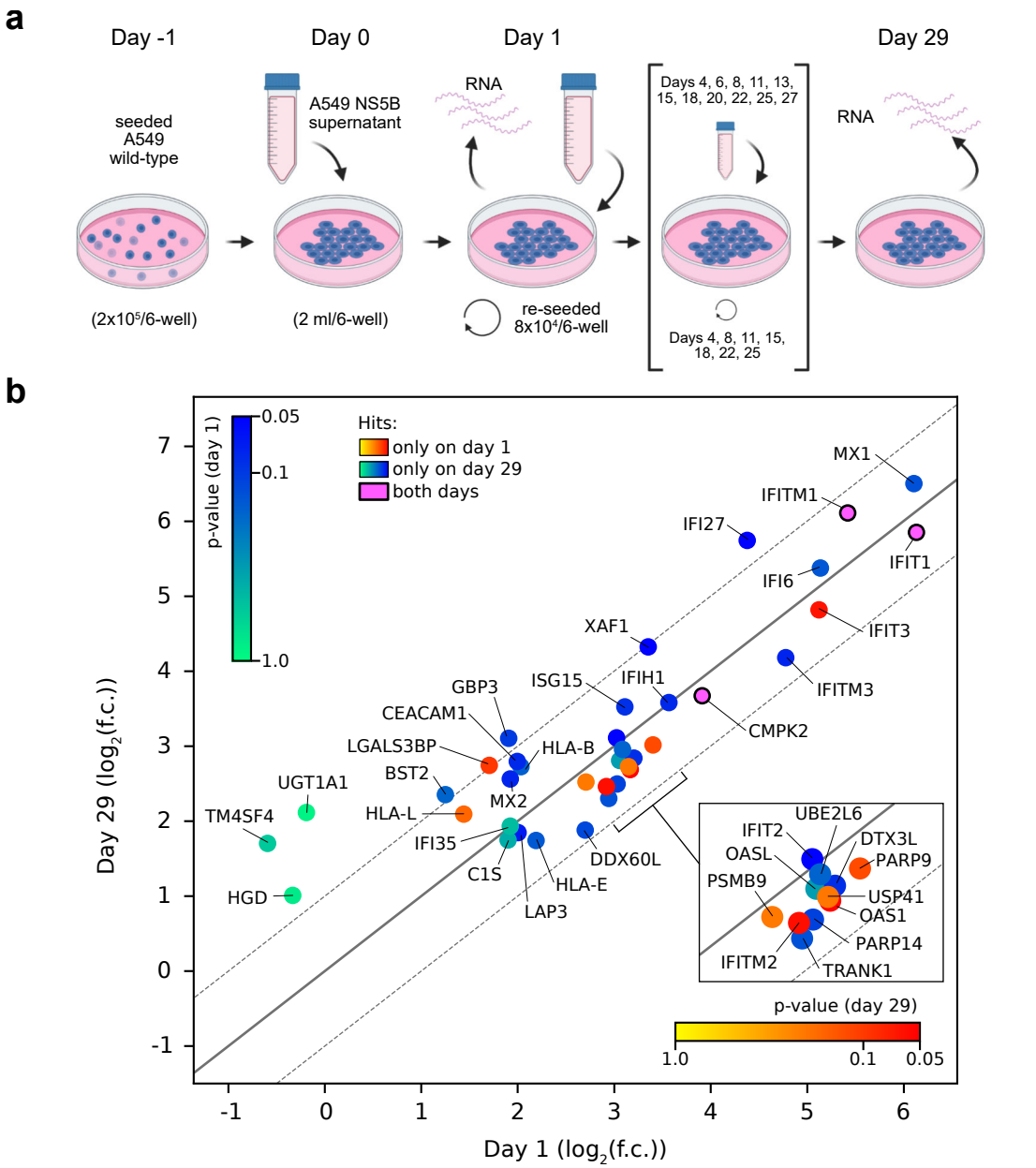

Figure 22: RNA expression profiles of A549 cells cultured in supernatant derived from NS5B-transduced cells.

(**a**) Schematic process of long-term supernatant treatment experiment. (**b**) Scatter plot displaying mRNA level fold changes (f.c.) of significantly regulated genes in A549 wild-type cells cultured in supernatant (sup) derived from $NS5B^{WT}$-expressing A549 cells for 1 or 29 days (log_2(mean f.c.) over $NS5B^{GND}$ of n = 3 independent experiments). Genes were classified as significantly regulated if they fulfilled the requirements of i) at least 2-fold up- or downregulation, and ii) p-value < 0.05 (after Benjamini-Hochberg correction for multiple testing). Gene color indicates whether a gene was significantly regulated at both time points (pink with black border) or only at one time point (day 1: yellow to red; day 29: green to blue). The color of a gene significantly regulated only at one time point also indicates the p-value at the respective other time point (see color bars in the top left and bottom right). Diagonal lines indicate fold change difference between day 1 and day 29 (continuous line: no difference; dashed lines: 2-fold difference). Detailed volcano plots for each time point are shown in Fig. S5e-f.

Some genes were not annotated on the most specific GO term level. Cytidine/uridine monophosphate kinase 2 (CMPK2) was significantly upregulated to very similar levels at both time points. CMPK2 phosphorylates deoxyuridine monophosphate (dUMP) during its conversion to deoxyuridine triphosphate (dUTP)[290]. CMPK2's ISG property seems to be highly conserved[142], however, its molecular function is not well understood. Antiviral properties against HIV have been reported, possibly connected to involvement of CMPK2 in uracilation of retroviral genomes[291]. A lncRNA from the CMPK2 gene locus, however, has been reported to negatively regulate antiviral signaling during HCV infection *in vitro* and showed elevated levels in livers from HCV-infected patients[292].

Genes significantly upregulated only on day 1 after treatment start that were not annotated included ubiquitin specific protease 14 (USP14), proteasome 20S subunit beta 9 (PSMB9), lectin galactoside-binding soluble 3-binding protein (LGALS3BP), and HLA-L (a pseudogene). USP14 is a protease that belongs to the group of deubiquitinating enzymes (DUBs). It has been reported to show isopeptidase activity against ISG15, which increases when USP14 is complexed with the proteasome[293]. It furthermore inhibits specifically RLR signaling via TBK1 deubiqitination, while stabilizing cGAS/STING sig-

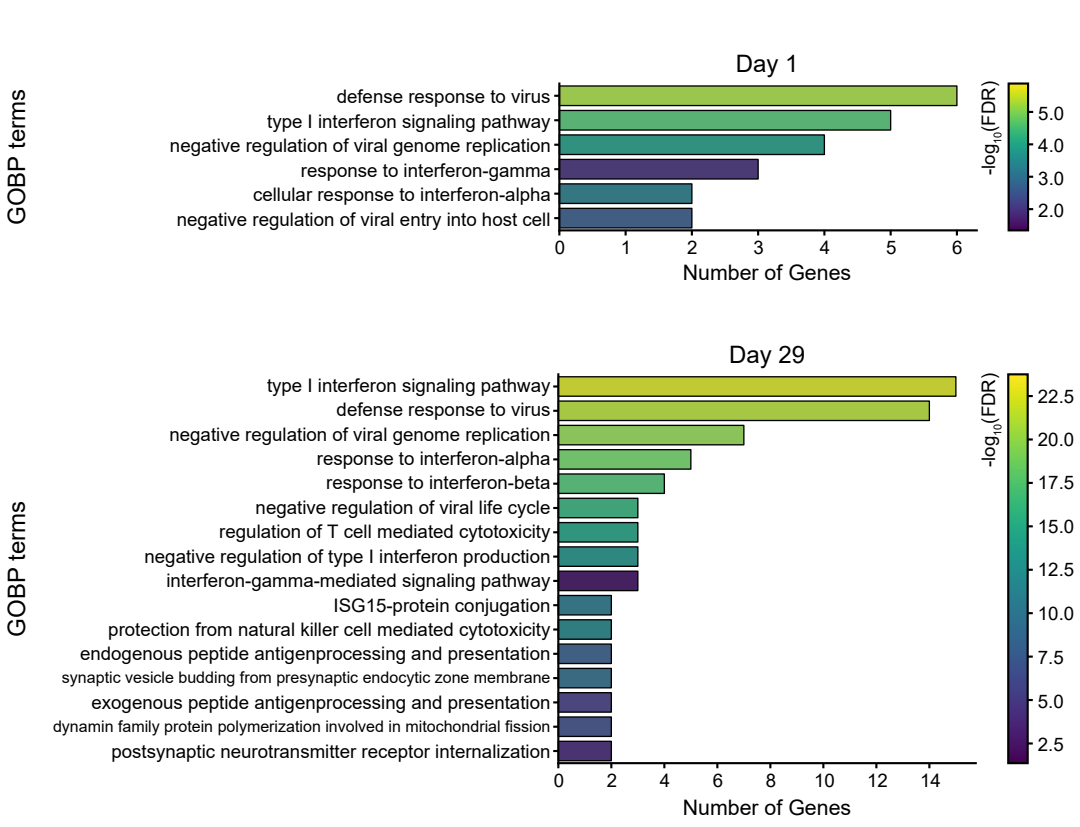

Figure 23: GOBP term enrichment analysis of A549 cells cultured in supernatant derived from NS5B-transduced cells.

Gene ontology (GO) terms for biological processes (BP) enriched in A549 cells cultured in supernatant derived from $NS5B^{WT}$-transduced A549 cells for 1 (a) or 29 (b) days (false discovery rate (FDR) < 0.05). For each day, the set of genes determined as significantly regulated (see Fig. 22) was analyzed for enriched BP terms with PANTHER, and most specific terms from the hierarchically sorted results are shown (lists of annotated genes: Table S4 and S5).

naling[294]. PSMB9 is a subunit of the immunoproteasome, a specialized version of the central protein degradation machinery in the cell[295]. Protein cleavage by the immunoproteasome is optimized to produce peptides for presentation via MHC class proteins[295]. LGALS3BP has been very recently described as a central negative modulator of the ISG response, interacting with several cellular proteins[272].

Genes significantly upregulated only on day 29 after treatment start that were not annotated included C1S, DExD/H-Box 60 like (DDX60L), poly(ADP-Ribose) polymerase family member 14 (PARP14), tetratricopeptide repeat and ankyrin repeat containing 1 (TRANK1), leucine aminopeptidase 3 (LAP3), UDP glucuronosyltransferase family 1 member A1 (UGT1A1), transmembrane 4 L six family member 4 (TM4SF4) and homogentisate 1,2-dioxygenase (HGD). The cytoplasmic helicase DDX60L has been shown to restrict HCV replication and moderately impact RIG-I activation in Huh-7 cells[285]. PARP14's role in innate immune regulation is yet poorly understood. Recent studies have shown antiviral properties against coronaviruses that depended on its polymerase activity and acted on IFN type I signaling (reviewed in [296]). TRANK1 is conserved among mammals and has been reported as an ISG before, although no known function has been determined as of yet[297,298]. Located in the cytosol, LAP3 is a metallopeptidase that was induced by IFN type I and II signaling in a time-dependent fashion[299]. Moreover, LAP3 levels were elevated in livers of CHC patients and were proposed as a biomarker for treatment outcome prediction[300,301].

Transcript levels of most genes did not change over the course of one month. Three genes, however, did not show significantly altered transcript levels after 24 h treatment, but were significantly upregulated after four weeks. HGD (2-fold upregulated) is involved in the amino acid catabolism of tyrosine and phenylalanine[302]. Pathway analysis[303] connects this gene with viral mRNA translation, however, we are not aware of any study investigating HGDs role in antiviral immunity. Active in the glucuronidation pathway, UGT1A1 (4.3-fold) is involved in the transformation of small, lipophilic molecules (e.g. hormones, steroids, and bilirubin) into hydrophilic metabolites[304]. Interestingly, UGT1A1 activity has been reported to be inhibited by the HCV NS3/4A protease inhibitor paritaprevir[305]. TM4SF4 (3.3-fold) belongs to the tetraspanin L6 family of cell surface receptors[306]. Although other tetraspanins are implicated in viral infection[307], such as the HCV entry receptor CD81, literature on TM4SF4 does not indicate a connection to infectious diseases. Surprisingly, however, a recent meta-analysis of severe acute respiratory syndrome coronavirus 2 (SARS-CoV2) transcriptomes ranked TM4SF4 among the top 20 transcripts significantly regulated in the collection of SARS-CoV2 transcriptomes, termed "SARS2 consensome"[308]. Here, SARS-CoV2 infection lead to a decrease in TM4SF4 transcript levels, which was also the case in A549 cells treated with NS5B supernatant for 1 day.

After one month of constant exposure to $NS5B^{WT}$-derived stimulatory factors, the transcriptional response exhibited overall remarkably little changes. Many well-studied ISGs

were among the strongly upregulated transcripts after 24 hours of treatment and more or less remained at the same levels four weeks later. For example, transcript levels increased the most for hit ISGs IFI27 (~2.6-fold up), guanylate binding protein 3 (GBP3; ~2.3-fold), and tetherin (BST2; ~2.2-fold) (Fig. 22b, dashed lines). Interferon induced protein 44 like (IFI44L), which was narrowly excluded for both time points due to p-values slightly above the cutoff, experienced the highest transcript fold increase over time (~5-fold up; from 7.8-fold over $NS5B^{GND}$-treated ($p = 0.09$) at day 1 to 39-fold ($p = 0.1$) at day 29). Conversely, among the significantly regulated genes, DDX60L experienced the strongest downregulation over time (~1.8-fold). In general, genes downregulated more than 2-fold over time were not as strongly affected by $NS5B^{WT}$ supernatant treatment as upregulated genes, in that their transcript levels changed less than 5-fold compared to $NS5B^{GND}$ (data not shown). For instance, among genes downregulated after one month that were excluded based on p-values, the bone morphogenic protein antagonist gremlin 1 (GREM1) experienced the strongest downregulation (~3.3-fold down; from 1.9-fold over $NS5B^{GND}$-treated ($p = 0.08$) at day 1 to 0.6-fold ($p = 0.12$) at day 29).

Finally, we analyzed the transcriptome datasets of $NS5B^{WT}$ supernatant-treated cells for differentially regulated genes that are not known transcriptional targets of IFN type I or III signaling. We extended the set of significantly regulated genes with i) genes that showed at least a fold difference of > 2, and ii) genes with a fold difference $<= 2$, but a p-value < 0.05. This extended gene set then was compared to genes listed in the Interferome database[253]. Here, genes significantly upregulated (f.c. > 2, p-value < 0.05) in patient samples or human cell lines after IFN type I or type III treatment were classified by us as ISGs. Consequently, genes from the long-term treatment experiment that were not listed in the database were classified as non-ISGs. This approach resulted in the classification of all hits from the transcriptome sets as well as the majority of genes from the extended gene sets as ISGs. In the long-term treatment setting, only four non-ISGs were found (Table 10). Beta-carotene oxygenase 1 (BCO1) was over 2-fold upregulated at day 1 and experienced slight downregulation over time. BCO1 catalyzes the oxidative cleavage of beta-carotene into retinaldehyde, a precursor of vitamin A[309]. The enzyme itself is not implicated in innate immunity or viral infections, but the important role of vitamin A in the immune system has been studied in detail[310]. The chemokine CXCL8/IL-8 as well as endoplasmic reticulum oxidoreductase 1 alpha (ERO1A) were both upregulated over time. Regulation of IL-8 has been extensively studied: Transcription is repressed under homeostatic conditions, but derepression can occur as a result of a variety of signals, including TNF and IL-1, and IL-8 expression requires NF-κB[311]. IL-8 is generally considered pro-inflammatory and pro-tumorigenic[311,312]. ERO1A re-oxidizes protein disulfide isomerase (PDI), a chaperone facilitating disulfide bond formation during protein folding, and is upregulated as part of the unfolded protein response[313,314]. Lastly, spexin hormone (SPX) was upregulated over time. SPX has been identified in 2007 due to similarities with galanin and is implicated in regulation of metabolism, mood and behavior[315].

Table 10: Non-ISGs.

Genes classified as non-ISGs by comparison of long-term NS5B^{WT} supernatant treatment experiment transcriptome data with genes listed in the Interferome database[253]. Genes were classified as non-ISGs if they have not been significantly regulated (f.c. > 2, p < 0.05) in IFN type I or type III treated samples or cell lines of human origin according to the database. Listed are fold changes (f.c.) over NS5B^{GND} supernatant treated cells and corrected p-values for time points day 1 (d1) and day 29 (d29). f.c.(d29/d1): fold difference between day 29 and day 1.

Gene	f.c.(d1)	p(d1)	f.c.(d29)	p(d29)	f.c.(d29/d1)
BCO1	2.12	0.072	1.71	0.116	0.81
CXCL8	1.34	0.840	2.23	0.480	1.66
ERO1A	1.20	0.840	2.25	0.288	1.87
SPX	0.65	0.771	2.44	0.701	3.73

The three differentially regulated genes – TM4SF4, UGT1A1, and HGD – were returned as ISGs from the database search. Of note, Interferome data indicated a slight downregulation of TM4SF4 upon IFN type I treatment within 4-6 hours after treatment start[253], which is in line with transcript levels after 24 h of NS5B supernatant treatment (Fig. 22b). Long-term treatment data, such as in this study, was not available in the database.

We concluded that in both, A549 and PH5CH, transcriptional changes induced by immunostimulatory factors secreted by NS5B^{WT}-expressing cells encompassed predominantly ISGs. Their induction can very likely be attributed to the combined effects of IFN type I and III signaling via IFN-β and IFN-λ. The prolonged stimulation with interferons furthermore did not affect transcription of most genes over time in A549 cells, with the exception of UGT1A1, HGD, and TM4SF4 that show disproportionate increase in mRNA levels after one month.

5 Discussion

Patients infected with HCV frequently progress to chronicity, in which the virus permanently replicates within the liver[5]. This is accompanied by a constant immune response that puts the liver into a state of chronic inflammation. Despite lacking the capacity to effectively clear the viral infection, inflammation-associated processes damage the liver and promote the development of malignancies[6]. In this study, we simulated aspects of a chronic inflammation state in a virus-free cell culture model of epithelial cells, thus being able to investigate the effects of persistent stimulation of all-intrinsic antiviral signaling without interference of viral countermeasures.

5.1 The NS5B Cell Culture Model of Continuous Innate Antiviral Signaling

We employed ectopic expression of the HCV RdRp NS5B to stimulate antiviral signaling pathways. NS5B transgene expression has been shown before to generate dsRNA and induce the production of cytokines. These reports also state the involvement of several PRRs, namely RIG-I[256,258], TLR3[257,316], and the NLR NOD1[317], in sensing the NS5B-derived dsRNA. Using CRISPR/Cas9-mediated gene knockout, we could show that a strong innate immune response, i.e. IFN production and subsequent ISG expression, depends exclusively on functional RIG-I in the immune-competent lung adenocarcinoma cell line A549 (Fig. 4). Based on our experimental approach, we cannot rule out that other signaling pathways might later add to, or are positively regulated by RIG-I signaling; however, RIG-I seems to be the driving force in detecting intracellular dsRNA produced by transgenic NS5B.

We could show that transgene expression of NS5B is an effective tool to induce an antiviral response in cells (Fig. 1–4). We argue that this method is superior to classical transfection of RLR agonists for several reasons. For example, it prevents the stress put on cells during transfection. Furthermore, we argue that the RNA species synthesized by NS5B are more closely related to physiological RIG-I agonists. We assume that NS5B incorporates 5'-ppp into nascent RNA during amplification of non-viral RNA templates, as it is the case for HCV genome replication[78]. In the absence of viral RNA genomes, NS5B has to rely on endogenous RNA as a template. NS5B without the C-terminal membrane anchor alternates between a closed and a more open confirmation, where the enzyme is less specific in terms of template RNA structures[36,45,318,319]. Although the precise structure of RNA molecules produced by ectopically expressed NS5B is not known, Yu *et al.* have reported that NS5B-derived RNAs are not based on specific RNA sequences, although a large fraction of sequences corresponded to non-coding RNAs[256]. The authors have hypothesized that these RNA species, as opposed to mRNA, might be more

accessible since they are not masked by the translational machinery[256]. In order to characterize the dsRNA produced by NS5B in A549 cells, we tried to isolate dsRNA from cells expressing NS5B. This, however, as well as using an immune fluorescence method to visualize dsRNA in fixed cells, was unsuccessful (data now shown). Possible explanations include low concentration and/or diffuse distribution of dsRNA, since NS5B is not concentrated in replication organelles, and short dsRNA molecule length.

The expression of GFP-tagged NS5B allowed us to investigate its subcellular localization. We observed an aggregation of $NS5B^{WT}$ and $NS5B^{GND}$ in clusters that seemed to be localized within the nucleus (Fig. 2e). A nucleolar localization of NS5B variants lacking the C-terminal membrane anchor has been reported before and was assigned to an interaction with nucleolin, a protein which is enriched in nucleoli[320–322]. In contrast to these findings, however, we observed no nucleolar or even nuclear enrichment of $NS5B^{\Delta}$ (Fig. 1e). This NS5B variant lacks a 10 amino acid stretch covering the GDD motif, but the reported nucleolin interaction sites do not overlap with the deleted section[321,322]. We argued that nucleolar enrichment could be due to NS5B binding to rRNA molecules, which are highly enriched in nucleoli[259], and that this binding might be impaired in $NS5B^{\Delta}$ due to the extent of the deletion. Alternatively, changes in tertiary protein structure related to the deletion could alter nucleolin binding affinity. It is unclear how NS5B proteins could translocate into the nucleus, since no NLS or interaction with nuclear pore complex proteins has been shown[323]. Many nuclear proteins lack a classical NLS and thus have to use alternative means of transport into the nucleus, for example via transport regulated by unconventional NLS or by piggybacking other proteins destined for nuclear import[324]. As viral proteins commonly integrate multiple functions and properties, a putative ability of NS5B to interact with proteins that can enter the nucleus is not unlikely. Since NS5B-derived dsRNA is sensed by RIG-I, a cytosolic PRR, it is unclear whether dsRNA produced in the nucleus would be detected at all. Interestingly, a recent study could show that a fraction of RIG-I molecules is present within the nucleus and is able to activate the canonical RLR pathway upon ligand binding[325].

Another advantage, and considered by us to be most important, is that transgenic expression of NS5B presumably provides a constant supply of dsRNA. This is in contrast to transfection methods, which introduce dsRNA more or less in a pulse-like fashion, and NS5B-derived dsRNA production should more closely resemble the build-up of dsRNA molecules during viral RNA genome replication. The NS5B cell culture model reported in this work exhibited constant RIG-I pathway activation and subsequent IFN production and ISG expression for a period of over 14 days (Fig. 5). This allowed us to study the phenotypes of a constantly active antiviral signaling over the course of several days, which will be discussed in the following paragraphs. Furthermore, the continuous RIG-I activation allowed for production of cytokines and other secreted factors at concentrations that are, presumably, closer to a steady-state condition than after RLR agonist transfection. This allowed us to study the composition of the NS5B-derived secretome and its effects on bystander cells without active RIG-I signaling (discussed in later sections).

We showed that cells expressing catalytically active NS5B exhibited impaired proliferation (Fig. 10). This finding was published in 2020 together with our collaboration partners from the Pichlmair lab (ref. [247]). In the publication, we stated that the observed growth defect depends on IRF3, but unlikely on IFNs. The IFN argument was made based on treatment of an A549-IFIT1-eGFP reporter cell line with IFN-α, IFN-β, and IFN-λ, respectively, where the concentrations of IFN-β and IFN-λ were adjusted to yield the same IFIT1-GFP expression as observed in IFN-α-treated cells. Here, cells experienced normal cell growth after treatment with 8.25 ng/ml IFN-α, 17 IU/ml IFN-β, or 9 ng/ml IFN-λ compared to untreated control cells[247]. When we later investigated the supernatant composition of NS5B-expressing cells in more detail in this work, we measured IFN-β levels almost 8-times higher, in the range of 130 IU/ml (Fig. 17a). While A549 proliferation was indeed only weakly impaired even by high concentrations of IFN-α (1000 IU/ml) or IFN-λ (100 ng), IFN-β had significant effects at 200 IU/ml (Fig. 16). We proceeded to show that proliferation is impaired through interferon signaling, where IFN-β is the main antiproliferative factor, and IFN-λ is slightly amplifying the effect (Fig. 16–18). An antiproliferative role has been reported before for IFNs (reviewed in [113]). Analogous to their antiviral properties, also the antiproliferative properties of IFNs correlate with their receptor binding affinity[90, 113]. It is therefore comprehensible that IFN-β, which exhibits greater affinity towards IFNAR2 than IFN-α subtypes or type III IFNs to IFNLR1[90], respectively, also possesses the strongest antiproliferative power. Importantly, though, IFNs elicit their antiviral effects already at concentrations about 3 magnitudes lower than necessary for antiproliferative effects: IFN-β and IFN-α, when used at concentrations that induce a comparable antiviral response, would differ about 50-fold in their antiproliferative potency[113]. Hence, adjusting IFN concentrations based on antiviral effects, as done in the first part of our work (ref. [247]), turns out to be not advisable when investigating antiproliferative effects of IFNs.

Using flow cytometry and FACS-based cell sorting, we could show that NS5B protein levels differed considerably on a single cell level, and that NS5B expression positively correlated with IFN-λ1 transcript levels (Fig. 8, Fig. 12). Furthermore, the gradual decrease in ISG expression coincided with a gradual disappearance of cells expressing high levels of NS5B (Fig. 9). In NS5B-transduced cells, we observed an increased frequency of cell death events at low, but reproducible, frequencies (Fig. 11). The induction of apoptosis can be a direct effect of RLR signaling[229–231]. IFN signaling may amplify RLR signaling and thus facilitate and/or accelerate apoptosis, but IFNs alone were unable to cause cell death in our experiments (Fig. 16). We could show that, in the context of overall proliferation activity, the role of cell death was neglectable compared to cytostatic effects of IFNs (Fig. 14–15). Nevertheless, we suspect that NS5B high-expressing cells could be over-proportionally affected by dsRNA-induced apoptosis. Data from our group indicated that cell death rates in response to dsRNA correlate with the concentration of dsRNA and with the duration of the stimulus, in that case the duration of lipofectamine-based dsRNA transfection[260]. We therefore argue that cells expressing high levels of NS5B, and/or

cells that do not downregulate NS5B expression over time, have a high chance to be subject to programmed cell death. Hence, NS5B high-expressing cells would sooner or later disappear from the cell pool, which could in part explain the observed reduction of overall NS5B protein levels in the population (Fig. 5, Fig. 9). Of note, this counterselection does not necessarily have to be exclusively due to extreme effects such as cell death. Already a growth disadvantage would remove NS5B high-expressers more effectively from the cell pool. One study reported that the overexpression of IRF3 in HeLa cells conferred an anti-proliferative effect that depended on IRF3 binding to DNA[326]. Whether IRF3 after RIG-I signaling-mediated phosphorylation exerts anti-proliferative effects in a similar fashion, however, is not known.

Intriguingly, the properties of the NS5B cell culture model discussed above display similarities to the distribution of HCV-infected cells within the liver. In fact, while a patient's liver as a whole is considered to be persistently infected, the infection seems to be highly dynamic on a single cell level[243,247,327,328]. Studies have reported that the infection is restricted to clusters of infected cells that are surrounded by non-infected tissue[247,327,328]. Interestingly, the clusters themselves were determined to be not older than a week, suggesting that HCV is constantly infecting previously uninfected cells and establishing new clusters[247,328]. Infected clusters as well as the surrounding bystander cells both experienced elevated ISG levels, which is likely due to IFN secretion from infected cells[243,247]. In this regard, our NS5B cell culture model, consisting of a minority of NS5B high-expressing and IFN-producing cells and a majority of NS5B low-expressing bystander cells, exhibits a comparable composition[247]. By design, however, it lacks two properties that seem to be necessary for HCV to establish a persistent infection. First, no re-infection takes place that would introduce or reinstate NS5B expression, as cells are transduced with replication-incompetent lentiviral vectors. Second, the immune response to dsRNA is not modulated by viral components that are present in HCV infected cells. HCV can inhibit RLR signaling through NS3/4A-mediated cleavage of MAVS[103,104,247]. Moreover, dsRNA levels, and thus the potency to trigger antiviral signaling and apoptosis, are reduced in HCV-infected cells via self-limiting replication and export of dsRNA replication intermediates[247,329,330]. These combined measures could be necessary for HCV to reduce or delay antiviral effects, such as apoptosis, until progeny virions are produced that can infect other cells. This would give HCV always just enough time to move to other cells before the immune response could clear the infection on the single cell level.

A goal of this work was to establish a cell culture model where a cells' antiviral system is constantly activated. As described before, this was achieved for a period of 2–3 weeks; however, NS5B levels, and subsequently ISG levels, decreased over time, until no antiviral activity could be detected about 3 weeks after NS5B transduction (Fig. 5). Extensive characterization of the system shed some light on the processes that resulted in the immune response to cease. Transduction of cells – even if done multiple times – resulted in a very heterogeneous population (Fig. 8). The fraction of NS5B low-expressing cells that survived antibiotic selection increased over time, as cells down-regulated transgene

expression independently of NS5B's catalytic activity. Gene silencing is a very dynamic process that is affected, among others, by components of the viral vector and the position of integration into the genome[331,332]. During the generation of transgene-overexpressing cell lines, cells are usually passaged several times before the generation process is considered to be completed. It is very likely that early after transduction, i.e. in the first days to weeks, transgene down-regulation constitutes a normal process during cell line generation, but is simply not monitored by the experimenter.

Protein levels of NS5B correlated on a single cell level with the production of IFN-λ1 mRNA, presumably because more dsRNA was generated that could activate RIG-I signaling (Fig. 8). ISG expression on the other hand was determined to be independent of the NS5B levels in an individual cell and depended on paracrine IFN signaling. Here, an important property of the IFN response comes into play. Since many components of the RLR signaling pathways are themselves ISGs and positively influence their pathway activity, IFN signaling effectively sensitizes all cells to respond to RLR agonists[121]. In our NS5B cell culture model, many cells exhibiting medium-to-low NS5B levels might on their own be unresponsive to their low intracellular dsRNA levels. Conversely, cells with high NS5B levels are able to produce enough dsRNA to effectively induce IFN production. Through autocrine and paracrine stimulation, these IFNs would then sensitize all cells, thus lowering the concentration threshold for dsRNA detection and allowing IFN production in previously unresponsive cells. Over time, however, with decreasing NS5B levels and the counterselection of NS5B high-expressing cells, IFN production and therefore sensitization would cease, until no immune response is detectable any more on a cell pool level.

Our experiences so far suggest that constant RLR signaling bears disadvantages for a cell, which will, sooner or later, lead to the disappearance of that cell from the cell pool. Nevertheless, it would be desirable to design an NS5B-based cell culture system that is truly able to exhibit persistent activation of antiviral signaling pathways. For future projects, it might be advantageous to envisage how this could be achieved. It has been reported that N-terminal modification decreases the activity of NS5B[333–335], which would result in lower amounts of dsRNA. We did not observe striking differences between the untagged and the N-terminally HA-tagged variants of NS5B in terms of immune stimulation, and our experimental data suggests that rather NS5B protein abundance plays a significant role. Thus, one important technical aspect would be to maintain a more stable NS5B expression rate. For this, other viral vector systems and different promoters could be tested. In this study, we have used the EF1α promoter, which is a ubiquitous promoter known for high transgene expression levels[332]. Low-level NS5B expression by the weak ROSA promoter did not result in measurable ISG expression (data not shown). It could be beneficial to use a promoter with a medium expression rate, or a cell type-specific promoter, as these are less likely to be the target of gene silencing than ubiquitous promoters[332]. The expression rate could be even more fine-tuned by using an inducible expression system[332,336]. Ultimately, though, our data suggest that it will be important

to strike a balance between two parameters: On one side, RLR stimulation has to be potent enough to produce IFNs, as their amplifying properties seem to be necessary for establishing a potent ISG response. On the other side, the immune response must not be too severe to avoid the (early) onset of detrimental effects such as cell death.

5.2 The NS5B Secretome

The NS5B system permits for continuous stimulation of the RLR/IFN axis for several days. This ensures constant production and secretion, and thus accumulation, not only of IFNs, but also of other factors induced by active RLR signaling. This allowed us to study the whole of secreted factors – the secretome – produced by cells in response to RLR signaling. In this work, we have analyzed 22 cytokines in the supernatant from two epithelial cell lines of different tissue origin (Fig. 17, Fig. 19). A549 and PH5CH cells displayed the same cytokine expression pattern after NS5B transduction, with levels of TNF, IL-6, CCL3, -4, -17, and CXCL10 being significantly increased in the supernatant. The expression of cytokines and chemokines in response to dsRNA or synthetic analogs has been investigated before by several groups, and next to RIG-I, also TLR3 and PKR were reported to induce their expression[66, 256, 337–339]. For the 6 cytokines detected in this study, our group could confirm through dsRNA-transfection experiments in A549 RIG-I knockout cells that a measurable production in response to intracellular dsRNA depends on functional RIG-I signaling (S. Wüst, unpublished data). The two detected pro-inflammatory cytokines, TNF and IL-6, both have central roles in inflammatory processes, where especially IL-6 is known as a driver for the establishment of chronic inflammation[193, 340]. Levels of the other pro-inflammatory cytokines included in the multiplex panel were not altered by NS5B activity. For some, such as IL-4 and IL-13, this was not unexpected, since they are known to be expressed primarily by cells of the adaptive immune system[341], while A549 and PH5CH are of epithelial origin. Unchanged IL-1β levels indicate that pyroptosis is not induced to significant levels upon NS5B transduction. To completely exclude the presence of inflammatory forms of cell death, other marker cytokines such as IL-18, IL-1α and IL-33 should be measured as well.

The detected chemokines – CCL3, -4, -17, and CXCL10 – are all associated with HCV infection, where their levels usually correlate with viral load and disease progression[177]. CCL3, CCL4, and CXCL10 are known drivers of fibrosis[177]. CXCL10 is thought to activate CXCR3-bearing HSCs to differentiate into myofibroblasts and produce connective tissue, while at the same time inhibiting NK cells in their function to negatively regulate HSC activity[177]. Furthermore, one study showed that CXCL10 can drive apoptosis in hepatocytes via TLR4[177, 280]. According to our transcriptome data, PH5CH cells exhibit ~2.5-fold higher basal TLR4 mRNA levels than A549 cells, and this difference could factor into why PH5CH, but not A549, displayed a low cell death rate upon treatment with supernatant from NS5B^{WT}-transduced cells (Fig. 17). Recently it was also shown that

CXCL10 expression in PHH and HepG2 cells is induced by Hepatitis A virus infection directly via RIG-I signaling and, unlike CCL4 and CCL5, was independent of IFN-λ signaling[342]. Interestingly, CXCL10 possesses biomarker properties for viral hepatitis: Elevated CXCL10 levels in HCV infected patients were reported to predict a poor response to antiviral therapy consisting of PEG-IFN-α and ribavirin[177,343]. Another chemokine typical for HCV infection, and also classified as pro-fibrogenic, is CCL5[177]. It acts similar to CCL3 and CCL4 on CCR1- and CCR5-presenting NK cells and T cells, and additionally on HSCs[177,344]. Although not covered in the chemokine panel in this study, we argue that NS5B-expressing cells likely also produce CCL5. A study reported expression of CCL5 in HCV-infected hepatoma cells and in primary human hepatocytes (PHH) treated with poly(I:C), and other cytokines detected in that study included CXCL10, CCL3 and -4, IL-6, and TNF[66]. The chemokine CCL17 is involved in the recruitment of regulatory T cells[344]. CCL17 was reported to be expressed in A549 cells infected with Respiratory syncytial virus (RSV) in a NF-κB-dependent way[345]. It was also shown to be expressed by DCs upon detection of HCV-infected hepatocytes[177,346,347]. Here, CCL17 is recruiting immunosuppressive T_{reg} cells[177], and in the context of CHC, this could play a role in the weakened T cell response observed in CHC patients.

When studying the vast field of cytokines in the context of infection and chronic inflammation, it quickly becomes apparent how important the immune-crosstalk between different cell types is. Immune cells are considered to be the primary targets of cytokines expressed by epithelial cells, although epithelial cells themselves can respond to these cytokines as well[174]. Of note, our transcriptome data indicated that neither NS5B supernatant nor the mix of IFN-β and IFN-λ1 significantly altered transcript levels of chemokine receptors, TNF receptor subunits, or IL6R in A549 and PH5CH cells (data not shown). Conversely, some cytokines are primarily produced by non-epithelial cells, but play important roles in the regulation of cytokine expression in epithelial cells. For example, T_h cell-derived cytokines IL-4, IL-13, and IL-17A were shown to synergize with dsRNA or poly(I:C) in inducing the expression of several cytokines in epithelial cells[348,349]. Therefore, it would be interesting to extend the NS5B cell culture model into a co-culture system that also contains different types of T cells. Likewise, a co-culture system with Kupffer cells, HSCs and other non-parenchymal liver cells could allow one to study the interplay of cell types in the progression of liver fibrosis.

Our secretome analysis is by far not exhaustive. Novel methods combining click-chemistry labeling of secreted proteins with unbiased mass spectrometry analysis could help to elucidate the whole composition of the secretome of cells with activated RIG-I signaling[350]. Of note, since most adherent cell lines cultured for several days produce components of the extracellular matrix, which potentially immobilize chemokines[175,177,351], chemokine concentrations measured in the NS5B supernatants may deviate from the local concentrations in the cell layer. Furthermore, studies have shown that cells, for example upon infection with HCV or after stimulation with IFNs, release exosomes[352–354]. These membrane vesicles constitute another way of cell-to-cell communication, as they

can shuttle proteins with antiviral properties and a variety of RNA species, such as mRNA, dsRNA, miRNAs, and lncRNAs, into recipient cells[353]. It is important to note that, since the supernatants used in this study were frozen and stored at -80 °C, exosomes could have been destroyed before treatment of cells.

5.3 Impact of the NS5B Secretome on "Uninfected" Bystander Cells

We had observed that IFNs are responsible for the cell growth inhibition and the ISG induction in $NS5B^{WT}$-transduced cells. Without knowing the exact composition of the secretome, we wanted to test whether any factors other than IFNs would affect cells on the transcriptional level as well. Treatment of naïve cells for 24 h with either NS5B supernatant or IFNs β and λ1 alone, however, induced very similar responses. In A549 cells and in PH5CH cells, both treatments induced the expression of mostly known ISGs (Fig. 20–21). The analysis of the micro-array data sets put us into a position where we had to choose between many potential hits (by disregarding statistical correction for multiple testing) or restricting the hit list to reduce the number of false positive hits (by choosing corrected p-values). For this work, we chose a hybrid approach when comparing transcript levels from two compositions, where we considered both fold-change values if at least one of them was statistically significant. Many genes that experienced a several-fold increase in transcript levels after treatment, but had p-values above the cutoff value, were also known ISGs (Fig. S5). Thus, even though NS5B-transduced cells express many different cytokines, the effect on the transcriptional landscape in epithelial cells seems to be largely dependent on IFNs. It has been suggested that IFN signaling may affect up to 10 % of the human genome[118, 142], but many transcriptional changes could be rather subtle and would therefore be below the resolution of the microarray. Nevertheless, data-mining the expression profiles beyond corrected p-values could uncover potential transcriptional patterns that change upon IFN or supernatant treatment and that could be used as primers for future studies.

mRNA transcript levels do not necessarily translate into protein abundance or activity, as those parameters are also affected by – to name a few – posttranscriptional modification, degradation, sequestration and complex formation. A more comprehensive approach would therefore be to integrate transcript profile analysis with other *omics* analysis methods. For example, unbiased proteome analysis such as the mass spectrometry analyses performed in this study would add valuable protein level data to the picture. More specialized mass spectrometry methods even allow for discriminating the PTM status of a protein, for example the phosphorylation state[355].

5.4 Stimulation with IFNs and Beyond: Long-Term Effects and Implications for Hepatocellular Carcinoma

The interferon response is a rapid and usually transient process, and its dynamics have been studied extensively in the context of immediate responses. The roles of continuous IFN signaling, which is a common characteristic of CHC, are only beginning to emerge[356]. To study those effects in cell culture, we figured that a month of constant exposure to the supernatant from NS5B-transduced cells would constitute a suitable first step towards simulating a chronic immunostimulatory state. Strikingly, the expression profile did not change significantly, and cells maintained a classical ISG response throughout (Fig. 22). Importantly, established ISGs with negative regulatory properties were not strongly downregulated over time. USP18, a prime inhibitor of type I IFN signaling[90], was initially upregulated and mRNA levels decreased only ~1.4-fold (Fig. S5). In fact, transcript levels of negative regulators such as ISG15 and the recently discovered LGALS3BP even increased. IFI44L exhibited the strongest fold increase over time (described in section 4.9.3). Recently, several studies examined this poorly studied ISG and its paralog, IFI44, in more detail. IFI44L was shown to negatively modulate the antiviral response by interfering with IKK activity, thus impairing IRF3 phosphorylation and NF-κB activation[357]. This activity of IFI44L represents a negative feedback loop that acts downstream of PAMP recognition. We argue that IFI44L upregulation probably had no effect on the antiviral response in the long-term treatment experiment, since no dsRNA or other intracellular PAMPs were introduced, but a contribution to dampening the immune response in NS5B-transduced cells cannot be ruled out. Additionally, IFI44 and IFI44L were assigned antiproliferative roles[358]. In the context of HCC, a study showed that IFI44L acts as a tumor suppressor, inhibiting the Met/Src signaling pathway in cancer stem cells and thereby reducing migration, invasion, and metastasis formation, and attenuating the development of chemoresistance to doxorubicin[359].

Only three genes – HGD, UGT1A1, and TM4SF4 – changed their expression pattern clearly over the course of one month. Based on their functions (described in section 4.9.3), no obvious common connection to a specific pathway or a specific role in the antiviral response arises for the three genes. Of note, the temporal resolution of transcript level changes was rather low in our long-term experiment, as we only compared day 1 and day 29 after treatment. It is therefore necessary to measure transcript levels at other time points to determine whether these genes reach the levels observed on day 29 already a couple of days after treatment start or if mRNA levels gradually increase. Additionally, long-term treatment with NS5B supernatant should be compared to long-term treatment with IFN-β and IFN-λ1, and results should be confirmed in other cell lines such as PH5CH. One of the three differentially regulated genes, the tetraspanin TM4SF4, was among the central hits in a meta-analysis of transcriptome data sets from human cells infected with SARS-CoV2[308]. SARS-CoV2, a (+)ssRNA betacoronavirus that is sensed

in epithelial cells by MDA5, is the causative agent responsible for the coronavirus disease 2019 (COVID-19) pandemic[360]. It mainly infects the lung and induces respiratory illness as well as an inflammatory response that, when accelerating out of control, can lead to cytokine storm syndrome, acute respiratory distress syndrome and respiratory failure[360–362]. Furthermore, TM4SF4 has been implicated in cancer. As opposed to IFI44Ls suggested role as a tumor suppressor, TM4SF4 was reported to protect lung cancer cells from γ-radiation, and to induce and maintain cancer stemness[363,364]. More precisely, loss of promoter methylation leads to increased TM4SF4 expression, which in turn activates a positive feedback loop involving the expression of the cytokine osteopontin and the activation of IGF1Rβ/PI3K/AKT/NF-κB and JAK2/STAT3 signaling pathways[364]. TM4SF4 was also shown to be upregulated in regenerating rat liver tissue[364,365] and in human hepatocellular carcinomas, where it accelerated tumor cell growth[364,366,367]. We argue that TM4SF4's implication in cancer development and the novel link to viral infection makes it the most interesting candidate to further investigate.

A couple of reports have described the concept of IFN refractoriness, where cells *in vivo* and *in vitro* became unresponsive to IFNs after a few hours of stimulation[368–370]. The most recent studies narrowed down IFN refractoriness only to IFN-α due to negative feedback regulation via USP18[139,370]. Our results from several experiments, where cells received IFN-α for 2 weeks (Fig. 7) or NS5B supernatant for 2–4 weeks (Fig. 13, Fig. 22), do not indicate any form of refractoriness. In the case of IFN-α, these contradicting results could be due to differences in host organism and cell type, as IFN refractoriness was reported in mice[139,369,370] and human fibroblasts[368], respectively. Furthermore, the time between IFN-α treatments differed between our experiment (every 3 days) and the reports (within 24 h)[139,370]. USP18 has been shown to be unable to significantly inhibit IFN-β signaling or type III IFN signaling[90], and our data from long-term NS5B supernatant treatment experiments in A549 cells supports the notion that cells do not become refractory to IFN-β or IFN-λ. Interestingly, the effects of prolonged activation of the innate immune response have been studied in mice with the help of a viral RdRp. In a mouse model, which systemically expresses a picornavirus RdRp under the control of the ubiquitous ubiquitin c promoter, RdRp activity resulted in RLR signaling via MDA5 and MAVS, and in IFNAR-dependent induction of ISGs[371–374]. Moreover, RdRp expression was reported to be stable and life-long. It is not clear to us why the mice, in contrast to our NS5B-expressing A549 cells, seemingly do not lose RdRp expression; however, various parameters differ between the two experimental approaches, such as *in vivo* versus *in vitro* systems; differences in organisms, RdRp type, and expression control; and the fact that the picornavirus RdRp produces PAMPs that activate MDA5, while NS5B-derived dsRNA is sensed by RIG-I. The series of publications demonstrated that the present IFN signaling created a protective effect against infection with viruses from several families, including picornavirus, rhabdovirus, herpesvirus, and retrovirus[371–374]. Interestingly, mice did not exhibit any negative effects despite consistent and systemic IFN production, which was expected to induce interferonopathy-like disease manifesta-

tions[374]. Studies have shown that the knockout of adenosine deaminase acting on RNA 1 (ADAR1) in mice is lethal during embryo development[375,376]. ADAR1 is responsible for adenosine to inosine conversion in dsRNA, which is required to prevent detection of endogenous dsRNA by MDA5[376]. Impaired ADAR1 RNA editing function led to the activation of MDA5 by endogenous dsRNA, and MDA5 knockout rescued lethality and normalized development in the ADAR1 knockout[376]. Since constant MDA5 activation was proven to be the cause for *in utero* lethality[376], it is unclear how RdRp-expressing mice could develop normally; however, since these mice presumably possess functional ADAR1, it is possible that MDA5 activation is fine-tuned by the enzyme's RNA editing activity. Taken together, these reports underline the potential of viral RdRps as molecular tools able to induce specific antiviral signaling pathways, and support our findings that cells retain the ability to sense IFNs even after prolonged exposure periods.

Gene transcription is heavily modulated by epigenetic remodeling, where various histone modifications and DNA methylation control the condensation state of chromatin and thus regulate whether a gene is accessible for the transcriptional machinery[377]. In a recent review article, Barrat *et al.* explained the basic concepts of IFN-mediated epigenetic remodeling[254]. The effect of IFN signaling on chromatin state is thought to be primarily conducted through the actions of STAT and IRF proteins, which bind to DNA and recruit epigenetic remodelers. For example, IFN type I signaling can induce transcription-promoting histone modifications H3K4me3 and H3K36me3[254,378,379]. IFN signaling furthermore induces the recruitment of transcription factors and regulators and the establishment of latent enhancer complexes[254,379,380]. These concepts are termed "bookmarking" and "priming"[254,378,381,382], and the general idea is that IFN signaling prepares sets of genes for fast and amplified transcription once the cell detects IFNs again[254]. Importantly, IFN-mediated epigenetic remodeling can persist for weeks without active IFN signaling, and it can extend to non-ISGs, such as inflammatory mediators, although the full extent of affected regions has yet to be determined[254]. The field of epigenetics is constantly improving methods to determine the type and location of certain epigenetic markers. Bisulfite sequencing is able to reveal whether a nucleotide was methylated or not, while chromatin immunoprecipitation can be used to identify genome segments that are associated with certain histone modifications[377,383,384]. Methods like assay for transposase-accessible chromatin using sequencing (ATAC-seq), or sequencing following DNase or MNase digestion, can be employed to map genome regions that are accessible for transcription[377,385]. An understanding of changes in the epigenome in response to IFN will be a valuable addition to transcriptomic data generated in this work. Important questions for future studies include whether/how the epigenetic landscape is remodeled over the course of extended IFN signaling, and whether IFN-mediated epigenetic remodeling plays a role in epithelial cells as important as it does in immune cells, where most studies have been conducted so far[254]. Additionally, as cells primed by IFN will presumably react differently to secondary stimulations, it would be interesting to test at different time points during long-term IFN treatment how cells respond to secondary

IFN treatment, virus infection, or various signaling molecules such as death ligands or growth factors.

IFNs play key roles in the immune response initiation upon detection of pathogens or danger signals[121]. Interestingly, though, the impact of type I IFNs changes with the establishment of chronic infections, where they are thought to drive a pro-inflammatory, but immunosuppressive milieu[356]. Snell *et al.* have summarized key features of type I IFN-derived immunosuppressive processes and have drawn parallels to the immune-suppressed microenvironment of tumors[356]. Fundamentally, prolonged type I IFN production results in the expression of several factors with immunosuppressive properties, such as the cell surface receptor programmed cell death 1 (PD-1) and its ligand PD-L1, indoleamine 2,3-deoxygenase (IDO), and IL-10[356]. These factors inhibit immune cell subtypes that could effectively target infected or cancerous cells (e.g. $CD8^+$ T cells), or inhibit cells that could aid in the immune response (e.g. $CD4^+$ T_h cells)[356]. At the same time, the milieu promotes differentiation and proliferation of certain immune cell subtypes that possess a more regulatory phenotype (e.g. plasmacytoid DCs, T_{reg} cells) and thus suppress effective cellular immune responses[356]. Of note, studies showed that inhibition of IFN signaling in a lymphocytic choriomeningitis virus (LCMV) chronic infection model resulted in control of viral infection, reduced viral titers, and abolishment of many immune dysfunctions, thus supporting the notion of persistence-favoring roles of type I IFNs in virus infections[356,386,387]. Cancers of the liver constitute an especially interesting subject, as they may develop in the immune-suppressed environment of chronically inflamed liver tissue[388]. HCC, the most common form of primary liver cancer, is responsible for the second-most cancer-related deaths worldwide[389–391]. The majority of HCCs develop in the context of liver cirrhosis and chronic inflammation, and the already damaged liver tissue in combination with often late-stage detection and a high recurrence rate result in an overall poor prognosis for patients[232,390–394]. HCV has both direct and indirect roles in the development of HCC. Several HCV proteins have been reported to induce epigenetic remodeling that leads to silencing of tumor suppressor genes and activation of oncogenes (reviewed in [395]). A recent study could show that HCV infection leaves an epigenetic “scar”, which remains long after DAA treatment has lead to a sustained virologic response, and which correlates with increased risk of HCC occurrence[396]. The authors furthermore demonstrated, using a HCV subgenomic replicon system in Huh7.5 hepatoma cells, that these epigenetic changes required the presence of HCV RNA and/or HCV non-structural proteins, and were not transmitted to uninfected bystander cells in a transwell co-culture setting. Since Huh7.5 cells lack functional RIG-I signaling[397], we assume that no IFNs, cytokines, or other soluble factors were secreted in those experiments as done by NS5B-expressing cell lines with functional RIG-I. Thus, we argue that the treatment with the NS5B secretome is well-suited to study differences between the epigenetic signatures present in HCV infected cells and uninfected bystander cells. HCV infection also favors tumor development indirectly through the establishment of chronic inflammation. Pro-inflammatory signaling has been shown to promote HCC develop-

ment. For example, the continued IL-6 production in the chronically inflamed liver drives pro-tumorigenic processes via STAT3 signaling (reviewed in [390]). In contrast, signaling via STAT1 and STAT2, which are the main signal transducers downstream of IFN receptors, are considered to be anti-tumorigenic, in part due to anti-proliferative properties[390]. These findings suggest that IFNs could have a direct inhibitory effect on tumor cell proliferation; however, the anti-proliferative properties of IFNs could also exert an evolutionary pressure on the tumor, and tumor cells escaping the IFN-induced arrest would likely be highly malignant in terms of proliferative speed. Hence, we consider that studying the effects of prolonged IFN or NS5B secretome treatment on different HCC cell lines could give valuable insights into HCC disease progression.

5.5 Conclusion

In this work, we have described the potential of the HCV RdRp NS5B as a molecular tool to induce near-physiological activation of RIG-I signaling. While NS5B expression itself was limited due to gene silencing and counterselection processes, and thus warrants further fine-tuning, a novel application emerged in the production of a “NS5B secretome”, which is the whole of factors secreted upon NS5B-activated RIG-I signaling. We showed that the NS5B secretome, although containing at least several pro-inflammatory cytokines and chemokines, exerted its antiproliferative role and the transcriptional upregulation of (mostly well-known) ISGs through IFN type I and III signaling. Long-term treatment results support the notion that cells do not become refractory to IFN signaling, and differentially regulated genes HGD, UGT1A1, and especially TM4SF4 constitute interesting candidates for further analysis. The findings presented in this work lay the foundation for improving the NS5B cell culture model, and we suggest focusing future research on supernatant transfer or co-culture applications. First, (transwell) co-culture systems of NS5B-expressing cells with immune cells and/or non-parenchymal liver cells could shed light on the dynamics of cytokine signaling and the processes responsible for the transition from acute to chronic inflammation. Second, the NS5B secretome may be employed to study the effects of continuous IFN signaling on the epigenetic landscape in epithelial cells. And third, it would be intriguing to elucidate the long-term effects of IFNs and other NS5B secretome components on the evolution of hepatocellular carcinoma cells.

Although nowadays an HCV infection can be effectively treated in most patients using DAAs, CHC-related liver damage and chronic inflammation-related HCC still pose major medical problems[388]. At the same time, novel viruses such as SARS-CoV2 emerge as global health threats and demonstrate how the deregulation of the immune response, as observed in serious cases of COVID-19, can have detrimental effects on a patient’s body[360]. We hope that the results obtained in this work may be used as primers for future studies that further elucidate the complex dynamics of the immune signaling networks at the core of these diseases.

Bibliography

[1] Parkin, J. & Cohen, B. An Overview of the Immune System. *Lancet* **357**, 1777–1789 (2001).

[2] Duggal, N. K. & Emerman, M. Evolutionary Conflicts Between Viruses and Restriction Factors Shape Immunity. *Nat. Rev. Immunol.* **12**, 687–695 (2012).

[3] Paul, D. & Bartenschlager, R. Architecture and Biogenesis of Plus-Strand RNA Virus Replication Factories. *World J. Virol.* **2**, 32–48 (2013).

[4] McCarthy, M. K. & Morrison, T. E. Persistent RNA Virus Infections: Do PAMPs Drive Chronic Disease? *Curr. Opin. Virol.* **23**, 8–15 (2017).

[5] Heim, M. H. & Thimme, R. Innate and Adaptive Immune Responses in HCV Infections. *J. Hepatol.* **61**, S14–25 (2014).

[6] Tanwar, S., Rhodes, F., Srivastava, A., Trembling, P. M. & Rosenberg, W. M. Inflammation and Fibrosis in Chronic Liver Diseases Including Non-Alcoholic Fatty Liver Disease and Hepatitis C. *World J. Gastroenterol.* **26**, 109–133 (2020).

[7] WHO | Global Hepatitis Report, 2017. http://www.who.int/hepatitis/publications/global-hepatitis-report2017/en/.

[8] Simmonds, P. The Origin of Hepatitis C Virus. In Bartenschlager, R. (ed.) *Hepatitis C Virus: From Molecular Virology to Antiviral Therapy*, Current Topics in Microbiology and Immunology, 1–15 (Springer, Berlin, Heidelberg, 2013).

[9] Guzman, M. G. & Harris, E. Dengue. *Lancet* **385**, 453–465 (2015).

[10] Yun, S.-I. & Lee, Y.-M. Zika Virus: An Emerging Flavivirus. *J. Microbiol.* **55**, 204–219 (2017).

[11] Kaito, M. *et al.* Hepatitis C Virus Particle Detected by Immunoelectron Microscopic Study. *J. Gen. Virol.* **75 (Pt 7)**, 1755–1760 (1994).

[12] Moradpour, D. & Penin, F. Hepatitis C Virus Proteins: From Structure to Function. In Bartenschlager, R. (ed.) *Hepatitis C Virus: From Molecular Virology to Antiviral Therapy*, Current Topics in Microbiology and Immunology, 113–142 (Springer, Berlin, Heidelberg, 2013).

[13] Gong, Y. & Cun, W. The Role of ApoE in HCV Infection and Comorbidity. *Int. J. Mol. Sci.* **20** (2019).

[14] Neufeldt, C. J., Cortese, M., Acosta, E. G. & Bartenschlager, R. Rewiring Cellular Networks by Members of the Flaviviridae Family. *Nat. Rev. Microbiol.* **16**, 125–142 (2018).

[15] Houghton, M. Hepatitis C Virus: 30 Years after Its Discovery. *Cold Spring Harb. Perspect. Med.* **9**, a037069 (2019).

[16] Alter, M. J. HCV Routes of Transmission: What Goes Around Comes Around. *Semin. Liver Dis.* **31**, 340–346 (2011).

[17] Colpitts, C. C., Tsai, P.-L. & Zeisel, M. B. Hepatitis C Virus Entry: An Intriguingly Complex and Highly Regulated Process. *Int. J. Mol. Sci.* **21**, 2091 (2020).

[18] Koutsoudakis, G. *et al.* Characterization of the Early Steps of Hepatitis C Virus Infection by Using Luciferase Reporter Viruses. *J. Virol.* **80**, 5308–5320 (2006).

[19] Zeisel, M. B. *et al.* Scavenger Receptor Class B Type I Is a Key Host Factor for Hepatitis C Virus Infection Required for an Entry Step Closely Linked to CD81. *Hepatology* **46**, 1722–1731 (2007).

[20] Harris, H. J. *et al.* CD81 and Claudin 1 Coreceptor Association: Role in Hepatitis C Virus Entry. *J. Virol.* **82**, 5007–5020 (2008).

[21] Evans, M. J. *et al.* Claudin-1 Is a Hepatitis C Virus Co-Receptor Required for a Late Step in Entry. *Nature* **446**, 801–805 (2007).

[22] Benedicto, I. *et al.* The Tight Junction-Associated Protein Occludin Is Required for a Postbinding Step in Hepatitis C Virus Entry and Infection. *J. Virol.* **83**, 8012–8020 (2009).

[23] Krieger, S. E. *et al.* Inhibition of Hepatitis C Virus Infection by Anti-Claudin-1 Antibodies Is Mediated by Neutralization of E2–CD81–Claudin-1 Associations. *Hepatology* **51**, 1144–1157 (2010).

[24] Brazzoli, M. *et al.* CD81 Is a Central Regulator of Cellular Events Required for Hepatitis C Virus Infection of Human Hepatocytes. *J. Virol.* **82**, 8316–8329 (2008).

[25] Lupberger, J. *et al.* EGFR and EphA2 Are Host Factors for Hepatitis C Virus Entry and Possible Targets for Antiviral Therapy. *Nat. Med.* **17**, 589–595 (2011).

[26] Zona, L. *et al.* HRas Signal Transduction Promotes Hepatitis C Virus Cell Entry by Triggering Assembly of the Host Tetraspanin Receptor Complex. *Cell Host Microbe* **13**, 302–313 (2013).

[27] Blanchard, E. *et al.* Hepatitis C Virus Entry Depends on Clathrin-Mediated Endocytosis. *J. Virol.* **80**, 6964–6972 (2006).

[28] Liu, S. *et al.* The Second Extracellular Loop Dictates Occludin-Mediated HCV Entry. *Virology* **407**, 160–170 (2010).

[29] Farquhar, M. J. *et al.* Hepatitis C Virus Induces CD81 and Claudin-1 Endocytosis. *J. Virol.* **86**, 4305–4316 (2012).

[30] Niepmann, M. & Gerresheim, G. K. Hepatitis C Virus Translation Regulation. *Int. J. Mol. Sci.* **21**, 2328 (2020).

[31] Pietschmann, T., Lohmann, V., Rutter, G., Kurpanek, K. & Bartenschlager, R. Characterization of Cell Lines Carrying Self-Replicating Hepatitis C Virus RNAs. *J. Virol.* **75**, 1252–1264 (2001).

[32] Romero-Brey, I. *et al.* Three-Dimensional Architecture and Biogenesis of Membrane Structures Associated with Hepatitis C Virus Replication. *PLOS Pathog.* **8**, e1003056 (2012).

[33] Paul, D. & Bartenschlager, R. Flaviviridae Replication Organelles: Oh, What a Tangled Web We Weave. *Annu. Rev. Virol.* **2**, 289–310 (2015).

[34] Lohmann, V. *et al.* Replication of Subgenomic Hepatitis C Virus RNAs in a Hepatoma Cell Line. *Science* **285**, 110–113 (1999).

[35] Paul, D., Hoppe, S., Saher, G., Krijnse-Locker, J. & Bartenschlager, R. Morphological and Biochemical Characterization of the Membranous Hepatitis C Virus Replication Compartment. *J. Virol.* **87**, 10612–10627 (2013).

[36] Lohmann, V. Hepatitis C Virus RNA Replication. In Bartenschlager, R. (ed.) *Hepatitis C Virus: From Molecular Virology to Antiviral Therapy*, Current Topics in Microbiology and Immunology, 167–198 (Springer, Berlin, Heidelberg, 2013).

[37] Ferrari, E. *et al.* Characterization of Soluble Hepatitis C Virus RNA-Dependent RNA Polymerase Expressed in Escherichia Coli. *J. Virol.* **73**, 1649–1654 (1999).

[38] Ivashkina, N. *et al.* The Hepatitis C Virus RNA-Dependent RNA Polymerase Membrane Insertion Sequence Is a Transmembrane Segment. *J. Virol.* **76**, 13088–13093 (2002).

[39] Bressanelli, S. *et al.* Crystal Structure of the RNA-Dependent RNA Polymerase of Hepatitis C Virus. *Proc. Natl. Acad. Sci. U.S.A.* **96**, 13034–13039 (1999).

[40] Lescar, J. & Canard, B. RNA-Dependent RNA Polymerases from Flaviviruses and Picornaviridae. *Curr. Opin. Struct. Biol.* **19**, 759–767 (2009).

[41] Appleby, T. C. *et al.* Structural Basis for RNA Replication by the Hepatitis C Virus Polymerase. *Science* **347**, 771–775 (2015).

[42] Li, H.-C., Yang, C.-H. & Lo, S.-Y. Hepatitis C Viral Replication Complex. *Viruses* **13**, 520 (2021).

[43] Sun, X. L., Johnson, R. B., Hockman, M. A. & Wang, Q. M. De Novo RNA Synthesis Catalyzed by HCV RNA-Dependent RNA Polymerase. *Biochem. Biophys. Res. Commun.* **268**, 798–803 (2000).

[44] Zhong, W., Uss, A. S., Ferrari, E., Lau, J. Y. & Hong, Z. De Novo Initiation of RNA Synthesis by Hepatitis C Virus Nonstructural Protein 5B Polymerase. *J. Virol.* **74**, 2017–2022 (2000).

[45] Shim, J. H., Larson, G., Wu, J. Z. & Hong, Z. Selection of 3'-Template Bases and Initiating Nucleotides by Hepatitis C Virus NS5B RNA-Dependent RNA Polymerase. *J. Virol.* **76**, 7030–7039 (2002).

[46] Biswal, B. K. *et al.* Crystal Structures of the RNA-dependent RNA Polymerase Genotype 2a of Hepatitis C Virus Reveal Two Conformations and Suggest Mechanisms of Inhibition by Non-nucleoside Inhibitors. *J. Biol. Chem.* **280**, 18202–18210 (2005).

[47] Mosley, R. T. *et al.* Structure of Hepatitis C Virus Polymerase in Complex with Primer-Template RNA. *J. Virol.* **86**, 6503–6511 (2012).

[48] Simister, P. *et al.* Structural and Functional Analysis of Hepatitis C Virus Strain JFH1 Polymerase. *J. Virol.* **83**, 11926–11939 (2009).

[49] Powdrill, M. H. *et al.* Contribution of a Mutational Bias in Hepatitis C Virus Replication to the Genetic Barrier in the Development of Drug Resistance. *Proc. Natl. Acad. Sci. U.S.A.* **108**, 20509–20513 (2011).

[50] Vieyres, G. & Pietschmann, T. HCV Pit Stop at the Lipid Droplet: Refuel Lipids and Put on a Lipoprotein Coat before Exit. *Cells* **8** (2019).

[51] Neumann, A. U. *et al.* Hepatitis C Viral Dynamics in Vivo and the Antiviral Efficacy of Interferon-Alpha Therapy. *Science* **282**, 103–107 (1998).

[52] Thimme, R., Binder, M. & Bartenschlager, R. Failure of Innate and Adaptive Immune Responses in Controlling Hepatitis C Virus Infection. *FEMS Microbiol. Rev.* **36**, 663–683 (2012).

[53] Takeuchi, O. & Akira, S. Pattern Recognition Receptors and Inflammation. *Cell* **140**, 805–820 (2010).

[54] Liu, G. & Gack, M. U. Distinct and Orchestrated Functions of RNA Sensors in Innate Immunity. *Immunity* **53**, 26–42 (2020).

[55] Vautier, S., MacCallum, D. M. & Brown, G. D. C-Type Lectin Receptors and Cytokines in Fungal Immunity. *Cytokine* **58**, 89–99 (2012).

[56] Reikine, S., Nguyen, J. B. & Modis, Y. Pattern Recognition and Signaling Mechanisms of RIG-I and MDA5. *Front. Immunol.* **5**, 342 (2014).

[57] Choi, A. J. S. & Ryter, S. W. Inflammasomes: Molecular Regulation and Implications for Metabolic and Cognitive Diseases. *Mol. Cells* **37**, 441–448 (2014).

[58] Holm, C. K., Paludan, S. R. & Fitzgerald, K. A. Dna Recognition in Immunity and Disease. *Curr. Opin. Immunol.* **25**, 13–18 (2013).

[59] Sun, L., Wu, J., Du, F., Chen, X. & Chen, Z. J. Cyclic GMP-AMP Synthase Is a Cytosolic DNA Sensor That Activates the Type I Interferon Pathway. *Science* **339**, 786–791 (2013).

[60] Rehwinkel, J. & Gack, M. U. RIG-I-Like Receptors: Their Regulation and Roles in RNA Sensing. *Nat. Rev. Immunol.* **20**, 537–551 (2020).

[61] Maelfait, J., Liverpool, L. & Rehwinkel, J. Nucleic Acid Sensors and Programmed Cell Death. *J. Mol. Biol* **432**, 552–568 (2020).

[62] Metz, P., Reuter, A., Bender, S. & Bartenschlager, R. Interferon-Stimulated Genes and Their Role in Controlling Hepatitis C Virus. *J. Hepatol.* **59**, 1331–1341 (2013).

[63] O'Neill, L. A. J., Golenbock, D. & Bowie, A. G. The History of Toll-Like Receptors — Redefining Innate Immunity. *Nat. Rev. Immunol.* **13**, 453–460 (2013).

[64] Jin, M. S. & Lee, J.-O. Structures of the Toll-like Receptor Family and Its Ligand Complexes. *Immunity* **29**, 182–191 (2008).

[65] Gay, N. J., Gangloff, M. & O'Neill, L. A. J. What the Myddosome Structure Tells Us About the Initiation of Innate Immunity. *Trends Immunol.* **32**, 104–109 (2011).

[66] Li, K. *et al.* Activation of Chemokine and Inflammatory Cytokine Response in Hepatitis C Virus–Infected Hepatocytes Depends on Toll-Like Receptor 3 Sensing of Hepatitis C Virus Double-Stranded RNA Intermediates. *Hepatology* **55**, 666–675 (2012).

[67] Yamamoto, M. *et al.* Role of Adaptor TRIF in the MyD88-Independent Toll-Like Receptor Signaling Pathway. *Science* **301**, 640–643 (2003).

[68] Oshiumi, H., Matsumoto, M., Funami, K., Akazawa, T. & Seya, T. TICAM-1, an Adaptor Molecule That Participates in Toll-Like Receptor 3-Mediated Interferon-β Induction. *Nat. Immunol.* **4**, 161–167 (2003).

[69] Uchikawa, E. *et al.* Structural Analysis of dsRNA Binding to Anti-viral Pattern Recognition Receptors LGP2 and MDA5. *Mol. Cell* **62**, 586–602 (2016).

[70] Rothenfusser, S. *et al.* The RNA Helicase LGP2 Inhibits TLR-Independent Sensing of Viral Replication by Retinoic Acid-Inducible Gene-I. *J. Immunol.* **175**, 5260–5268 (2005).

[71] Childs, K. S., Randall, R. E. & Goodbourn, S. LGP2 Plays a Critical Role in Sensitizing mda-5 to Activation by Double-Stranded RNA. *PLOS ONE* **8**, e64202 (2013).

[72] Deddouche, S. *et al.* Identification of an LGP2-Associated MDA5 Agonist in Picornavirus-Infected Cells. *eLife* **2014** (2014).

[73] Schlee, M. *et al.* Recognition of 5′ Triphosphate by RIG-I Helicase Requires Short Blunt Double-Stranded RNA as Contained in Panhandle of Negative-Strand Virus. *Immunity* **31**, 25–34 (2009).

[74] Schlee, M. & Hartmann, G. Discriminating Self from Non-Self in Nucleic Acid Sensing. *Nat. Rev. Immunol.* **16**, 566–580 (2016).

[75] Saito, T., Owen, D. M., Jiang, F., Marcotrigiano, J. & Jr, M. G. Innate Immunity Induced by Composition-Dependent RIG-I Recognition of Hepatitis C Virus RNA. *Nature* **454**, 523–527 (2008).

[76] Hornung, V. *et al.* 5'-Triphosphate RNA Is the Ligand for RIG-I. *Science* **314**, 994–997 (2006).

[77] Pichlmair, A. *et al.* RIG-I-Mediated Antiviral Responses to Single-Stranded RNA Bearing 5'-Phosphates. *Science* **314**, 997–1001 (2006).

[78] Decroly, E., Ferron, F., Lescar, J. & Canard, B. Conventional and Unconventional Mechanisms for Capping Viral mRNA. *Nat. Rev. Microbiol.* **10**, 51–65 (2012).

[79] Binder, M., Kochs, G., Bartenschlager, R. & Lohmann, V. Hepatitis C Virus Escape from the Interferon Regulatory Factor 3 Pathway by a Passive and Active Evasion Strategy. *Hepatology* **46**, 1365–1374 (2007).

[80] Devarkar, S. C. *et al.* Structural Basis for m7G Recognition and 2′-O-Methyl Discrimination in Capped RNAs by the Innate Immune Receptor RIG-I. *Proc. Natl. Acad. Sci. U.S.A.* **113**, 596–601 (2016).

[81] Binder, M. *et al.* Molecular Mechanism of Signal Perception and Integration by the Innate Immune Sensor Retinoic Acid-inducible Gene-I (RIG-I). *J. Biol. Chem.* **286**, 27278–27287 (2011).

[82] Kowalinski, E. *et al.* Structural Basis for the Activation of Innate Immune Pattern-Recognition Receptor RIG-I by Viral RNA. *Cell* **147**, 423–435 (2011).

[83] Jiang, F. *et al.* Structural Basis of RNA Recognition and Activation by Innate Immune Receptor RIG-I. *Nature* **479**, 423–427 (2011).

[84] Luo, D. *et al.* Structural Insights into RNA Recognition by RIG-I. *Cell* **147**, 409–422 (2011).

[85] Gack, M. U. *et al.* TRIM25 Ring-Finger E3 Ubiquitin Ligase Is Essential for Rig-I-Mediated Antiviral Activity. *Nature* **446**, 916–920 (2007).

[86] Oshiumi, H., Matsumoto, M., Hatakeyama, S. & Seya, T. Riplet/RNF135, a RING Finger Protein, Ubiquitinates RIG-I to Promote Interferon-beta Induction during the Early Phase of Viral Infection. *J. Biol. Chem.* **284**, 807–817 (2009).

[87] Oshiumi, H., Miyashita, M., Matsumoto, M. & Seya, T. A Distinct Role of Riplet-Mediated K63-Linked Polyubiquitination of the RIG-I Repressor Domain in Human Antiviral Innate Immune Responses. *PLOS Pathog.* **9**, e1003533 (2013).

[88] Cadena, C. *et al.* Ubiquitin-Dependent and -Independent Roles of E3 Ligase RIPLET in Innate Immunity. *Cell* **177**, 1187–1200.e16 (2019).

[89] Negishi, H., Taniguchi, T. & Yanai, H. The Interferon (IFN) Class of Cytokines and the IFN Regulatory Factor (IRF) Transcription Factor Family. *Cold Spring Harb. Perspect. Biol.* **10**, a028423 (2018).

[90] Mesev, E. V., LeDesma, R. A. & Ploss, A. Decoding Type I and III Interferon Signalling During Viral Infection. *Nat. Microbiol.* **4**, 914–924 (2019).

[91] Berke, I. C. & Modis, Y. MDA5 Cooperatively Forms Dimers and ATP-Sensitive Filaments Upon Binding Double-Stranded RNA. *EMBO J.* **31**, 1714–1726 (2012).

[92] Kato, H. *et al.* Length-Dependent Recognition of Double-Stranded Ribonucleic Acids by Retinoic Acid–Inducible Gene-I and Melanoma Differentiation–Associated Gene 5. *J. Exp. Med.* **205**, 1601–1610 (2008).

[93] Pichlmair, A. *et al.* Activation of MDA5 Requires Higher-Order RNA Structures Generated during Virus Infection. *J. Virol.* **83**, 10761–10769 (2009).

[94] Peisley, A. *et al.* Cooperative Assembly and Dynamic Disassembly of MDA5 Filaments for Viral dsRNA Recognition. *Proc. Natl. Acad. Sci. U.S.A.* **108**, 21010–21015 (2011).

[95] Wu, B. *et al.* Structural Basis for dsRNA Recognition, Filament Formation, and Antiviral Signal Activation by MDA5. *Cell* **152**, 276–289 (2013).

[96] Wies, E. *et al.* Dephosphorylation of the RNA Sensors RIG-I and MDA5 by the Phosphatase PP1 Is Essential for Innate Immune Signaling. *Immunity* **38**, 437–449 (2013).

[97] Lang, X. *et al.* TRIM65-Catalized Ubiquitination Is Essential for MDA5-Mediated Antiviral Innate Immunity. *J. Exp. Med.* **214**, 459–473 (2016).

[98] Munier, C. C., Ottmann, C. & Perry, M. W. D. 14-3-3 Modulation of the Inflammatory Response. *Pharmacol. Res.* **163**, 105236 (2021).

[99] Takeuchi, O. & Akira, S. Recognition of Viruses by Innate Immunity. *Immunol. Rev.* **220**, 214–224 (2007).

[100] Hou, F. *et al.* MAVS Forms Functional Prion-like Aggregates to Activate and Propagate Antiviral Innate Immune Response. *Cell* **146**, 448–461 (2011).

[101] Xu, H. *et al.* Structural Basis for the Prion-Like MAVS Filaments in Antiviral Innate Immunity. *eLife* **3**, e01489 (2014).

[102] Liu, S. *et al.* MAVS Recruits Multiple Ubiquitin E3 Ligases to Activate Antiviral Signaling Cascades. *eLife* **2** (2013).

[103] Meylan, E. *et al.* Cardif Is an Adaptor Protein in the RIG-I Antiviral Pathway and Is Targeted by Hepatitis C Virus. *Nature* **437**, 1167–1172 (2005).

[104] Li, X.-D., Sun, L., Seth, R. B., Pineda, G. & Chen, Z. J. Hepatitis C Virus Protease NS3/4A Cleaves Mitochondrial Antiviral Signaling Protein Off the Mitochondria to Evade Innate Immunity. *Proc. Natl. Acad. Sci. U.S.A.* **102**, 17717–17722 (2005).

[105] Li, K. *et al.* Immune Evasion by Hepatitis C Virus NS3/4A Protease-Mediated Cleavage of the Toll-Like Receptor 3 Adaptor Protein TRIF. *Proc. Natl. Acad. Sci. U.S.A.* **102**, 2992–2997 (2005).

[106] Fitzgerald, K. A. *et al.* IKKε and TBK1 Are Essential Components of the IRF3 Signaling Pathway. *Nat. Immunol.* **4**, 491–496 (2003).

[107] Mogensen, T. H. IRF and STAT Transcription Factors - From Basic Biology to Roles in Infection, Protective Immunity, and Primary Immunodeficiencies. *Front. Immunol.* **9** (2019).

[108] Honda, K. & Taniguchi, T. IRFs: Master Regulators of Signalling by Toll-Like Receptors and Cytosolic Pattern-Recognition Receptors. *Nat. Rev. Immunol.* **6**, 644–658 (2006).

[109] Dinarello, C. A. Historical Insights into Cytokines. *Eur. J. Immunol.* **37**, S34–S45 (2007).

[110] Pestka, S., Krause, C. D. & Walter, M. R. Interferons, Interferon-Like Cytokines, and Their Receptors. *Immunol. Rev.* **202**, 8–32 (2004).

[111] Schroder, K., Hertzog, P. J., Ravasi, T. & Hume, D. A. Interferon-γ: An Overview of Signals, Mechanisms and Functions. *J. Leukoc. Biol.* **75**, 163–189 (2004).

[112] Lavoie, T. B. *et al.* Binding and Activity of All Human Alpha Interferon Subtypes. *Cytokine* **56**, 282–289 (2011).

[113] Schreiber, G. The Molecular Basis for Differential Type I Interferon Signaling. *J. Biol. Chem.* **292**, 7285–7294 (2017).

[114] Walter, M. R. *et al.* Crystal Structure of a Complex Between Interferon-γ and Its Soluble High-Affinity Receptor. *Nature* **376**, 230–235 (1995).

[115] Walter, M. R. The Role of Structure in the Biology of Interferon Signaling. *Front. Immunol.* **11** (2020).

[116] Stanifer, M. L., Pervolaraki, K. & Boulant, S. Differential Regulation of Type I and Type III Interferon Signaling. *Int. J. Mol. Sci.* **20**, 1445 (2019).

[117] Darnell, J. E., Kerr, I. M. & Stark, G. R. Jak-STAT Pathways and Transcriptional Activation in Response to IFNs and Other Extracellular Signaling Proteins. *Science* **264**, 1415–1421 (1994).

[118] Schoggins, J. W. Interferon-Stimulated Genes: What Do They All Do? *Annu. Rev. Virol.* **6**, 567–584 (2019).

[119] González-Navajas, J. M., Lee, J., David, M. & Raz, E. Immunomodulatory Functions of Type I Interferons. *Nat. Rev. Immunol.* **12**, 125–135 (2012).

[120] Kak, G., Raza, M. & Tiwari, B. K. Interferon-Gamma (IFN-γ): Exploring Its Implications in Infectious Diseases. *Biomol. Concepts* **9**, 64–79 (2018).

[121] Schneider, W. M., Chevillotte, M. D. & Rice, C. M. Interferon-Stimulated Genes: A Complex Web of Host Defenses. *Annu. Rev. Immunol.* **32**, 513–545 (2014).

[122] Cheon, H. *et al.* IFN-β-Dependent Increases in STAT1, STAT2, and IRF9 Mediate Resistance to Viruses and DNA Damage. *EMBO J.* **32**, 2751–2763 (2013).

[123] Marié, I., Durbin, J. E. & Levy, D. E. Differential Viral Induction of Distinct Interferon-α Genes by Positive Feedback Through Interferon Regulatory Factor-7. *EMBO J.* **17**, 6660–6669 (1998).

[124] Ning, S., Pagano, J. S. & Barber, G. N. IRF7: Activation, Regulation, Modification and Function. *Genes Immun.* **12**, 399–414 (2011).

[125] Civas, A., Island, M.-L., Génin, P., Morin, P. & Navarro, S. Regulation of Virus-Induced Interferon-α Genes. *Biochimie* **84**, 643–654 (2002).

[126] Osterlund, P. I., Pietilä, T. E., Veckman, V., Kotenko, S. V. & Julkunen, I. IFN Regulatory Factor Family Members Differentially Regulate the Expression of Type III IFN (IFN-λ) Genes. *J. Immunol.* **179**, 3434–3442 (2007).

[127] Iversen, M. B. & Paludan, S. R. Mechanisms of Type III Interferon Expression. *J. Interferon Cytokine Res.* **30**, 573–578 (2010).

[128] Zheng, Y.-w. *et al.* Interferon-λs: Special Immunomodulatory Agents and Potential Therapeutic Targets. *J. Innate Immun.* **5**, 209–218 (2013).

[129] Uggenti, C., Lepelley, A. & Crow, Y. J. Self-Awareness: Nucleic Acid–Driven Inflammation and the Type I Interferonopathies. *Annu. Rev. Immunol.* **37**, 247–267 (2019).

[130] Quicke, K. M., Diamond, M. S. & Suthar, M. S. Negative Regulators of the RIG-I-Like Receptor Signaling Pathway. *Eur. J. Immunol.* **47**, 615–628 (2017).

[131] Arimoto, K.-i. *et al.* Negative Regulation of the RIG-I Signaling by the Ubiquitin Ligase RNF125. *Proc. Natl. Acad. Sci. U.S.A.* **104**, 7500–7505 (2007).

[132] Fan, Y. *et al.* USP21 Negatively Regulates Antiviral Response by Acting as a RIG-I Deubiquitinase. *J. Exp. Med.* **211**, 313–328 (2014).

[133] Willemsen, J. *et al.* Phosphorylation-Dependent Feedback Inhibition of RIG-I by DAPK1 Identified by Kinome-wide siRNA Screening. *Mol. Cell* **65**, 403–415.e8 (2017).

[134] Zanin, N., Viaris de Lesegno, C., Lamaze, C. & Blouin, C. M. Interferon Receptor Trafficking and Signaling: Journey to the Cross Roads. *Front. Immunol.* **11** (2021).

[135] Babon, J. J. *et al.* Suppression of Cytokine Signaling by SOCS3: Characterization of the Mode of Inhibition and the Basis of Its Specificity. *Immunity* **36**, 239–250 (2012).

[136] Piganis, R. A. R. *et al.* Suppressor of Cytokine Signaling (SOCS) 1 Inhibits Type I Interferon (IFN) Signaling via the Interferon α Receptor (IFNAR1)-associated Tyrosine Kinase Tyk2. *J. Biol. Chem.* **286**, 33811–33818 (2011).

[137] Blumer, T., Coto-Llerena, M., Duong, F. H. T. & Heim, M. H. SOCS1 Is an Inducible Negative Regulator of Interferon λ (IFN-λ)–Induced Gene Expression in Vivo. *J. Biol. Chem.* **292**, 17928–17938 (2017).

[138] François-Newton, V. *et al.* USP18-Based Negative Feedback Control Is Induced by Type I and Type III Interferons and Specifically Inactivates Interferon α Response. *PLOS ONE* **6**, e22200 (2011).

[139] Makowska, Z., Duong, F. H. T., Trincucci, G., Tough, D. F. & Heim, M. H. Interferon-β and Interferon-λ Signaling Is Not Affected by Interferon-Induced Refractoriness to Interferon-α in Vivo. *Hepatology* **53**, 1154–1163 (2011).

[140] Speer, S. D. *et al.* ISG15 Deficiency and Increased Viral Resistance in Humans but Not Mice. *Nat. Commun.* **7**, 11496 (2016).

[141] Zhang, D. & Zhang, D.-E. Interferon-Stimulated Gene 15 and the Protein ISGylation System. *J. Interferon Cytokine Res.* **31**, 119–130 (2011).

[142] Shaw, A. E. *et al.* Fundamental Properties of the Mammalian Innate Immune System Revealed by Multispecies Comparison of Type I Interferon Responses. *PLOS Biol.* **15**, e2004086 (2017).

[143] Forster, S. C., Tate, M. D. & Hertzog, P. J. MicroRNA as Type I Interferon-Regulated Transcripts and Modulators of the Innate Immune Response. *Front. Immunol.* **6** (2015).

[144] Zhang, Y. & Cao, X. Long Noncoding RNAs in Innate Immunity. *Cell. Mol. Immunol.* **13**, 138–147 (2016).

[145] Megger, D. A., Philipp, J., Le-Trilling, V. T. K., Sitek, B. & Trilling, M. Deciphering of the Human Interferon-Regulated Proteome by Mass Spectrometry-Based Quantitative Analysis Reveals Extent and Dynamics of Protein Induction and Repression. *Front. Immunol.* **8** (2017).

[146] Zhao, X., Li, J., Winkler, C. A., An, P. & Guo, J.-T. IFITM Genes, Variants, and Their Roles in the Control and Pathogenesis of Viral Infections. *Front. Microbiol.* **9** (2019).

[147] Desai, T. M. *et al.* IFITM3 Restricts Influenza A Virus Entry by Blocking the Formation of Fusion Pores following Virus-Endosome Hemifusion. *PLOS Pathog.* **10**, e1004048 (2014).

[148] Spence, J. S. *et al.* IFITM3 Directly Engages and Shuttles Incoming Virus Particles to Lysosomes. *Nat. Chem. Biol.* **15**, 259–268 (2019).

[149] Liu, S.-Y. *et al.* Interferon-Inducible Cholesterol-25-Hydroxylase Broadly Inhibits Viral Entry by Production of 25-Hydroxycholesterol. *Immunity* **38**, 92–105 (2013).

[150] Haller, O., Staeheli, P., Schwemmle, M. & Kochs, G. Mx GTPases: Dynamin-Like Antiviral Machines of Innate Immunity. *Trends Microbiol.* **23**, 154–163 (2015).

[151] Itsui, Y. *et al.* Expressional Screening of Interferon-Stimulated Genes for Antiviral Activity Against Hepatitis C Virus Replication. *J. Viral Hepat.* **13**, 690–700 (2006).

[152] Hartmann, G. Nucleic Acid Immunity. *Adv. Immunol.* **133**, 121–169 (2017).

[153] Garaigorta, U. & Chisari, F. V. Hepatitis C Virus Blocks Interferon Effector Function by Inducing Protein Kinase R Phosphorylation. *Cell Host Microbe* **6**, 513–522 (2009).

[154] Kristiansen, H., Gad, H. H., Eskildsen-Larsen, S., Despres, P. & Hartmann, R. The Oligoadenylate Synthetase Family: An Ancient Protein Family with Multiple Antiviral Activities. *J. Interferon Cytokine Res.* **31**, 41–47 (2010).

[155] Schoggins, J. W. Recent Advances in Antiviral Interferon-Stimulated Gene Biology. *F1000Research* **7**, 309 (2018).

[156] Pichlmair, A. *et al.* IFIT1 Is an Antiviral Protein That Recognizes 5'-Triphosphate RNA. *Nat. Immunol.* **12**, 624–630 (2011).

[157] Raychoudhuri, A. *et al.* ISG56 and IFITM1 Proteins Inhibit Hepatitis C Virus Replication. *J. Virol.* **85**, 12881–12889 (2011).

[158] Stavrou, S. & Ross, S. R. APOBEC3 Proteins in Viral Immunity. *J. Immunol.* **195**, 4565–4570 (2015).

[159] Richardson, R. B. *et al.* A CRISPR Screen Identifies IFI6 as an ER-Resident Interferon Effector That Blocks Flavivirus Replication. *Nat. Microbiol.* **3**, 1214–1223 (2018).

[160] Neil, S. J. D., Zang, T. & Bieniasz, P. D. Tetherin Inhibits Retrovirus Release and Is Antagonized by HIV-1 Vpu. *Nature* **451**, 425–430 (2008).

[161] Dafa-Berger, A. *et al.* Modulation of Hepatitis C Virus Release by the Interferon-Induced Protein BST-2/Tetherin. *Virology* **428**, 98–111 (2012).

[162] Szretter, K. J. *et al.* The Interferon-Inducible Gene Viperin Restricts West Nile Virus Pathogenesis. *J. Virol.* **85**, 11557–11566 (2011).

[163] Wang, S. *et al.* Viperin Inhibits Hepatitis C Virus Replication by Interfering with Binding of NS5A to Host Protein hVap-33. *J. Gen. Virol.* **93**, 83–92 (2012).

[164] Helbig, K. J. *et al.* Viperin Is Induced following Dengue Virus Type-2 (DENV-2) Infection and Has Anti-viral Actions Requiring the C-terminal End of Viperin. *PLOS Negl. Trop. Dis.* **7**, e2178 (2013).

[165] Mitchell, S., Vargas, J. & Hoffmann, A. Signaling Via the NF-κB System. *Wiley Interdiscip. Rev. Syst. Biol. Med.* **8**, 227–241 (2016).

[166] Xiao, G., Rabson, A. B., Young, W., Qing, G. & Qu, Z. Alternative Pathways of NF-κB Activation: A Double-Edged Sword in Health and Disease. *Cytokine Growth Factor Rev.* **17**, 281–293 (2006).

[167] Karin, M. & Ben-Neriah, Y. Phosphorylation Meets Ubiquitination: The Control of NF-κB Activity. *Annu. Rev. Immunol.* **18**, 621–663 (2000).

[168] Li, Q. & Verma, I. M. NF-κB Regulation in the Immune System. *Nat. Rev. Immunol.* **2**, 725–734 (2002).

[169] Hoffmann, A. & Baltimore, D. Circuitry of Nuclear Factor κB Signaling. *Immunol. Rev.* **210**, 171–186 (2006).

[170] Hoffmann, A., Levchenko, A., Scott, M. L. & Baltimore, D. The IκB-NF-κB Signaling Module: Temporal Control and Selective Gene Activation. *Science* **298**, 1241–1245 (2002).

[171] Platanitis, E. & Decker, T. Regulatory Networks Involving STATs, IRFs, and NF-κB in Inflammation. *Front. Immunol.* **9** (2018).

[172] Panne, D., Maniatis, T. & Harrison, S. C. An Atomic Model of the Interferon-β Enhanceosome. *Cell* **129**, 1111–1123 (2007).

[173] Wang, J. & Knaut, H. Chemokine Signaling in Development and Disease. *Development* **141**, 4199–4205 (2014).

[174] Hughes, C. E. & Nibbs, R. J. B. A Guide to Chemokines and Their Receptors. *FEBS J.* **285**, 2944–2971 (2018).

[175] Salanga, C. L. & Handel, T. M. Chemokine Oligomerization and Interactions with Receptors and Glycosaminoglycans: The Role of Structural Dynamics in Function. *Exp. Cell Res.* **317**, 590–601 (2011).

[176] Proudfoot, A. *et al.* Glycosaminoglycan Binding and Oligomerization Are Essential for the in Vivo Activity of Certain Chemokines. *Proc. Natl. Acad. Sci. U.S.A.* **100**, 1885–1890 (2003).

[177] Marra, F. & Tacke, F. Roles for Chemokines in Liver Disease. *Gastroenterology* **147**, 577–594.e1 (2014).

[178] Nourshargh, S. & Alon, R. Leukocyte Migration into Inflamed Tissues. *Immunity* **41**, 694–707 (2014).

[179] Kufareva, I., Salanga, C. L. & Handel, T. M. Chemokine and Chemokine Receptor Structure and Interactions: Implications for Therapeutic Strategies. *Immunol. Cell Biol.* **93**, 372–383 (2015).

[180] Kleist, A. B. *et al.* New Paradigms in Chemokine Receptor Signal Transduction: Moving Beyond the Two-Site Model. *Biochem. Pharmacol.* **114**, 53–68 (2016).

[181] Kehrl, J. H. Chemoattractant Receptor Signaling and the Control of Lymphocyte Migration. *Immunol. Res.* **34**, 211–227 (2006).

[182] Nibbs, R. J. B. & Graham, G. J. Immune Regulation by Atypical Chemokine Receptors. *Nat. Rev. Immunol.* **13**, 815–829 (2013).

[183] Plotkin, J., Prockop, S. E., Lepique, A. & Petrie, H. T. Critical Role for CXCR4 Signaling in Progenitor Localization and T Cell Differentiation in the Postnatal Thymus. *J. Immunol.* **171**, 4521–4527 (2003).

[184] Stone, M. J., Hayward, J. A., Huang, C., E. Huma, Z. & Sanchez, J. Mechanisms of Regulation of the Chemokine-Receptor Network. *Int. J. Mol. Sci.* **18** (2017).

[185] Fahey, S., Dempsey, E. & Long, A. The Role of Chemokines in Acute and Chronic Hepatitis C Infection. *Cell. Mol. Immunol.* **11**, 25–40 (2014).

[186] von Hundelshausen, P. *et al.* Chemokine Interactome Mapping Enables Tailored Intervention in Acute and Chronic Inflammation. *Sci. Transl. Med.* **9** (2017).

[187] Beck, L. A. *et al.* Functional Analysis of the Chemokine Receptor CCR3 on Airway Epithelial Cells. *J. Immunol.* **177**, 3344–3354 (2006).

[188] Kany, S., Vollrath, J. T. & Relja, B. Cytokines in Inflammatory Disease. *Int. J. Mol. Sci.* **20**, 6008 (2019).

[189] Shakhov, A. N., Collart, M. A., Vassalli, P., Nedospasov, S. A. & Jongeneel, C. V. κB-Type Enhancers Are Involved in Lipopolysaccharide-Mediated Transcriptional Activation of the Tumor Necrosis Factor Alpha Gene in Primary Macrophages. *J. Exp. Med.* **171**, 35–47 (1990).

[190] Libermann, T. A. & Baltimore, D. Activation of Interleukin-6 Gene Expression Through the NF-κB Transcription Factor. *Mol. Cell. Biol.* **10**, 2327–2334 (1990).

[191] Webster, J. D. & Vucic, D. The Balance of TNF Mediated Pathways Regulates Inflammatory Cell Death Signaling in Healthy and Diseased Tissues. *Front. Cell Dev. Biol.* **8** (2020).

[192] Brenner, D., Blaser, H. & Mak, T. W. Regulation of Tumour Necrosis Factor Signalling: Live or Let Die. *Nat. Rev. Immunol.* **15**, 362 (2015).

[193] Unver, N. & McAllister, F. IL-6 Family Cytokines: Key Inflammatory Mediators as Biomarkers and Potential Therapeutic Targets. *Cytokine Growth Factor Rev.* **41**, 10–17 (2018).

[194] Rose-John, S. Interleukin-6 Signalling in Health and Disease. *F1000Research* **9**, 1013 (2020).

[195] Rose-John, S. & Heinrich, P. C. Soluble Receptors for Cytokines and Growth Factors: Generation and Biological Function. *Biochem. J.* **300 (Pt 2)**, 281–290 (1994).

[196] Mackiewicz, A., Schooltink, H., Heinrich, P. C. & Rose-John, S. Complex of Soluble Human IL-6-Receptor/IL-6 up-Regulates Expression of Acute-Phase Proteins. *J. Immunol.* **149**, 2021–2027 (1992).

[197] Jiang, M. *et al.* Dysregulation of SOCS-Mediated Negative Feedback of Cytokine Signaling in Carcinogenesis and Its Significance in Cancer Treatment. *Front. Immunol.* **8** (2017).

[198] Ho, H. H. & Ivashkiv, L. B. Role of STAT3 in Type I Interferon Responses: Negative Regulation of STAT1-Dependent Inflammatory Gene Activation. *J. Biol. Chem.* **281**, 14111–14118 (2006).

[199] Barbier, L. *et al.* Interleukin-1 Family Cytokines: Keystones in Liver Inflammatory Diseases. *Front. Immunol.* **10** (2019).

[200] Frank, D. & Vince, J. E. Pyroptosis Versus Necroptosis: Similarities, Differences, and Crosstalk. *Cell Death Differ.* **26**, 99–114 (2019).

[201] Elmore, S. Apoptosis: A Review of Programmed Cell Death. *Toxicol. Pathol.* **35**, 495–516 (2007).

[202] Nagata, S. Apoptosis and Clearance of Apoptotic Cells. *Annu. Rev. Immunol.* **36**, 489–517 (2018).

[203] Edlich, F. BCL-2 Proteins and Apoptosis: Recent Insights and Unknowns. *Biochem. Biophys. Res. Commun.* **500**, 26–34 (2018).

[204] Peña-Blanco, A. & García-Sáez, A. J. Bax, Bak and Beyond — Mitochondrial Performance in Apoptosis. *FEBS J.* **285**, 416–431 (2018).

[205] Chinnaiyan, A. M. The Apoptosome: Heart and Soul of the Cell Death Machine. *Neoplasia* **1**, 5–15 (1999).

[206] Hill, M. M., Adrain, C., Duriez, P. J., Creagh, E. M. & Martin, S. J. Analysis of the Composition, Assembly Kinetics and Activity of Native Apaf-1 Apoptosomes. *EMBO J.* **23**, 2134–2145 (2004).

[207] McIlwain, D. R., Berger, T. & Mak, T. W. Caspase Functions in Cell Death and Disease. *Cold Spring Harb. Perspect. Biol.* **5**, a008656 (2013).

[208] Hardwick, J. M. & Soane, L. Multiple Functions of BCL-2 Family Proteins. *Cold Spring Harb. Perspect. Biol.* **5** (2013).

[209] Hrdinka, M. & Yabal, M. Inhibitor of Apoptosis Proteins in Human Health and Disease. *Genes Immun.* **20**, 641–650 (2019).

[210] So, T. & Ishii, N. The TNF–TNFR Family of Co-signal Molecules. In Azuma, M. & Yagita, H. (eds.) *Co-Signal Molecules in T Cell Activation: Immune Regulation in Health and Disease*, Advances in Experimental Medicine and Biology, 53–84 (Springer, Singapore, 2019).

[211] Wajant, H. The Fas Signaling Pathway: More Than a Paradigm. *Science* **296**, 1635–1636 (2002).

[212] Grimm, S., Stanger, B. Z. & Leder, P. RIP and FADD: Two "Death Domain"-Containing Proteins Can Induce Apoptosis by Convergent, but Dissociable, Pathways. *Proc. Natl. Acad. Sci. U.S.A.* **93**, 10923–10927 (1996).

[213] Hsu, H., Xiong, J. & Goeddel, D. V. The TNF Receptor 1-Associated Protein TRADD Signals Cell Death and NF-κB Activation. *Cell* **81**, 495–504 (1995).

[214] Kischkel, F. C. *et al.* Cytotoxicity-Dependent Apo-1 (Fas/CD95)-Associated Proteins Form a Death-Inducing Signaling Complex (DISC) with the Receptor. *EMBO J.* **14**, 5579–5588 (1995).

[215] Chávez-Galán, L., Arenas-Del Angel, M. C., Zenteno, E., Chávez, R. & Lascurain, R. Cell Death Mechanisms Induced by Cytotoxic Lymphocytes. *Cell. Mol. Immunol.* **6**, 15–25 (2009).

[216] Pardo, J. *et al.* Apoptotic Pathways Are Selectively Activated by Granzyme a and/or Granzyme B in CTL-Mediated Target Cell Lysis. *J. Cell Biol.* **167**, 457–468 (2004).

[217] Trapani, J. A. & Smyth, M. J. Functional Significance of the Perforin/Granzyme Cell Death Pathway. *Nat. Rev. Immunol.* **2**, 735–747 (2002).

[218] Martinvalet, D., Zhu, P. & Lieberman, J. Granzyme A Induces Caspase-Independent Mitochondrial Damage, a Required First Step for Apoptosis. *Immunity* **22**, 355–370 (2005).

[219] Vivier, E., Tomasello, E., Baratin, M., Walzer, T. & Ugolini, S. Functions of Natural Killer Cells. *Nat. Immunol.* **9**, 503–510 (2008).

[220] Fink, S. L. & Cookson, B. T. Apoptosis, Pyroptosis, and Necrosis: Mechanistic Description of Dead and Dying Eukaryotic Cells. *Infect. Immun.* **73**, 1907–1916 (2005).

[221] Degterev, A. *et al.* Chemical Inhibitor of Nonapoptotic Cell Death with Therapeutic Potential for Ischemic Brain Injury. *Nat. Chem. Biol.* **1**, 112–119 (2005).

[222] Holler, N. *et al.* Fas Triggers an Alternative, Caspase-8-Independent Cell Death Pathway Using the Kinase RIP as Effector Molecule. *Nat. Immunol.* **1**, 489–495 (2000).

[223] Sun, L. *et al.* Mixed Lineage Kinase Domain-Like Protein Mediates Necrosis Signaling Downstream of RIP3 Kinase. *Cell* **148**, 213–227 (2012).

[224] Kaczmarek, A., Vandenabeele, P. & Krysko, D. V. Necroptosis: The Release of Damage-Associated Molecular Patterns and Its Physiological Relevance. *Immunity* **38**, 209–223 (2013).

[225] Grootjans, S., Vanden Berghe, T. & Vandenabeele, P. Initiation and Execution Mechanisms of Necroptosis: An Overview. *Cell Death Differ.* **24**, 1184–1195 (2017).

[226] Brault, M. & Oberst, A. Controlled Detonation: Evolution of Necroptosis in Pathogen Defense. *Immunol. Cell Biol.* **95**, 131–136 (2017).

[227] Naderer, T. & Fulcher, M. C. Targeting Apoptosis Pathways in Infections. *J. Leukoc. Biol.* **103**, 275–285 (2018).

[228] Broz, P. & Dixit, V. M. Inflammasomes: Mechanism of Assembly, Regulation and Signalling. *Nat. Rev. Immunol.* **16**, 407–420 (2016).

[229] Maadidi, S. E. *et al.* A Novel Mitochondrial MAVS/Caspase-8 Platform Links RNA Virus–Induced Innate Antiviral Signaling to Bax/Bak-Independent Apoptosis. *J. Immunol.* **192**, 1171–1183 (2014).

[230] Yu, C.-Y., Chiang, R.-L., Chang, T.-H., Liao, C.-L. & Lin, Y.-L. The Interferon Stimulator Mitochondrial Antiviral Signaling Protein Facilitates Cell Death by Disrupting the Mitochondrial Membrane Potential and by Activating Caspases. *J. Virol.* **84**, 2421–2431 (2010).

[231] Chattopadhyay, S. & Sen, G. C. RIG-I-Like Receptor-Induced IRF3 Mediated Pathway of Apoptosis (RIPA): A New Antiviral Pathway. *Protein Cell* **8**, 165–168 (2017).

[232] Ringelhan, M., Pfister, D., O'Connor, T., Pikarsky, E. & Heikenwalder, M. The Immunology of Hepatocellular Carcinoma. *Nat. Immunol.* **19**, 222–232 (2018).

[233] Hofmann, M., Tauber, C., Hensel, N. & Thimme, R. CD8+ T Cell Responses during HCV Infection and HCC. *J. Clin. Med.* **10**, 991 (2021).

[234] Shin, E.-C., Sung, P. S. & Park, S.-H. Immune Responses and Immunopathology in Acute and Chronic Viral Hepatitis. *Nat. Rev. Immunol.* **16**, 509–523 (2016).

[235] Ehrlich, A., Duche, D., Ouedraogo, G. & Nahmias, Y. Challenges and Opportunities in the Design of Liver-on-Chip Microdevices. *Annu. Rev. Biomed. Eng.* **21**, 219–239 (2019).

[236] Li, H., Huang, M.-H., Jiang, J.-D. & Peng, Z.-G. Hepatitis C: From Inflammatory Pathogenesis to Anti-Inflammatory/Hepatoprotective Therapy. *World J. Gastroenterol.* **24**, 5297–5311 (2018).

[237] Bonilla, F. A. & Oettgen, H. C. Adaptive Immunity. *J. Allergy Clin. Immunol.* **125**, S33–S40 (2010).

[238] Chatzileontiadou, D. S. M., Sloane, H., Nguyen, A. T., Gras, S. & Grant, E. J. The Many Faces of CD4+ T Cells: Immunological and Structural Characteristics. *Int. J. Mol. Sci.* **22**, 73 (2021).

[239] Janeway, C. A., Travers, P., Walport, M. & Shlomchik, M. J. The Course of the Adaptive Response to Infection. In *Immunobiology: The Immune System in Health and Disease. 5th Edition* (Garland Science, 2001).

[240] Shin, E.-C. *et al.* Delayed Induction, Not Impaired Recruitment, of Specific CD8+ T Cells Causes the Late Onset of Acute Hepatitis C. *Gastroenterology* **141**, 686–695, 695.e1 (2011).

[241] Pestka, J. M. *et al.* Rapid Induction of Virus-Neutralizing Antibodies and Viral Clearance in a Single-Source Outbreak of Hepatitis C. *Proc. Natl. Acad. Sci. U.S.A.* **104**, 6025–6030 (2007).

[242] Santantonio, T., Wiegand, J. & Tilman Gerlach, J. Acute Hepatitis C: Current Status and Remaining Challenges. *J. Hepatol.* **49**, 625–633 (2008).

[243] Wieland, S. *et al.* Simultaneous Detection of Hepatitis C Virus and Interferon Stimulated Gene Expression in Infected Human Liver. *Hepatology* **59**, 2121–2130 (2013).

[244] Sarhan, M., Land, W. G., Tonnus, W., Hugo, C. P. & Linkermann, A. Origin and Consequences of Necroinflammation. *Physiol. Rev.* **98**, 727–780 (2018).

[245] Khatun, M. & Ray, R. B. Mechanisms Underlying Hepatitis C Virus-Associated Hepatic Fibrosis. *Cells* **8**, 1249 (2019).

[246] Schlabe, S. & Rockstroh, J. K. Advances in the Treatment of HIV/HCV Coinfection in Adults. *Expert Opin. Pharmacother.* **19**, 49–64 (2018).

[247] Urban, C., **Welsch**, H. *et al.* Persistent Innate Immune Stimulation Results in IRF3-Mediated but Caspase-Independent Cytostasis. *Viruses* **12**, 635 (2020).

[248] Bender, S. *et al.* Activation of Type I and III Interferon Response by Mitochondrial and Peroxisomal MAVS and Inhibition by Hepatitis C Virus. *PLOS Pathog.* **11**, e1005264 (2015).

[249] Thomas, P. D. *et al.* PANTHER: A Library of Protein Families and Subfamilies Indexed by Function. *Genome Res.* **13**, 2129–2141 (2003).

[250] Mi, H., Muruganujan, A. & Thomas, P. D. PANTHER in 2013: Modeling the Evolution of Gene Function, and Other Gene Attributes, in the Context of Phylogenetic Trees. *Nucleic Acids Res.* **41**, D377–386 (2013).

[251] Pfaffl, M. W. A New Mathematical Model for Relative Quantification in Real-Time RT–PCR. *Nucleic Acids Res.* **29**, e45–e45 (2001).

[252] Jo, J. *et al.* Analysis of CD8+ T-Cell–Mediated Inhibition of Hepatitis C Virus Replication Using a Novel Immunological Model. *Gastroenterology* **136**, 1391–1401 (2009).

[253] Rusinova, I. *et al.* INTERFEROME V2.0: An Updated Database of Annotated Interferon-Regulated Genes. *Nucleic Acids Res.* **41**, D1040–D1046 (2013).

[254] Barrat, F. J., Crow, M. K. & Ivashkiv, L. B. Interferon Target-Gene Expression and Epigenomic Signatures in Health and Disease. *Nat. Immunol.* **20**, 1574–1583 (2019).

[255] Kim, T. K. & Eberwine, J. H. Mammalian Cell Transfection: The Present and the Future. *Anal Bioanal Chem* **397**, 3173–3178 (2010).

[256] Yu, G.-Y. *et al.* Hepatic Expression of HCV RNA-dependent RNA Polymerase Triggers Innate Immune Signaling and Cytokine Production. *Mol. Cell* **48**, 313–321 (2012).

[257] Naka, K., Dansako, H., Kobayashi, N., Ikeda, M. & Kato, N. Hepatitis C Virus NS5B Delays Cell Cycle Progression by Inducing Interferon-β via Toll-Like Receptor 3 Signaling Pathway Without Replicating Viral Genomes. *Virology* **346**, 348–362 (2006).

[258] Ranjith-Kumar, C. T., Wen, Y., Baxter, N., Bhardwaj, K. & Kao, C. C. A Cell-Based Assay for RNA Synthesis by the HCV Polymerase Reveals New Insights on Mechanism of Polymerase Inhibitors and Modulation by NS5A. *PLOS ONE* **6**, e22575 (2011).

[259] Bersaglieri, C. & Santoro, R. Genome Organization in and Around the Nucleolus. *Cells* **8**, 579 (2019).

[260] Strauß, L. Characterization of RIG-I Mediated Cell Death (Master's Thesis, DKFZ, Heidelberg). (2019).

[261] Kato, N. *et al.* Replication of Hepatitis C Virus in Cultured Non-neoplastic Human Hepatocytes. *Jpn. J. Cancer Res.* **87**, 787–792 (1996).

[262] Faísca, P. & Desmecht, D. Sendai Virus, the Mouse Parainfluenza Type 1: A Longstanding Pathogen That Remains up-to-Date. *Res. Vet. Sci.* **82**, 115–125 (2007).

[263] Seth, R. B., Sun, L., Ea, C.-K. & Chen, Z. J. Identification and Characterization of MAVS, a Mitochondrial Antiviral Signaling Protein that Activates NF-κB and IRF3. *Cell* **122**, 669–682 (2005).

[264] Rehwinkel, J. *et al.* RIG-I Detects Viral Genomic RNA during Negative-Strand RNA Virus Infection. *Cell* **140**, 397–408 (2010).

[265] Hogan, K. A., Chini, C. C. S. & Chini, E. N. The Multi-Faceted Ecto-Enzyme CD38: Roles in Immunomodulation, Cancer, Aging, and Metabolic Diseases. *Front. Immunol.* **10**, 1187 (2019).

[266] Glaría, E. & Valledor, A. F. Roles of CD38 in the Immune Response to Infection. *Cells* **9** (2020).

[267] Chowdhury, D. *et al.* The Exonuclease TREX1 Is in the SET Complex and Acts in Concert with NM23-H1 to Degrade DNA during Granzyme A-Mediated Cell Death. *Mol. Cell* **23**, 133–142 (2006).

[268] Yan, N. Immune Diseases Associated with TREX1 and STING Dysfunction. *J. Interferon Cytokine Res.* **37**, 198–206 (2017).

[269] Vidoni, S. *et al.* MR-1S Interacts with PET100 and PET117 in Module-Based Assembly of Human Cytochrome C Oxidase. *Cell Rep.* **18**, 1727–1738 (2017).

[270] Murthy, S. E. *et al.* OSCA/TMEM63 Are an Evolutionarily Conserved Family of Mechanically Activated Ion Channels. *eLife* **7**, e41844 (2018).

[271] Du, H. *et al.* The Cation Channel TMEM63B Is an Osmosensor Required for Hearing. *Cell Rep.* **31**, 107596 (2020).

[272] Hubel, P. *et al.* A Protein-Interaction Network of Interferon-Stimulated Genes Extends the Innate Immune System Landscape. *Nat. Immunol.* **20**, 493–502 (2019).

[273] Wang, W., Xu, L., Su, J., Peppelenbosch, M. P. & Pan, Q. Transcriptional Regulation of Antiviral Interferon-Stimulated Genes. *Trends Microbiol.* **25**, 573–584 (2017).

[274] Ashley, C. L., Abendroth, A., McSharry, B. P. & Slobedman, B. Interferon-Independent Upregulation of Interferon-Stimulated Genes during Human Cytomegalovirus Infection is Dependent on IRF3 Expression. *Viruses* **11**, 246 (2019).

[275] Imai, T. *et al.* The T Cell-directed CC Chemokine TARC Is a Highly Specific Biological Ligand for CC Chemokine Receptor 4. *J. Biol. Chem.* **272**, 15036–15042 (1997).

[276] Bernardini, G. *et al.* Identification of the CC Chemokines TARC and Macrophage Inflammatory Protein-1β as Novel Functional Ligands for the CCR8 Receptor. *Eur. J. Immunol.* **28**, 582–588 (1998).

[277] Korbecki, J. *et al.* CC Chemokines in a Tumor: A Review of Pro-Cancer and Anti-Cancer Properties of the Ligands of Receptors CCR1, CCR2, CCR3, and CCR4. *Int. J. Mol. Sci.* **21**, 8412 (2020).

[278] Zeremski, M. *et al.* Intrahepatic Levels of CXCR3-Associated Chemokines Correlate with Liver Inflammation and Fibrosis in Chronic Hepatitis C. *Hepatology* **48**, 1440–1450 (2008).

[279] Zeremski, M. *et al.* Peripheral CXCR3-Associated Chemokines as Biomarkers of Fibrosis in Chronic Hepatitis C Virus Infection. *J. Infect. Dis.* **200**, 1774–1780 (2009).

[280] Sahin, H. *et al.* Proapoptotic Effects of the Chemokine, CXCL10 Are Mediated by the Noncognate Receptor TLR4 in Hepatocytes. *Hepatology* **57**, 797–805 (2013).

[281] Noris, M. & Remuzzi, G. Overview of Complement Activation and Regulation. *Semin. Nephrol.* **33**, 479–492 (2013).

[282] Thery, F. *et al.* Ring Finger Protein 213 Assembles into a Sensor for ISGylated Proteins with Antimicrobial Activity. *bioRxiv* 2021.06.03.446796 (2021).

[283] Kuroda, M. *et al.* Identification of Interferon-Stimulated Genes That Attenuate Ebola Virus Infection. *Nat. Commun.* **11**, 2953 (2020).

[284] Karki, S. *et al.* Multiple Interferon Stimulated Genes Synergize with the Zinc Finger Antiviral Protein to Mediate Anti-Alphavirus Activity. *PLOS ONE* **7**, e37398 (2012).

[285] Grünvogel, O. *et al.* DDX60L Is an Interferon-Stimulated Gene Product Restricting Hepatitis C Virus Replication in Cell Culture. *J. Virol.* **89**, 10548–10568 (2015).

[286] Grünvogel, O. *et al.* Type I and Type II Interferon Responses in Two Human Liver Cell Lines (Huh-7 and Huh6). *Genom. Data* **7**, 166–170 (2016).

[287] Nielsen, H. L., Rønnov-Jessen, L., Villadsen, R. & Petersen, O. W. Identification of EPSTI1, a Novel Gene Induced by Epithelial-Stromal Interaction in Human Breast Cancer. *Genomics* **79**, 703–710 (2002).

[288] Kim, Y.-H., Lee, J.-R. & Hahn, M.-J. Regulation of Inflammatory Gene Expression in Macrophages by Epithelial-Stromal Interaction 1 (Epsti1). *Biochem. Biophys. Res. Commun.* **496**, 778–783 (2018).

[289] Meng, X., Yang, D., Yu, R. & Zhu, H. EPSTI1 Is Involved in IL-28A-Mediated Inhibition of HCV Infection. *Mediators Inflamm.* **2015**, e716315 (2015).

[290] Xu, Y., Johansson, M. & Karlsson, A. Human UMP-CMP Kinase 2, a Novel Nucleoside Monophosphate Kinase Localized in Mitochondria. *J. Biol. Chem.* **283**, 1563–1571 (2008).

[291] El-Diwany, R. *et al.* CMPK2 and BCL-G Are Associated with Type 1 Interferon–Induced HIV Restriction in Humans. *Sci. Adv.* **4** (2018).

[292] Kambara, H. *et al.* Negative Regulation of the Interferon Response by an Interferon-Induced Long Non-Coding RNA. *Nucleic Acids Res.* **42**, 10668–10680 (2014).

[293] Catic, A. *et al.* Screen for ISG15-crossreactive Deubiquitinases. *PLOS ONE* **2**, e679 (2007).

[294] Liu, Q. *et al.* Broad and Diverse Mechanisms Used by Deubiquitinase Family Members in Regulating the Type I Interferon Signaling Pathway During Antiviral Responses. *Sci. Adv.* **4**, eaar2824 (2018).

[295] Ferrington, D. A. & Gregerson, D. S. Immunoproteasomes: Structure, Function, and Antigen Presentation. *Prog. Mol. Biol. Transl. Sci.* **109**, 75–112 (2012).

[296] Tauber, A. L., Schweiker, S. S. & Levonis, S. M. The Potential Association Between PARP14 and SARS-CoV-2 Infection (COVID-19). *Future Med. Chem.* **13**, 587–592 (2021).

[297] Glennon, N. B., Jabado, O., Lo, M. K. & Shaw, M. L. Transcriptome Profiling of the Virus-Induced Innate Immune Response in Pteropus vampyrus and Its Attenuation by Nipah Virus Interferon Antagonist Functions. *J. Virol.* **89**, 7550–7566 (2015).

[298] Ignatius Irudayam, J. *et al.* Characterization of Type I Interferon Pathway During Hepatic Differentiation of Human Pluripotent Stem Cells and Hepatitis C Virus Infection. *Stem Cell Res.* **15**, 354–364 (2015).

[299] He, X.-S. *et al.* Differential Transcriptional Responses to Interferon-α and Interferon-γ in Primary Human Hepatocytes. *J. Interferon Cytokine Res.* **30**, 311–320 (2009).

[300] Chen, L. *et al.* Hepatic Gene Expression Discriminates Responders and Nonresponders in Treatment of Chronic Hepatitis C Viral Infection. *Gastroenterology* **128**, 1437–1444 (2005).

[301] Chen, L. *et al.* Cell-Type Specific Gene Expression Signature in Liver Underlies Response to Interferon Therapy in Chronic Hepatitis C Infection. *Gastroenterology* **138**, 1123–1133.e3 (2010).

[302] Titus, G. P. *et al.* Crystal Structure of Human Homogentisate Dioxygenase. *Nat. Struct. Biol.* **7**, 542–546 (2000).

[303] Belinky, F. *et al.* PathCards: Multi-Source Consolidation of Human Biological Pathways. *Database* **2015** (2015).

[304] Rowland, A., Miners, J. O. & Mackenzie, P. I. The UDP-Glucuronosyltransferases: Their Role in Drug Metabolism and Detoxification. *The International Journal of Biochemistry & Cell Biology* **45**, 1121–1132 (2013).

[305] Alam, N., Angeli, M. G. & Greenblatt, D. J. Mechanism of In-Vitro Inhibition of UGT1A1 by Paritaprevir. *J. Pharm. Pharmacol.* **69**, 1794–1801 (2017).

[306] Wright, M. D., Ni, J. & Rudy, G. B. The L6 Membrane Proteins–a New Four-Transmembrane Superfamily. *Protein Sci.* **9**, 1594–1600 (2000).

[307] Florin, L. & Lang, T. Tetraspanin Assemblies in Virus Infection. *Front. Immunol.* **9** (2018).

[308] Ochsner, S. A., Pillich, R. T. & McKenna, N. J. Consensus Transcriptional Regulatory Networks of Coronavirus-Infected Human Cells. *Sci. Data* **7**, 314 (2020).

[309] Harrison, E. H. & Kopec, R. E. Enzymology of Vertebrate Carotenoid Oxygenases. *Biochim. Biophys. Acta* **1865**, 158653 (2020).

[310] Huang, Z., Liu, Y., Qi, G., Brand, D. & Zheng, S. G. Role of Vitamin A in the Immune System. *J. Clin. Med.* **7**, 258 (2018).

[311] Jundi, K. & Greene, C. M. Transcription of Interleukin-8: How Altered Regulation Can Affect Cystic Fibrosis Lung Disease. *Biomolecules* **5**, 1386–1398 (2015).

[312] Kim, J.-H. Interleukin-8 in the Tumor Immune Niche: Lessons from Comparative Oncology. In Birbrair, A. (ed.) *Tumor Microenvironment: The Role of Interleukins – Part A*, Advances in Experimental Medicine and Biology, 25–33 (Springer International Publishing, Cham, 2020).

[313] Zito, E. ERO1: A Protein Disulfide Oxidase and H_2O_2 Producer. *Free Radic. Biol. Med.* **83**, 299–304 (2015).

[314] Shergalis, A. G., Hu, S., Bankhead, A. & Neamati, N. Role of the ERO1-PDI Interaction in Oxidative Protein Folding and Disease. *Pharmacol. Ther.* **210**, 107525 (2020).

[315] Mills, E. G., Izzi-Engbeaya, C., Abbara, A., Comninos, A. N. & Dhillo, W. S. Functions of Galanin, Spexin and Kisspeptin in Metabolism, Mood and Behaviour. *Nat. Rev. Endocrinol.* **17**, 97–113 (2021).

[316] Moriyama, M. *et al.* Interferon-β Is Activated by Hepatitis C Virus NS5B and Inhibited by NS4A, NS4B, and NS5A. *Hepatol. Int.* **1**, 302–310 (2007).

[317] Vegna, S. *et al.* NOD1 Participates in the Innate Immune Response Triggered by Hepatitis C Virus Polymerase. *J. Virol.* **90**, 6022–6035 (2016).

[318] Binder, M. *et al.* Identification of Determinants Involved in Initiation of Hepatitis C Virus RNA Synthesis by Using Intergenotypic Replicase Chimeras. *J. Virol.* **81**, 5270–5283 (2007).

[319] Ranjith-Kumar, C. T. & Kao, C. C. Recombinant Viral RdRps Can Initiate RNA Synthesis from Circular Templates. *RNA* **12**, 303–312 (2006).

[320] Yamashita, T. *et al.* RNA-dependent RNA Polymerase Activity of the Soluble Recombinant Hepatitis C Virus NS5B Protein Truncated at the C-terminal Region. *J. Biol. Chem.* **273**, 15479–15486 (1998).

[321] Hirano, M. *et al.* Direct Interaction Between Nucleolin and Hepatitis C Virus NS5B. *J. Biol. Chem.* **278**, 5109–5115 (2003).

[322] Shimakami, T. *et al.* Effect of Hepatitis C Virus (HCV) NS5B-Nucleolin Interaction on HCV Replication with HCV Subgenomic Replicon. *J. Virol.* **80**, 3332–3340 (2006).

[323] Levin, A. *et al.* Functional Characterization of Nuclear Localization and Export Signals in Hepatitis C Virus Proteins and Their Role in the Membranous Web. *PLOS ONE* **9**, e114629 (2014).

[324] Tessier, T. M., MacNeil, K. M. & Mymryk, J. S. Piggybacking on Classical Import and Other Non-Classical Mechanisms of Nuclear Import Appear Highly Prevalent within the Human Proteome. *Biology* **9** (2020).

[325] Liu, G. *et al.* Nuclear-Resident RIG-I Senses Viral Replication Inducing Antiviral Immunity. *Nat. Commun.* **9**, 3199 (2018).

[326] Kim, T. Y. *et al.* Oncogenic Potential of a Dominant Negative Mutant of Interferon Regulatory Factor 3. *J. Biol. Chem.* **278**, 15272–15278 (2003).

[327] Kandathil, A. J. *et al.* Use of Laser Capture Microdissection to Map Hepatitis C Virus-Positive Hepatocytes in Human Liver. *Gastroenterology* **145**, 1404–1413.e1–10 (2013).

[328] Graw, F. *et al.* Inferring Viral Dynamics in Chronically HCV Infected Patients from the Spatial Distribution of Infected Hepatocytes. *PLOS Comput. Biol.* **10**, e1003934 (2014).

[329] Binder, M. *et al.* Replication Vesicles are Load- and Choke-Points in the Hepatitis C Virus Lifecycle. *PLOS Pathog.* **9**, e1003561 (2013).

[330] Grünvogel, O. *et al.* Secretion of Hepatitis C Virus Replication Intermediates Reduces Activation of Toll-Like Receptor 3 in Hepatocytes. *Gastroenterology* **154**, 2237–2251.e16 (2018).

[331] Tolmachov, O. E., Subkhankulova, T. & Tolmachova, T. Silencing of Transgene Expression: A Gene Therapy Perspective. In *Gene Therapy - Tools and Potential Applications (DOI: 10.5772/53379)* (IntechOpen, 2013).

[332] Goyvaerts, C., Liechtenstein, T., Bricogne, C., Escors, D. & Breckpot, K. Targeted Lentiviral Vectors: Current Applications and Future Potential. In *Gene Therapy - Tools and Potential Applications (DOI: 10.5772/52770)* (IntechOpen, 2013).

[333] Lohmann, V., Körner, F., Herian, U. & Bartenschlager, R. Biochemical Properties of Hepatitis C Virus NS5B RNA-Dependent RNA Polymerase and Identification of Amino Acid Sequence Motifs Essential for Enzymatic Activity. *J. Virol.* **71**, 8416–8428 (1997).

[334] Lohmann, V., Roos, A., Körner, F., Koch, J. O. & Bartenschlager, R. Biochemical and Kinetic Analyses of NS5B RNA-Dependent RNA Polymerase of the Hepatitis C Virus. *Virology* **249**, 108–118 (1998).

[335] Ranjith-Kumar, C. T. & Kao, C. C. Biochemical Activities of the HCV NS5B RNA-Dependent RNA Polymerase. In Tan, S.-L. (ed.) *Hepatitis C Viruses: Genomes and Molecular Biology* (Horizon Bioscience, Norfolk (UK), 2006).

[336] Goverdhana, S. *et al.* Regulatable Gene Expression Systems for Gene Therapy Applications: Progress and Future Challenges. *Mol. Ther.* **12**, 189–211 (2005).

[337] Matsukura, S. *et al.* Synthetic Double-Stranded RNA Induces Multiple Genes Related to Inflammation Through Toll-Like Receptor 3 Depending on NF-κB and/or IRF-3 in Airway Epithelial Cells. *Clin. Exp. Allergy* **36**, 1049–1062 (2006).

[338] Meusel, T. R. & Imani, F. Viral Induction of Inflammatory Cytokines in Human Epithelial Cells Follows a p38 Mitogen-Activated Protein Kinase-Dependent but NF-κB-Independent Pathway. *J. Immunol.* **171**, 3768–3774 (2003).

[339] Gern, J. E. *et al.* Double-Stranded RNA Induces the Synthesis of Specific Chemokines by Bronchial Epithelial Cells. *Am. J. Respir. Cell Mol. Biol.* **28**, 731–737 (2003).

[340] Mehta, A. K., Gracias, D. T. & Croft, M. TNF Activity and T cells. *Cytokine* **101**, 14–18 (2018).

[341] Ho, I.-C. & Miaw, S.-C. Regulation of IL-4 Expression in Immunity and Diseases. In Ma, X. (ed.) *Regulation of Cytokine Gene Expression in Immunity and Diseases*, Advances in Experimental Medicine and Biology, 31–77 (Springer Netherlands, Dordrecht, 2016).

[342] Sung, P. S. *et al.* CXCL10 Is Produced in Hepatitis A Virus-Infected Cells in an IRF3-Dependent but IFN-Independent Manner. *Sci. Rep.* **7**, 6387 (2017).

[343] Ferrari, S. M. *et al.* Immunomodulation of CXCL10 Secretion by Hepatitis C Virus: Could CXCL10 Be a Prognostic Marker of Chronic Hepatitis C? *J. Immunol. Res.* **2019**, e5878960 (2019).

[344] Brass, A. & Brenndörfer, E. D. The Role of Chemokines in Hepatitis C Virus-Mediated Liver Disease. *Int. J. Mol. Sci.* **15**, 4747–4779 (2014).

[345] Monick, M. M. *et al.* Respiratory Syncytial Virus Synergizes with Th2 Cytokines to Induce Optimal Levels of TARC/CCL17. *J. Immunol.* **179**, 1648–1658 (2007).

[346] Oo, Y. H. *et al.* Distinct Roles for CCR4 and CXCR3 in the Recruitment and Positioning of Regulatory T Cells in the Inflamed Human Liver. *J. Immunol.* **184**, 2886–2898 (2010).

[347] Riezu-Boj, J.-I. *et al.* Hepatitis C Virus Induces the Expression of CCL17 and CCL22 Chemokines That Attract Regulatory T Cells to the Site of Infection. *J. Hepatol.* **54**, 422–431 (2011).

[348] Tsuji, K. *et al.* dsRNA Enhances Eotaxin-3 Production Through Interleukin-4 Receptor Upregulation in Airway Epithelial Cells. *Eur. Respir. J.* **26**, 795–803 (2005).

[349] Matsuzaki, H. *et al.* Interleukin-17A and Toll-Like Receptor 3 Ligand Poly(I:C) Synergistically Induced Neutrophil Chemoattractant Production by Bronchial Epithelial Cells. *PLOS ONE* **10**, e0141746 (2015).

[350] Ma, Y. & Yates, J. R. Proteomics and Pulse Azidohomoalanine Labeling of Newly Synthesized Proteins: What Are the Potential Applications? *Expert Rev. Proteomics* **15**, 545–554 (2018).

[351] Harris, G. M., Raitman, I. & Schwarzbauer, J. E. Cell-Derived Decellularized Extracellular Matrices. In Mecham, R. P. (ed.) *Methods in Cell Biology*, vol. 143 of *Methods in Extracellular Matrix Biology*, 97–114 (Academic Press, 2018).

[352] Li, J. *et al.* Exosomes Mediate the Cell-to-Cell Transmission of IFN-α-Induced Antiviral Activity. *Nat. Immunol.* **14**, 793–803 (2013).

[353] Schorey, J. S., Cheng, Y., Singh, P. P. & Smith, V. L. Exosomes and Other Extracellular Vesicles in Host–Pathogen Interactions. *EMBO Rep.* **16**, 24–43 (2015).

[354] Devhare, P. B. *et al.* Exosome-Mediated Intercellular Communication between Hepatitis C Virus-Infected Hepatocytes and Hepatic Stellate Cells. *J. Virol.* **91** (2017).

[355] Ke, M. *et al.* Identification, Quantification, and Site Localization of Protein Posttranslational Modifications via Mass Spectrometry-Based Proteomics. In Mirzaei, H. & Carrasco, M. (eds.) *Modern Proteomics – Sample Preparation, Analysis and Practical Applications*, Advances in Experimental Medicine and Biology, 345–382 (Springer International Publishing, Cham, 2016).

[356] Snell, L. M., McGaha, T. L. & Brooks, D. G. Type I Interferon in Chronic Virus Infection and Cancer. *Trends Immunol.* **38**, 542–557 (2017).

[357] DeDiego, M. L., Martinez-Sobrido, L. & Topham, D. J. Novel Functions of IFI44L as a Feedback Regulator of Host Antiviral Responses. *J. Virol.* **93** (2019).

[358] Busse, D. C. *et al.* Interferon-Induced Protein 44 and Interferon-Induced Protein 44-Like Restrict Replication of Respiratory Syncytial Virus. *J. Virol.* **94** (2020).

[359] Huang, W.-C., Tung, S.-L., Chen, Y.-L., Chen, P.-M. & Chu, P.-Y. IFI44L Is a Novel Tumor Suppressor in Human Hepatocellular Carcinoma Affecting Cancer Stemness, Metastasis, and Drug Resistance Via Regulating Met/Src Signaling Pathway. *BMC Cancer* **18**, 609 (2018).

[360] Hu, B., Guo, H., Zhou, P. & Shi, Z.-L. Characteristics of SARS-CoV-2 and COVID-19. *Nat. Rev. Microbiol.* **19**, 141–154 (2021).

[361] Yin, X. *et al.* MDA5 Governs the Innate Immune Response to SARS-CoV-2 in Lung Epithelial Cells. *Cell Rep.* **34**, 108628 (2021).

[362] Rebendenne, A. *et al.* SARS-CoV-2 Triggers an MDA-5-Dependent Interferon Response Which Is Unable To Control Replication in Lung Epithelial Cells. *J. Virol.* **95** (2021).

[363] Choi, S.-I., Kim, S.-Y., Lee, J., Cho, E.-W. & Kim, I.-G. TM4SF4 Overexpression in Radiation-Resistant Lung Carcinoma Cells Activates IGF1R Via Elevation of IGF1. *Oncotarget* **5**, 9823–9837 (2014).

[364] Choi, S. I. *et al.* Osteopontin Production by TM4SF4 Signaling Drives a Positive Feedback Autocrine Loop with the STAT3 Pathway to Maintain Cancer Stem Cell-Like Properties in Lung Cancer Cells. *Oncotarget* **8**, 101284–101297 (2017).

[365] Liu, Z., Zhao, M., Yokoyama, K. K. & Li, T. Molecular Cloning of a cDNA for Rat TM4SF4, a Homolog of Human il-TMP (TM4SF4), and Enhanced Expression of the Corresponding Gene in Regenerating Rat Liver. *Biochim. Biophys. Acta* **1518**, 183–189 (2001).

[366] Li, Y. *et al.* Human Tetraspanin Transmembrane 4 Superfamily Member 4 or Intestinal and Liver Tetraspan Membrane Protein Is Overexpressed in Hepatocellular Carcinoma and Accelerates Tumor Cell Growth. *Acta Biochim. Biophys. Sin.* **44**, 224–232 (2012).

[367] Wang, L. *et al.* Adenovirus-Mediated Delivery of siRNA Targeting TM4SF4 Attenuated Liver Cancer Cell Growth in Vitro and in Vivo. *Acta Biochim. Biophys. Sin.* **45**, 213–219 (2013).

[368] Larner, A. C., Chaudhuri, A. & Darnell, J. E. Transcriptional Induction by Interferon. New Protein(s) Determine the Extent and Length of the Induction. *J. Biol. Chem.* **261**, 453–459 (1986).

[369] Borden, E. C. & Murphy, F. A. The Interferon Refractory State: In Vivo and in Vitro Studies of Its Mechanism. *J. Immunol.* **106**, 134–142 (1971).

[370] Sarasin-Filipowicz, M. *et al.* Alpha Interferon Induces Long-Lasting Refractoriness of JAK-STAT Signaling in the Mouse Liver through Induction of USP18/UBP43. *Mol. Cell. Biol.* **29**, 4841–4851 (2009).

[371] Kerkvliet, J. *et al.* Transgenic Expression of the 3D Polymerase Inhibits Theiler's Virus Infection and Demyelination. *J. Virol.* **83**, 12279–12289 (2009).

[372] Kerkvliet, J., Papke, L. & Rodriguez, M. Antiviral Effects of a Transgenic RNA-Dependent RNA Polymerase. *J. Virol.* **85**, 621–625 (2011).

[373] Painter, M. M. *et al.* Antiviral Protection via RdRP-Mediated Stable Activation of Innate Immunity. *PLOS Pathog.* **11**, e1005311 (2015).

[374] Miller, C. M. *et al.* Systemic Expression of a Viral RdRP Protects against Retrovirus Infection and Disease. *J. Virol.* **94** (2020).

[375] Wang, Q., Khillan, J., Gadue, P. & Nishikura, K. Requirement of the RNA Editing Deaminase ADAR1 Gene for Embryonic Erythropoiesis. *Science* **290**, 1765–1768 (2000).

[376] Liddicoat, B. J., Chalk, A. M. & Walkley, C. R. ADAR1, Inosine and the Immune Sensing System: Distinguishing Self from Non-Self. *Wiley Interdiscip. Rev. RNA* **7**, 157–172 (2016).

[377] Klemm, S. L., Shipony, Z. & Greenleaf, W. J. Chromatin Accessibility and the Regulatory Epigenome. *Nat. Rev. Genet.* **20**, 207–220 (2019).

[378] Park, S. H. *et al.* Type I Interferons and the Cytokine TNF Cooperatively Reprogram the Macrophage Epigenome to Promote Inflammatory Activation. *Nat. Immunol.* **18**, 1104–1116 (2017).

[379] Kamada, R. *et al.* Interferon Stimulation Creates Chromatin Marks and Establishes Transcriptional Memory. *Proc. Natl. Acad. Sci. U.S.A.* **115**, E9162–E9171 (2018).

[380] Ostuni, R. *et al.* Latent Enhancers Activated by Stimulation in Differentiated Cells. *Cell* **152**, 157–171 (2013).

[381] Qiao, Y. *et al.* Synergistic Activation of Inflammatory Cytokine Genes by Interferon-γ-Induced Chromatin Remodeling and Toll-like Receptor Signaling. *Immunity* **39**, 454–469 (2013).

[382] Daniel, B. *et al.* The Nuclear Receptor PPARγ Controls Progressive Macrophage Polarization as a Ligand-Insensitive Epigenomic Ratchet of Transcriptional Memory. *Immunity* **49**, 615–626.e6 (2018).

[383] Gouil, Q. & Keniry, A. Latest Techniques to Study DNA Methylation. *Essays Biochem.* **63**, 639–648 (2019).

[384] Park, P. J. ChIP–Seq: Advantages and Challenges of a Maturing Technology. *Nat. Rev. Genet.* **10**, 669–680 (2009).

[385] Shashikant, T. & Ettensohn, C. A. Genome-Wide Analysis of Chromatin Accessibility Using ATAC-Seq. In Hamdoun, A. & Foltz, K. R. (eds.) *Methods in Cell Biology*, vol. 151 of *Echinoderms, Part B*, 219–235 (Academic Press, 2019).

[386] Wilson, E. B. *et al.* Blockade of Chronic Type I Interferon Signaling to Control Persistent LCMV Infection. *Science* **340**, 202–207 (2013).

[387] Teijaro, J. R. *et al.* Persistent LCMV Infection Is Controlled by Blockade of Type I Interferon Signaling. *Science* **340**, 207–211 (2013).

[388] Dash, S., Aydin, Y., Widmer, K. E. & Nayak, L. Hepatocellular Carcinoma Mechanisms Associated with Chronic HCV Infection and the Impact of Direct-Acting Antiviral Treatment. *J. Hepatocell. Carcinoma* **7**, 45–76 (2020).

[389] Bray, F. *et al.* Global Cancer Statistics 2018: GLOBOCAN Estimates of Incidence and Mortality Worldwide for 36 Cancers in 185 Countries. *CA Cancer J. Clin.* **68**, 394–424 (2018).

[390] Hin Tang, J. J., Hao Thng, D. K., Lim, J. J. & Toh, T. B. JAK/STAT Signaling in Hepatocellular Carcinoma. *Hepat. Oncol.* **7** (2020).

[391] Bakiri, L. & Wagner, E. F. Mouse Models for Liver Cancer. *Mol. Oncol.* **7**, 206–223 (2013).

[392] Llovet, J. M., Schwartz, M. & Mazzaferro, V. Resection and Liver Transplantation for Hepatocellular Carcinoma. *Semin. Liver Dis.* **25**, 181–200 (2005).

[393] Liu, C.-Y., Chen, K.-F. & Chen, P.-J. Treatment of Liver Cancer. *Cold Spring Harb. Perspect. Med.* **5**, a021535 (2015).

[394] Llovet, J. M. *et al.* Hepatocellular Carcinoma. *Nat. Rev. Dis. Primers* **2**, 1–23 (2016).

[395] Kgatle, M. M., Setshedi, M. & Hairwadzi, H. N. Hepatoepigenetic Alterations in Viral and Nonviral-Induced Hepatocellular Carcinoma. *BioMed Res. Int.* **2016**, e3956485 (2016).

[396] Perez, S. *et al.* Hepatitis C Virus Leaves an Epigenetic Signature Post Cure of Infection by Direct-Acting Antivirals. *PLOS Genet.* **15**, e1008181 (2019).

[397] Sumpter, R. *et al.* Regulating Intracellular Antiviral Defense and Permissiveness to Hepatitis C Virus RNA Replication through a Cellular RNA Helicase, RIG-I. *J. Virol.* **79**, 2689–2699 (2005).

Supplement

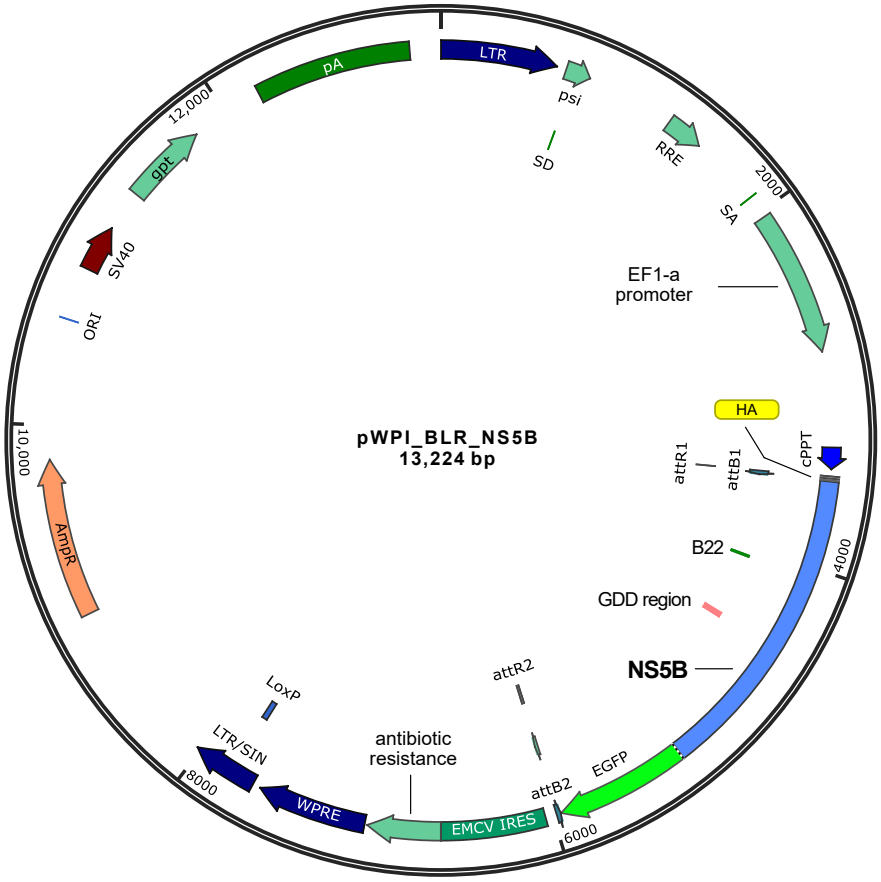

Figure S1: Plasmid map of pWPI NS5B vector.

Map of a lentiviral pWPI vector coding for NS5B expression under the control of the EF1α promoter. The RNA transcript contains an internal ribosomal entry site (IRES) and the coding sequence for blasticidin or puromycin resistance downstream of the NS5B coding sequence. All NS5B variants used in this study lacked 21 amino acids at the C-terminus, and additionally versions of all variants tagged C-terminally with eGFP were generated as shown in the vector map. In NS5B$^{\Delta}$, a 30 bp stretch around the catalytic triad GDD was deleted, while a point mutation converted GDD to GND in NS5B^{GND}. The latter variant and its accompanying wild-type version NS5B^{WT} were mutated for improved epitope detection (B22) and tagged N-terminally with HA. Further vector elements: LTR: long terminal repeat; psi: HIV packaging signal; RRE: Rev responsive element; SD and SE: 5' and 3' splicing sites; cPPT: central polypurine tract; attB and attR sites: relevant regions for Gateway cloning; WPRE: Woodchuck Hepatitis virus (WHV) posttranscriptional regulatory element; LoxP: locus of X-over P1; LTR/SIN: long terminal repeat/self-inactivating; AmpR: ampicillin resistence for prokaryotic selection; ORI: origin of replication; SV40: Simian virus 40; pA: SV40 poly adenylation signal. Vector map was generated with SnapGene.

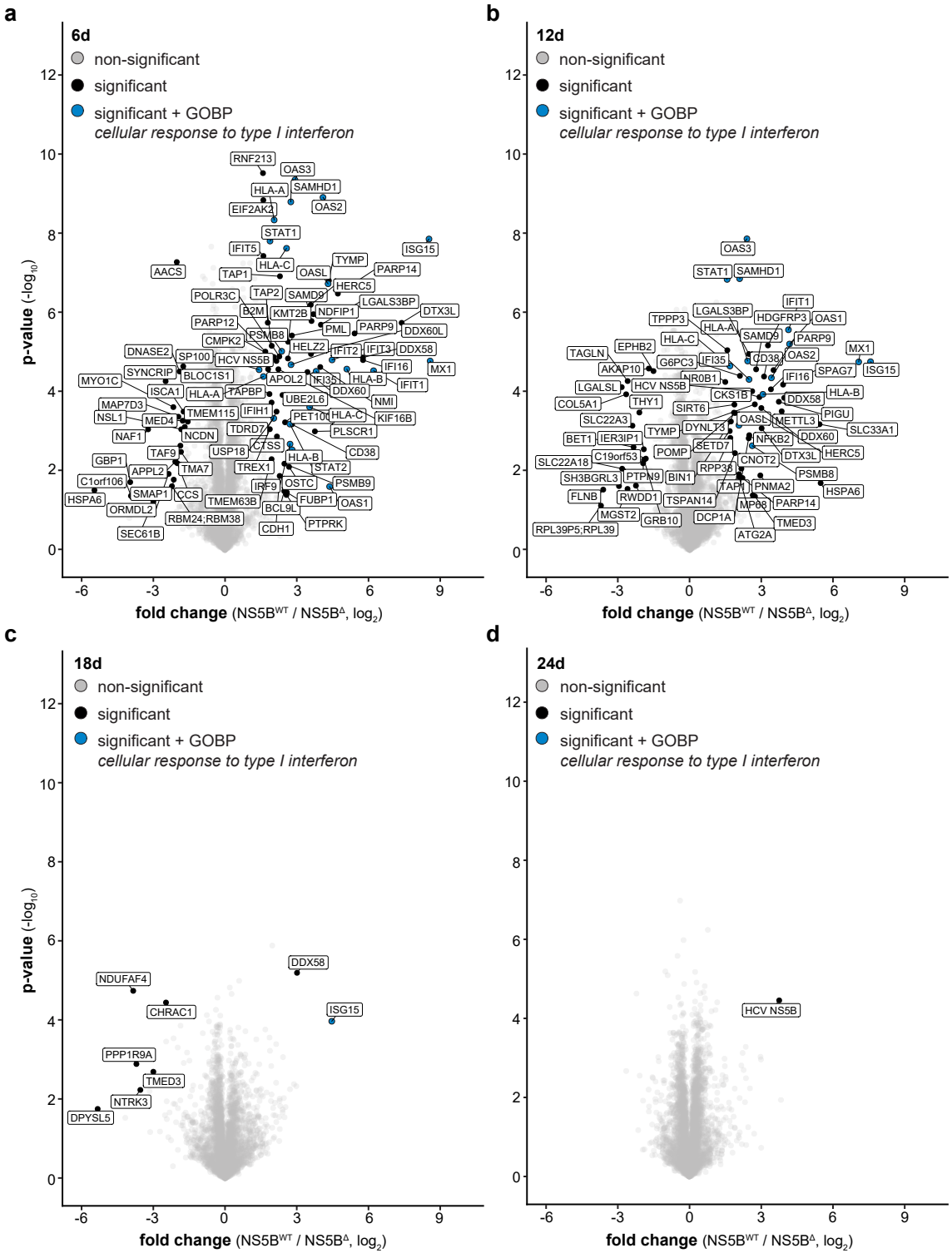

Figure S2: Total cell proteomics of NS5B-transduced A549 cells.

Volcano plots displaying total cell proteomics of A549 cells 6 (a), 12 (b), 18 (c) and 24 (d) days post transduction with $NS5B^{WT}$ (fold change over $NS5B^{\Delta}$ from n = 4 technical replicates). Significantly regulated genes (two-sided t-test, S0 = 1, corrected for multiple testing with permutation based false discovery rate < 0.01) are shown in black, while proteins connected to the GOBP term "cellular response to type I interferon" are shown in blue. This figure is based on mass spectrometry measurements and data analysis performed by Christian Urban and Andreas Pichlmair. Figure adapted from joint publication [247].

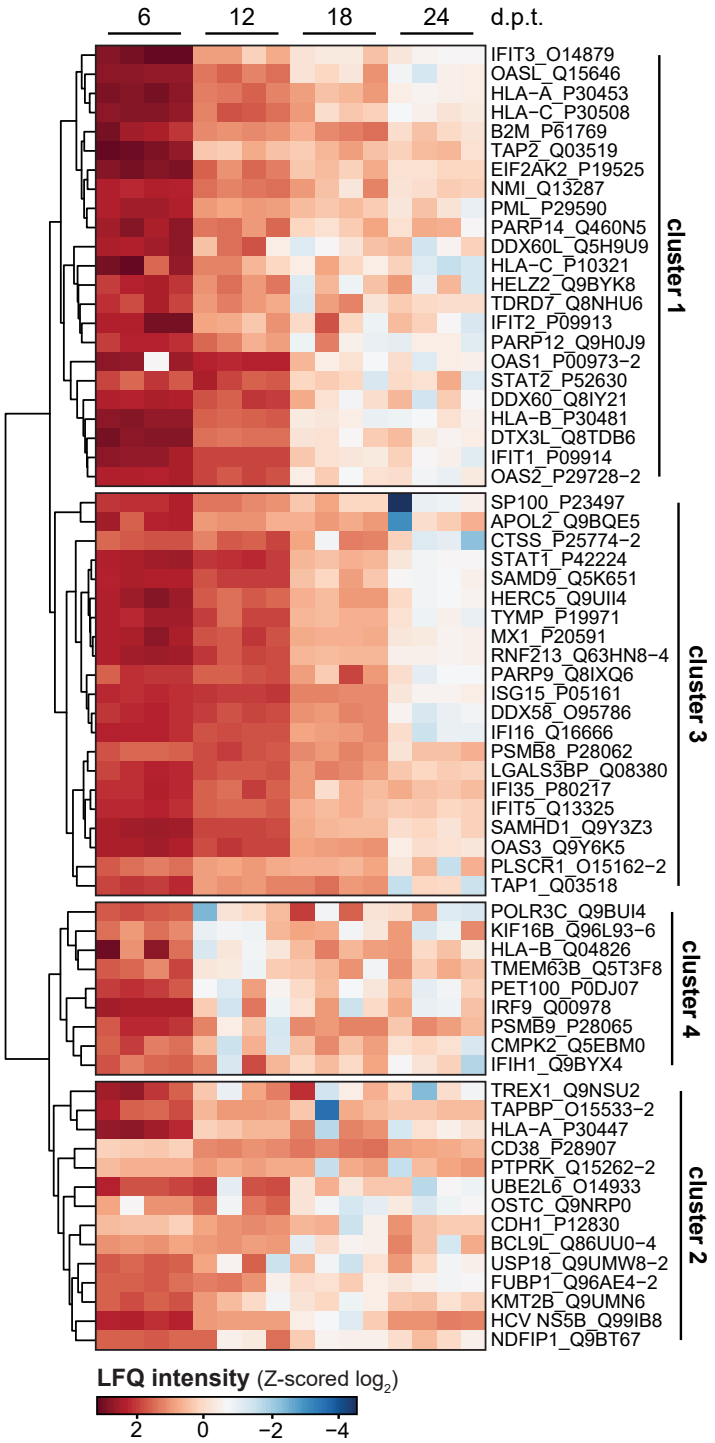

Figure S3: Differentially upregulated proteins in NS5B^{WT} A549 cells.

Hierarchical clustering of proteins significantly upregulated in NS5B^{WT}-transduced A549 cells 6 days post transduction (d.p.t.) (Z-scored $\log_2$ LFQ intensities compared to NS5B$^{\Delta}$). Clustering (Euclidean distances and Ward agglomeration) identified four clusters of differentially regulated proteins (gene names and majority protein IDs are shown). This figure is based on mass spectrometry measurements and data analysis performed by Christian Urban and Andreas Pichlmair. Figure adapted from joint publication [247].

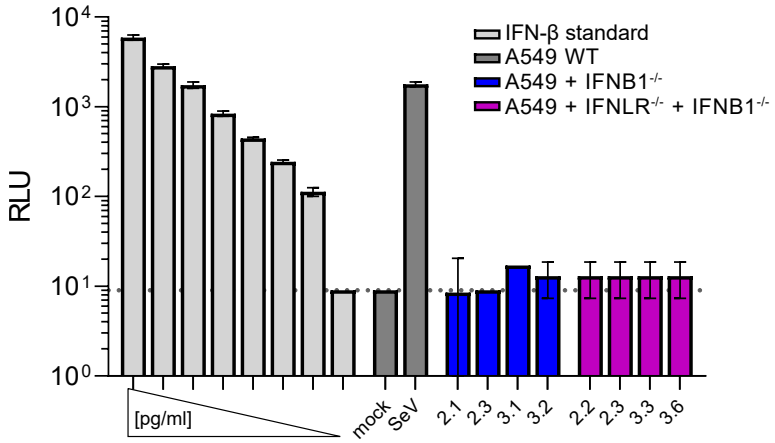

Figure S4: Validation of IFNB1 knockout single cell clones.

IFNB1 knockout single cell clones in A549 wild-type and in A549 IFNLR knockout cells were validated by IFN-β ELISA 16 hours after infection with Sendai virus (SeV) (mean ± s.d. of relative light units (RLU) from n = 2 technical replicates). IFN-β levels in SeV-infected knockout single cell clones were compared to SeV- and mock-infected wild-type A549 as well as to the internal IFN-β standard at concentrations of 1000, 500, 250, 125, 62.5, 31.25, 15.625, and 0 pg/ml. Dashed line indicates the assay background signal.

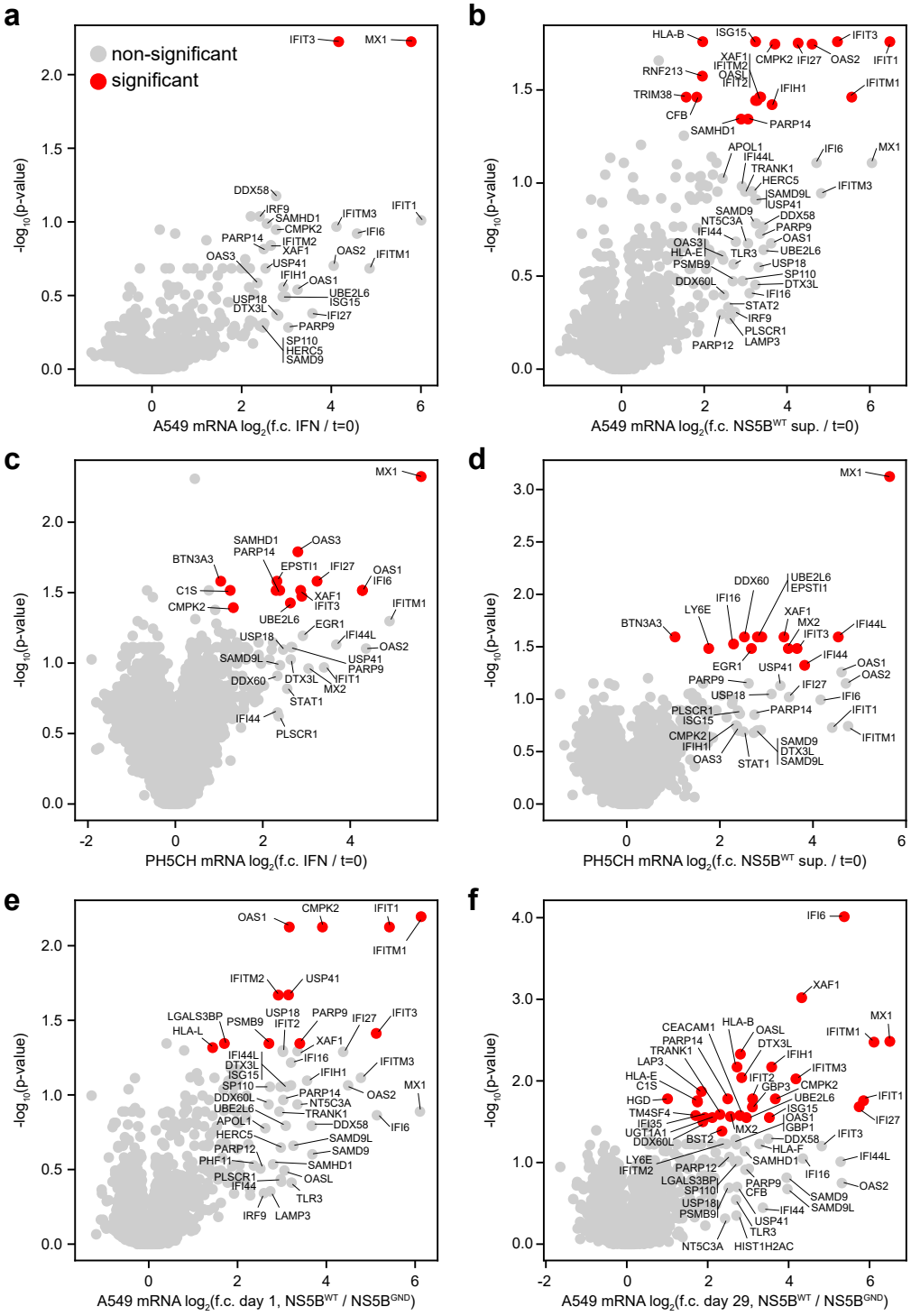

Figure S5: Expression profiles of cells stimulated with NS5B-derived supernatant or defined IFNs.

Volcano plots displaying mRNA fold changes (f.c.) of cells stimulated with interferons or supernatant from NS5B-transduced cells (log_2(mean f.c.) of n = 3 independent experiments). Significantly regulated genes (at least two-fold up- or downregulation and p-value < 0.05 after Benjamini-Hochberg correction for multiple testing) are highlighted in red. Non-significant genes with labels showed fold change > 5 and B.H.-corrected p-value < 0.1. (**a-b**) A549 cells treated with IFN-β (130 IU/ml) and IFN-λ1 (12 ng/ml) (a) or $NS5B^{WT}$ supernatant (b) for 24 h (f.c. over t = 0 h). (**c-d**) PH5CH cells treated with IFN-β (110 IU/ml) and IFN-λ1 (2.5 ng/ml) (e) or $NS5B^{WT}$ supernatant (f) for 24 h (f.c. over t = 0 h). (**e-f**) A549 cells treated with $NS5B^{WT}$ supernatant for 1 day (d) or 29 days (f.c. over $NS5B^{GND}$).

Table S1: GOBP terms enriched in A549 cells after NS5B^{WT} supernatant treatment.

Gene ontology (GO) terms for biological processes enriched in A549 cells cultured for 24 h in supernatant derived from NS5B^{WT}-transduced A549 cells. False discovery rate (FDR) < 0.05. GOBP term enrichment analysis was performed with PANTHER, and most specific terms from the hierarchically sorted results are listed.

Term	GO ID	FDR	Genes
type I interferon signaling pathway	GO:0060337	2.90E-21	IFITM1, IFITM2, IFI27, OAS2, HLA-B, ISG15, IFIT1, SAMHD1, XAF1, IFIT3, IFIT2, OASL
defense response to virus	GO:0051607	1.85E-14	IFIH1, IFITM1, IFITM2, IFI27, OAS2, ISG15, IFIT1, SAMHD1, IFIT3, IFIT2, OASL
negative regulation of viral genome replication	GO:0045071	9.00E-09	IFITM1, IFITM2, OAS2, ISG15, IFIT1, OASL
viral process	GO:0016032	2.96E-02	IFIH1, IFI27, HLA-B, ISG15, IFIT1, SAMHD1
interferon-gamma-mediated signaling pathway	GO:0060333	2.71E-04	OAS2, HLA-B, TRIM38, OASL
response to interferon-beta	GO:0035456	1.46E-03	IFITM1, IFITM2, XAF1
regulation of viral entry into host cell	GO:0046596	4.23E-03	IFITM1, IFITM2, TRIM38
negative regulation of innate immune response	GO:0045824	1.14E-02	HLA-B, SAMHD1, PARP14
regulation of ribonuclease activity	GO:0060700	1.61E-02	OAS2, OASL
cellular response to interferon-alpha	GO:0035457	2.61E-02	IFIT3, IFIT2
deoxyribonucleoside triphosphate metabolic process	GO:0009200	4.12E-02	CMPK2, SAMHD1
cellular response to exogenous dsRNA	GO:0071360	4.52E-02	IFIH1, IFIT1

Table S2: GOBP terms enriched in PH5CH after IFN treatment

Gene ontology (GO) terms for biological processes enriched in PH5CH cells treated with IFN-β (110 IU/ml) and IFN-λ1 (2.5 ng/ml) for 24 h. False discovery rate (FDR) < 0.05. GOBP term enrichment analysis was performed with PANTHER, and most specific terms from the hierarchically sorted results are listed. Table continued on next page.

Term	GO ID	FDR	Genes
type I interferon signaling pathway	GO:0060337	1.74E-12	OAS1, IFI27, OAS3, MX1, IFI6, SAMHD1, XAF1, IFIT3
defense response to virus	GO:0051607	1.21E-07	OAS1, IFI27, OAS3, MX1, IFI6, SAMHD1, IFIT3

Term	GO ID	FDR	Genes
negative regulation of viral genome replication	GO:0045071	5.68E-03	OAS1, OAS3, MX1
regulation of ribonuclease activity	GO:0060700	1.81E-02	OAS1, OAS3
cellular response to interferon-alpha	GO:0035457	2.58E-02	OAS1, IFIT3
deoxyribonucleoside triphosphate metabolic process	GO:0009200	4.04E-02	CMPK2, SAMHD1

Table S3: GOBP terms enriched in PH5CH cells after NS5B^{WT} supernatant treatment.

Gene ontology (GO) terms for biological processes enriched in PH5CH cells cultured for 24 h in supernatant derived from NS5B^{WT}-transduced PH5CH cells. False discovery rate (FDR) < 0.05. GOBP term enrichment analysis was performed with PANTHER, and most specific terms from the hierarchically sorted results are listed.

Term	GO ID	FDR	Genes
defense response to virus	GO:0051607	8.78E-06	IFI16, MX2, MX1, DDX60, IFI44L, IFIT3
type I interferon signaling pathway	GO:0060337	6.41E-06	EGR1, MX2, MX1, XAF1, IFIT3
negative regulation of viral process	GO:0048525	2.16E-02	IFI16, MX1, LY6E
synaptic vesicle budding from presynaptic endocytic zone membrane	GO:0016185	1.41E-02	MX2, MX1
dynamin family protein polymerization involved in mitochondrial fission	GO:0003374	1.67E-02	MX2, MX1
postsynaptic neurotransmitter receptor internalization	GO:0098884	1.76E-02	MX2, MX1
mitochondrial fission	GO:0000266	4.76E-02	MX2, MX1

Table S4: GOBP terms enriched in A549 cells after NS5B^{WT} supernatant treatment for 1 day.

Gene ontology (GO) terms for biological processes enriched in A549 cells cultured for 1 day (= 24 h) in supernatant derived from NS5B^{WT}-transduced A549 cells. False discovery rate (FDR) < 0.05. GOBP term enrichment analysis was performed with PANTHER, and most specific terms from the hierarchically sorted results are listed. Table continued on next page.

Term	GO ID	FDR	Genes
defense response to virus	GO:0051607	1.33E-06	IFITM1, IFITM2, OAS1, IFIT1, PARP9, IFIT3
type I interferon signaling pathway	GO:0060337	2.54E-06	IFITM1, IFITM2, OAS1, IFIT1, IFIT3

Term	GO ID	FDR	Genes
negative regulation of viral genome replication	GO:0045071	2.99E-05	IFITM1, IFITM2, OAS1, IFIT1
response to interferon-gamma	GO:0034341	4.52E-02	IFITM1, IFITM2, OAS1
cellular response to interferon-alpha	GO:0035457	1.48E-02	OAS1, IFIT3
negative regulation of viral entry into host cell	GO:0046597	3.31E-02	IFITM1, IFITM2

Table S5: GOBP terms enriched in A549 cells after NS5B^{WT} supernatant treatment for 29 days.

Gene ontology (GO) terms for biological processes enriched in A549 cells cultured for 29 days in supernatant derived from NS5B^{WT}-transduced A549 cells. False discovery rate (FDR) < 0.05. GOBP term enrichment analysis was performed with PANTHER, and most specific terms from the hierarchically sorted results are listed. Table continued on next page.

Term	GO ID	FDR	Genes
type I interferon signaling pathway	GO:0060337	1.78E-24	IFITM3, IFITM1, MX2, MX1, HLA-B, IFI6, ISG15, IFI35, IFIT1, IFIT2, HLA-E, OASL, BST2, IFI27, XAF1
defense response to virus	GO:0051607	1.73E-16	IFITM3, IFITM1, DTX3L, MX2, MX1, IFI6, ISG15, IFIT1, IFIT2, OASL, BST2, IFIH1, IFI27, GBP3
negative regulation of viral genome replication	GO:0045071	3.17E-09	IFITM3, BST2, IFITM1, MX1, ISG15, IFIT1, OASL
response to interferon-alpha	GO:0035455	3.36E-07	IFITM3, BST2, IFITM1, MX2, IFIT2
response to interferon-beta	GO:0035456	8.79E-05	IFITM3, BST2, IFITM1, XAF1
negative regulation of viral life cycle	GO:1903901	4.39E-03	IFITM3, BST2, IFITM1
regulation of T cell mediated cytotoxicity	GO:0001914	1.17E-02	CEACAM1, HLA-B, HLA-E
negative regulation of type I interferon production	GO:0032480	1.76E-02	IFIH1, ISG15, UBE2L6
interferon-gamma-mediated signaling pathway	GO:0060333	4.30E-02	HLA-B, HLA-E, OASL
ISG15-protein conjugation	GO:0032020	1.99E-02	ISG15, UBE2L6
protection from natural killer cell mediated cytotoxicity	GO:0042270	1.96E-02	HLA-B, HLA-E

Term	GO ID	FDR	Genes
antigen processing and presentation of endogenous peptide antigen via MHC class I via ER pathway, TAP-independent	GO:0002486	2.39E-02	HLA-B, HLA-E
synaptic vesicle budding from presynaptic endocytic zone membrane	GO:0016185	2.31E-02	MX2, MX1
antigen processing and presentation of exogenous peptide antigen via MHC class I, TAP-independent	GO:0002480	2.75E-02	HLA-B, HLA-E
dynamin family protein polymerization involved in mitochondrial fission	GO:0003374	2.70E-02	MX2, MX1
postsynaptic neurotransmitter receptor internalization	GO:0098884	3.11E-02	MX2, MX1